

SOILS and ROCKS

An International Journal of Geotechnical and Geoenvironmental Engineering

Editor

Renato Pinto da Cunha
University of Brasília, Brazil

Co-editor

Ana Vieira
National Laboratory for Civil Engineering, Portugal

Associate Editors

António Alberto S. Correia
University of Coimbra, Portugal

Cristiana Ferreira
University of Porto, Portugal

Fernando Feitosa Monteiro
Unichristus, Brazil

Gilson de F. N. Gitirana Jr.
Federal University of Goiás, Brazil

José A. Schiavon
Aeronautics Institute of Technology, Brazil

Leandro Neves Duarte
Federal University of São João del-Rei, Brazil

Luciano Soares da Cunha
University of Brasília, Brazil

Marcio Leão
Federal University of Viçosa / IBMEC-BH, Brazil

Margarida Pinho Lopes
University of Aveiro, Portugal

Neusa M. B. Mota
University Center of Brasília, Brazil

Nuno Cristelo
University of Trás-os-Montes and Alto Douro, Portugal

Paulo J. R. Albuquerque
Campinas State University, Brazil

Rui Carrilho Gomes
Technical University of Lisbon, Portugal

Ricardo Pontes Resende
University Institute of Lisbon, Portugal

Rui Carrilho Gomes
Technical University of Lisbon, Portugal

Sara Rios
University of Porto, Portugal

Silvrano Adonias Dantas Neto
Federal University of Ceará, Brazil

Teresa M. Bodas Freitas
Technical University of Lisbon, Portugal

Advisory Panel

Alejo O. Sfriso
University of Buenos Aires, Argentina

Harry Poulos
University of Sidney, Australia

Luis A. Vallejo
Complutense University of Madrid, Spain

Emanuel Maranha das Neves
Technical University of Lisbon, Portugal

Michele Jamiolkowski
Studio Geotecnico Italiano, Italy

Roger Frank
École des Ponts ParisTech, France

Willy Lacerda
Federal University of Rio de Janeiro, Brazil

Editorial Board

Abdelmalek Bouazza
Monash University, Australia

Alessandro Mandolini
University of Naples Federico II, Italy

Alessio Ferrari
École Polytechnique Fédérale de Lausanne, Switzerland

Antônio Roque
National Laboratory for Civil Engineering, Portugal

Antônio Viana da Fonseca
University of Porto, Portugal

Armando Antão
NOVA University Lisbon, Portugal

Beatrice Baudet
University College of London, UK

Catherine O'Sullivan
Imperial College London, UK

Cristhian Mendoza
National University of Colombia, Colombia

Cristina Tsuha
University of São Paulo at São Carlos, Brazil

Daniel Dias
Antea Group / Grenoble-Alpes University, France

Debasis Roy
Indian Institute of Technology Kharagpur, India

Denis Kalumba
Cape Town University, South Africa

Fangwei Yu
Inst. Mt. Haz. Env. Chinese Acad. of Sci. China

Ian Schumann M. Martins
Federal University of Rio de Janeiro, Brazil

Jean Rodrigo Garcia
Federal University of Uberlândia, Brazil

José Muralha
National Laboratory for Civil Engineering, Portugal

Kátia Vanessa Bicalho
Federal University of Espirito Santo, Brazil

Krishna R. Reddy
University of Illinois at Chicago, USA

Limin Zhang
The Hong Kong Univ. of Science Technology, China

Márcio de Souza Soares de Almeida
Federal University of Rio de Janeiro, Brazil

Marcelo Javier Sanchez Castilla
Texas A&M University College Station, USA

Marco Barla
Politecnico di Torino, Italy

Marcos Arroyo
Polytechnic University of Catalonia, Spain

Marcos Massao Futai
University of São Paulo, Brazil

Maria de Lurdes Lopes
University of Porto, Portugal

Maurício Martines Sales
Federal University of Goiás, Brazil

Nilo Cesar Consoli
Federal University of Rio Grande do Sul, Brazil

Olavo Francisco dos Santos Júnior
Federal University of Rio Grande do Norte, Brazil

Orianne Jenck
Grenoble-Alpes University, France

Paulo Venda Oliveira
University of Coimbra, Portugal

Pijush Samui
National Institute of Technology Patna, India

Rafaela Cardoso
Technical University of Lisbon, Portugal

Roberto Quental Coutinho
Federal University of Pernambuco, Brazil

Sai K. Vanapalli
University of Ottawa, Canada

Samir Maghous
Federal University of Rio Grande do Sul, Brazil

Satoshi Nishimura
Hokkaido University, Japan

Siang Huat Goh
National University of Singapore, Singapore

Tácio Mauro Campos
Pontifical Catholic University of Rio de Janeiro, Brazil

Tiago Miranda
University of Minho, Portugal

Zhen-Yu Yin
Hong Kong Polytechnic University, China

Zhongxuan Yang
Zhejiang University, China

Honorary Members

André Pacheco de Assis
Clovis Ribeiro de M. Leme (in memoriam)
Delfino L. G. Gambetti
Eduardo Soares de Macedo
Ennio Marques Palmeira
Eraldo Luporini Pastore
Francisco de Rezende Lopes
Francisco Nogueira de Jorge
Jaime de Oliveira Campos
João Augusto M. Pimenta

José Carlos A. Cintra
José Carlos Virgili
José Couto Marques
José Jorge Nader
José Maria de Camargo Barros
Manuel Matos Fernandes
Maurício Abramento
Maurício Erlich
Newton Moreira de Souza
Orencio Monje Villar

Osni José Pejón
Paulo Eduardo Lima de Santa Maria
Paulo Scarano Hemi
Ricardo Oliveira
Ronaldo Rocha
Rui Taiji Mori (in memoriam)
Susumu Niyama
Vera Cristina Rocha da Silva
Waldemar Coelho Hachich
Willy Lacerda

Soils and Rocks reviewers in 2021

Soils and Rocks is grateful for the diligent contributions of anonymous referees who provided their manuscript assessments in 2021.

Abbas Al-Taie	Fernando Saboya Albuquerque Junior	Matheus Praciano Sampaio
Ahmad Rajabian	Francisco Rezende Lopes	Matheus Viana de Souza
Alessio Ferrari	Gilson de F. N. Gitirana Jr.	Mauricio Abramento
Alex Sy	Giovani Jordi Bruschi	Md. Abu Taiyab
Alfran Sampaio Moura	Gisleiva Cristina dos Santos Ferreira	Michael Jefferies
Amirhossein Hashemi	Gregório Luis Silva Araujo Araújo	Michele Dal Toé Casagrande
Ana Elisa Silva de Abreu	Hamed Sadeghi	Miguel Alfaro Soto
Ana Patricia Bandeira	Heitor Cardoso Bernardes	Muhammad Safdar
Anderson Borghetti Soares	Heraldo Luiz Giacheti	Naloan Coutinho Sampa
Andre Luis Brasil Cavalcante	Hossein Bahmyari	Nilo Cesar Consoli
André Pacheco de Assis	Ignacio Escuder Bueno	Nuno Raposo
André Vinicius Azevedo Borgatto	Ingrid Milena Reyes Martinez Belchior	Olavo Santos
Andy Fourie	Isabel Gonçalves Falorca	Orêncio M. Vilar
Anna Chiaradonna	John S. McCartney	Pablo Trejo
Anna Silvia Palcheco Peixoto	Jair de Jesús Baldovino Arrieta	Paulo Coelho
Antônio Viana da Fonseca	Jamie Standing	Paulo Cesar Lodi
Armando Nunes Antão	Jean Rodrigo Garcia	Paulo Venda Oliveira
Asaad Alomari	João Marcelino	Raimundo Leidimar Bezerra
Bahadir Ok	João Marcos Miranda Vaillant	Renato Santos Paulinelli Raposo
Beatrice Baudet	Joel Oliveira	Ricardo Bergan Born
Bendadi Hanumantha Rao	José Leitão Borges	Rodrigo Palma
Bernadete Ragoni Danziger	José Maria de Camargo Barros	Roger Augusto Rodrigues
Bosco Intriago Álvarez	Juan Felix Rodríguez Rebolledo	Sai K. Vanapalli
Breno Padovezi Rocha	Karla Maria Wingler Rebelo	Samuel França Amorim
Bruno Guimarães Delgado	Katia Vanessa Bicalho	Sandra Oda
Bruno Teixeira Lima	Kostas Senetakis	Sandra Houston
Camila Woldam Clemente	Larissa de Brum Passini	Sandro Lemos Machado
Carlos Emmanuel Ribeiro Lautenschläger	Lazaro Valentim Zuquette	Satoshi Nishimura
Cassio Eduardo Lima de Paiva	Lucas Festugato	Sayed Mohammad Alipoori
Cecília Vale	Lucia Mele	Sergio Tibana
Cristhian Mendoza	Luciana Barbosa Amancio	Sérgio Filipe Veloso Marques
Cristina de Hollanda Cavalcanti Tsuha	Lucio Vilar	Sérgio Paraíso
Duong Nguyen	Luis Altarejos-García	Silvio Romero de Melo Ferreira
Eda Freitas Quadros	Luis Araújo Santos	Tácio Mauro Pereira de Campos
Eder Carlos Guedes dos Santos	Luiz Guilherme de Mello	Talita Caroline Miranda
Edgar Rodriguez Rincon	Luiz Russo Neto	Thomas Pabst
Eduardo Dell'Avanzi	Márcia Maria dos Anjos Mascarenha	Tiago Miranda
Efrain Ovando Shelley	Marcio Fernandes Leão	Vitor Nascimento Aguiar
Eugenio Pabst Vieira da Cunha	Maria das Graças Gardoni Almeida	Washington Peres Núñez
Eurípedes do A. Vargas Jr.	Maria Esther Soares Marques	Xiong Zhang
Fabrizio Panico	Maria Lurdes Lopes	Yuri Barbosa
Felipe de Campos Loch	Mariana Vela Silveira	Zhong Han
Fernando A. M. Marinho	Marta Luz	

Soils and Rocks publishes papers in English in the broad fields of Geotechnical Engineering, Engineering Geology, and Geoenvironmental Engineering. The Journal is published quarterly in March, June, September and December. The first issue was released in 1978, under the name *Solos e Rochas*, being originally published by the Graduate School of Engineering of the Federal University of Rio de Janeiro. In 1980, the Brazilian Association for Soil Mechanics and Geotechnical Engineering took over the editorial and publishing responsibilities of *Solos e Rochas*, increasing its reach. In 2007, the journal was renamed Soils and Rocks and acquired the status of an international journal, being published jointly by the Brazilian Association for Soil Mechanics and Geotechnical Engineering, by the Portuguese Geotechnical Society, and until 2010 by the Brazilian Association for Engineering Geology and the Environment.

Soils and Rocks

1978,	1 (1, 2)
1979,	1 (3), 2 (1,2)
1980-1983,	3-6 (1, 2, 3)
1984,	7 (single number)
1985-1987,	8-10 (1, 2, 3)
1988-1990,	11-13 (single number)
1991-1992,	14-15 (1, 2)
1993,	16 (1, 2, 3, 4)
1994-2010,	17-33 (1, 2, 3)
2011,	34 (1, 2, 3, 4)
2012-2019,	35-42 (1, 2, 3)
2020,	43 (1, 2, 3, 4)
2021,	44 (1, 2, 3, 4)
2022,	45 (1,

ISSN 1980-9743
ISSN-e 2675-5475

CDU 624.131.1

Soils and Rocks

An International Journal of Geotechnical and Geoenvironmental Engineering
ISSN 1980-9743 ISSN-e 2675-5475

Publication of

ABMS - Brazilian Association for Soil Mechanics and Geotechnical Engineering
SPG - Portuguese Geotechnical Society
Volume 45, N. 1, January-March 2022

Special Issue
Thermal Applications in Geotechnical Engineering

Guest Editors

Fernando Saboya
Universidade Estadual do Norte Fluminense Darcy Ribeiro, Brazil
John S. McCartney
University of California San Diego, USA

Table of Contents

EDITORIAL

Introduction to the Special Issue of Soils and Rocks entitled: "Thermal Applications in Geotechnical Engineering"

Fernando Saboya Albuquerque Junior, John S. McCartney

ARTICLES

Thermo-energy performance of neighbouring energy piles

Hassam Ayaz, Mohammed Faizal, Abdelmalek Bouazza

Thermal performance assessment of an energy lining for the Lyon-Turin base tunnel

Maria Romana Alvi, Alessandra Insana, Marco Barla

Site characterization for a study on shallow geothermal energy exploitation in Southern Brazil

Bianca Penteado de Almeida Tonus, Carlos Emmanuel Ribeiro Lautenschläger, Amanda Fetzer Visintin, Vitor Pereira Faro, Cristina de Hollanda Cavalcanti Tsuha

Centrifuge modeling of temperature effects on the pullout capacity of torpedo piles in soft clay

Ismaail Ghaoowd, John S. McCartney, Fernando Saboya

Physical modeling of thermal improvement in normally consolidated and overconsolidated soil

João Alberto Machado Leite, Sérgio Tibana

Numerical study on heat transfer performance of geothermal piles in a Brazilian sandy soil

Caique Roberto de Almeida, Cyro Albuquerque Neto, Cristina de Hollanda Cavalcanti Tsuha, Maria Eugenia Gimenez Boscov

Laboratory experimental and numerical thermal response tests in thermal piles prototypes in tropical soil

Charles Pereira Chaves, Juan Deyvson José Camilo da Silva, Renato Pinto da Cunha, André Luis Brasil Cavalcante

Experimental analysis of improved bearing capacity in offshore foundations due to thermal consolidation

Marina de Souza Ferreira, Fernando Saboya Albuquerque Junior, Sérgio Tibana, Ricardo Garske Borges

CASE STUDY

Thermal design of energy piles for a hotel building in subtropical climate: a case study in São Paulo, Brazil

Letícia Menezes Santos Sá, Alberto Hernandez Neto, Cristina de Hollanda Cavalcanti Tsuha, Juliana Pessin, Milena Cardoso de Freitas, Thaise da Silva Oliveira Moraes

REVIEW ARTICLES

Thermo-hydro-mechanical behaviour of partially saturated fine-grained soils in the context of energy geostructures

Amirhossein Hashemi, Melis Sutman

Site characterization for the design of thermoactive geostructures

Ana Vieira, Maria Alberdi-Pagola, Marco Barla, Paul Christodoulides, Georgios Florides, Alessandra Insana, Saqib Javed, João Maranhã, Dejan Milenic, Iulia Prodan, Diana Salciarini

EDITORIAL

Soils and Rocks
v. 45, n. 1

Introduction to the Special Issue of Soils and Rocks entitled: “Thermal Applications in Geotechnical Engineering”

Fernando Saboya Albuquerque Junior^{1#} , John S. McCartney^{2#} 

EDITORIAL

This special issue of Soils and Rocks includes 8 state-of-the-art research studies, a case history, and 2 review papers on the behavior of energy geostructures and the thermo-hydro-mechanical behavior of soils. Energy geostructures are an emerging technology, which permit geotechnical engineering structures to be used as geothermal heat exchangers as well as structural support. This dual use not only permits cost-effective use of materials but also helps expand the portfolio of renewable energy technologies. Many types of energy geostructures are evaluated in this special issue, from conventional cast-in place energy piles, to energy tunnel linings, to steel offshore energy piles. Implementation of energy geostructures in countries like Brazil poses unique challenges due to the regional geological setting and the cooling dominated climate, which require careful site characterization, in-situ thermal assessment, and design considering thermo-mechanical effects. New infrastructure development in Brazil including retrofitting existing cooling systems for buildings and offshore oil exploration provides opportunities to develop new types of energy geostructures. It is critical to combine the development of energy geostructures with research on the thermo-hydro-mechanical behavior of soils, as recent research indicates that heat transfer can have potentially beneficial effects on soil-structure interaction in cooling dominated climates. Overall, this collection of papers from both Brazilian and international researchers provides an excellent contribution to the area of energy geotechnics that will hopefully form the basis of additional research studies in the future. The guest editors of this special issue would like to gratefully acknowledge the efforts of all the authors and peer reviewers of these papers, and the dedication of the Soils and Rocks publication staff in producing this special issue.

Guest Editors

[#]Corresponding author. E-mail address: saboya@uenf.br; mccartney@ucsd.edu

¹Universidade Estadual do Norte Fluminense Darcy Ribeiro, Department of Civil Engineering, Campos do Goytacazes, RJ, Brasil.

²University of California San Diego, Department of Structural Engineering, La Jolla, USA.






This is an Open Access article distributed under the terms of the Creative Commons Attribution License, which permits unrestricted use, distribution, and reproduction in any medium, provided the original work is properly cited.

ARTICLES

Soils and Rocks
v. 45, n. 1

Thermo-energy performance of neighbouring energy piles

Hassam Ayaz¹ , Mohammed Faizal¹ , Abdelmalek Bouazza^{1#} 

Article

Keywords

Energy piles
Operating modes
Thermal interaction
Energy

Abstract

Energy piles are often closely spaced such that the thermal response of one pile might affect the response of neighbouring piles through heat transfer in the soil. This paper examines the changes in extracted energy and ground temperature of two cast-in-place bored energy piles installed below a six-storey building, with a diameter of 0.6 m, length of 10 m and 3.5 m centre-to-centre distance. Field experiments were conducted on singular and dual piles for cooling and cyclic temperatures, continuous daily operation of the ground source heat pump (GSHP) and intermittent cyclic operations with stoppage-to-operating ratios of 2:1 and 1:2. Compared to single pile operations, greater energy was extracted from dual piles for all operating modes despite thermal interaction through the soil volume between the dual piles. The larger stoppage-to-operating ratio of the GSHP induced lower pile and ground temperature changes and higher energy extraction than continuous operation for single and dual pile operations. The larger stoppage-to-operating ratio of the GSHP reduced the thermal interaction between the dual piles by imposing lower ground temperature changes compared to continuous operation. The results demonstrate the practical significance of managing the GSHPs operating modes for optimal thermal performance of multiple closely spaced energy piles.

1. Introduction

Improving energy performances of buildings is critical in the efforts to transit to a low carbon future. A significant portion of building energy is taken up by indoor heating/cooling. For new buildings that require foundation piles for structural support, ground source heat pumps (GSHP) are increasingly used for indoor heating/cooling by utilizing on-site shallow geothermal energy by converting the piles to underground heat exchangers, known as energy piles. Multiple piles are constructed as energy piles in a building footprint, depending on the heating/cooling requirements of the structure. The neighbouring energy piles would be expected to interact thermally due to the presence of multiple heat sources in the soil, which will enhance heat transfer in the soil, and could affect the thermal performance of the piles. The thermo-energy performance of neighbouring energy piles has received little attention under field conditions and currently remains largely hypothetical.

Current literature on the energy and ground temperature variations at a field scale is mostly related to isolated energy piles behaviour under monotonic temperatures (e.g. Li et al., 2006; Gao et al., 2008; Bourne-Webb et al., 2009; Jalaluddin et al., 2011; Singh et al., 2015; Wang et al., 2015; Faizal et al., 2016; Chen et al., 2017; Faizal & Bouazza, 2018; Guo et al., 2018) and daily cyclic temperatures from intermittent operations of the GSHP (You et al., 2014;

Park et al., 2015, 2019; Faizal et al., 2016; Faizal & Bouazza, 2018). The above studies showed that cyclic temperature operations of isolated energy piles impose lower ground temperature changes and higher geothermal energy extraction/rejection than the monotonic temperature operation of the piles. Furthermore, these field studies led to the hypothesis that cyclic temperature operations of multiple energy piles would improve the geothermal energy utilization of the piles and reduce the ground temperature changes between the piles, hence decreasing the thermal interaction between neighbouring piles. Further field tests on the influence of temperature cycles are required to validate this hypothesis.

Even though several field studies have been conducted on the thermo-mechanical behaviour of energy piles in groups (Wood et al., 2009; You et al., 2014; Jeong et al., 2014; Mimouni & Laloui, 2015; Murphy et al., 2015; Rotta Loria & Laloui, 2017; You et al., 2018; Kong et al., 2019; Fang et al., 2020; Moradshahi et al., 2021a, b), these studies did not provide comprehensive insights into the energy, ground temperature responses and thermal interaction between neighbouring energy piles under temperature cycles. The energy utilization of multiple energy piles would be expected to be larger than isolated energy piles due to the increased surface area for heat transfer between the piles and the soil, as has been shown in field studies based on monotonic temperatures of energy piles by You et al. (2014). However, the assumption of obtaining higher geothermal energy with a higher number of energy

[#]Corresponding author. E-mail address: malek.bouazza@monash.edu

¹Monash University, Department of Civil Engineering, Vic., Australia.

Submitted on October 29, 2021; Final Acceptance on December 22, 2021; Discussion open until May 31, 2022.

<https://doi.org/10.28927/SR.2022.076521>



This is an Open Access article distributed under the terms of the Creative Commons Attribution License, which permits unrestricted use, distribution, and reproduction in any medium, provided the original work is properly cited.

piles cannot be put into practice without understanding the ground temperature variations due to thermal interaction between the piles. Also, extrapolating the energy obtained from isolated energy pile field tests to represent multiple energy piles could be inaccurate due to the lack of understanding of thermal interaction between neighbouring piles through the soil. Greater ground temperature changes and increased thermal interaction between the piles due to multiple heat sources in the soil may reduce the geothermal energy utilization and degrade the performance of the GSHP. Therefore, field investigations on neighbouring energy piles are critical to understand the piles' energy and ground thermal responses.

This paper explores the influence of temperature cycles on the energy and ground temperature changes between two neighbouring cast-in-place bored energy piles installed under a six-storey residential building. Field investigations were conducted for singular and dual pile operations.

2. Field setup and experiments

The experiments were conducted on two energy piles installed below a six-storey student residential building at Monash University, Melbourne, Australia. The building is founded on the Brighton Group of materials consisting of mostly dense sand (Barry-Macaulay et al., 2013; Singh et al., 2015). A summary of the site's ground conditions is given in Table 1. The soil is inferred to be unsaturated since no groundwater was encountered up to the piles' drill depth during installation. The piles had a diameter of 0.6 m and length of 10 m and were spaced at a centre-to-centre distance of 3.5 m. A schematic of the field setup is shown in Figure 1. Four high-density polyethylene (HDPE) pipe U-loops were installed in each pile with an inner diameter of 20 mm and an outer diameter of 25 mm.

The ground temperatures were monitored using Type T thermocouples installed at depths of 1 m, 3.05 m, 5 m, 7.28 m, 9.5 m and 12 m in two boreholes, BH1 and BH2, located at 0.63 m and 1.95 m radial distances, respectively, from the edge of pile 1 (referred to herein as EP1). The inlet and outlet water temperatures were monitored using Type T thermocouples installed in the plumbing manifold. A WaterFurnace commercial 2-5 kW Envision GSHP was used to circulate water in the piles. Pico Technology's USB-TC08 data loggers recorded temperatures from the

thermocouples. The water flowrates were recorded using Flomec TM series digital water flowmeters. The pile temperatures were obtained from Geokon 4200 vibrating wire strain gauges installed at five depths in EP1 using Campbell Scientific CR1000 data loggers. A detailed description of the instrumentation and installation of the energy piles is given in Faizal et al. (2019a, b).

A total of five experiments were conducted, two on a single energy pile (EP1) and three on the dual piles operating together and connected in series (EP1 + EP2). The five tests were as follows: (1) single pile cooled daily for 24 hours (referred to as 1P-24C), (2) single pile cooled daily for 8 hours with 16 hours of natural ground thermal recovery (referred to as 1P-8C16N), (3) dual piles cooled daily for 24 hours (referred to as 2P-24C), (4) dual piles cooled daily for 16 hours with 8 hours of natural ground thermal recovery (referred to as 2P-16C8N), and (5) dual piles cooled daily for 8 hours with 16 hours of natural ground thermal recovery (referred to as 2P-8C16N). The 8C16N and 16C8N operating modes represented the stoppage to operating time intermittent ratios of 2:1 and 1:2, respectively. The details of all experiments are summarised in Table 2. Water was used as the heat exchange fluid flowing in the HDPE pipes. The water flowrates were higher for the single pile experiments and were approximately 15 litres per minute (LPM); they were 11.5 LPM for the dual piles experiments. An evaluation of the temperatures of EP1, ground temperatures between the two piles and energy extracted for single and dual piles were conducted based on the experimental results obtained in the current investigation.

The inlet, outlet, and change in water temperatures between inlet and outlet for all the experiments are shown in Figure 2. Only 12 days of results are presented for all experiments for the sake of clarity on the comparative analysis. The water temperatures for the 24C mode are shown in Figures 2a-c. The lowest inlet water temperature was close to 0 °C for the single pile test (Figure 2a) and 5 °C for the dual piles test (Figure 2b). The fluctuation in inlet and outlet water temperatures on day 9 of the 1P-24C test was due to heat pump performance issues encountered on the day. The change in water temperature was approximately 2 °C for single pile and 3 °C for dual piles (Figure 2c). There were some limitations in controlling the inlet water temperatures in the 24C mode, which led to differences in the pile and ground temperatures (discussed later in the paper). The water temperatures for the 8C16N mode are shown in Figures 2d-f. During cooling, the inlet water temperatures were between 8 - 16 °C for the single pile (Figure 2d) and 8-14 °C for the dual piles (Figure 2e). The change in water temperatures was between 2-3 °C for the single pile and 3-4 °C for the dual piles (Figure 2f). The water temperatures for 16C8N mode are shown in Figures 2g-h. The only test for this mode was conducted on the dual piles, with an inlet temperature of 6-13 °C (Figure 2g) and a change in water temperature of 3-4 °C (Figure 2h).

Table 1. Summary of ground conditions (modified from Faizal et al. 2019a, b).

Depth (m)	Soil type	Soil description
0-0.4	Fill material	Crushed rock silt, sand, moist, medium dense
0.4-3.5	Sandy clay	Silt, sand (sand lenses) moist, stiff - very stiff
3.5-12.5	Sand	Sand, clay lenses, silt, cemented lenses, moist, dense

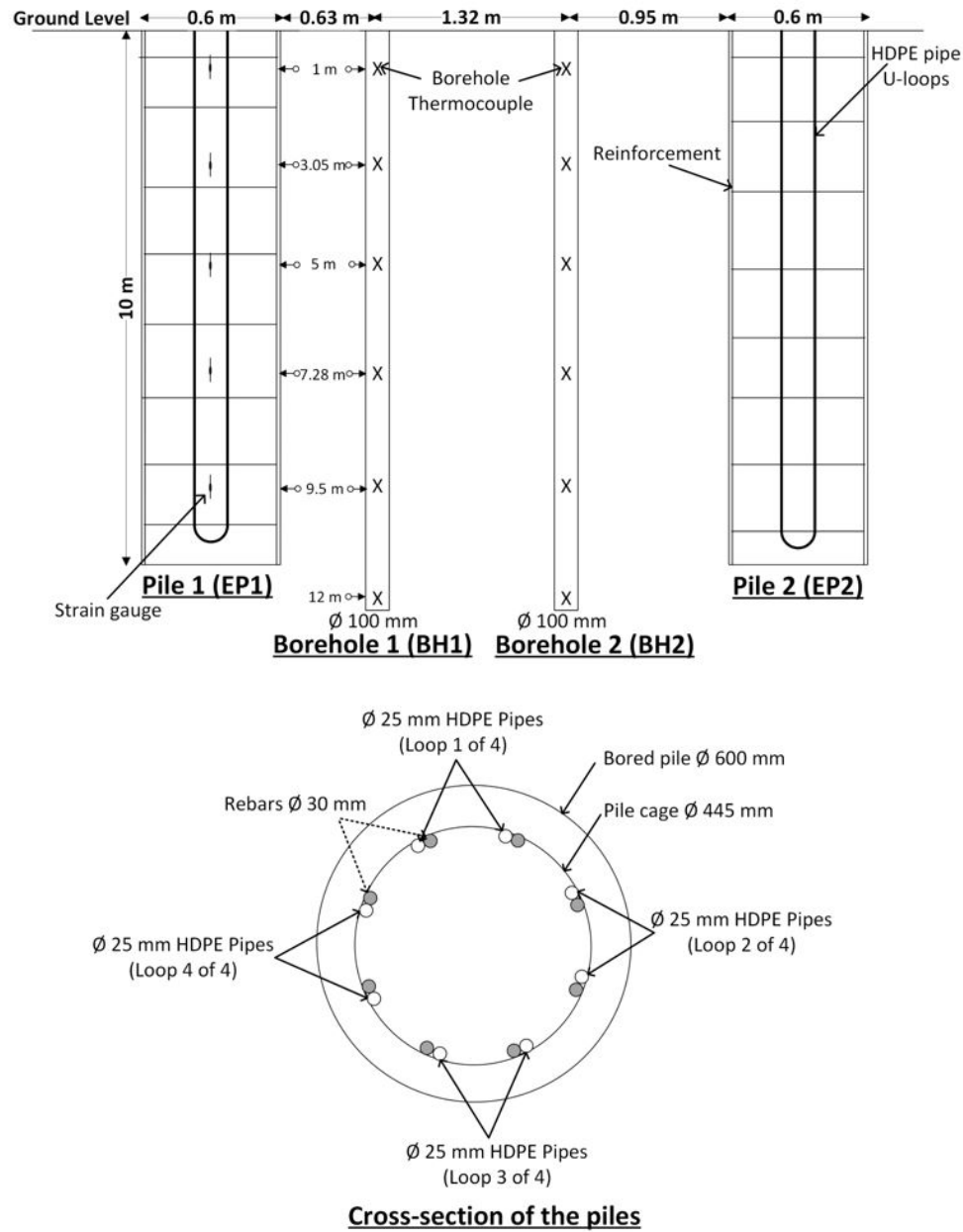


Figure 1. Schematics of the two energy piles installed under the six-storey residential building at Monash University, Australia (modified from Faizal et al., 2019a, b).

Table 2. Summary of experiments.

Operating mode	Description	Start date	End date
1) 1P-24C	Single energy pile cooled daily for 24 hours	2 September 2019	23 September 2019
2) 1P-8C16N	Single energy pile cooled daily for 8 hours with 16 hours of natural ground thermal recovery	12 April 2019	7 May 2019
3) 2P-24C	Dual-energy piles cooled daily for 24 hours	10 June 2019	24 June 2019
4) 2P-16C8N	Dual-energy piles cooled daily for 16 hours with 8 hours of natural ground thermal recovery	5 June 2020	19 June 2020
5) 2P-8C16N	Dual-energy piles cooled daily for 8 hours with 16 hours of natural ground thermal recovery	10 July 2020	24 July 2020

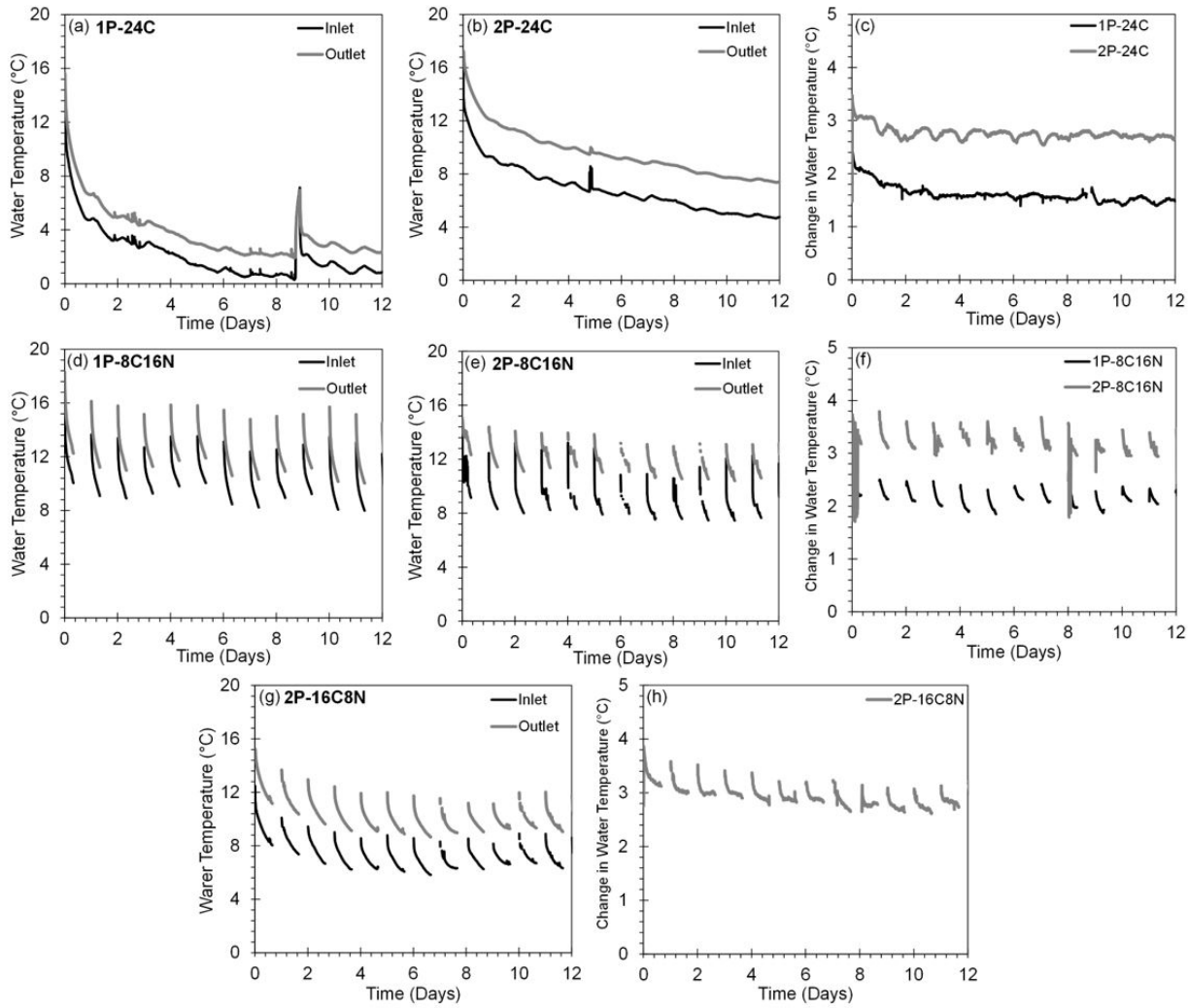


Figure 2. Water temperatures: (a) inlet and outlet (1P-24C); (b) inlet and outlet (2P-24C); (c) change in fluid temperature (24C); (d) inlet and outlet (1P-8C16N); (e) inlet and outlet (2P-8C16N); (f) change in fluid temperature (8C16N); (g) inlet and outlet (2P-16C8N); and (h) change in fluid temperature (16C8N).

3. Results and discussions

3.1 Pile temperatures

The change in temperatures of EP1 at a middle depth of 5 m for all experiments are shown in Figure 3 and Figure 4 (note that only EP1 was instrumented to obtain pile temperatures). The pile temperatures closely followed the trends of the inlet water temperatures shown in Figure 2. A comparison of the influence of different operating modes on the temperatures of EP1 for single and dual piles is shown in Figure 3. The temperature changes of EP1 in the 1P-24C and 1P-8C16N modes were approximately 14 °C and between 2-8 °C, respectively (Figure 3a). The fluctuation in pile temperature on Day 9 for the 1P-24C test was caused by water

temperature fluctuation due to heat pump performance issues. The maximum pile temperature reduction in the 1P-8C16N mode was approximately 43% lower than 1P-24C mode.

The temperature changes of EP1 in the 2P-24C, 2P-16C8N and 2P-8C16N modes were approximately 12 °C, between 1-7 °C, and between 2-6 °C, respectively (Figure 3b). The maximum temperatures reductions in the 2P-16C8N and 2P-8C16N modes were approximately 42% and 50% lower than the 2P-24C mode. The largest change in pile temperatures is in the 24C mode due to the continuous operation of the GSHP. The temperatures of EP1 remained closer to initial undisturbed conditions in the cyclic operating modes for both single and dual piles due to frequent ground temperature recoveries during non-operating times of the GSHP, particularly for the 8C16N mode with greater natural ground thermal recovery time. Cyclic operating modes of the

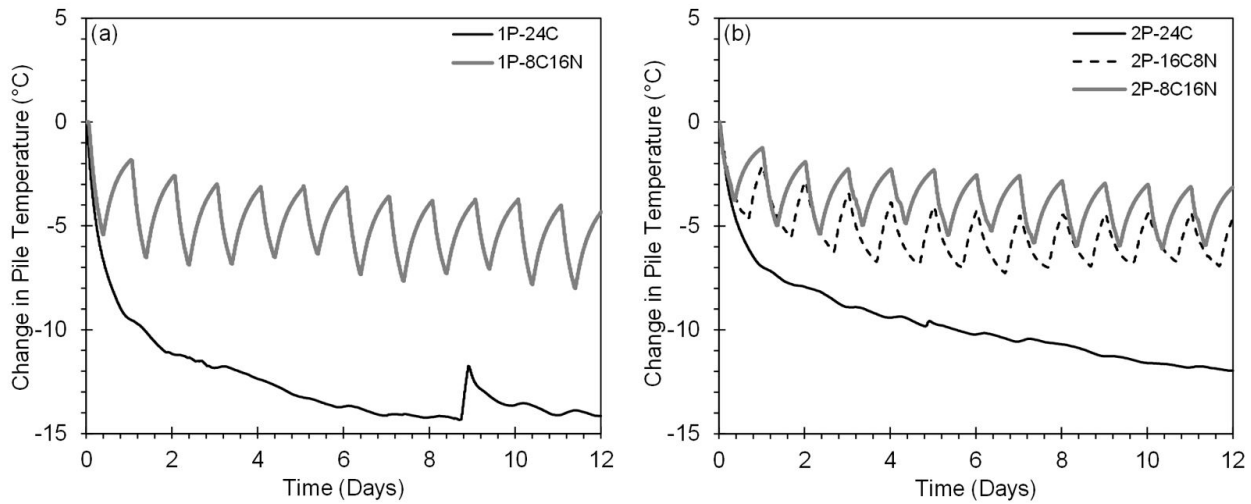


Figure 3. Comparison of change in pile temperatures of EP1 between different operation modes of the GSHP for: (a) single pile; and (b) dual piles.

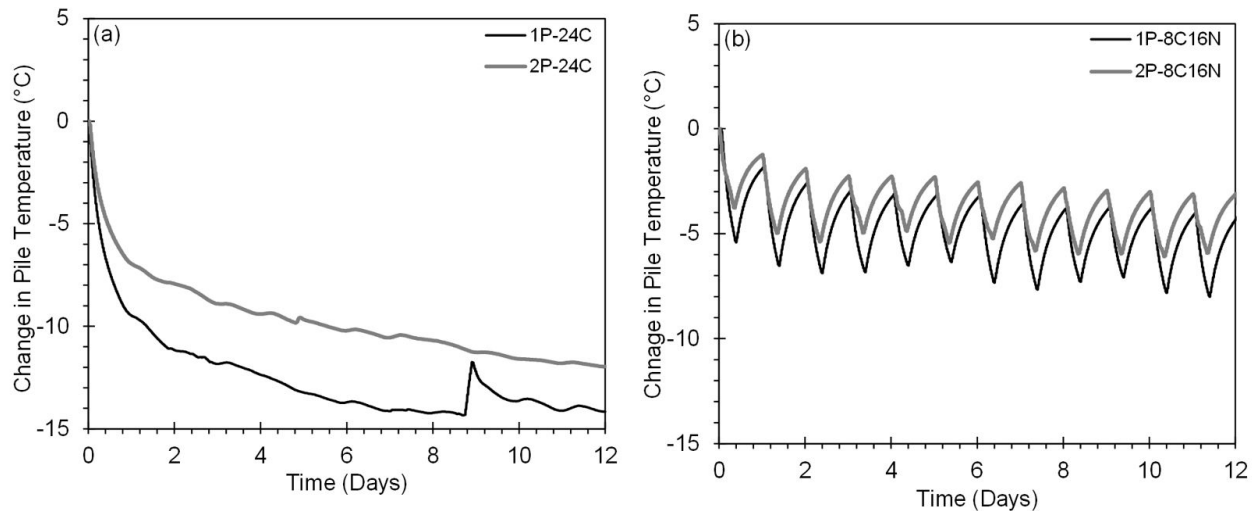


Figure 4. Comparison of change in pile temperatures of EP1 between single and dual piles experiments for: (a) 24C mode; and (b) 8C16N mode.

GSHP with greater stoppage to operating time intermittent ratios (2:1 in the present case) will therefore develop lower pile temperatures, and hence likely lower thermal stresses in the piles, for long term operations. Similar observations were also reported by Faizal et al. (2016) for a single field-scale energy pile.

A comparison of EP1 temperature changes for a single pile against dual piles experiments for a given operating mode is shown in Figure 4. Due to issues in controlling the inlet water temperatures in the 24C modes, the pile temperatures are different for single and dual piles experiments (Figure 4a). However, the pile temperatures are similar in the 8C16N modes (Figure 4b), indicating that the influence of operation

of the second pile (i.e. EP2) in dual piles experiments is not significant on the temperature variations of EP1, for the given pile spacing. The temperatures of EP1 would also have been similar for the 24C modes for single and dual piles experiments (Figure 4a) if the inlet water temperatures were similar (Figure 2a, b).

3.2 Ground temperatures

The change in ground temperatures in BH1 and BH2, with respect to the initial undisturbed conditions, at a depth of 5 m is shown in Figures 5 and 6 for all experiments. The radial distance, R , of BH1 is 0.63 m from the edge of

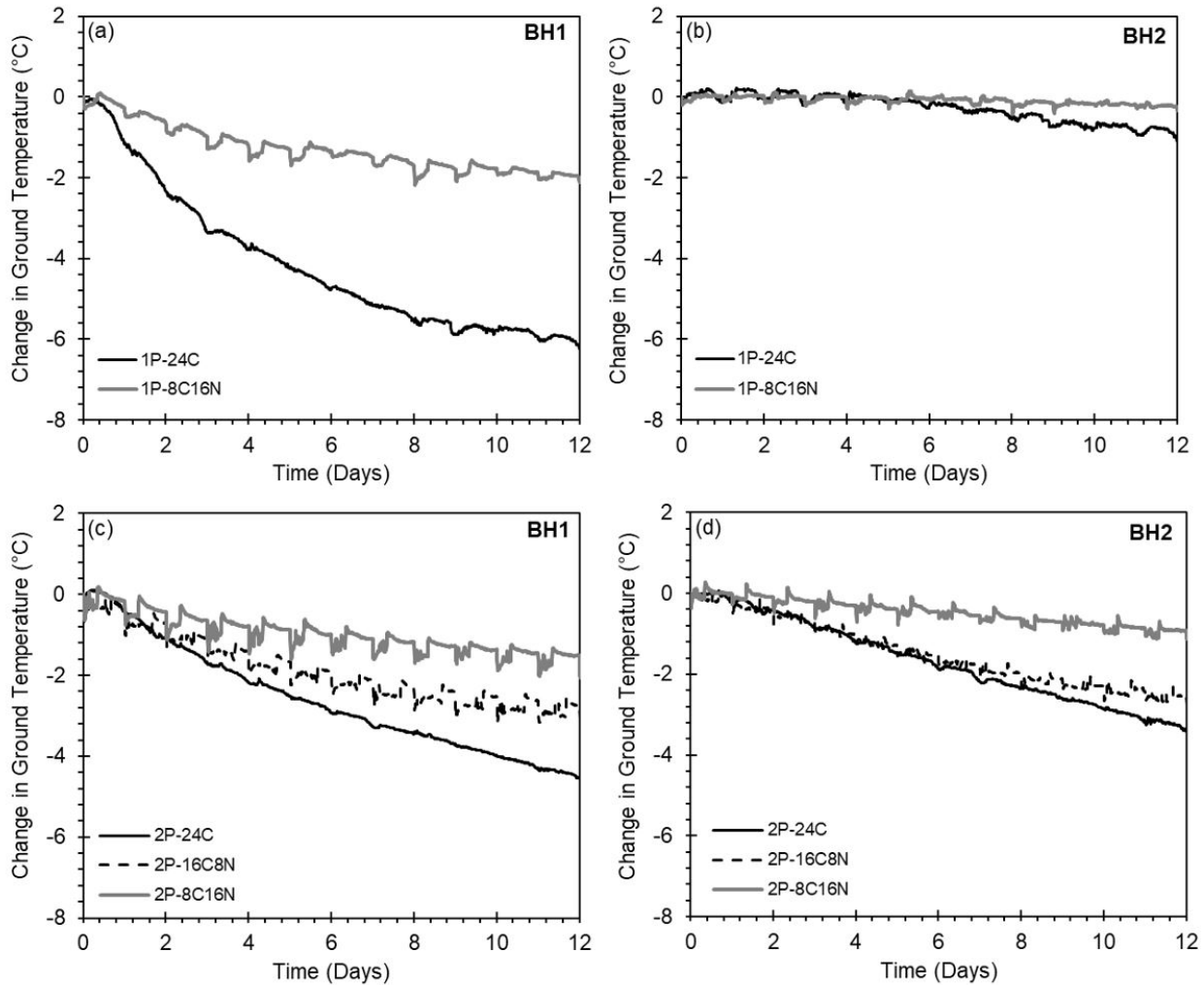


Figure 5. Comparison of change in ground temperatures between different operation modes of the GSHP for: (a) single pile at BH1; (b) single pile at BH2; (c) dual piles at BH1; and (d) dual piles at BH2.

EP1 and 2.27 m from the edge of EP2, whereas BH2 is at $R = 1.95$ m from the edge of EP1 and at $R = 0.95$ m from the edge of EP2 (Figure 1). The undisturbed ground temperature at the test site was between 17°C and 19°C .

A comparison of the influence of different operating modes on the ground temperature changes for single and dual piles is shown in Figures 5a, b and 5c, d, respectively. For the single pile 1P-24C and 1P-8C16N modes, the ground temperatures at BH1 (Figure 5a) decreased by 5.6°C and 2.1°C , respectively, and by 1°C and 0.3°C , respectively, at BH2 (Figure 5b). The 1P-8C16N mode had approximately 63% and 70% smaller temperature changes at BH1 and BH2, respectively, than the 1P-24C mode. A smaller change in ground temperatures in the 1P-8C16N mode is due to the presence of 16 hours of natural ground recovery time daily, which alleviates the ground temperature changes. The temperature changes at BH1 were greater than BH2 for the single pile operating modes as the thermal influence of energy piles

on the ground reduced in the radial direction. Field studies conducted on isolated energy piles have also shown that ground temperature changes are largest closest to the energy pile and diminish with increasing radial distance from the edge of the pile (Amis et al., 2008; Bourne-Webb et al., 2009; Chen et al., 2017; Faizal & Bouazza, 2018; Faizal et al., 2016; Guo et al., 2018; Murphy et al., 2015; Singh et al., 2015).

For the dual piles 2P-24C, 2P-16C8N and 2P-8C16N modes, the ground temperatures at BH1 (Figure 5c) decreased by 4.6°C , 2.7°C and 1.5°C , respectively, and by 3.4°C , 2.5°C and 0.9°C , respectively, at BH2 (Figure 5d). Compared to the 2P-24C mode, the 2P-16C8N and 2P-8C16N modes had approximately 41% and 67% smaller temperature changes at BH1, respectively, and about 26% and 74% smaller temperature change at BH2, respectively. Similar to the single pile test results shown in Figures 5a and 5b, the ground temperature changes were highest in the 24C mode. However, due to the presence of dual heat sources in

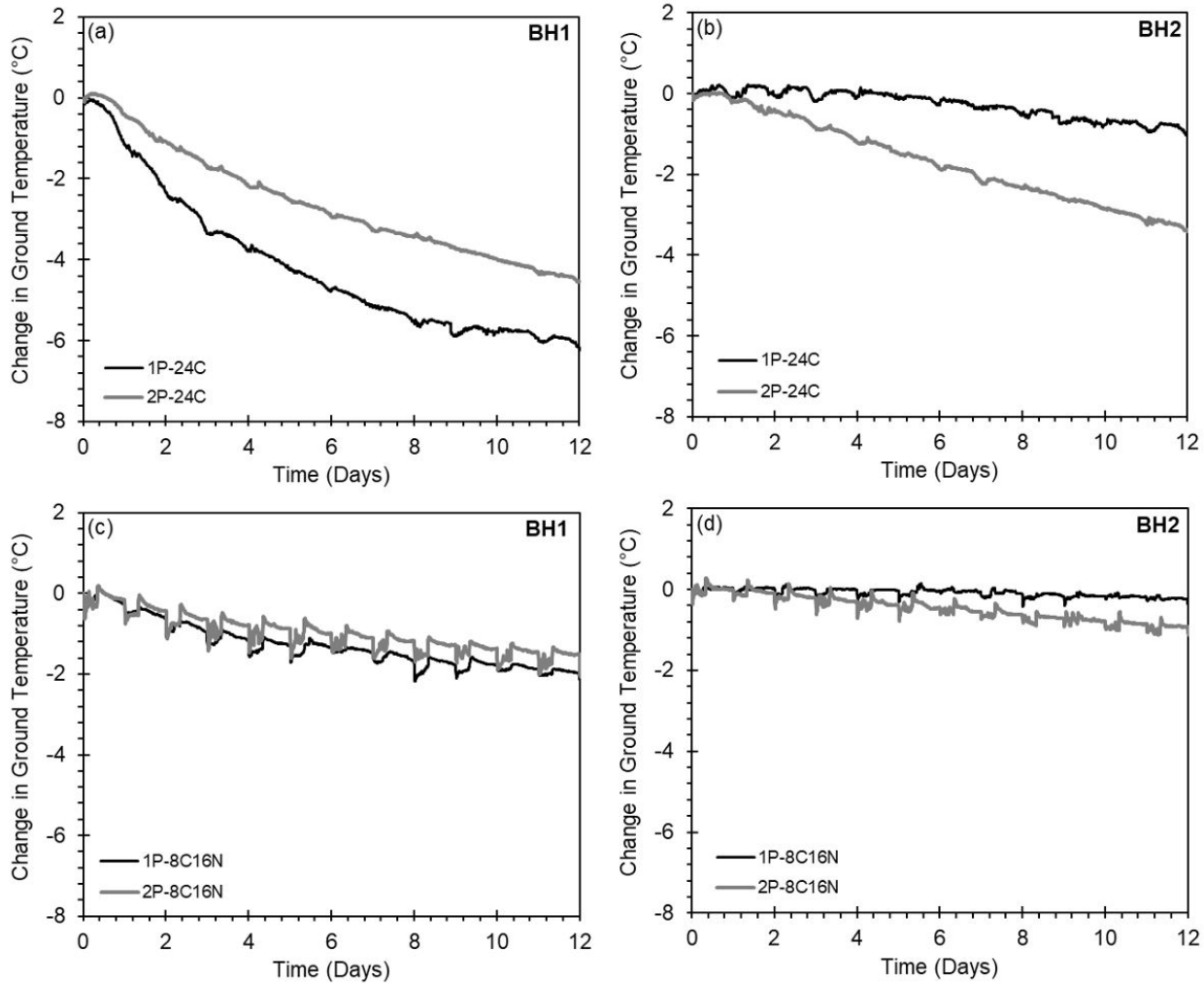


Figure 6. Comparison of change in ground temperatures between single and dual piles experiments for (a) 24C mode at BH1; (b) 24C mode at BH2; (c) 8C16N mode at BH1; and (d) 8C16N mode at BH2.

the ground, the ground temperature changes at BH2 were more significant in the dual piles experiments than that of single pile experiments, indicating the presence of thermal interaction between the two piles through the ground.

A comparison of ground temperature changes for a single pile against dual piles experiments for a given operating mode is shown in Figure 6. The ground temperatures for the 24C mode at BH1, shown in Figure 6a, are different due to the differences in the inlet water and EP1 temperatures, as discussed in relation to Figures 2-4. The ground temperatures for the 8C16N mode at BH1, shown in Figure 6c, are similar for both single and dual piles experiments, indicating a negligible influence of EP2 on ground temperatures at BH1 which is at $R = 2.27$ m from the edge of EP2 during dual piles experiments. The influence of the 1P-24C mode on the ground temperatures at BH2 is lower than that of the 2P-24C mode because BH2 is at $R = 1.95$ m from the edge of EP1 and at $R = 0.95$ m from the edge of EP2 (Figure 6b). Similarly, the 2P-8C16N mode

had a bigger influence on the ground temperatures at BH2 than the 1P-8C16N mode (Figure 6d).

The ground temperature results shown in Figures 5 and 6 indicate that thermal interaction exists between the piles during dual piles experiments due to increased ground temperature changes. The lower temperature changes at BH2 for dual piles experiments for the intermittent operating modes, particularly for higher recovery times in the 8C16N mode, compared to continuous operating mode indicates that intermittent operation of the GSHP will be beneficial in reducing the thermal interaction between multiple energy piles and hence improve the energy extracted/rejected by the piles for long-term operations.

3.3 Energy

The average daily energy extracted for all the experiments is shown in Figures 7 and 8. The energy extracted, \dot{Q} , was calculated as follows:

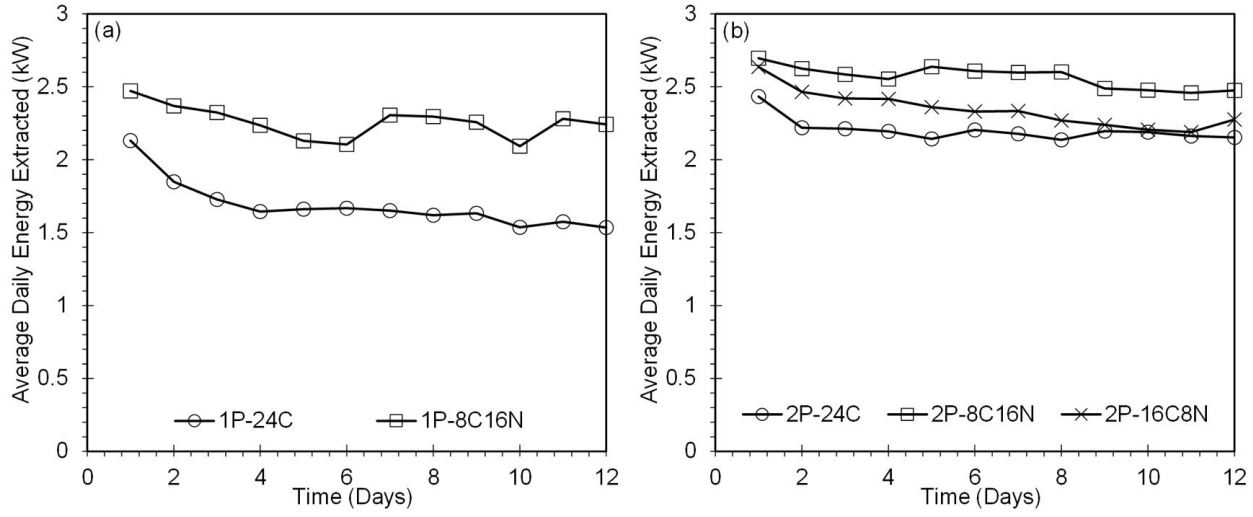


Figure 7. Comparison of average daily energy between different operation modes of the GSHP for: (a) single pile; and (b) dual piles.

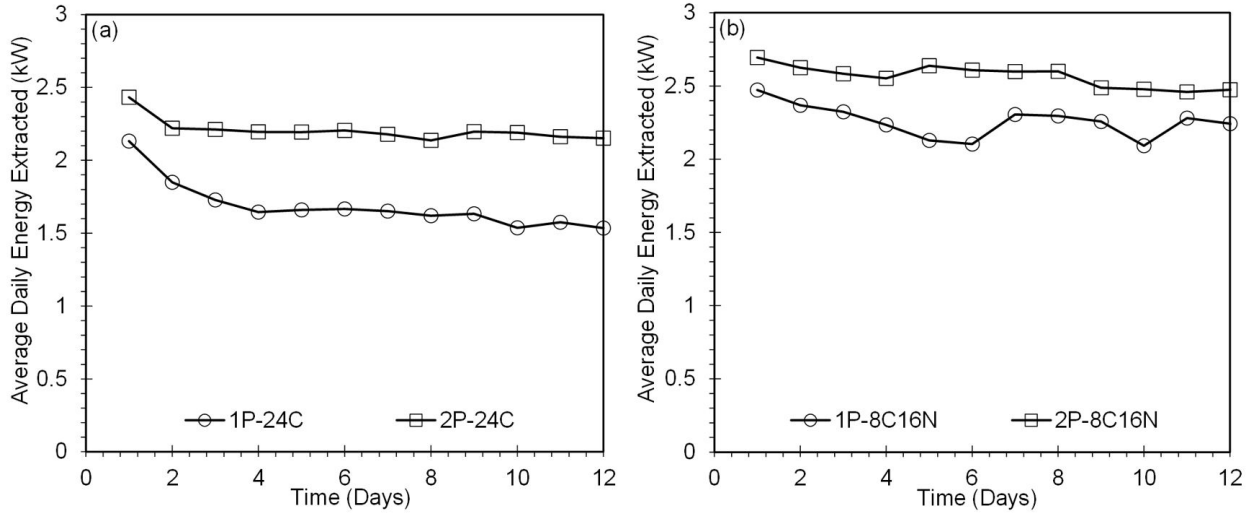


Figure 8. Comparison of average daily energy between single and dual piles experiments for (a) 24C mode; and (b) 8C16N.

$$\dot{Q} = \rho \dot{V} C_p (T_{outlet} - T_{inlet}) \quad (1)$$

where ρ is the density of the water, \dot{V} is the water flow rate, C_p is the specific heat capacity of the water, and T_{outlet} and T_{inlet} are the outlet and inlet water temperatures, respectively.

A comparison of the influence of different operating modes on the energy extracted for single and dual piles is shown in Figures 7a and 7b, respectively. The average energy extracted for single pile 1P-24C and 1P-8C16N modes, shown in Figure 7a, was 1.69 kW and 2.26 kW, respectively. The 1P-24C mode had a 25% lower average energy extracted than the 1P-8C16N mode. The average energy extracted for the 2P-24C, 2P-16C8N and the 2P-8C16N modes, shown in Figure 7b, was 2.21 kW, 2.35 kW and 2.57 kW, respectively. The 2P-24C

mode had 6% and 14% lower average energy extracted than the 2P-16C8N and 2P-8C16N modes, respectively, because of continuous reduction in pile and ground temperatures in the 24C mode, hence decreasing the energy efficiency of the system. The results shown in Figures 7a and 7b indicate that intermittent operating modes of the GSHP, particularly with higher ground thermal recovery times, lead to higher energy extracted than the continuous operation of the GSHP and would be beneficial for long-term operations of the pile. A higher energy extraction rate for intermittent operation of the GSHP compared to the continuous operation was also reported by Ren et al. (2020) for dual field micro-steel-pipe piles and by Faizal et al. (2016) and Faizal & Bouazza (2018) for a single field energy piles.

A comparison of the average daily energy extracted for single pile against dual piles experiments for a given operating mode is presented in Figures 8a and 8b. Compared to the single pile, the average energy extracted by dual piles was 31% greater for the 24C mode (Figure 8a) and 14% greater for the 8C16N mode (Figure 8b). The average energy extracted is larger during dual piles operation due to the greater length of the heat exchanger pipes, which increases the heat transfer between the water and the ground. These results indicate that a higher number of energy piles with the intermittent operation of the GSHP would provide higher thermal loads to the building with reduced thermal interaction between the piles. The reduction in thermal interaction between the piles during intermittent operation results in alleviation of ground temperature changes (as discussed for Figures 5 and 6), leading to an increased temperature difference between the pile and the ground, and hence increase in heat transfer and energy efficiency of the dual piles.

4. Conclusions

This paper investigated the impact of different operating modes of the GSHP on the energy extracted from the ground and temperature changes around single and closely spaced dual-energy piles and the effect of single and dual-energy piles operation on the energy and ground temperature responses. Monotonic and cyclic cooling experiments, resulting from continuous and intermittent operations of the GSHP, respectively, were conducted on the two piles spaced at a centre-to-centre distance of 3.5 m. The cyclic operation of the GSHP induced lower pile and ground temperature changes than continuous operation for both single and dual piles experiments. The ground temperature changes indicated thermal interaction took place between the piles during the dual pile operation. However, the cyclic operation of the GSHP was found to be beneficial in reducing the ground temperature changes and reducing the thermal interaction between the two energy piles when operated together. The intermittent operation of the GSHP, particularly with higher rest times of the GSHP, also showed larger geothermal energy extracted than the continuous operating modes for both single and dual piles experiments. The higher energy extracted during dual piles experiments indicated that a higher number of energy piles would provide higher thermal loads to the building despite the thermal interaction between the piles through the ground.

Acknowledgements

The first author was supported by a Monash University Graduate Scholarship. This support and support of all the sponsors (Geotechnical Engineering Pty Ltd, Golder Associates Pty Ltd., Geoexchange Australia Pty. Ltd and Brookfield-Multiplex) are gratefully acknowledged.

Declaration of interest

The authors have no conflicts of interests.

Authors' contributions

Hassam Ayaz: Conceptualization; Formal analysis; Investigation; Data Curation; Writing - Original Draft; Visualization. Mohammed Faizal: Conceptualization; Methodology; Writing - Review & Editing; Supervision. Abdelmalek Bouazza: Methodology; Resources; Writing - Review & Editing; Supervision; Project administration; Funding acquisition.

References

- Barry-Macaulay, D., Bouazza, A., Singh, R.M., Wang, B., & Ranjith, P.G. (2013). Thermal conductivity of soils and rocks from the Melbourne (Australia) region. *Engineering Geology*, 164, 131-138. <http://dx.doi.org/10.1016/j.enggeo.2013.06.014>.
- Bourne-Webb, P.J., Amatya, B., Soga, K., Amis, T., Davidson, C., & Payne, P. (2009). Energy pile test at Lambeth College, London: geotechnical and thermodynamic aspects of pile response to heat cycles. *Geotechnique*, 59(3), 237-248. <http://dx.doi.org/10.1680/geot.2009.59.3.237>.
- Chen, Y., Xu, J., Li, H., Chen, L., Ng, C., & Liu, H. (2017). Performance of a prestressed concrete pipe energy pile during heating and cooling. *Journal of Performance of Constructed Facilities*, 31(3), 06017001. [http://dx.doi.org/10.1061/\(ASCE\)CF.1943-5509.0000982](http://dx.doi.org/10.1061/(ASCE)CF.1943-5509.0000982).
- Faizal, M., & Bouazza, A. (2018). Energy utilisation and ground temperature distribution of a field scale energy pile under monotonic and cyclic temperature changes. *Proceedings of China-Europe Conference on Geotechnical Engineering*, 2, 1591-1594. http://dx.doi.org/10.1007/978-3-319-97115-5_151.
- Faizal, M., Bouazza, A., & Singh, R.M. (2016). An experimental investigation of the influence of intermittent and continuous operating modes on the thermal behaviour of a full-scale geothermal energy pile. *Geomechanics for Energy and the Environment*, 8, 8-29. <http://dx.doi.org/10.1016/j.gete.2016.08.001>.
- Faizal, M., Bouazza, A., McCartney, J.S., & Haberfield, C. (2019a). Axial and radial thermal responses of energy pile under six-storey residential building. *Canadian Geotechnical Journal*, 56(7), 1019-1033. <http://dx.doi.org/10.1139/cgj-2018-0246>.
- Faizal, M., Bouazza, A., McCartney, J.S., & Haberfield, C. (2019b). Effects of cyclic temperature variations on the thermal response of an energy pile under a residential building. *Journal of Geotechnical and Geoenvironmental Engineering*, 145(10), 04019066. [http://dx.doi.org/10.1061/\(ASCE\)GT.1943-5606.0002147](http://dx.doi.org/10.1061/(ASCE)GT.1943-5606.0002147).

- Fang, J., Kong, G., Meng, Y., Wang, L., & Yang, Q. (2020). Thermomechanical behavior of energy piles and interactions within energy pile-raft foundations. *Journal of Geotechnical and Geoenvironmental Engineering*, 146(9), 04020079. [http://dx.doi.org/10.1061/\(ASCE\)GT.1943-5606.0002333](http://dx.doi.org/10.1061/(ASCE)GT.1943-5606.0002333).
- Gao, J., Zhang, X., Liu, J., Li, K.S., & Yang, K. (2008). Thermal performance and ground temperature of vertical pile-foundation heat exchangers: A case study. *Applied Thermal Engineering*, 28(17-18), 2295-2304. <http://dx.doi.org/10.1016/j.applthermaleng.2008.01.013>.
- Guo, Y., Zhang, G., & Liu, S. (2018). Investigation on the thermal response of full-scale PHC energy pile and ground temperature distribution in multi-layer strata. *Applied Thermal Engineering*, 143, 836-848. <http://dx.doi.org/10.1016/j.applthermaleng.2018.08.005>.
- Jalaluddin, M., Miyara, A., Tsubaki, K., Inoue, S., & Yoshida, K. (2011). Experimental study of several types of ground heat exchanger using a steel pile foundation. *Renewable Energy*, 36(2), 764-771. <http://dx.doi.org/10.1016/j.renene.2010.08.011>.
- Jeong, S., Lim, H., Lee, J.K., & Kim, J. (2014). Thermally induced mechanical response of energy piles in axially loaded pile groups. *Applied Thermal Engineering*, 71(1), 608-615. <http://dx.doi.org/10.1016/j.applthermaleng.2014.07.007>.
- Kong, L., Qiao, L., Xiao, Y., & Li, Q. (2019). A study on heat transfer characteristics and pile group influence of enhanced heat transfer energy piles. *Journal of Building Engineering*, 24(Jul), 100768. <http://dx.doi.org/10.1016/j.jobte.2019.100768>.
- Li, X., Chen, Y., Chen, Z., & Zhao, J. (2006). Thermal performances of different types of underground heat exchangers. *Energy and Building*, 38(5), 543-547. <http://dx.doi.org/10.1016/j.enbuild.2005.09.002>.
- Mimouni, T., & Laloui, L. (2015). Behaviour of a group of energy piles. *Canadian Geotechnical Journal*, 52(12), 1913-1929. <http://dx.doi.org/10.1139/cgj-2014-0403>.
- Moradshahi, A., Faizal, M., Bouazza, A., & McCartney, J.S. (2021a). Effect of nearby piles and soil properties on the thermal behaviour of a field-scale energy pile. *Canadian Geotechnical Journal*, 58(9), 1351-1364. <http://dx.doi.org/10.1139/cgj-2020-0353>.
- Moradshahi, A., Faizal, M., Bouazza, A., & McCartney, J.S. (2021b). Cross-sectional thermo-mechanical responses of energy piles. *Computers and Geotechnics*, 138, 104320. <http://dx.doi.org/10.1016/j.compgeo.2021.104320>.
- Murphy, K.D., McCartney, J.S., & Henry, K.S. (2015). Evaluation of thermo-mechanical and thermal behavior of full-scale energy foundations. *Acta Geotechnica*, 10(2), 179-195. <http://dx.doi.org/10.1007/s11440-013-0298-4>.
- Park, S., Lee, S., Choi, H., Jung, K., & Choi, H. (2015). Relative constructability and thermal performance of cast-in-place concrete energy pile: coil-type GHEX (ground heat exchanger). *Energy*, 81, 56-66. <http://dx.doi.org/10.1016/j.energy.2014.08.012>.
- Park, S., Lee, S., Lee, D., Ahn, D., & Choi, H. (2019). Effect of thermal interference on energy piles considering various configurations of heat exchangers. *Energy and Building*, 199, 381-401. <http://dx.doi.org/10.1016/j.enbuild.2019.07.008>.
- Ren, L., Xu, J., Kong, G., & Liu, H. (2020). Field tests on thermal response characteristics of micro-steel-pipe pile under multiple temperature cycles. *Renewable Energy*, 147(1), 1098-1106. <http://dx.doi.org/10.1016/j.renene.2019.09.084>.
- Rotta Loria, A.F., & Laloui, L. (2017). Thermally induced group effects among energy piles. *Geotechnique*, 67(5), 374-393. <http://dx.doi.org/10.1680/jgeot.16.P.039>.
- Singh, R.M., Bouazza, A., & Wang, B. (2015). Near-field ground thermal response to heating of a geothermal energy pile: observations from a field test. *Soil and Foundation*, 55(6), 1412-1426. <http://dx.doi.org/10.1016/j.sandf.2015.10.007>.
- Wang, B., Bouazza, A., Singh, R.M., Haberfield, C., Barry-Macaulay, D., & Baycan, S. (2015). Posttemperature effects on shaft capacity of a full-scale geothermal energy pile. *Journal of Geotechnical and Geoenvironmental Engineering*, 141(4), 04014125. [http://dx.doi.org/10.1061/\(ASCE\)GT.1943-5606.0001266](http://dx.doi.org/10.1061/(ASCE)GT.1943-5606.0001266).
- Wood, C., Liu, H., & Riffat, S.B. (2009). Use of energy piles in a residential building, and effects on ground temperature and heat pump efficiency. *Geotechnique*, 59(3), 287-290. <http://dx.doi.org/10.1680/geot.2009.59.3.287>.
- You, S., Cheng, X., Guo, H., & Yao, Z. (2014). In-situ experimental study of heat exchange capacity of CFG pile geothermal exchangers. *Energy and Building*, 79, 23-31. <http://dx.doi.org/10.1016/j.enbuild.2014.04.021>.
- You, T., Li, X., Cao, S., & Yang, H. (2018). Soil thermal imbalance of ground source heat pump systems with spiral-coil energy pile groups under seepage conditions and various influential factors. *Energy Conversion and Management*, 178, 123-136. <http://dx.doi.org/10.1016/j.enconman.2018.10.027>.

Thermal performance assessment of an energy lining for the Lyon-Turin base tunnel

Maria Romana Alvi¹ , Alessandra Insana¹ , Marco Barla^{1#} 

Article

Keywords

Energy tunnel
Thermal performance
Geothermal energy
Sensitivity analysis
Numerical coupled analysis

Abstract

The use of geothermal energy for heating and cooling purposes is an environmentally-friendly and cost-effective alternative with the potential to replace fossil fuels and help to mitigate global warming as well. The paper illustrates the geothermal potential evaluation of a portion of the Lyon-Turin base tunnel considering the thermal activation of the tunnel concrete segmental lining. The international infrastructure will connect Italy to France, crossing the Alps and meeting uncommon climate conditions, reaching a peak temperature of 47 °C, due to its significant rock overburden (up to 2500 m) under the Ambin massif. A thermo-hydraulic numerical model was used to simulate the heat exchange of the system and quantify the power achievable by thermally activating a 10 km-long section of the base tunnel. Sensitivity analyses were performed to investigate the influence of the heat carrier fluid and the air flow velocities as well as the inlet temperature on the heat exchange. Moreover, four different operational conditions were compared to allow for assessing the overall thermal performance of the energy lining in terms of heat exploited and of the capacity of cooling the tunnel.

1. Introduction

Despite the importance of the heating and cooling sector, renewable energy technologies currently supply only a small percentage of global and European heat demand per year (Seyboth et al., 2008; European Union, 2012; IEA, 2012) with the vast majority of heat currently generated by burning fossil fuels. However, sustainable solutions relying both on decreasing the consumption of non-renewable energy and developing technologies that harvest non-polluting energy sources are possible. The IPCC Special Report on Renewable Energy Sources and Climate Change Mitigation (IPCC, 2012) predicted the annual global CO₂ savings from renewable energy technologies in four deployment scenarios for 2030 and 2050 and highlighted the good potential of geothermal energy in reducing the greenhouse gas (GHG) emissions.

Geothermal energy is a good alternative to fossil fuels and its usage is among the most innovative and significant, contributing to environmental protection and providing substantial energy, long term cost savings and minimized maintenance (Kanth & Chakraborty, 2015).

So-called energy geostructures are earth-contact structures that embed a piping circuit with a circulating heat carrier fluid to achieve a heat exchange between the ground and any building or infrastructure (Brandl, 2006; Adam & Markiewicz, 2009; Barla & Perino, 2015). They combine the role of the structural support with the role of the thermal energy carrier in a unique technology to serve all types of buildings and infrastructure.

During recent years, increasing considerations have been paid on how this heat transfer technology could be extended to tunnels. In comparison with other energy geostructures, energy tunnels are characterized by their much more extensive linear development so that a bigger surface is in contact with the ground and can be thermally activated. Concerning the overburden and presence of potential heat end-users, considerable differences exist between city tunnels (metro lines, railway city crossings) and mountain tunnels (for railways and highways). Regarding the former, energy tunnels can serve as a renewable energy source for heating and cooling networks on a city scale (Epting et al., 2020; Baralis et al., 2020). In this context, a recent feasibility study was indeed carried out to assess the energy potential of the

[#]Corresponding author. E-mail address: marco.barla@polito.it

¹Politecnico di Torino, Department of Structural, Building and Geotechnical Engineering, Turin, Italy.

Submitted on January 18, 2022; Final Acceptance on February 4, 2022; Discussion open until May 31, 2022.

<https://doi.org/10.28927/SR.2022.000722>



This is an Open Access article distributed under the terms of the Creative Commons Attribution License, which permits unrestricted use, distribution, and reproduction in any medium, provided the original work is properly cited.

thermal activation of the Turin Metro line 2 (Barla et al., 2021). With reference to deep mountain tunnels, some insights on possible applications were given by Tinti et al. (2017) and Barla & Di Donna (2018) with reference to the Mules Access Tunnel of the Brenner Base Tunnel (BBT) and the Lyon-Turin tunnel. Additionally, Baralis et al. (2021) investigated the thermal activation of a tunnel lining in an Alpine context in relation to an application for bridge deck deicing showing that it can provide enough heat to keep the paved surface unfrozen.

In the case of TBM tunnelling, the absorber pipes can be tied to the reinforcement cage during the concrete segment prefabrication as for the 'Energietübbing' (Franzius & Pralle, 2011) and the 'Enertun' (Barla & Di Donna, 2016; Barla et al., 2019; Insana & Barla, 2020) systems. In the 'Enertun' system, two configurations exist, 'Ground' which comprehends a circuit of pipes installed nearby the extrados of the lining (surface in contact with the ground) and 'Air' where the pipes are closer to the intrados (surface in contact with the tunnel air).

This paper describes a possible application of the 'Air' configuration of the 'Enertun' system for a deep tunnel, namely the Lyon-Turin base tunnel, in a 10 km-long portion of the infrastructure under the huge cover of the Ambin massif. Thanks to the mining of the available geothermal energy potential due to the high rock mass and tunnel air

temperatures, not only a system able to exploit energy from a renewable resource (which would be otherwise ignored) could be achieved, but the tunnel internal climate conditions would be monitored and adjusted as well. In the following a description of the case study will be provided, followed by the presentation of numerical modelling setup and results.

2. The case study of the Lyon-Turin Base Tunnel

2.1 General description

The Lyon-Turin high-speed railway is a rail line under construction between the cities of Lyon (France) and Turin (Italy). It is intended to link the French and Italian high-speed rail networks and will be 270 km long. The core of the project is the Base Tunnel which will cross the Alps between the Susa Valley in Piedmont and the Maurienne in Savoie. The 57.5 km twin-tube tunnel beneath the Mont Cenis mountain, 45 km of which in France and 12.5 km on the Italian side, will replace the 150-year-old Frejus rail tunnel and will stand between 570 m and 750 m above sea level (Figure 1). Upon opening the tunnel, it will be the longest rail tunnel in the world, followed by the Gotthard

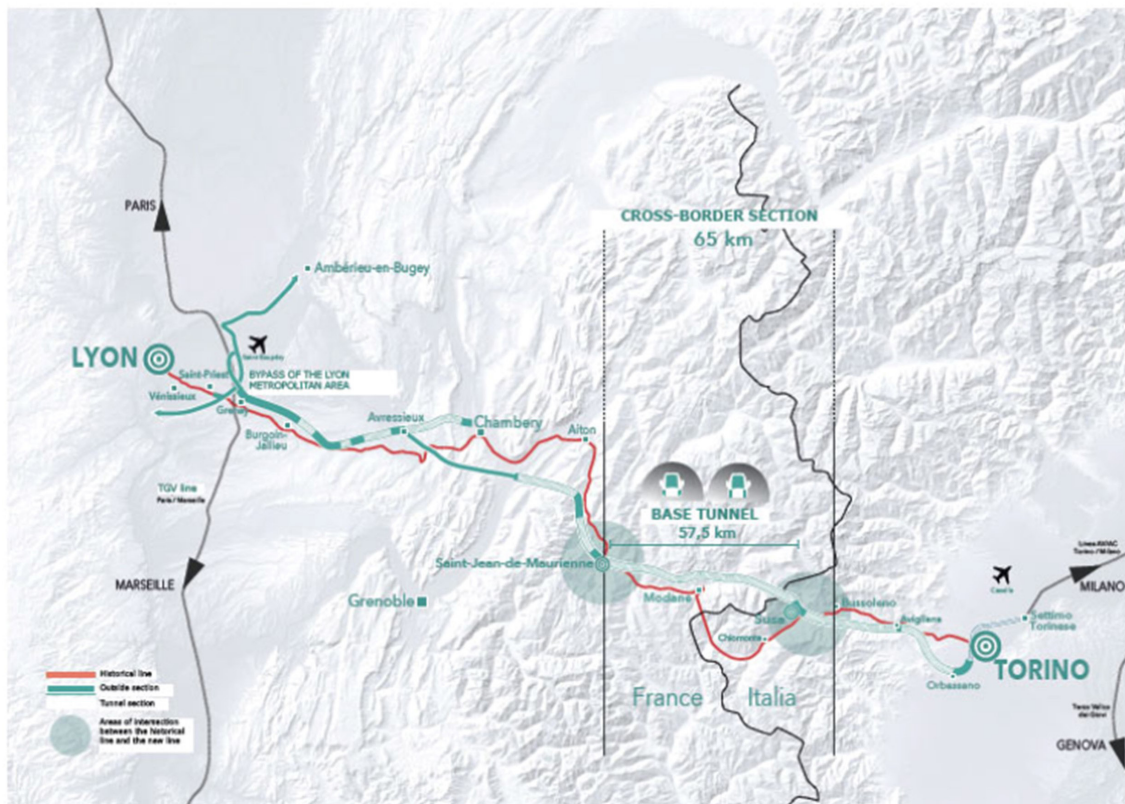


Figure 1. Cross-border section of the Lyon-Turin railway line overview (Italy, 2021).

Base Tunnel (57.1 km) and the Brenner Base Tunnel (55 km, currently under construction).

The reference geological and geomechanical model is based on the data obtained during the excavation of the inclined access adits at Saint-Martin-La-Porte, La Praz and Modane, including the La Maddalena exploratory tunnel (Bufalini et al., 2017). The base tunnel will encounter different geological contexts along its alignment including loose granular soils (alluvial deposits, glacial deposits), complex rock mass formations (arenaceous shale, coal-rich shale), evolutionary ground (anhydrites), high strength (mica schist and gneiss) or abrasive rock masses (quartzite). Thanks to the geological and geotechnical model developed, the most suitable methods to be adopted for excavation were identified, as well as the main geological risks, mitigation and management measures. Attention was devoted to critical conditions such as fault and severely fractured zones, high temperatures anomalies, squeezing, presence of swelling or soluble minerals. Hydrological investigations were carried out in order to assess the expected interference with aquifers such as water ingress into the tunnel and possible impacts on water resources, surface streams and rivers. Except for the first 350-400 m on the Susa side, the base tunnel is to be excavated with a slurry shield TBM (Tunnel Boring Machine), capable of creating a back pressure at the face greater than the groundwater hydrostatic pressure, in order to prevent water ingress into the tunnel. Immediately behind the TBM shield,

gaskets are to be adopted with the segmental lining to make it waterproof around the entire perimeter of the tunnel, when the water pressure is lower than 10 bar. Expected residual water flows at the portals are exploited for both drinking water and heating purposes (Bufalini et al., 2017).

2.2 The proposal for the thermal activation of a tunnel section

A specific study concerning the possible energy uses of the hot water intercepted during the excavation of the base tunnel in Chiomonte was recently carried out by TELT (2021). In this mentioned study, the heat exploited along the total length of the base tunnel (57.5 km), which ranges between 3.2 MW and 9.3 MW (for the least and the best conditions respectively), is to be used to supply a portion of the energy needs (district heating, swimming pools, greenhouses, etc.) of the Susa Valley. The close cities of Susa and Chiomonte for example could take advantage of this power to supply a swimming pool, greenhouses and the tunnel construction site area energy needs and for district heating.

From the geothermal profile evaluated for the base tunnel (Figure 2) it can be seen that in the core of the Ambin massif the temperature field reaches 47 °C, due to the overburden of 2500 m. This leads to the possibility of exploiting geothermal energy not only through the drained water but also by taking

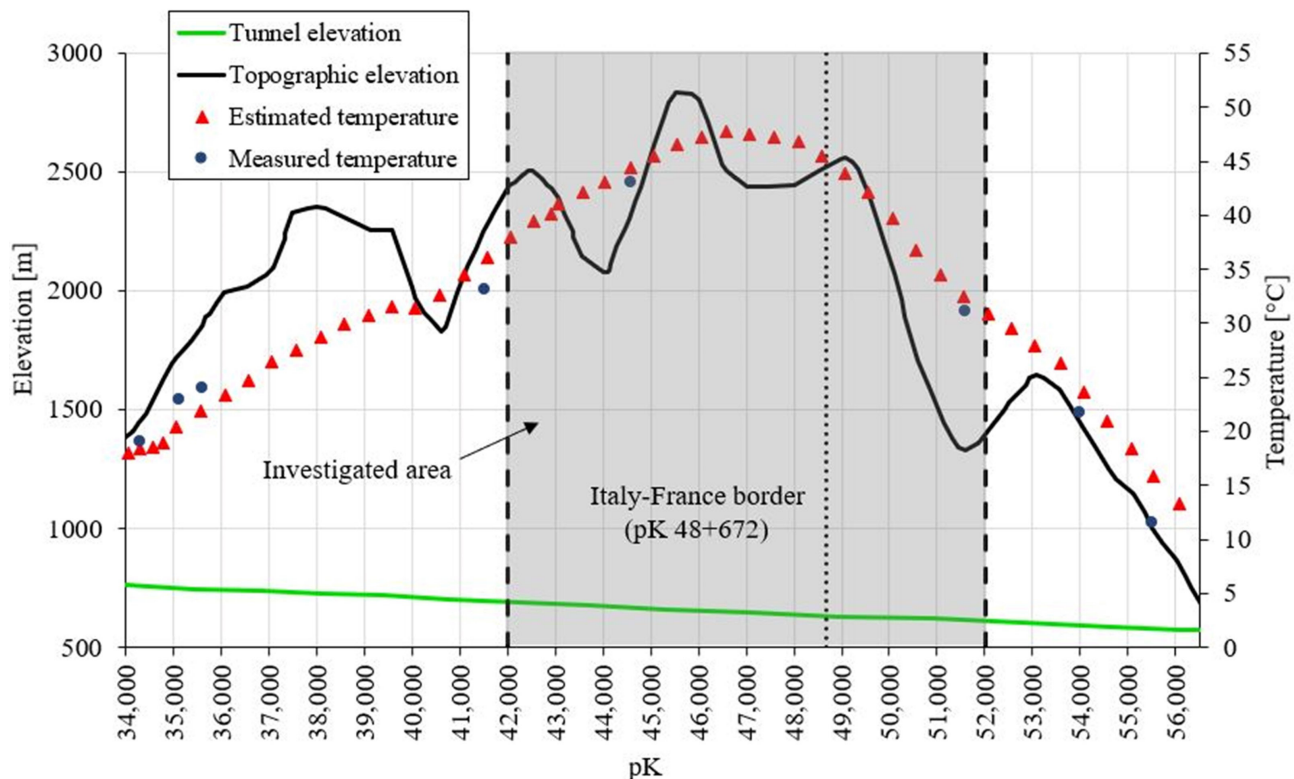


Figure 2. Geothermal profile of the Lyon-Turin railway base tunnel with indication of the investigated area (modified from LTF, 2001).

advantage of the high temperatures of the rock mass and of the air inside the infrastructure.

Diversely from prior studies, this paper will investigate the potential of thermally activating the tunnel lining thanks to the ‘Enertun’ system. The focus will be on the central 10 km-long section of the infrastructure (from pk 42 to pk 52, as shown in Figure 2) which also corresponds to the portion with the highest expected temperatures. The Air configuration of the ‘Enertun’ system is considered so that the circuit of embedded pipes is found at the intrados of the concrete lining segments and allows for heat exchange with the air inside the tunnel (Figure 3). The rings are hydraulically connected in pairs forming a subcircuit and the circuit of each segment is linked to that of the adjacent ones by hydraulic connections to form lining ring circuits (Barla et al., 2019; Rosso et al., 2021). The pipes are included in the concrete segments close to the internal boundary (at 10 cm from the air-lining interface), with a spacing of 30 cm, external diameter of 20 mm and thickness of 2.0 mm (cross-section area of 201 mm²).

The system may allow cooling the tunnel from the actual temperature down to the required working temperature (set to a maximal value of 32 °C by LTF, 2013). Potentially, the heat exploited during cooling of the 10 km-plant could be transferred to the nearest tunnel portal and used to satisfy energy needs in the area.

3. Description of the finite element model

To evaluate the potential of the proposed system described in 2.2, a 3D finite element model with thermo-hydraulic coupling was adopted. The thermo-hydraulic (TH) analyses were conducted by the software FEFLOW® (Diersch, 2009), where the thermo-hydraulic problem is governed by the following equations: the mass conservation, the Darcy’s law and the energy conservation for a saturated medium composed of a solid and a liquid (water) phase. In this chapter, the model set-up will be described together with the boundary conditions adopted and the thermo-physical properties of each component (surrounding ground, internal air and concrete energy lining).

The 3D model was built to reproduce a portion of the Lyon-Turin base tunnel, whose geometry is shown in Figure 4 with the indication of dimensions, materials and boundary conditions. It is composed of 240537 nodes and 465048 triangular prismatic three-noded elements distributed in 37 slices. A 30 cm-thick segmental lining with an outer diameter of 9 m was adopted. The whole domain is 200 m high and 200 m wide so that both the height and width are equal to twenty times the outer tunnel diameter, which allows the boundary effects to be ignored. The modelled tunnel has a longitudinal length of 8.4 m with 6 rings of a hypothesizing length of 1.4 m, each ring composed of 6 concrete segments. The absorber pipes were reproduced by 1D elements called

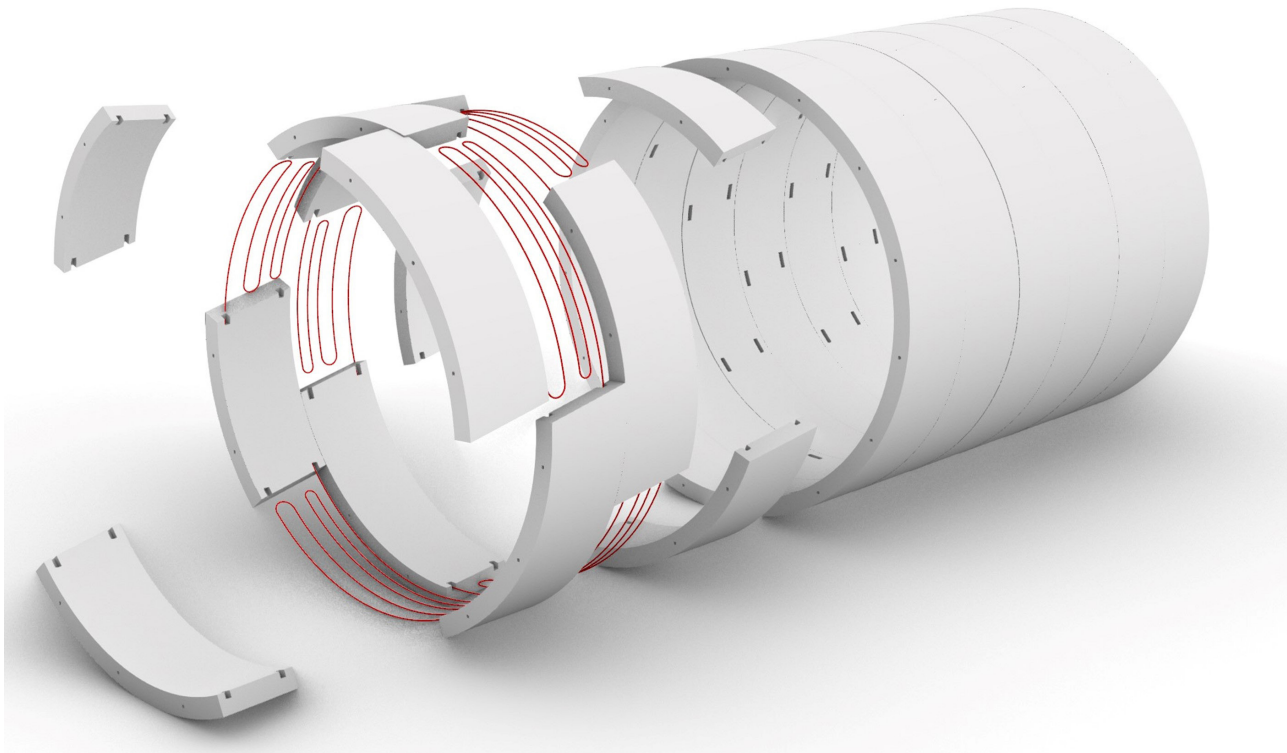


Figure 3. Exploded view of the ‘Air’ pipes embedded in the segmental lining.

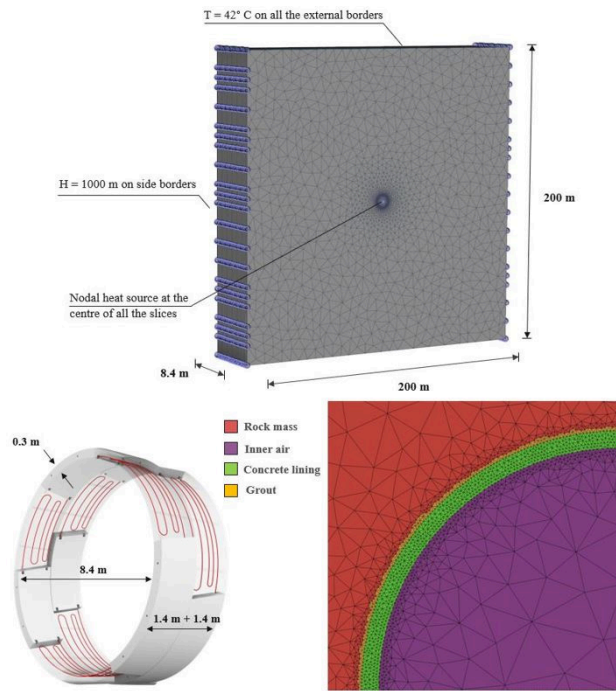


Figure 4. 3D FEM model with the indication of external and internal dimensions, materials and boundary conditions.

“discrete features” (distributed throughout the tunnel as shown in Figure 5), provided by the software FEFLOW®. Their properties are summarized in Table 1.

In these elements, the thermal resistance of the plastic pipes is neglected. This could lead to a very small temperature error in terms of numerical analysis results. However, the use of the 1D pipe elements was validated for similar systems and showed good agreement when compared to analytical solutions (Diersch, 2009). The mass and energy conservation equations governing the convection-diffusion problem, are satisfied for these elements, while the fluid flow inside them is described by the Hagen–Poiseuille law. Accordingly, fluid particles are assumed to move in pure translation with constant velocity, similarly to what occurs in circular tubes. An insulation layer able to prevent heat losses was placed around the network of pipes along the connection from the first to the second ring (and from the third to the fourth and so on) like it would be in reality, although in the model the connection takes place within the rock mass. The internal air was also discretized not only to investigate the heat exchange between the absorber pipes and the tunnel environment but also to monitor the internal climate conditions. The material properties were assigned to all the elements of the model, adding a 10 cm-thick layer of grout between the concrete lining and the surrounding ground for the sake of likelihood (Figure 4). All the thermo-hydraulic material properties are listed in Table 2.

Considering the scale of the problem, an equivalent continuum model was considered appropriate to represent

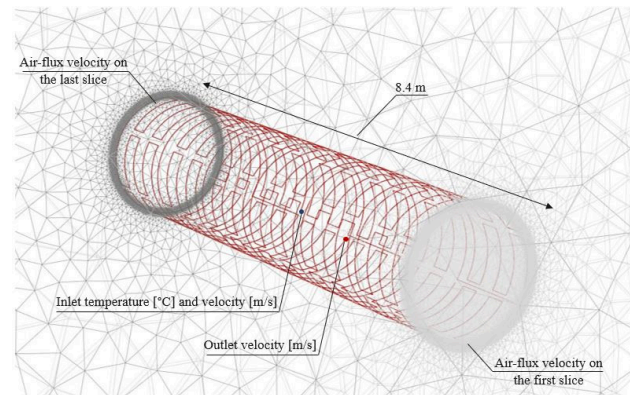


Figure 5. 3D discretisation of the piping system in the lining segments and boundary conditions.

Table 1. Discrete features properties adopted for the simulation of absorber pipes.

Property	Symbol	Unit	Value
External diameter	D	mm	20
Tube thickness	s	mm	2
Spacing	i	mm	300
Cross-sectional area	A	mm ²	201.06
Hydraulic aperture	r_{yd}	mm	8.0

the surrounding fractured rock mass. Due to the presence of discontinuities, the thermal conductivity of the rock mass is expected to be lower than that of the intact rock. This effective conductivity parameter depends on multiple factors such as fracture density, trace length and fracture thermal contact resistance (Li et al., 2021). Because of the preliminary stage of the analysis, such information could not be retrieved for the fracture network present in the studied area and the intact rock value was assumed for the following analyses. This may lead to computing a higher outlet temperature of the heat carrier inside the pipes and, thus, a slightly higher exploitable thermal power. Despite the Authors believe that this will only marginally affect the results obtained, it is an aspect that should be more deeply explored in a future stage of the research.

The fractures in the rock mass are supposed to be completely saturated and no flow occurs. To consider this, a constant hydraulic head of 1000 m was set all over the domain as an initial condition and at the lateral sides of the model. Moreover, a temperature of 42 °C (mean value of the estimated temperatures at the tunnel depth, Figure 2) was set throughout the domain as the initial condition and fixed equal at all the edges of the model. A heat nodal source boundary condition of -12 W was imposed in the central node of the tunnel cross-section, reproducing a constant injection of thermal energy to simulate the possible increase of the internal air temperature due to fast-moving vehicles or additional sources of heat (shown in Figure 4).

Table 2. Thermo-hydraulic material properties.

Material	Property	Symbol	Unit	Value
Ground	Horizontal hydraulic conductivity	$K_x = K_z$	m/s	$4.1 \cdot 10^{-8}$
	Vertical hydraulic conductivity	K_y	m/s	$4.1 \cdot 10^{-8}$
	Specific storage	S	m^{-1}	10^{-4}
	Porosity	n	—	0.02
	Fluid-phase thermal conductivity	λ_w	W/ (m ¹ K ¹)	0.65
	Solid-phase thermal conductivity	λ_s	W/ (m ¹ K ¹)	2.74
	Fluid-phase volumetric thermal capacity	$\rho_w c_w$	MJ/ (m ³ K ¹)	4.2
	Solid-phase volumetric thermal capacity	$\rho_s c_s$	MJ/ (m ³ K ¹)	2.4
	Transverse aquifer thermal dispersivity	α_T	m	0.5
	Longitudinal aquifer thermal dispersivity	α_L	m	5
Tunnel lining	Specific storage	S	m^{-1}	10^{-4}
	Solid-phase thermal conductivity	λ_s	W/ (m ¹ K ¹)	1.5
	Solid-phase volumetric thermal capacity	$\rho_s c_s$	MJ/ (m ³ K ¹)	2.19
	Horizontal hydraulic conductivity	$K_x = K_z$	m/s	10^{-16}
	Vertical hydraulic conductivity	K_y	m/s	10^{-16}
	Porosity	n	—	0
Grout	Specific storage	S	m^{-1}	10^{-4}
	Solid-phase thermal conductivity	λ_s	W/ (m ¹ K ¹)	2.0
	Solid-phase volumetric thermal capacity	$\rho_s c_s$	MJ/ (m ³ K ¹)	2.19
	Horizontal hydraulic conductivity	$K_x = K_z$	m/s	10^{-16}
	Vertical hydraulic conductivity	K_y	m/s	10^{-16}
	Porosity	n	—	0
Insulation	Specific storage	S	m^{-1}	10^{-4}
	Solid-phase thermal conductivity	λ_s	W/ (m ¹ K ¹)	0.0255
	Solid-phase volumetric thermal capacity	$\rho_s c_s$	MJ/ (m ³ K ¹)	0.001
	Horizontal hydraulic conductivity	$K_x = K_z$	m/s	10^{-16}
	Vertical hydraulic conductivity	K_y	m/s	10^{-16}
	Porosity	n	—	0
Internal air	Specific storage	S	m^{-1}	10^{-4}
	Fluid-phase thermal conductivity	λ_w	W/ (m ¹ K ¹)	0.53
	Fluid-phase volumetric thermal capacity	$\rho_w c_w$	MJ/ (m ³ K ¹)	10^{-3}
	Horizontal hydraulic conductivity	$K_x = K_z$	m/s	10^{-2}
	Vertical hydraulic conductivity	K_y	m/s	10^{-2}
	Porosity	n	—	1
	Transverse thermal dispersivity	α_T	m	0.5
	Longitudinal thermal dispersivity	α_L	m	5

To simulate the environment inside the tunnel and the geothermal plant operation conditions, a proper air-flux velocity at the first and last model slices and an inlet fluid temperature and velocity, regarding the absorber pipes, at the beginning of the circuit must be added. Also, an outlet fluid velocity has to be set at the end of the pipes network. These additional boundary conditions applied are shown in Figure 5. Given the influence involving these last parameters, it was chosen to perform sensitivity analyses, whose results will be discussed in the next chapter (section 4.1).

4. Numerical modelling results

In this chapter, the results of the thermo-hydraulic (TH) coupled analyses performed will be described. A first

section will focus on some sensitivity analyses to assess the proper boundary value parameters with respect to the air-flux velocity, the temperature and the velocity of the heat carrier fluid. Then the attention is posed on the short and long term behaviour of the thermoactive system so to quantify the amount of exploitable geothermal energy in different operating modes.

To investigate the thermal feasibility of energy geostructures, when the pipes are explicitly modelled, the exchanged heat can be computed from the results of the numerical analysis, as in Equation 1:

$$Q = m c (T_{in} - T_{out}) \quad (1)$$

where Q (in Watt) is the exploitable heat of the site, m (in kg/s) is the mass flow rate, c (in $J \cdot kg^{-1} \cdot ^\circ C^{-1}$) is the heat capacity of the circulating fluid at constant pressure, T_{in} (in $^\circ C$) is the inlet temperature and T_{out} (in $^\circ C$) is the outlet temperature of the heat carrier fluid running in the pipes.

4.1 Sensitivity analyses

The tunnel internal air is influenced by the motion of the vehicles running into it and, especially for railways and motorways tunnels, this needs to be accounted for when analysing the thermal behaviour of the infrastructure. Thus, a parametric analysis on the air-flux velocity was performed, showing that a higher flow velocity is able to facilitate the heat distribution inside the tunnel, while with a lower air-flux a more inhomogeneous distribution of the air temperature was seen both radially and axially. Based on this, a constant value of 8 m/s was imposed on the air nodes of the first and last cross-section of the numerical model in the subsequent analyses. The adoption of this value represents the most conservative choice among all the investigated velocities since the temperatures at the intrados of the lining were the highest experienced amongst all.

A second set of parametric analyses were conducted to study the influence of the inlet velocity and temperature of the heat carrier fluid. Such initial and boundary conditions have been varied one by one to determine the most suitable pair and optimise the plant performance. The operational conditions of the geothermal system were simulated by circulating fluid in the pipes network at a given inlet temperature and velocity, defined as Dirichlet and Neumann boundary conditions

respectively. Figure 6a shows the difference between the inlet and outlet fluid temperature (which influences the heat exchanged according to Equation 1) computed as a function of the heat carrier fluid velocity and temperature. Figure 6b depicts the thermal power calculated, in kW/m and after 1 year of continuous heat extraction, for a certain combination of fluid velocity and inlet temperature. It is evident that, for the tested ranges, the lower the temperature the higher the quantified exploitable heat, along with a higher fluid velocity. From the picture, it can also be seen that the fluid input temperature (ranging between 20–28 $^\circ C$) was the parameter that mostly affected the heat exchange in terms of exploitable geothermal power, at least from a certain heat carrier fluid velocity onwards.

Finally, the optimal input values were selected looking also at the difference ΔT between the outlet fluid temperature and that of the undisturbed rock mass at the end of the year investigated. A bigger difference would lead to a higher geothermal power per meter and a dimensionally less costly geothermal plant, but, at the same time, it would imply the worse performance of the heat pump, also affecting the ground thermal equilibrium. For this reason, to properly balance the heat pump efficiency with the overall system dimensions, a maximum of 17 $^\circ C$ was adopted as the limit value between the outlet fluid temperature and that of the undisturbed ground (Capozza et al., 2012). Based on the above, 24 $^\circ C$ and 0.8 m/s were imposed on the first node of the absorber pipes circuit, in the first, third and fifth ring, as this combination allowed to fulfil the above mentioned limit value and to maximise thermal power. From now onwards, the

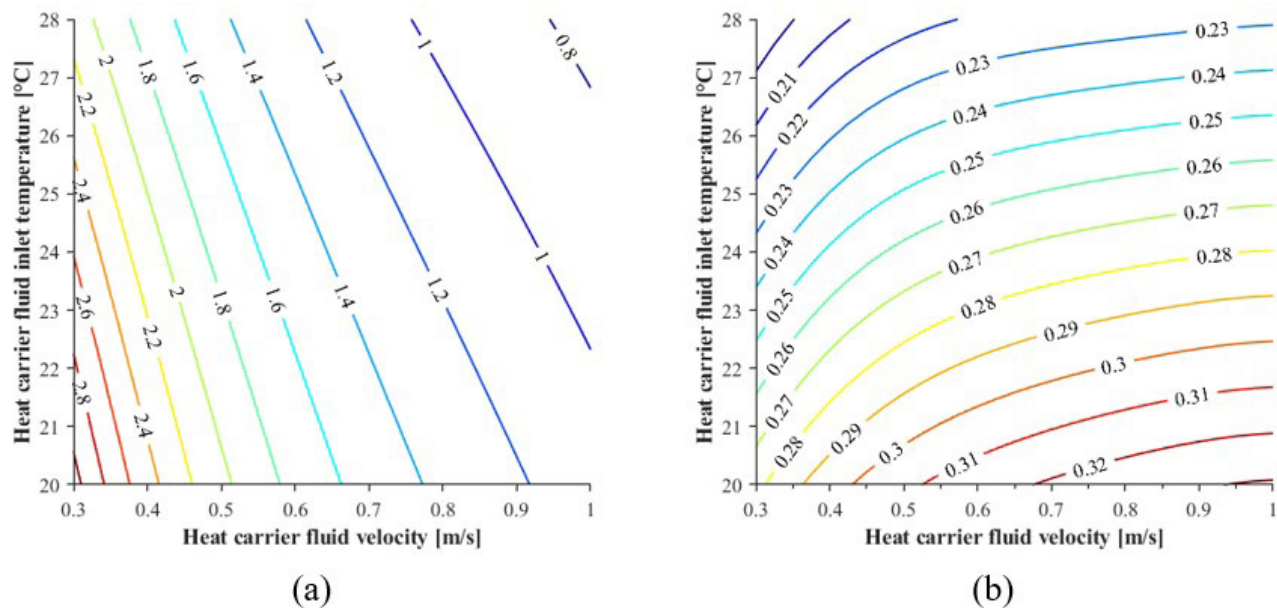


Figure 6. (a) Difference ($^\circ C$) between the outlet and inlet fluid temperature; and (b) thermal power (kW/m) exploited at the end of the year investigated depending on the fluid velocity and inlet temperature.

numerical simulations will refer only to the results obtained adopting these two boundary values for the heat carrier fluid.

4.2 Short term behaviour

The optimised model was used to quantify the heat that could be exchanged with the tunnel internal environment and the surrounding ground all over the year. Four types of operating conditions have been studied:

- the geothermal heat exchanger is active all the year-round,
- the geothermal heat exchanger is suspended during the summer season (three months),
- the geothermal heat exchanger is suspended for a longer period (five months from May to September),
- the geothermal heat exchanger is activated cyclically monthly (with on-and-off cycles for the heat pump being 30 days long).

To apply the above conditions, the temperature and velocity boundary conditions were imposed to the corresponding nodes through time histories in which the fluid motion circulation in the pipes is controlled. The imposed inlet temperature and the computed outlet temperature during the first year of the TH numerical simulations are shown in Figure 7 for each operational mode. The beginning of the analysis ($t=0$) corresponds to January, while the summer period (considering it from June to September) goes from day 151 to 243.

The computed temperature difference, the power per meter and the total power for the 10 km long section (considering that the inlet fluid temperature corresponds to 24 °C after 365 days of service) are shown in Table 3. Except for the continuous operating condition a), at the end of the first year, the geothermal plant would be able to extract at least 3 MW of thermal power for the base tunnel length

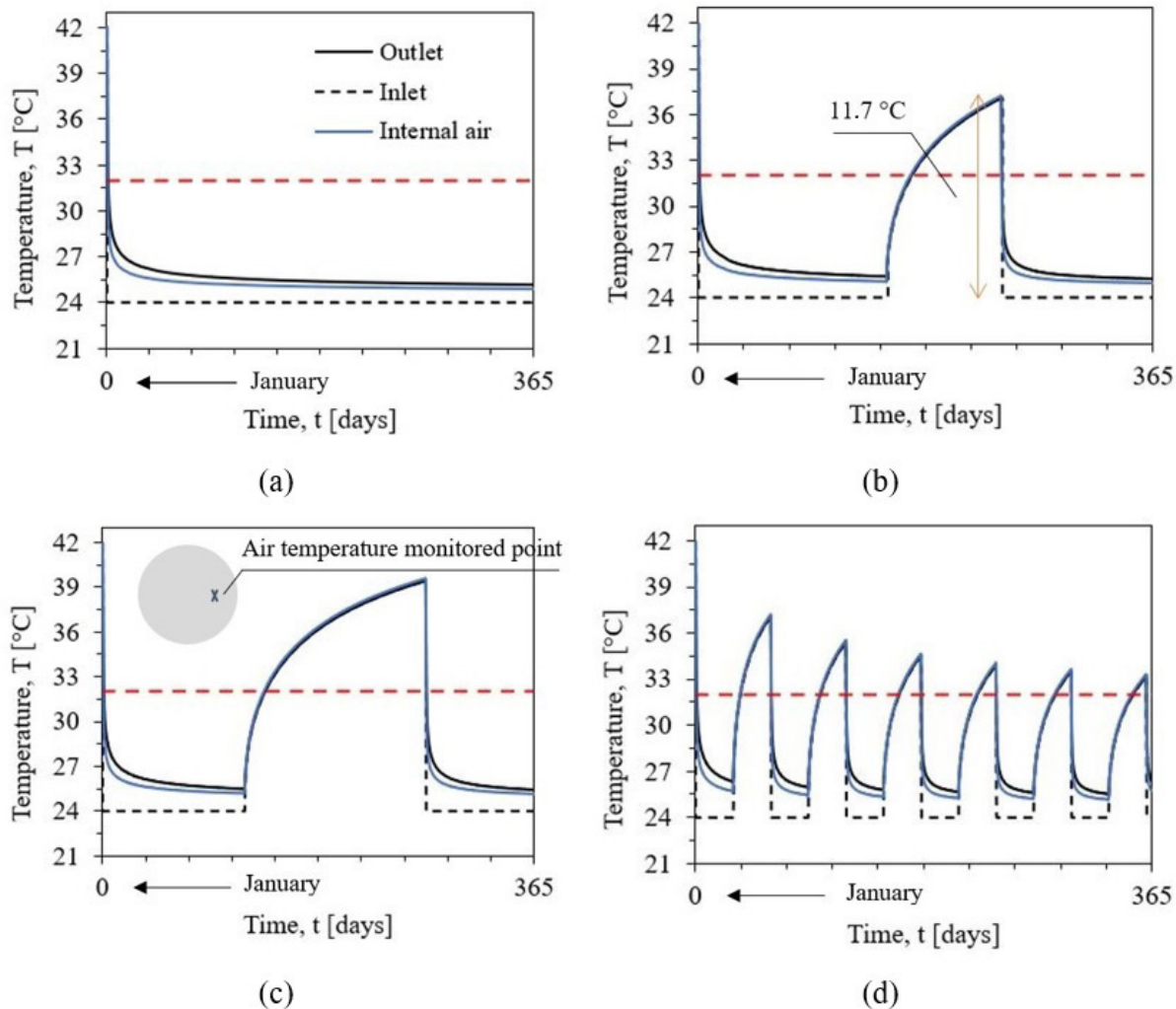


Figure 7. Imposed inlet temperature, computed outlet temperature and internal air temperature for (a) continuous; (b) cyclic (no 3 months); (c) cyclic (no 5 months); and (d) cyclic monthly activation (in red is the established temperature threshold of 32 °C for internal air).

Table 3. Temperature difference (ΔT), thermal power per meter of tunnel (q) and total power for the 10 km section (Q) in all the operating conditions considered.

Operating mode	Time	ΔT (°C)	q (kW/m)	Q (MW)
a) Continuous	1 year	1.14	0.28	2.84
	10 years	0.75	0.18	1.81
b) Cyclic (no 3 months)	1 year	1.27	0.30	3.04
	10 years	0.88	0.21	2.11
c) Cyclic (no 5 months)	1 year	1.46	0.34	3.43
	10 years	1.04	0.25	2.51
d) Cyclic monthly activation	1 year	1.50	0.36	3.61
	10 years	1.06	0.26	2.55

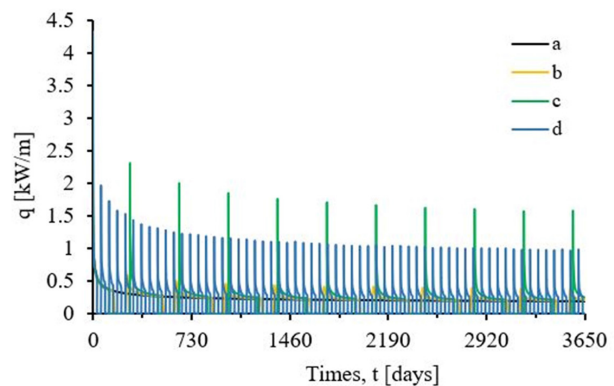
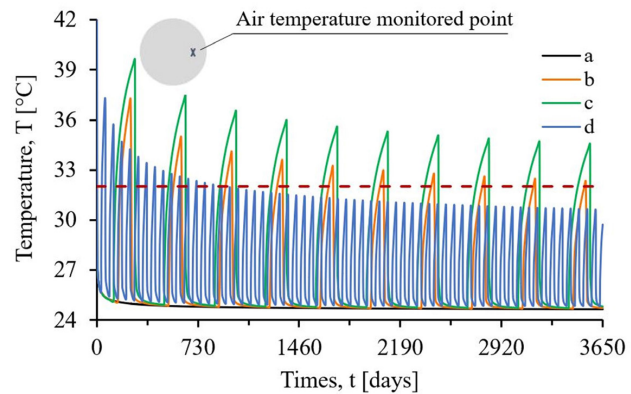
examined, with a maximum of 3.6 MW if the heat pump worked according to mode d).

The importance of seasonal activation is the need to avoid source depletion. The constant heat extraction of the continuous mode a), in fact, and the absence of groundwater flow will decrease the efficiency of the heat pump in the long term (Capozza et al., 2012). To avoid this, temporary breaks are introduced with the operating modes b), c) and d) to facilitate the thermal recharge of the ground. This would also result in a temperature variation of the tunnel internal environment. For example, in the operating mode b), during the three months in which the geothermal plant is switched off the climate conditions inside the tunnel would rise of about 11.7 °C (Figure 7b). Surely, in the first year at least, the continuous operating mode is the only one of those considered able to keep the internal air temperature under the acceptable limit of 32 °C (Figure 7a) imposed by LTF (2013). For such reason, there would be no need for a ventilation system implementation.

4.3 Exploitation in the long-term

To study the performance of the geothermal system in the long term, the coupled thermo-hydraulic analyses considering the four operational modes described above have been extended to a 10-year timespan. The results obtained in terms of specific thermal power are presented in Figure 8. As years go by, thermal efficiency changes in a different way depending on the operational mode considered, as quantified in Table 3.

In the long term, the system would provide a geothermal power per meter ranging between 0.18 and 0.26 kW/m, looking at all the scenarios. In terms of comparison, the power per meter evaluated by TELT (2021) with the exploitation of the drainage water heat would amount to around 0.162 kW/m in its most advantageous condition. According to the preliminary estimations shown, the thermal power per meter obtained through the thermal activation of the lining is similar, and even more favourable in selected cases. An additional advantage of the studied technology is that the system is a closed-loop

**Figure 8.** Extracted power per meter of tunnel with (a) continuous; (b) cyclic (no 3 months); (c) cyclic (no 5 months); and (d) cyclic monthly activation.**Figure 9.** Internal air temperature with (a) continuous; (b) cyclic (no 3 months); (c) cyclic (no 5 months); and (d) cyclic monthly activation (in red is the established temperature threshold of 32 °C for internal air).

and allows to avoid direct influence on the groundwater, reducing the concurrent environmental problems.

Lastly, Figure 9 presents the monitored internal air temperature. In comparison to the conditions experienced in

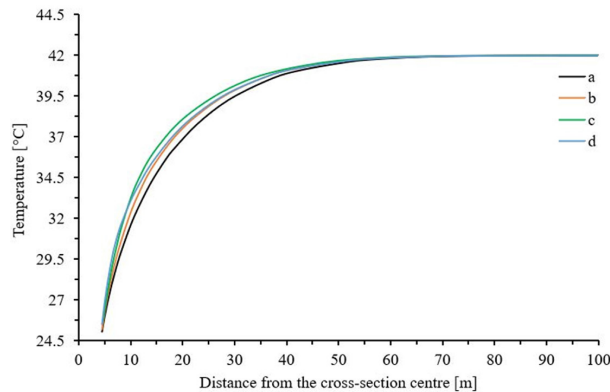


Figure 10. Worst scenario of ground temperature versus distance from the tunnel contour for (a) continuous; (b) cyclic (no 3 months); (c) cyclic (no 5 months); and (d) cyclic monthly activation.

the short-term (section 4.2) and with respect to the seasonal working modes b) and c), the 10 year-long analyses show a less pronounced growth of the internal air temperatures during the periods in which the geothermal plant is switched off. Specifically in the last year of the numerical analysis performed adopting mode b), the internal temperature during the three summer months of suspension will rise of just 7.3 °C, against the 11.7 °C of the first year (Figure 7b). However, the maximum limit of 32 °C imposed by LTF (2013) was only slightly exceeded for this case. On the contrary, assuming the cyclic monthly activation (mode d) for the heat pump, the tunnel internal air temperature, after 2 years and a half from the beginning of the heat extraction, would be maintained under this maximum value, as experienced with the continuous scenario a) (Figure 9).

Finally, the influence of the thermal activation on the surrounding ground temperature was checked for all the operating modes. Figure 10 depicts the temperature profile from the tunnel lining extrados to the model external boundary for modes a), b), c) and d) in their worst scenario, i.e. when the highest temperature reduction is experienced. For the operating mode a) and d), this corresponds to the end of the tenth year. Whereas, for mode b) and c), this condition occurs just before the seasonal break of the tenth year. In all situations, the ground affected zone lies within 50 m from the tunnel contour. However this trend is more or less constant only for mode a) while, for the other modes, it experiences variations throughout the year depending on the actual state of operation of the system (on/off cycles).

5. Conclusions

This work presents a numerical study conducted to evaluate the performance of the thermal activation of the tunnel linings for a 10 km-long section of the Lyon-Turin base tunnel. The aim is to take advantage of the high temperatures

expected at the base tunnel depth, exploit geothermal energy and, at the same time, improve the tunnel internal climate conditions. The portion of the base tunnel investigated fits into the category of hot tunnels, mainly due to the overburden, exceeding 2 km, experienced in the core of the Ambin massif. In addition, fast-moving trains or vehicles also contribute to raising the internal air temperature above the acceptable limits, and, hence, cooling is needed.

To enhance the heat exchange with the internal environment, the ‘Enertun air’ configuration of the circuit embedded into the concrete segmental lining was supposed to be installed.

Sensitivity analyses allowed to assess the most suitable boundary conditions for the inlet temperature and velocity of the fluid running into the absorber pipes. The ultimate values adopted in the model were an inlet temperature of 24 °C and a fluid velocity of 0.8 m/s, considering the exchangeable heat and the difference between the outlet fluid temperature and that of the undisturbed ground. The proper air-flux has been investigated as well and a velocity of 8 m/s has been set.

Four different theoretical scenarios for the geothermal plant behaviour have been considered to calculate the heat exchange obtained in the context investigated. The main issue was to find a satisfying compromise between the simulated most profitable thermal activation, in terms of exploitable power, and a safe internal climate (as assigned by LTF, 2013). With a continuous operating mode a), after 10 years the thermal power per meter is around 0.18 kW/m and the internal air temperature is maintained under the maximum limit (32 °C). In the other three hypotheses (b, c and d), cyclic operating conditions were implemented. Two of them (b and c) were seasonal, with the suspension of the heat extraction for three or five months, able to provide respectively 0.21 and 0.25 kW/m in a 10-year lifespan. In the last case d), the overall system was supposed to be activated according to monthly on-off cycles providing almost 0.26 kW/m in the long term. Acceptable climate conditions inside the tunnel were obtained for mode b) and d) after 10 and 2.5 years respectively, while it was not obtained in the 10 years period for operating mode c).

In conclusion, the ideal operating mode depends on the specific aim of the thermal activation project envisaged. If a constant energy provision along the year is requested, the continuous mode a) is to be chosen, also gaining in terms of cooling of the tunnel with relevant savings on ventilation and cooling system costs. In particular, if the focus is posed on the ventilation aspect, a cyclic monthly activation (mode d) should be evaluated as well, which develops a profitable geothermal plant in terms of power per meter, albeit it works for just half a year. Also mode b) may provide a reasonable compromise. In case the deep tunnel cooling is not mandatory, the seasonal alternative c) is another viable solution as it produces relevant thermal power. Nevertheless, the four operating modes represent theoretical limit conditions. In case of real operation, an equilibrium with the thermal needs should be sought thus implying on-and-off cycles designed ad hoc.

The work performed testifies that the ‘Enertun Air’ energy lining can be a highly competitive alternative, as a closed-loop system, to the thermal use of drainage water, also thanks to its additional advantages in terms of minor disturbance to the groundwater and the possibility to regulate the tunnel inner climate with savings on ventilation and cooling costs.

Declaration of interest

The authors have no conflicts of interest to declare. All co-authors have observed and affirmed the contents of the paper and there is no financial interest to report.

Authors’ contributions

Maria Romana Alvi: conceptualization, Data curation, Formal Analysis, Investigation, Methodology, Validation, Visualization, Writing – original draft, Writing – review & editing. Alessandra Insana: conceptualization, Data curation, Formal Analysis, Investigation, Methodology, Supervision, Visualization, Writing – review & editing. Marco Barla: conceptualization, Funding acquisition, Investigation, Methodology, Project administration, Resources, Supervision, Visualization, Writing – review & editing.

List of symbols



A	cross-sectional area of pipes
D	diameter
c	heat capacity of the circulating fluid at constant pressure
c_s	heat capacity of the solid phase
c_w	heat capacity of the liquid phase
H	hydraulic head
i	spacing
K_x, K_z, K_y	horizontal and vertical hydraulic conductivity
m	mass flow rate
n	porosity
q	thermal power per meter
Q	exchangeable heat in Watt
r_{yd}	hydraulic aperture
s	thickness
S	specific storage
T	temperature
T_{in}	Inlet temperature of the heat carrier fluid
T_{out}	Outlet temperature of the heat carrier fluid
v	velocity
α_L	longitudinal thermal dispersivity
α_T	transverse thermal dispersivity
λ_s	solid phase thermal conductivity
λ_w	liquid phase thermal conductivity
ρ_s	solid phase density
ρ_w	water or liquid phase density

References

- Adam, D., & Markiewicz, R. (2009). Energy from earth-coupled structures, foundations, tunnels and sewers. *Geotechnique*, 59(3), 229-236. <http://dx.doi.org/10.1680/geot.2009.59.3.229>.
- Baralis, M., Barla, M., Bogusz, W., Di Donna, A., Ryżyński, G., & Żeruć, M. (2020). Geothermal potential of the NE extension Warsaw (Poland) metro tunnels. *Environmental Geotechnics*, 7(4), 282-294. <http://dx.doi.org/10.1680/jenge.18.00042>.
- Baralis, M., Insana, A., & Barla, M. (2021). Energy tunnel for deicing of a bridge deck in Alpine region. In *International Conference of the International Association for Computer Methods and Advances in Geomechanics. Challenges and Innovations in Geomechanics (IACMAG 2021)* (Lecture Notes in Civil Engineering, No. 126, pp.1061-1068). Cambridge: Springer. http://dx.doi.org/10.1007/978-3-030-64518-2_126.
- Barla, M., & Di Donna, A. (2016). Conci energetici per il rivestimento delle gallerie. *Strade & Autostrade*, 5(119), 46-49.
- Barla, M., & Di Donna, A. (2018). Energy tunnels: concept and design aspects. *Underground Space*, 3(4), 268-276. <http://dx.doi.org/10.1016/j.undsp.2018.03.003>.
- Barla, M., & Perino, A. (2015). Energy from geo-structures: a topic of growing interest. *Environmental Geotechnics*, 2(1), 3-7. <http://dx.doi.org/10.1680/envgeo.13.00106>.
- Barla, M., Baralis, M., Insana, A., Santina, A., Antolini, F., Vigna, F., Azzarone, F., & Marchetti, P. (2021). On the thermal activation of Turin Metro Line 2 Tunnels. In *International Conference of the International Association for Computer Methods and Advances in Geomechanics. Challenges and Innovations in Geomechanics. IACMAG 2021* (Lecture Notes in Civil Engineering, No. 126, pp. 1069-1076). Cambridge: Springer. https://doi.org/10.1007/978-3-030-64518-2_127.
- Barla, M., Di Donna, A., & Insana, A. (2019). A novel real-scale experimental prototype of energy tunnel. *Tunnelling and Underground Space Technology*, 87, 1-14. <http://dx.doi.org/10.1016/j.tust.2019.01.024>.
- Brandl, H. (2006). Energy foundations and other thermo-active ground structures. *Geotechnique*, 56(2), 81-122. <http://dx.doi.org/10.1680/geot.2006.56.2.81>.
- Bufalini, M., Dati, G., Rocca, M., & Scevaroli, R. (2017). The Mont Cenis Base Tunnel. *Geomechanics and Tunnelling*, 10(3), 246-255. <http://dx.doi.org/10.1002/geot.201700009>.
- Capozza, A., De Carli, M., Galgaro, A., & Zarelle, A. (2012). *Linee guida per la progettazione dei campi geotermici per pompe di calore*. Milan: RSE (in Italian).
- Diersch, H.J.G. (2009). *DHI wasy software – Feflow 6.1 – Finite element subsurface flow & transport simulation system: reference manual*. Berlin: DHI-WASY GmbH.
- Epting, J., Baralis, M., Künze, R., Mueller, M. H., Insana, A., Barla, M., & Huggenberger, P. (2020). Geothermal potential

- of tunnel infrastructures: development of tools at the city-scale of Basel, Switzerland. *Geothermics*, 83, 101734. <http://dx.doi.org/10.1016/j.geothermics.2019.101734>.
- European Union. (2012). *EU - Energy in figures: statistical pocketbook 2012*. Luxembourg: European Commission. Retrieved in August 15, 2013, from <https://data.europa.eu/doi/10.2833/11169>
- Franzius, J.N., & Pralle, N. (2011). Turning segmental tunnels into sources of renewable energy. *Proceedings of the Institution of Civil Engineers. Civil Engineering*, 164(1), 35-40. <http://dx.doi.org/10.1680/cien.2011.164.1.35>.
- Insana, A., & Barla, M. (2020). Experimental and numerical investigations on the energy performance of a thermo-active tunnel. *Renewable Energy*, 152, 781-792. <http://dx.doi.org/10.1016/j.renene.2020.01.086>.
- Intergovernmental Panel on Climate Change – IPCC. (2012). *Renewable energy sources and climate change mitigation: summary for policymakers and technical summary*. Cambridge: Cambridge University Press.
- International Energy Agency – IEA. (2012). *Policies for renewable heat: an integrated approach* (Insight Series 2012). Paris: OECD/IEA.
- Italy. Ministero delle Infrastrutture e della Mobilità Sostenibili - MIMS. (2021). *Torino-Lione: al Piemonte 32 milioni di euro per opere di tutela ambientale e sociale*. Rome. Retrieved in August 15, 2013, from <https://mit.gov.it/> (in Italian).
- Kanth, A., & Chakraborty, T. (2015). Numerical analysis of geothermal tunnels. *IJRET: International Journal of Research in Engineering and Technology*, 4(2), 740-746. <http://dx.doi.org/10.15623/ijret.2015.0402102>.
- Li, Z.W., Liu, Y., Mei, S.M., Xing, S.C., & Wang, X.K. (2021). Effective thermal conductivity estimation of fractured rock masses. *Rock Mechanics and Rock Engineering*, 54(12), 6191-6206. <http://dx.doi.org/10.1007/s00603-021-02599-5>.
- Lyon Turin Ferroviarie – LTF. (2001). *Nuova linea Torino Lione: progetto preliminare in variante. Complementi di geologia – Modello geotermico*. Chambéry, France (in Italian).
- Lyon Turin Ferroviarie – LTF. (2013). *Ventilazione: studio degli scenari di estrazione fumi dal tunnel (Revisione del progetto definitivo)*. Chambéry, France (in Italian).
- Rosso, E., Insana, A., Vesipa, R., & Barla, M. (2021). Optimization of the hydraulic circuit for energy tunnels. In *EURO:TUN 2021, 5th International Conference on Computational Methods and Information Models in Tunneling*. Bochum: Ruhr University Bochum.
- Seyboth, K., Beurskens, L., Langniss, O., & Sims, R.E. (2008). Recognizing the potential for renewable energy heating and cooling. *Energy Policy*, 36(7), 2460-2463. <http://dx.doi.org/10.1016/j.enpol.2008.02.046>.
- Tinti, F., Boldini, D., Ferrari, M., Lanconelli, M., Kasmaee, S., Bruno, R., Egger, H., Voza, A., & Zurlo, R. (2017). Exploitation of geothermal energy using tunnel lining technology in a mountain environment: a feasibility study for the Brenner Base tunnel – BBT. *Tunnelling and Underground Space Technology*, 70, 182-203. <http://dx.doi.org/10.1016/j.tust.2017.07.011>.
- Tunnel Euralpin Lyon-Turin – TELT. (2021). *Acqua: Energia dal tunnel di base. La risorsa geotermica come opportunità di sviluppo green. TELT e dipartimenti DIATI e DENERG del Politecnico di Torino*. Italy (in Italian).

Site characterization for a study on shallow geothermal energy exploitation in Southern Brazil

Bianca Penteado de Almeida Tonus^{1,2#} , Carlos Emmanuel Ribeiro Lautenschläger² ,
Amanda Fetzer Visintin¹ , Vítor Pereira Faro¹ ,
Cristina de Hollanda Cavalcanti Tsuha³ 

Article

Keywords

Shallow geothermal energy
Tropical soils
Site characterization
Ground temperature

Abstract

The energy crisis scenario currently going on in Brazil, along with the need to reduce greenhouse emissions, lead to an urgent need to design buildings with greater energy efficiency. Shallow geothermal energy surges as a sustainable alternative to reduce the electricity consumption in buildings related to air conditioning and water heating systems. In Brazil, the use of this technique is still incipient due to the lack of studies that demonstrate its viability in the country's climatic conditions, as well as underground temperature and demand for acclimatization of buildings. The aim of the current work is to present a site characterization for the first geothermal energy investigation carried out in the Brazilian South region. This study is being conducted at the Geotechnical Experimental Site of the State University of Ponta Grossa, and this paper describes the physical, mineralogical, thermal and mechanical characteristics of this site, which comprises a thick layer of a lateritic sandy clay soil over a silty sand layer. The preliminary results of the ground temperatures are consistent with the common trends reported in the literature, showing more expressive oscillations near the ground surface, and becoming approximately constant at higher depths.

1. Introduction

The effects associated with climate change, such as the increase in global temperature and extreme weather events, have been worsened due to greenhouse gas emissions in the atmosphere. Among the international measures adopted to mitigate the effects of anthropically caused climate change is the Paris Agreement, signed in 2015 by Brazil and 194 other countries, aiming to contain the increase in global temperature associated with the emission of greenhouse gases by 1.5 °C (Sani et al., 2019). However, according to data from the Electric Energy Statistical Yearbook (Brasil, 2020a), in 2019 there was a 6.8% increase in greenhouse gas emissions from electricity generation in Brazil. Total greenhouse gas emissions in the National Interconnected System (SIN) increased by 3% between 2018 and 2019, with highlights being natural gas (+9.6%) and coal (+9.2%). Nevertheless, the most significant contribution was from the Isolated System, whose increase in 2019 was 134.4% over the previous year, due to the growth of diesel generation

(+72.9%) and the decisive entry of natural gas thermoelectric plants (+4,066.7%). This reality reinforces the need to reduce the global demand for fossil fuels, prioritizing renewable energy sources.

Regarding consumption, there has been a significant increase in global energy demand, driven by world population growth and the search for a better quality of life. According to Loveridge et al. (2020), the annual *per capita* energy consumption grew exponentially in the last century due to population growth. The growing demand must be absorbed by increasing the energy supply, increasing the existing installed capacity, and seeking previously unexplored sources with low greenhouse gas emissions. In Brazil, the building sector accounts for half of the country's total electricity consumption. Energy consumption with air conditioning systems is around 30% (Brasil, 2018). The Energy Research Company (EPE) projections point to significant growth in total energy consumption, with a considerable growth rate in air conditioners, which will practically double in fifteen years.

#Corresponding author. E-mail address: bpatonus@uepg.br

¹Universidade Federal do Paraná, Civil Construction Department, Curitiba, PR, Brasil.

²Universidade Estadual de Ponta Grossa, Civil Engineering Department, Ponta Grossa, PR, Brasil.

³Universidade de São Paulo, São Carlos School of Engineering, Civil Engineering Department, São Carlos, SP, Brasil.

Submitted on December 3, 2021; Final Acceptance on January 12, 2022; Discussion open until May 31, 2022.

<https://doi.org/10.28927/SR.2022.078221>



This is an Open Access article distributed under the terms of the Creative Commons Attribution License, which permits unrestricted use, distribution, and reproduction in any medium, provided the original work is properly cited.

Given the data presented above, there is an imminent need to design more sustainable buildings that seek more significant energy efficiency. In this context, shallow geothermal energy is an alternative for reducing electric energy consumption for the air conditioning of buildings. Besides being clean and renewable energy, its use system can be installed in the foundations of a building, using structures already foreseen in the project to exchange heat with the ground. Lee et al. (2007) also state that geothermal energy is available continuously, regardless of weather conditions and in any part of the Earth, which is advantageous compared to other renewable energy sources, such as solar and wind.

Amatya et al. (2012) comment that geothermal source heat pump (GSHP) has emerged as a promising technology for heating and cooling of buildings. In these systems, fluid is circulated between the heat pump and heat exchanger elements in the ground; with the cooler fluid being circulated to extract energy from the warmer ground for heating (winter) and the warmer fluid transferring heat from the building to the ground to provide cooling (summer). By incorporating the heat exchanger system between the building and the ground in the foundation elements, the advantage is that concrete is a suitable heat conduction medium, considering its thermal conductivity and thermal storage capacity.

The use of shallow geothermal energy is still developing in Brazil. However, the National Energy Plan (Brasil, 2020b) mentions the use of shallow geothermal energy as one of the disruptive technologies that can significantly change the energy market, highlighting China, the United States and Europe as leaders in these developments. The document points out that using this technology can reduce the final energy consumption for thermal energy production, above 60% for heating and between 20% and 60% for cooling, which may lead to a decrease in electricity consumption at peak hours. Finally, the Plan highlights that the technology is already viable in some international markets, based on concepts of energy efficiency, which may represent an opportunity for Brazil, that needs to expand the studies on this topic.

The first experimental study on shallow geothermal energy using the pile foundation as a ground heat exchanger in Brazil were carried out at the Experimental Site at São Carlos School of Engineering of University of São Paulo (EESC/USP), in the Southeast region of the country, in which Moraes (2019) evaluated the use this technology in unsaturated sandy soil with an average ground temperature of approximately 24 °C. Additionally, the first Brazilian building that will use heat exchanger piles for space cooling is being built at the USP campus in São Paulo city.

To expand the development and utilization of shallow geothermal energy in Brazil, it is essential to carried out experimental studies in different Brazilian regions and climatic conditions. To investigate the potential of the use of this technology for a given region, it is necessary to determine the local ground thermal and geotechnical characteristics. In this context, this work aims to present

the initial site characterization of an Experimental Site in the Southern region of Brazil, at the campus of the State University of Ponta Grossa, Paraná state, where the mean annual air temperature is below 20 °C.

2. Shallow geothermal energy

Geothermal energy can be defined, according to Laloui & Loria (2020), as the natural thermal energy or natural heat that exists inside the Earth, resulting from three processes: the formation of the planet, the radioactive decomposition of minerals and solar energy absorbed on the surface. The Earth is divided into the crust, mantle (upper and lower) and core (outer and inner). The average geothermal gradient is approximately 3 °C for every 100 meters depth to the upper mantle and may vary between 1 °C and 10 °C. According to the authors, the temperature variation in the Earth's most superficial layers, between 4 and 6 meters, presents a significant sensitivity to atmospheric conditions, being strongly influenced by daily and seasonal temperature fluctuations. Below this region, the temperature remains relatively stable throughout the year, between 10 °C and 25 °C depending on the region and is approximately equal to the mean annual outside air temperature, according to the typical behavior illustrated in Figure 1 for different seasons of the year. As mentioned in Narsilio et al. (2014), for most locations around the world, the soil tends to be warmer than the atmosphere during winter and cooler during summer, regardless of geology.

In order to use the heat from the ground, there are different types of geothermal systems, classified according to

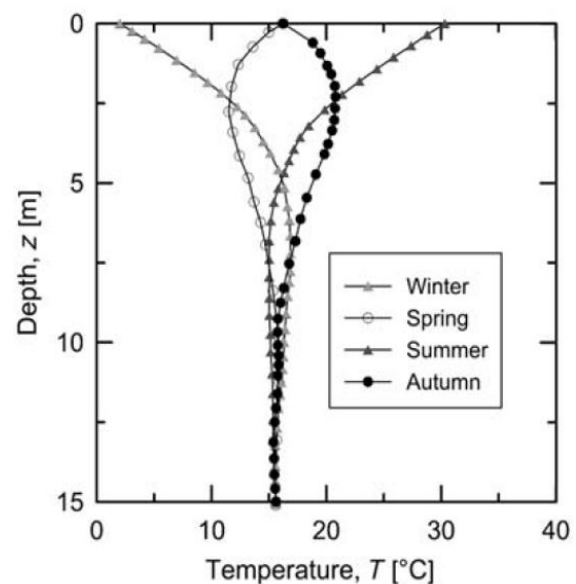


Figure 1. Typical temperature evolution with depth in the shallow subsurface throughout the year (Laloui & Loria, 2020).

the depth at which thermal energy is exploited. Geothermal systems with fewer than 400 meters are classified as shallow and work with low temperature and low enthalpy. Greater depths characterize deep geothermal systems with medium and high temperatures and enthalpies (Laloui & Loria, 2020).

Shallow geothermal systems can be used to provide space heating and cooling and water heating, using underground temperatures of up to 25 °C. These systems are suitable for domestic and small-scale use and can be used in almost all geographical locations. Deep geothermal systems can provide space and water heating using underground temperatures from 25 °C up to 200 °C, and electricity at temperatures above 175 °C. These systems are suitable for medium to large-scale use, requiring more specific deployment conditions than shallow systems (Narsilio et al., 2014).

Shallow geothermal systems are composed of three main components: a heat source, a heat sink and a heat exchanger (Sani et al., 2019). In winter, the heat source is the ground, and the heat sink is the built environment. In summer, the heat source is the built environment, and the heat sink is the ground. In both situations, the heat exchanger generally consists of one or more elements containing a fluid that transfers heat between the heat source and the heat sink. Heat exchanger pipes can be installed directly in specific trenches or attached to reinforce structures already planned for the construction, such as deep foundations, slabs, retaining walls and tunnel linings.

Regardless of the geothermal structure used, heat transfer is the physical phenomenon whereby energy is transferred between any two particles of matter at different temperatures. This heat transfer phenomenon can be quantified as a function of the amount of heat energy transferred per unit time. As heat transfer cannot be measured directly, its occurrence can be quantified by employing temperature, which is the variable that governs the heat transfer phenomenon (Laloui & Loria, 2020).

According to Rees et al. (2000), heat transfer in porous media can be induced by several mechanisms. The three most effective mechanisms are conduction, convection and heat transfer due to water phase change, also known as latent heat vaporization. Laloui & Loria (2020) point out that for engineering purposes, latent heat transfer processes are considered negligible. Sani et al. (2019) state that the portion referring to the mechanism of heat transfer by convection is small and that the conduction is the dominant mechanism, which depends on the type of soil, its porosity and moisture content.

A complete geotechnical characterization of the local soil is essential to understand the heat transfer mechanisms for the implementation of shallow geothermal energy utilization. Additionally, for the use of pile foundations as ground-coupled heat exchangers the characterization of the soil mechanical properties is also fundamental for the interpretation of the effect of thermal loads on the foundation mechanical behavior. As this subject has not yet been widely

studied in Brazil, new investigations must be carried out at different experimental sites, with an appropriate geotechnical characterization. Furthermore, new studies on the use of shallow geothermal energy in different regions is necessary, considering that the performance of these systems is dependent on the climatic and ground characteristics. In this context, this study is focused on the geotechnical, thermal and mechanical characterization of the soil of a particular site, for future studies on the thermal performance and thermomechanical behaviour of heat exchanger piles.

3. Experimental programme

To characterize the soil of a site located in the Southern Brazil for an investigation on the feasibility of shallow geothermal energy utilization, the chosen location was the Geotechnical Experimental Site (CEEG-PG) of the State University of Ponta Grossa, located in the Ponta Grossa city, Paraná State, Brazil with an area of 11,419 m².

Ponta Grossa city is in the Second Plateau of Paraná and is inserted in the Paraná Basin, large sedimentary basin located in the central-eastern of South America. Its area of occurrence encompasses mainly the center-south of Brazil, from the Mato Grosso state to the Rio Grande do Sul state. Away from Brazil, it is also present in northeastern Argentina and the eastern portion of Paraguay. Ponta Grossa city has a certain geological heterogeneity, in its urban area has a prevalence of the Ponta Grossa Formation and the Furnas Formation, both of the Paraná Group of the Devonian period, and the Campo Mourão Formation and the Taciba Formation, both of the Itararé Group of the Permian period.

The Experimental Site is in the Ponta Grossa Formation, mainly composed of clay rocks, called shales, and is close to the Furnas Formation, composed mainly of quartz sandstones. The Itararé Group is represented mainly by sandstones, diamictites and conglomerates. Both groups had their origin in the Paleozoic. Because they are softer, the clay rocks of the Ponta Grossa Formation are crossed in some points by dikes and diabase sills of the Serra Geral Formation of the Mesozoic, also close to the Experimental Site. Based on the geological information of the region, it can be concluded that a large part of the Ponta Grossa city is covered by residual soils from sedimentary rocks, except for the regions with the presence of more mature residual soils from magmatic rocks. There is also the presence of alluvial and colluvial sediments of a more recent age.

Besides knowing the local geology, the knowledge of the local temperature and precipitation variations are also crucial for the use of geothermal energy. Figure 2 presents the monthly average temperature at Ponta Grossa city registered during the last ten years, and indicates a mean temperature of ~18.2 °C. The precipitation data, provided by SIMEPAR (2021) for the same period, indicates 127mm for average monthly precipitation.

The soil characterization of the CEEG-PG was performed using field tests complemented by laboratory tests, for determining physical, mineralogical, mechanical, and thermal characteristics.

Three Standard Penetration Tests (SP01 to SP03) were conducted at this site in October 2018, and their samples were used for characterization tests in laboratory. After analyzing the SPT results, it was realized that the water circulation used during the tests probably influenced the strength results of the local soil; as normally observed for lateritic soils. For this reason, in October 2019, an additional Standard Penetration Test was performed (SP04) without water circulation. The excavation was performed only with an auger until the

depth of 5m, when it was no longer possible to advance without the addition of water. The samples from this borehole were stored for X-Ray diffraction tests, scanning electron microscopy, and disk method for tropical soil classification. The last Standard Penetration Test, SP05, was performed in September 2021 and it had its depth limited to 12.5m so that its borehole could be used for ground temperature measurements. Its samples were used to determine the natural soil moisture content.

Figure 3 illustrates the locations of the SPT tests in the Experimental Site and also indicates three trenches with 2m deep used to collect disturbed and undisturbed soil samples (TR01 to TR03). These trenches were opened in November

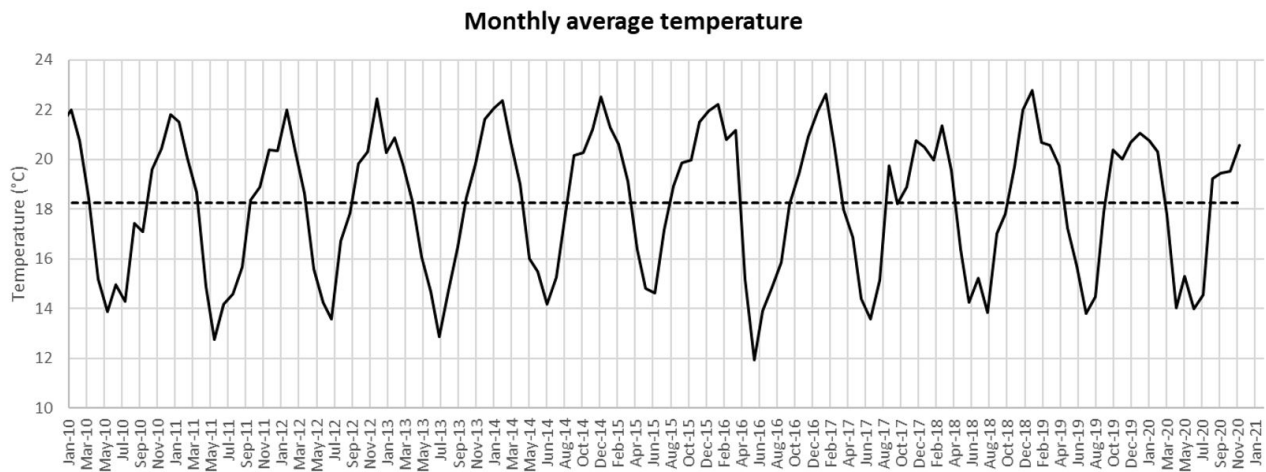


Figure 2. Monthly average temperature of Ponta Grossa city (Data provided by SIMEPAR, 2021).

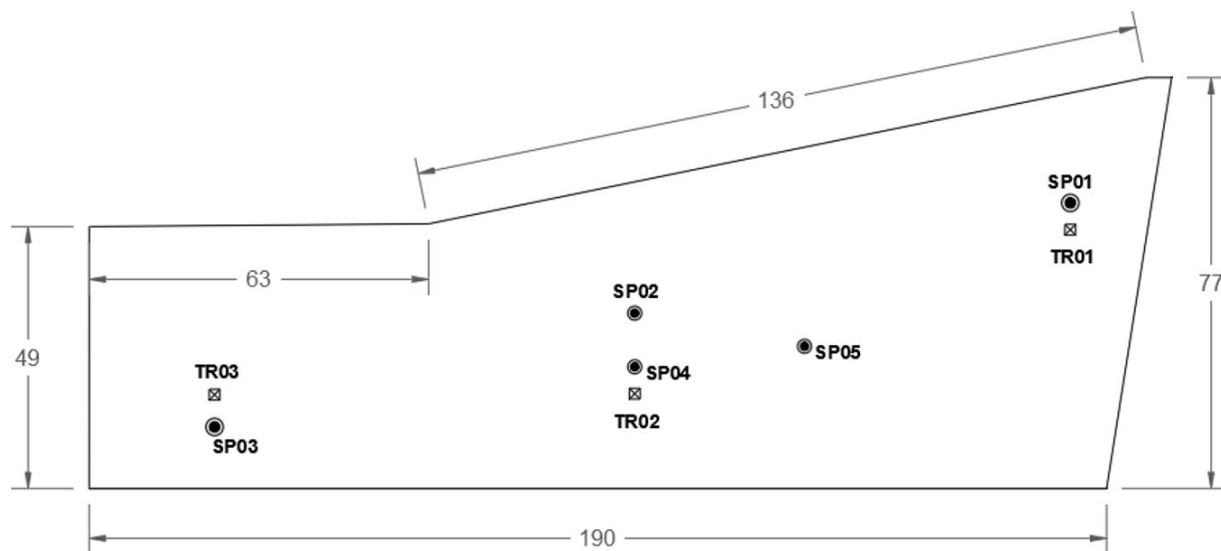


Figure 3. Location of Standard Penetration Tests and Trenches at the CEEG-PG site (distances in meters).

2019, and from each trench, three undisturbed soil blocks were collected. The disturbed soil samples were used for soil type characterization in laboratory and the undisturbed samples were used for obtaining soil strength information from direct shear tests.

From the Standard Penetration Tests, 76 soil samples were obtained at each meter depth, being 17 samples from borehole SP01, 15 samples from borehole SP02, 15 samples from borehole SP03, 17 samples from borehole SP04, and 12 samples from borehole SP05. The samples from boreholes SP01 to SP03 were taken to the Soil and Rock Mechanics Laboratory of UEPG to be tested for particle size analysis, density, liquid limit, and plastic limit. After these tests were performed, the soil was classified by the Unified Classification System (SUCS methodology). The samples from the SP04 borehole were used to perform the disk method to classify tropical soils (MCT methodology). Samples from the same borehole at depths of 3m, 6m, 9m, 12m, and 15m were sent to the Multiuser Laboratory Complex (C-Labmu) of UEPG to perform X-Ray diffraction tests and scanning electron microscopy tests intending to know the mineralogy of the local soil. The samples from borehole SP05, taken above the level where excavation with water circulation began, were immediately taken to the laboratory to determine their natural moisture content.

The undisturbed soil samples taken from the trenches (TR01 to TR03) were taken to the Materials and Structures Laboratory (LAME) of UFPR, kept in a humid chamber until the direct shear tests with flooded and natural moisture condition in samples of $50 \times 50 \times 20$ mm. For the tests in natural moisture, the samples were left for 24 hours in the consolidation phase followed by the rupture with a minimum of 200 minutes, the time recommended by ASTM D 3080 (ASTM, 2011) for the type of soil under study. To achieve the time established by the standard, a speed of 0.025 mm/min was used, corresponding to a total displacement of 5 mm, characterizing the rupture of the sample. The stresses defined for performing the two types of tests were 50kPa, 150kPa, and 300kPa. Deformed samples were also taken from each trench and were submitted to particle size analysis, density, liquid limit, and plastic limit in the Soil and Rock Mechanics Laboratory of UEPG.

Table 1 summarizes the number of laboratory tests performed in this research.

Regarding the thermal properties of the soil, the borehole of the test SP05 was used to install a 12m long steel bar with LM35 temperature sensors distributed in 8 different depths to measure the ground temperature variation over time. The LM35 sensor is a semiconductor temperature sensor, which consists of an integrated circuit based on PTAT (proportional to absolute temperature) and provides the temperature measurements as a function of the electrical voltage of the circuit, where 10mV is equivalent to 1 °C. The sensor has three pins, where pin 1 is the power input

Table 1. Laboratory tests.

Test	Quantity	Samples
Particle size analysis	49	SP01, SP02 and SP03 TR01, TR02 and TR03
Density	49	
Liquid limit	49	
Plastic limit	49	
Disk method	17	SP04
X-Ray diffraction	5	
Electron microscopy	5	
Natural moisture	8	SP05
Direct shear	18	TR01, TR02 and TR03

voltage from 4 to 30V, pin 2 is the data output and pin 3 is the negative (ground).

Sixteen sensors were fixed to an angle steel bar, with 2 sensors in each depth. The sensor pairs were located at 0.80m; 2.80m; 4.30m; 5.80m; 7.30m; 8.80m; 9.80m and 11.80m from the ground surface. They were fixed by epoxy glue, and they were electrically isolated with 3M ScotchcastMR resin. Figure 4a shows the bar before being inserted into the borehole, divided into 4 segments of 3 meters that were joined by screws at installation, Figure 4b shows the bar being inserted into the hole along with a tube through which the grout injection was made, and Figure 4c shows the readings being performed with a protoboard connected to a 9V battery and the wires connected to each pin of the sensors and a multimeter.

4. Laboratory results

4.1 Physical characterization tests

Figure 5 shows the results of the tests and the classification of the soils by the Unified System for the samples from Standard Penetration Test SP01. Observing the particle size distribution curves, one notices that the clay fraction is predominant from 2 to 11 meters depth, resulting in silty-sand clay soil. The samples at 8 and 9 meters depths have the highest percentages of fine soil. Successively, between 12 and 17 meters, the clay fraction decreases significantly, and the sand and silt fractions increase, characterizing silty-clay sand and followed by clayey-silt sand.

The density values found varied between 2.63 and 2.85 g/cm³ along the depth. The liquid limit values varied between 31% and 43% up to 14 meters depth, and below that decreased to approximately 25%. As for the plastic limit, up to 15 meters, it was impossible to perform the tests, that characterize non-plastic soil. Below that, the moistures obtained were between 18 and 22%, resulting in low plasticity index (between 3 and 8%). As for the classification by the Unified System, it is observed that up to 12 meters depth, the

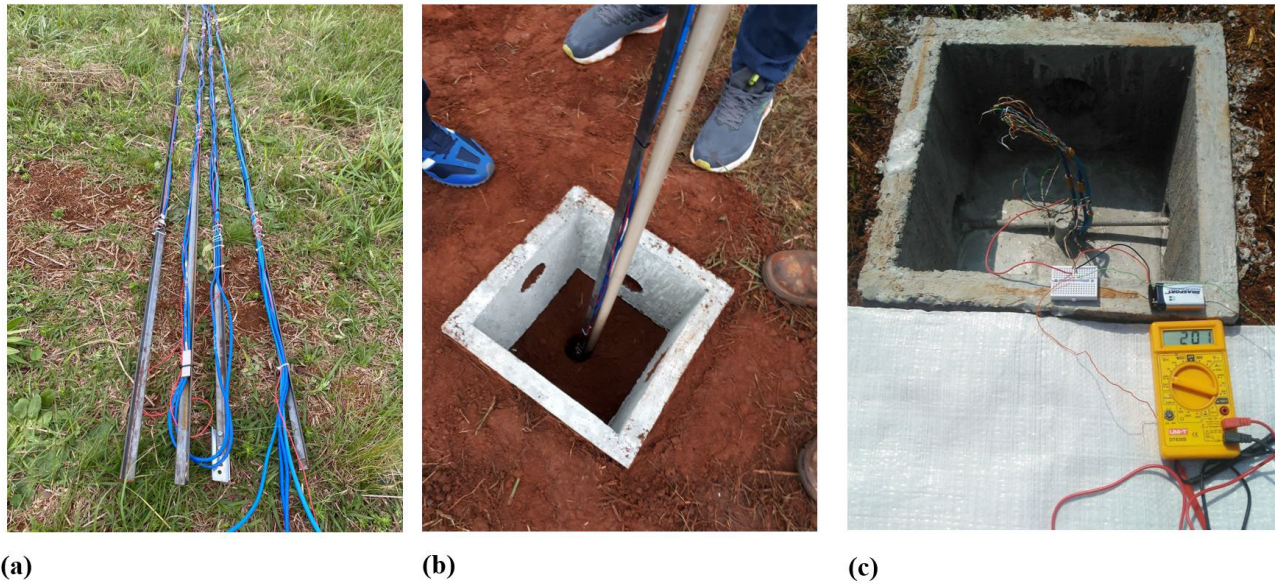


Figure 4. Instrumented bar with LM35 sensors (a) before insertion in the hole; (b) being inserted in the hole; and (c) submitted to temperature reading.

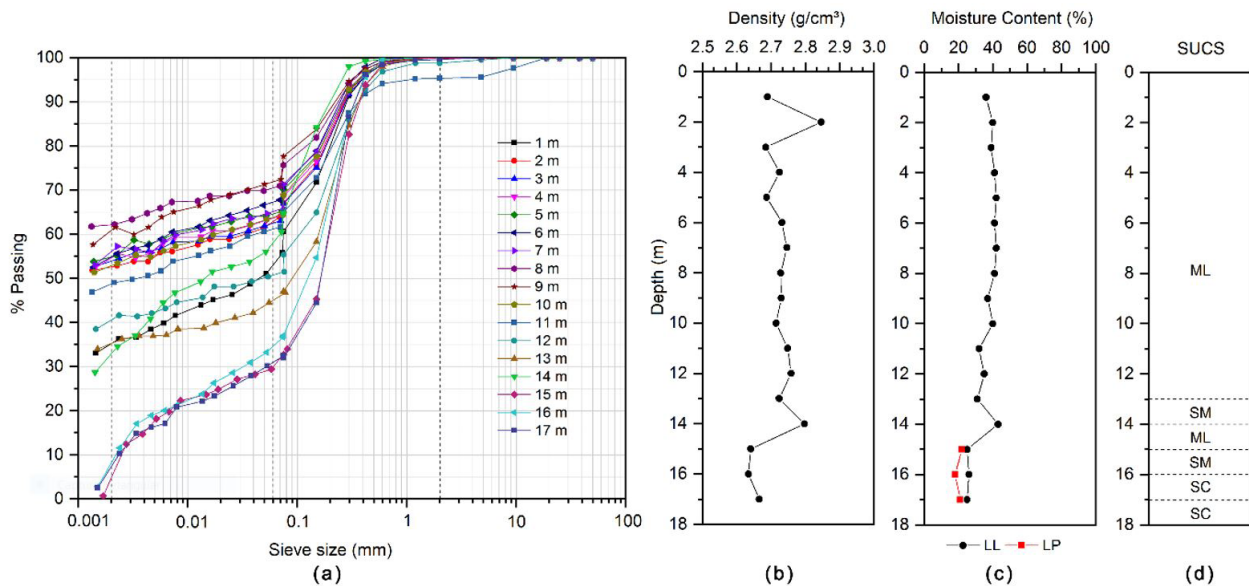


Figure 5. Characterization tests (SP01) - (a) Particle size curves (b) Density (c) Atterberg limits (d) SUCS classification.

soil is classified as silt of low plasticity (ML). In the sequence, from 15 to 17 meters, there is an intercalation between low plasticity silt (ML), silty sand (SM), and clayey sand (SC). For the samples from SP02 and SP03, very similar results were observed in the characterization tests.

The same characterization tests were performed for the deformed samples taken from trenches TR01 to TR03 at a depth of 2m and the three particle size curves obtained are very similar to those obtained for the shallowest samples from the boreholes. As for the density, the average value for

the three trenches was 2.68 g/cm^3 . For the liquid limit, the average value was 39%, and it was not possible to obtain a plastic limit value. Therefore, as expected, the tests performed with the samples from the trenches and with the samples from the boreholes were very similar.

So concluded that the subsoil of the Experimental Site is composed of a thick layer of predominantly thin, relatively homogeneous soil, around 12 meters. This soil is granulometric classified as silty-sand clay. However, as there is no plasticity when classified by the SUCS methodology, it

results in the silt of low plasticity, which may indicate that the behavior of this soil may be more similar to the behavior of a silty soil than clayey soil. Below this thick layer, there is a layer of silty sand.

In order to obtain a classification of the soils more faithful to tropical soils, the MCT methodology, developed by Nogami & Villibor (1981), was applied. This methodology classifies the soils according to their lateritic or non-lateritic behavior. This classification is performed through the execution of mini-MCV and mass loss by immersion tests. However, in 1994, the same authors proposed a method for the expeditious identification of the groups of the MCT classification, known as the Disk Method. This test is performed on cylindrical samples 20mm in diameter and 5mm in height, molded from a paste made of water and the soil fraction passing the 0.42mm sieve (Nogami & Villibor, 1994).

Three cylindrical samples were molded for each of the 17 meters of borehole SP04. First, the diametral contraction of each sample was measured after drying. Then the samples were placed on a saturated porous plate covered with filter paper. After two hours, each sample was penetrated using a standard penetrometer. With the diametral contraction (Ct) and penetration data, the MCT methodology classification chart was used to perform the classification, as illustrated in Figure 6.

It is observed that in the region called LG' (lateritic clayey soils), there is a large concentration of points, which correspond to the soils obtained from the surface up to 11 meters and the 14 meters sample. In this region there is great diametral contraction and small penetration. At 12 and 15 meters, a decrease in diametral contraction and a considerable increase in penetration values are observed.

The soils of these layers are in the LA'-LG' transition zone (lateritic sandy soils to lateritic clayey soils).

At 13, 16 and 17 meters, diametrical contractions were much smaller in relation to the other layers. At the last two depths the soils showed higher penetration values and were in the transition zone NA'-NS' (non-lateritic sandy soils and non-lateritic silty soils).

It is concluded that the subsoil of the Experimental Site is constituted in almost all the analyzed depth by lateritic soil, the first 12 meters being clay soil and, in the sequence, sandy soil, which confirms the results of the characterization analyses.

As the natural soil moisture significantly affects its thermal conductivity, the samples extracted from Standard Penetration Test SP05 were used to measure the natural soil moisture in depth. However, the excavation process during the drilling required water circulation from 7m, so the natural moistures could only be verified above this depth. There was not much variation in moisture for the depth studied, and the average value was around 36%. This unsaturated soil occurs until a depth of approximately 11m, where the water level is located, and the soil becomes saturated.

4.2 Mineralogical characterization tests

The mineralogical characterization of the CEEG-PG soil was performed through X-Ray diffraction (XRD) and scanning electron microscopy (SEM) at UEPG Multi-users Laboratories Complex (C-Labmu). Five samples, taken from Standard Penetration Test SP04 at depths of 3m, 6m, 9m, 12m, and 15m, were used. In the diffractogram analysis, a remarkable similarity between the results of the 3m, 6m, and 9m samples was noticed and between the 12m and 15m

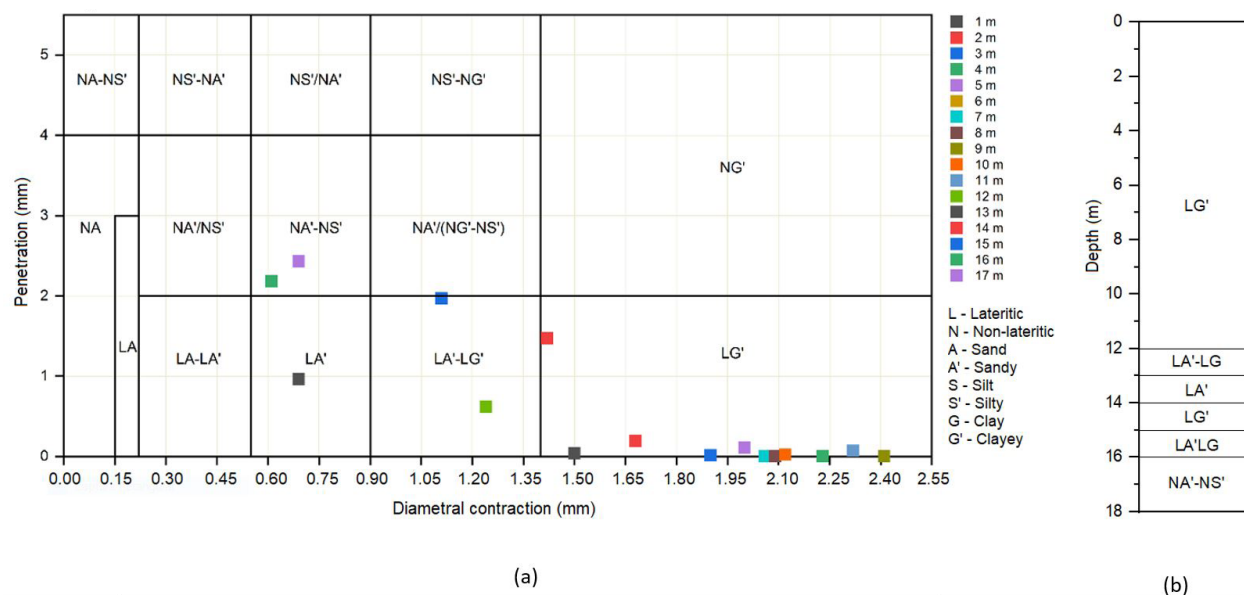


Figure 6. Classification test by Disk Method - (a) Classification chart (b) MCT classification.

samples. This was expected because the Standard Penetration Test and the physical characterizations in the laboratory indicated a thick upper layer of relatively homogeneous clay soil, followed by a layer of sandy soil. Figure 7 shows the XRD diffractograms for the clay soil (3m, 6m, and 9m samples), and Figure 8 shows the diffractograms for the sandy soil (12m and 15m samples).

Analyzing Figure 7, which corresponds to the diffractograms of the clayey soil, it is noted the presence of the quartz mineral, probably resulting from the weathering of the sandstone and mainly responsible for the portion of sand present in large quantities in this material, which makes it a sandy-clay soil as observed in the grain size curves. As for the lateritic nature of the soils, the presence of kaolinite, which is a hydrated

aluminum clay mineral, and iron oxide is observed. These minerals prove the lateritic behavior of the soil because the lateralization process results in the accumulation of large amounts of iron and aluminum oxides in the soil and gives it a reddish color. Another oxide observed was calcium oxide, which may result from the weathering of sandstone, which is a sedimentary rock composed of grains of silica or quartz, linked by siliceous, clay, or limestone cement.

For the sandy soil, with diffractograms shown in Figure 8, quartz and clay mineral kaolinite was also observed, probably quartz appears in greater quantity than in the clayey soil, the other oxides were not identified.

The analysis of these diffractograms reflects the geological origin of the soils in the region because the Experimental Site is located over the Ponta Grossa Formation, which is mainly composed of shales, which are clayey rocks, besides the presence of diabase dikes of the Serra Geral Formation. The topsoil layer in the Experimental Site is characterized as residual soil resulting from the rocks of these formations. Close by and beneath these formations is the Furnas Formation, composed of quartz sandstones, responsible for the presence of quartz in all the samples tested and for the residual origin of the lower sandy soil layer.

In the micrographs obtained for the same samples, a similarity in grain shape is noticed in the samples of 3m, 6m, and 9m. More angular grains are noted in the 15m sample, characteristic of sandy soils but with adhered clay minerals. The 12m sample shows a transition between the grain shapes. Figures 9 and 10 shows the scanning electron microscopy for the 3m and 15m samples.

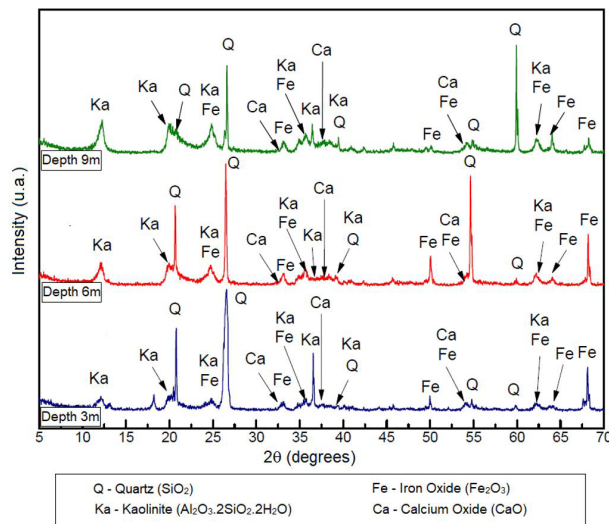


Figure 7. X-Ray diffractograms for the 3m, 6m, and 9m samples.

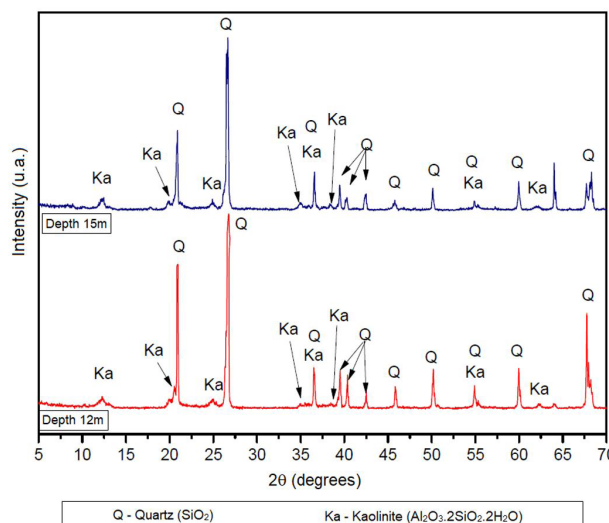


Figure 8. X-Ray diffractograms for the 12m, and 15m samples.

4.3 Mechanical characterization tests

The trenches were excavated to obtain undisturbed samples at a depth of 2 meters to carry out direct shear tests. As the clay soil layer is relatively homogeneous, it is understood that the results obtained from these tests can be representative of the entire surface layer.

Figure 11 and Figure 12 present the shear strength envelopes obtained in the direct shear tests for trenches TR01 and TR02, respectively, for stresses of 50kPa, 150kPa, and 300kPa. When comparing the results, it can be seen that there is an increase in the shear stress of the natural moisture condition compared to the test with the flooded sample.

Note that for the samples in the natural moisture condition of trench TR01, an internal friction angle (ϕ') of 21.0° and a cohesive intercept (c') of 56.6kPa were obtained. For the saturated samples, the internal friction angle increased to 24.3° , and the cohesive intercept decreased to 16.4kPa.

For the samples in trench TR02, the internal friction angle obtained for the two conditions were very close, being 21.9° for natural moisture and 22.3° for the flooded tests. There was also a significant decrease in the cohesive intercept with increasing saturation, going from 50.8kPa to 19.1kPa.

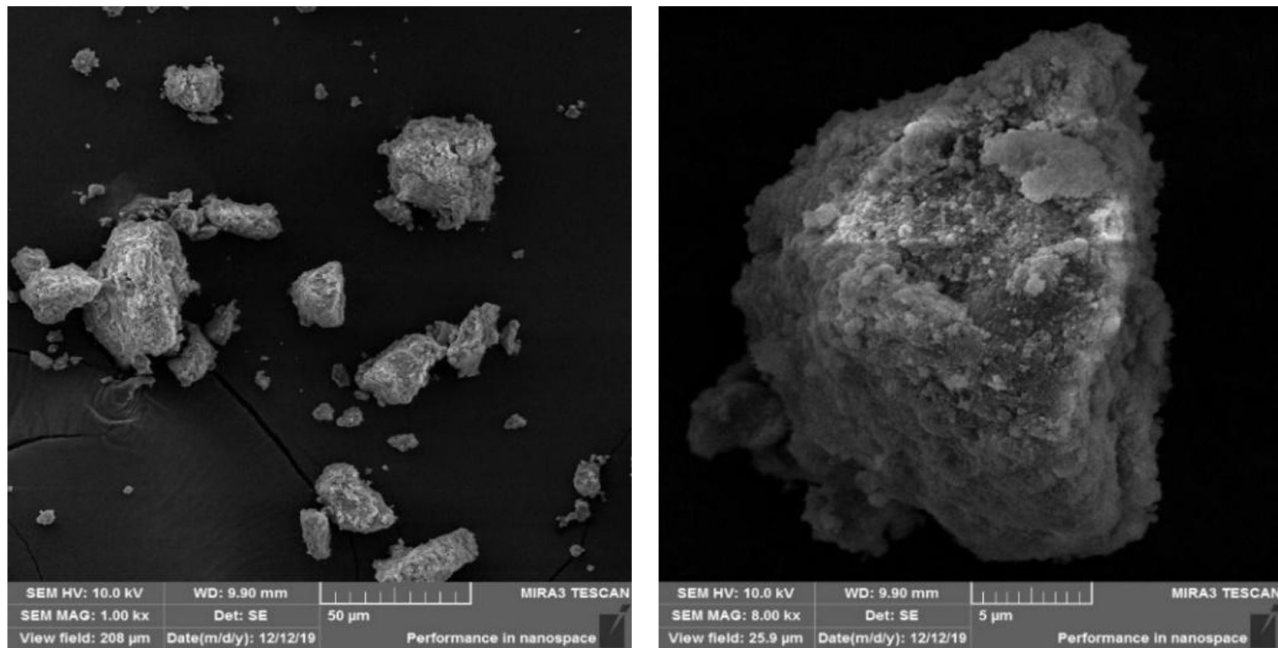


Figure 9. Scanning electron microscopy for the 3m sample.

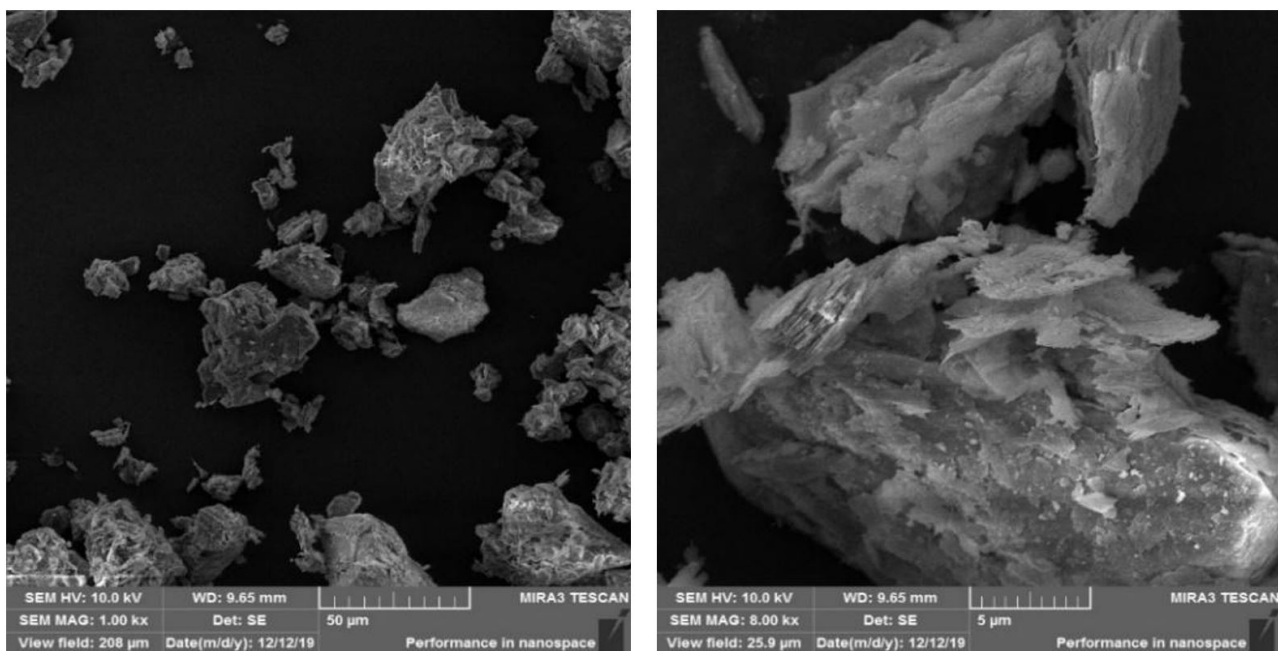


Figure 10. Scanning electron microscopy for the 15m sample.

The moisture variation in the direct shear test showed that the cohesive intercept showed more significant variability than the soil friction angle. As the water table is deep, the high cohesion at natural moisture results from the unsaturated soil suction.

5. Field results

The Standard Penetration Test (SPT) was performed in three separate stages, which totaled 5 tests. Table 2 summarizes the N_{SPT} obtained for each soil layer in the 5 boreholes and

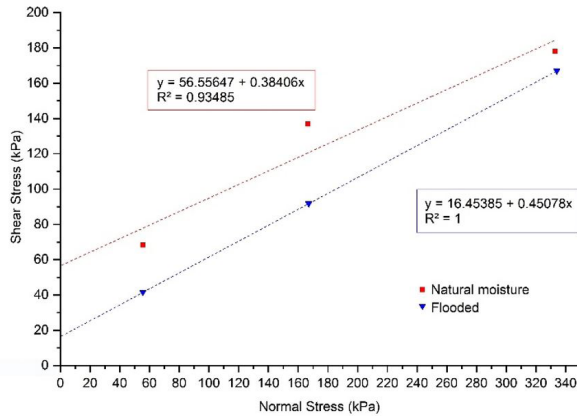


Figure 11. Shear strength envelopes for trench TR01.

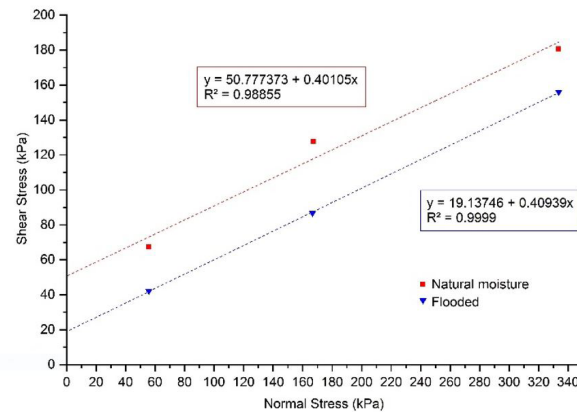


Figure 12. Shear strength envelopes for trench TR02.

presents information on soil type and water level position. It can be seen that all boreholes had a reasonably thick layer, around 12m, of sandy-silt clay with low consistency, followed by a layer of sand with a sudden increase in compactness. The average water level was found at 11.2m from the surface.

The present layer of clayey soil may have a probable residual origin of the Ponta Grossa Formation shale, and the sand may be a residual soil of the Furnas Formation, as the latter dips beneath the Ponta Grossa Formation. Petri (1948) named the interval between these two formations “transition layers” because it is a complicated contact to be observed in mapping since the shales of the Ponta Grossa Formation are little resistant to weathering, not forming relief breaks over the sandstones, besides presenting a relief aspect similar to the soil that occurs over the Furnas Formation.

Regarding the temperature measurements, they are being done using a multimeter and temperature sensors type LM35, which were fixed to a 12m long steel bar and inserted in the borehole SP05. Sixteen sensors were installed along the bar distributed in 8 different levels, 2 sensors at each level. The pair of sensors installed at the greatest depth, 11.80m from the surface, presented a defect, and it was not possible to take any readings. How these sensors were located below the water level, believed that they suffered some damage during installation that compromised the electrical isolation, leaving the sensors short-circuited.

After installing the bar, the readings were measured daily for two weeks, but as the variation in their value was small, the readings started to be taken every other day. The installation of the temperature sensors was done close to the writing of this article, so the history of readings collected is not yet significant for the analysis of temperature variation over time. However, Figure 13 shows the readings already

Table 2. Standard Penetration Test (SPT).

Dep. (m)	N _{SPT}					Soil
	SP01	SP02	SP03	SP04	SP05	
1	2/48	2/42	3	4	3	Silty-sandy clay
2	2	2	6	5	6	
3	2	2/45	2	3	8	
4	2	2	3	4	6	
5	2	2	3	8	9	
6	4	5	5	9	9	
7	5	7	7	5	6	
8	4	4	7	w6	7	
9	2/52	5	5	5	7	
10	1/45	6	5	7	11	
11	5	5	3	7	13	
12	5	7	5	11	14	
13	6	11	4	12	-	Silty Sand
14	9	8	10	15	-	
15	36	39/21	24	-	-	
16	48	-	-	-	-	
NA	10,2	11,9	12,1	10,2	11,8	m

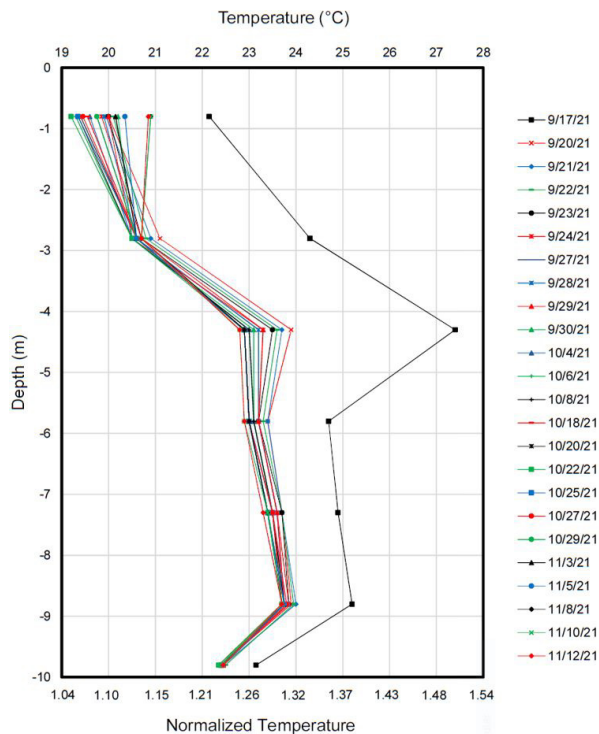


Figure 13. Underground temperature measurements and normalized temperature.

taken, and it is possible to verify the influence of the concrete heat hydration on the measurements taken the day after concreting, which resulted in much higher temperatures, which gradually decreased over the following days.

Even with a still small interval of readings, it can be seen that the temperature presents a greater variation in the first four meters of depth, becoming practically constant after this depth and reducing again when approaching the water level, which is approximately 11m. The observed behavior is comparable to that described by Laloui & Loria (2020), considering that the initial readings were taken in late winter and the most recent in spring.

On the lower axis in Figure 13 the soil temperature is shown divided by the local average temperature (18.2°C), and it is possible to notice that the measured soil temperatures are on average 30% higher than the local average temperature.

6. Final remarks

Field studies to evaluate the feasibility of the use of shallow geothermal energy as a new renewable energy source in regions of different climatic conditions is fundamental for the development of this technology in Brazil, due to its continental extension. In particular, in the Brazilian Southern region, where the current study is being developed, the use of shallow geothermal energy may be feasible considering the annual average temperatures.

A complete soil site characterization is needed for the development of field studies on the shallow geothermal energy exploitation. In Brazil, studies of this nature have already been developed in the country's Southeast region, and this paper presents the first site characterization programme carried out in the Southern region, expanding the scope of the knowledge base applicable to geothermal utilization in the country.

Considering that the main phenomenon that controls the performance of shallow geothermal energy systems is the heat transfer by conduction, and that the ground parameters influence this phenomenon, the complete characterization of the soil is fundamental. The geotechnical profile of the test site, obtained from field and laboratory tests, revealed a thick layer of sandy-silt clay soil (around 12m), with lateritic behavior evidenced by the Disk Method analysis. The deepest layer is composed of silty sand, with markedly higher penetration resistance than the clay layer. The water level depth was around 11m.

The mineralogical characterization through X-Ray diffraction tests and scanning electron microscopy corroborated the lateritic nature of the soil due to the identification of iron oxides in addition to quartz and kaolinite. These analyses also reflected the geological origin of the soils in the region since CEEG-PG is located over the Ponta Grossa Formation, which is mainly composed of shales and the presence of diabase dikes of the Serra Geral Formation. The thick layer of a clayey soil is characterized as residual soil resulting from these formations. The influence of the Furnas Formation, consisting of quartz sandstones, was denoted by the presence of quartz in all samples tested and the residual origin of the lower sandy layer.

The soil strength characterization is crucial for future studies on the use of foundation piles for geothermal energy application. From the results of direct shear tests on flooded soil samples and in its natural moisture condition, it was observed that the internal friction angle was less sensitive to saturation degree, varying between 21° and 24° for all cases. However, the cohesive intercepts for the unsaturated condition, resulted slightly higher compared to the flooded conditions, indicating the relevance of the suction effect on the unsaturated soil resistance.

It is important to emphasize the relevance of the soil resistance characterization along the depth through Standard Penetration Tests (SPT), because the foundations mechanical behavior by piles is estimated with these tests and, subsequently, the thermomechanical behavior is evaluated when the foundation works as a heat exchanger with the ground.

Finally, the preliminary results of the ground temperatures variations are in accordance with that reported in the literature for a typical soil temperature profile, showing more expressive oscillations near the ground surface and apparent constancy in the deeper layers. The constant temperature found at deeper depths is around 30% higher than the annual average air

temperature. This work also presents the thickness of the top soil zone influenced by the variation of the air temperature during the year (for different seasons).

Acknowledgements

The authors would like to thank the Postgraduate Program Civil Engineering (PPGECC) of Federal University of Parana (UFPR), the drilling company Gaioski Engenharia for the execution of the Standard Penetration Test, the Multi-User Laboratory Complex (C-Labmu) of UEPG for the help in performing the Scanning Electron Microscopy and X-Ray Diffraction tests, and SIMEPAR for providing the historical data on precipitation and temperature in the city of Ponta Grossa-PR.

Declaration of interest

The authors have no conflicts of interest to declare. All co-authors have observed and affirmed the contents of the paper and there is no financial interest to report.

Authors' contributions

Bianca Penteado de Almeida Tonus: conceptualization, data curation, funding acquisition, investigation, methodology, project administration, resources, supervision, validation, visualization, writing – original draft, writing – review & editing. Carlos Emmanuel Ribeiro Lautenschläger: conceptualization, funding acquisition, resources, validation, visualization, writing – review & editing. Amanda Fetzer Visintin: Visualization, Writing – review & editing. Vítor Pereira Faro: conceptualization, funding acquisition, methodology, project administration, resources, supervision, validation, writing – review & editing. Cristina de Hollanda Cavalcanti Tsuha: conceptualization, methodology, supervision, writing – review & editing.

List of symbols

<i>ASTM</i>	American Society for Testing and Materials
<i>c'</i>	Cohesive Intercept
<i>Ca</i>	Calcium Oxide
<i>CEEG-PG</i>	Geotechnical Experimental Site of Ponta Grossa City
<i>C-Labmu</i>	Multiuser Laboratory Complex of State University of Ponta Grossa
<i>Ct</i>	Diametral Contraction
<i>EESC/USP</i>	São Carlos School of Engineering of University of São Paulo
<i>EPE</i>	Energy Research Company
<i>Fe</i>	Iron Oxide
<i>GSHP</i>	Geothermal Source Heat Pump
<i>Ka</i>	Kaolinite

<i>LA'-LG'</i>	Lateritic Sandy Soils to Lateritic Clayey Soils
<i>LAME</i>	Materials and Structures Laboratory of Federal University of Parana
<i>LG'</i>	Lateritic Clayey Soils
<i>LM35</i>	Temperature sensor
<i>MCT</i>	Miniature, Compacted, Tropical
<i>ML</i>	Silt of Low Plasticity
<i>NA'-NS</i>	Non-lateritic Sandy Soils to Non-lateritic Silty Soils
<i>Q</i>	Quartz
<i>SIMEPAR</i>	Paraná Meteorological System
<i>SIN</i>	National Interconnected System
<i>SC</i>	Clayey Sand
<i>SEM</i>	Scanning Electron Microscopy
<i>SM</i>	Silty Sand
<i>SPT</i>	Standard Penetration Tests
<i>SUCS</i>	Unified Classification System
<i>UEPG</i>	State University of Ponta Grossa
<i>UFPR</i>	Federal University of Parana
<i>XRD</i>	X-Ray diffraction
ϕ'	Angle of Internal Friction

References

- Amatya, B.L., Soga, K., Bourne-Webb, P.J., Amis, T., & Laloui, L. (2012). Thermo-mechanical behaviour of energy piles. *Geotechnique*, 62(6), 503-519.
- American Society for Testing and Materials – ASTM. (2011). *ASTM D 3080: standard test method for direct shear test of soils under consolidated drained conditions*. Philadelphia: ASTM.
- Brasil. Ministry of Mines & Energy. (2018). *Uso de Ar Condicionado no Setor Residencial Brasileiro: Perspectivas e contribuições para o avanço em eficiência energética* (Nota Técnica EPE, No. 030/2018). Brasília, DF (in Portuguese). Retrieved in December 3, 2021, from <https://www.epe.gov.br/pt/publicacoes-dados-abertos/publicacoes/nota-tecnica-epe-030-2018>
- Brasil. Ministry of Mines & Energy. (2020a). *Anuário Estatístico de Energia Elétrica 2020: ano base 2019*. Brasília: Empresa de Pesquisa Energética. Retrieved in December 3, 2021, from <https://www.epe.gov.br/pt/publicacoes-dados-abertos/publicacoes/anuario-estatistico-de-energia-eletrica>
- Brasil. Ministry of Mines & Energy. (2020b). *Plano Nacional de Energia 2050*. Brasília: Empresa de Pesquisa Energética. Brasília: Empresa de Pesquisa Energética. Retrieved in December 3, 2021, from <https://www.epe.gov.br/sites-pt/publicacoes-dados-abertos/publicacoes/PublicacoesArquivos/publicacao-227/topico-563/Relatorio%20Final%20do%20PNE%202050.pdf>
- Laloui, L., & Loria, A.F.R. (2020). *Analysis and design of energy geostructures: theoretical essentials and practical application*. United Kingdom: Elsevier.

- Lee, S., Speight, J.G., & Loyalka, S.K. (2007). *Handbook of alternative fuel technologies*. Boca Raton: CRC Press.
- Loveridge, F., McCartney, J.S., Narsilio, G.A., & Sanchez, M. (2020). Energy geostructures: a review of analysis approaches, in situ testing and model scale experiments. *Geomechanics for Energy and the Environment*, 22, 100173.
- Morais, T.S.O. (2019). *Comportamento térmico e termomecânico de fundações por estacas trocadoras de calor em solos não saturados em região de clima subtropical* [PhD thesis]. Graduate Geotechnical Program, São Carlos School of Engineering, University of São Paulo.
- Narsilio, G.A., Bidarmaghaz, A., & Colls, S. (2014). Geothermal energy: introducing an emerging technology. *KSCE Journal of Civil Engineering*, 15, 643-653.
- Nogami, J.S., & Villibor, D.F. (1981). Uma nova classificação de solos para finalidades rodoviárias. In *Simpósio Brasileiro de Solos Tropicais em Engenharia* (Vol. 1, pp. 30-41), Rio de Janeiro, Brazil.
- Nogami, J.S., & Villibor, D.F. (1994). Identificação expedita dos grupos da classificação MCT para solos tropicais. In *Anais do X Congresso Brasileiro de Mecânica dos Solos e Engenharia de Fundações* (Vol. 4, pp. 1293-1300), Foz do Iguaçu, Brazil. (in Portuguese).
- Petri, S. (1948). *Contribuição ao estudo do Devoniano Paranaense* (Boletim DGM/DNPM). Rio de Janeiro. (in Portuguese).
- Rees, S.W., Adjali, M.H., Zhou, Z., Davies, M., & Thomas, H.R. (2000). Ground heat transfer effects on the thermal performance of earth-contact structures. *Renewable & Sustainable Energy Reviews*, 4(3), 213-265.
- Sani, A.K., Singh, R.M., Amis, T., & Cavarretta, I. (2019). A review on the performance of geothermal energy pile foundation, its design process and applications. *Renewable & Sustainable Energy Reviews*, 106, 54-78.
- Sistema Meteorológico do Paraná – SIMEPAR. (2021). *Ponta Grossa city temperature and precipitation data provided by email*. Curitiba.

Centrifuge modeling of temperature effects on the pullout capacity of torpedo piles in soft clay

Ismaail Ghaaowd¹ , John S. McCartney^{2#} , Fernando Saboya³ 

Article

Keywords

Thermal improvement
Torpedo piles
Centrifuge physical modelling
Pullout testing

Abstract

This study presents the results from centrifuge modeling experiments performed to understand the effects of temperature changes on the vertical pullout capacity of scale-model torpedo piles embedded in soft clay layers. The model torpedo pile is a pointed stainless-steel cylinder with fins at the top, installed by self-weight to the base of a clay layer using a stepper motor. An internal electrical resistance heater was used to control the pile temperature. The torpedo pile was first heated until the temperature and pore water pressure of the surrounding clay layer stabilized (drained conditions), after which the torpedo pile was cooled. Pullout tests performed on torpedo piles indicate that allowing drainage of excess pore water pressures induced by heating to different temperatures followed by cooling leads to an increase in axial pullout capacity with maximum temperature but does not affect the pullout stiffness. Push-pull T-bar penetration tests performed before and after pile heating indicate that an increase in undrained shear strength of the clay occurs near the torpedo pile, and post-test gravimetric water content measurements indicate a greater decrease in void ratio occurred in the soil layers heated to higher temperatures. The pullout capacity of the torpedo pile was found to follow a linear trend with maximum pile temperature change, but with a smaller slope than that observed for end-bearing energy piles tested in previous studies in the same clay.

1. Introduction

Torpedo piles are an economical method for anchoring offshore floating structures in deep water soil deposits (Bonfim dos Santos et al., 2004; Gilbert et al., 2008). Different sizes of torpedo piles are used in practice, with diameters varying from 0.75 to 1.10 m and lengths varying from 10 to 12 m. Larger torpedo piles are typically not encountered due to limitations in the capacities of transport vessels and offshore handling equipment. Although torpedo pile installation is cost effective as they are installed into the seafloor by self-weight penetration under high velocities associated with free fall through the water, the process of transporting the torpedo piles to a given location and rigging them for installation may be time consuming. Accordingly, any method to increase the pullout capacity of a torpedo pile so that the total number of piles required to anchor an offshore floating structure can be reduced will lead to significant cost savings. If the torpedo pile is embedded into clay layers in deep water conditions offshore, conventional soil improvement techniques like surcharge loading, vertical drains, electro-osmosis, are difficult

to implement. Instead, thermal consolidation may be a useful approach for improvement of the soil surrounding the pile.

The concept of soil improvement using thermal consolidation is shown in Figure 1 for a torpedo pile installed within a clay layer. In this method, the torpedo pile is equipped with an internal heating element powered by either an electrical resistance heater or a chemical reaction. After installation, the heater can be operated to reach a target temperature or energy output. Depending on the drainage conditions of the soil, changes in pore water pressure Δu_w and soil surface settlement ΔH are expected for a given change in temperature ΔT . For undrained conditions, it is well known that changes in temperature will lead to an increase in pore water pressure (Campanella & Mitchell, 1968), with a magnitude depending on the plasticity index, initial void ratio, and initial effective stress (Ghaaowd et al., 2017). Further, heating of soils in undrained conditions will coincide with an initial thermo-elastic expansion (upward ΔH) of the soil around the pile (Uchaipichat & Khalili, 2009). However, fully undrained conditions are not expected in the field for the boundary conditions shown in Figure 1. Instead, it is expected that the low permeability clay surrounding the heated torpedo pile

[#]Corresponding author. E-mail address: mccartney@ucsd.edu

¹Turner-Fairbank Highway Research Center, McLean, VA, USA.

²University of California San Diego, Department of Structural Engineering, La Jolla, CA, USA.

³Universidade Estadual do Norte Fluminense Darcy Ribeiro, Department of Civil Engineering, Rio de Janeiro, RJ, Brasil.

Submitted on January 20, 2022; Final Acceptance on February 11, 2022; Discussion open until May 31, 2022.

<https://doi.org/10.28927/SR.2022.000822>



This is an Open Access article distributed under the terms of the Creative Commons Attribution License, which permits unrestricted use, distribution, and reproduction in any medium, provided the original work is properly cited.

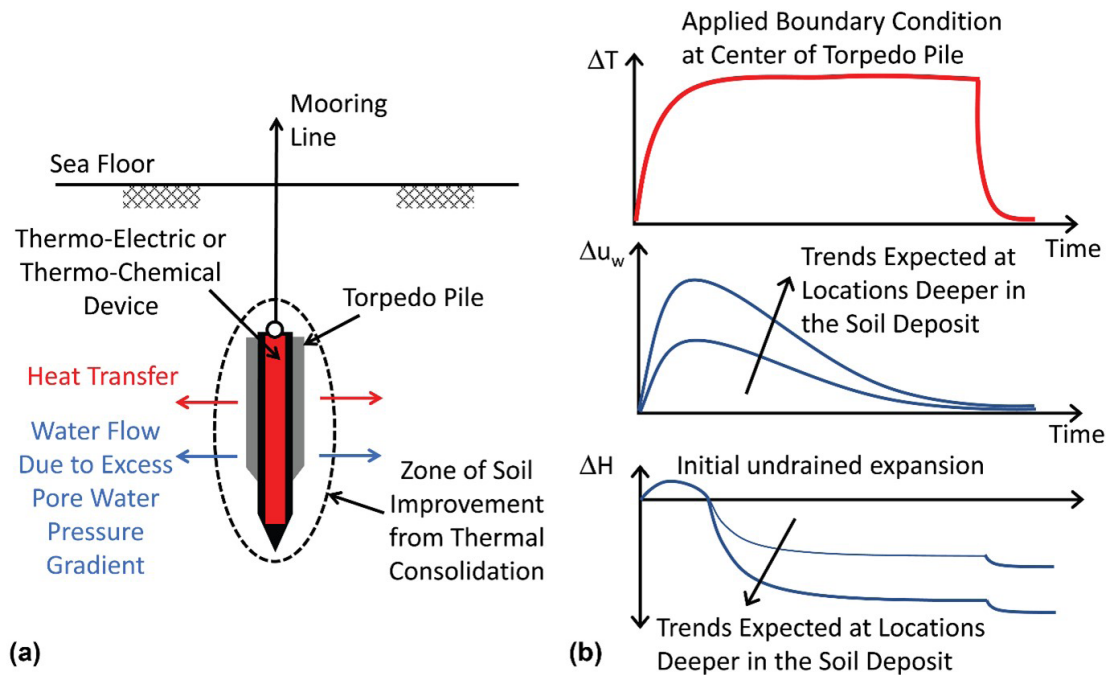


Figure 1. Concept of thermal improvement of soft clays around torpedo piles: (a) schematic of an installed torpedo pile with an internal heater; (b) hypothetical trends in pile temperature, excess pore water pressure in soil at different depths, and changes in soil volume surrounding the torpedo pile.

will have partial drainage conditions, with some increase in pore water pressure during heating but less than that observed in fully undrained conditions. Regardless, the increase in pore water pressure in the clay next to the heated pile will lead to a hydraulic gradient. This hydraulic gradient will cause water to flow away from the pile and dissipation of the excess pore water pressure, a process referred to as thermal consolidation (Zeinali & Abdelaziz, 2021). An increase then decrease in pore water pressure around a heating element in soft clay was observed in centrifuge modeling experiments by Maddocks & Savvidou (1984). It is important to maintain the elevated temperature during this water flow process, during which a permanent contraction of the soil is expected if the soil is normally consolidated or lightly overconsolidated (downward ΔH). The contraction of normally consolidated and lightly overconsolidated soils during drained heating has been observed in several element-scale studies (e.g., Baldi et al., 1988; Burghignoli et al., 2000; Cekerevac & Laloui, 2004; Abuel-Naga et al., 2007a, b; Towhata et al., 1993; Vega & McCartney, 2015; Takai et al., 2016; Samarakoon & McCartney, 2020). The coupling between changes in temperature and settlement have also been observed in the field. Bergenstahl et al. (1994) applied a change in temperature of approximately 60 °C to a 10 m-thick layer of clay over the course of 8.5 months and observed a thermally-induced settlement of 37 mm, while Pothiraksanon et al. (2010) applied a change in temperature of approximately 60 °C over the course of 200 days, and observed a thermally-induced

settlement of approximately 120 mm. Cooling is expected to lead to a further contraction of the soil surrounding the pile, although contraction during cooling may depend on the rate of cooling. Thermal improvement is only appropriate for normally consolidated and lightly consolidated soils, as heavily overconsolidated soils are expected to expand and contract elastically during heating and cooling, respectively.

The in-situ heating-cooling process shown in Figure 1 is expected to lead to a reduction in void ratio e of the normally consolidated or lightly overconsolidated soil surrounding the torpedo pile. This is expected to lead to an increase in the average undrained shear strength of the soil layer along the length of the torpedo pile, which will in turn lead to an increase in the pullout capacity of the torpedo pile. The mechanisms of thermal improvement in the undrained shear strength of soft clay have been evaluated in element-scale tests in studies like Houston et al. (1985), Abuel-Naga et al. (2007c) and Samarakoon et al. (2018). These studies generally found that undrained shearing of soils after drained heating will lead to an increase in undrained shear strength. Houston et al. (1985) found that shearing of soils after undrained heating will lead to a decrease in undrained shear strength associated with the reduction in effective stress associated with the thermally induced pore water pressures. Accordingly, it is critical to ensure that the heating process is sufficiently long for the excess pore water pressures to dissipate. While most previous of the studies mentioned above focused on the increase in undrained shear strength due to heating alone,

Samarakoon et al. (2018) found that a heating-cooling cycle leads to a further increase in shear strength of normally consolidated soil, and that the initial void ratio may play a role in the amount of change in shear strength of the soil. This observation is supported by the thermal consolidation experiments of Burghignoli et al. (2000) and Vega & McCartney (2015) who found that a heating-cooling cycle will lead to a further reduction in volume of soils than that encountered after heating alone.

There is evidence in the literature that thermal consolidation may be a useful technique to improve the pullout capacity of torpedo piles. Centrifuge modeling studies like Ghaaowd et al. (2018) and Ghaaowd & McCartney (2018, 2021) found that the pullout capacity of end-bearing piles embedded in soft clays could be improved by thermal consolidation induced by a heater embedded within the pile. The piles investigated in these previous studies extended through the full length of the clay layer, so thermal consolidation only affected the side shear resistance. Ng et al. (2014, 2021) performed centrifuge modeling studies on semi-floating energy piles in soft clay and observed settlement of the piles during cycles of heating and cooling, which can be attributed to thermal consolidation. However, they did not load the energy piles to failure after the heating-cooling cycles. McCartney & Murphy (2017) observed a transient change in axial stresses and strains within an energy pile in claystone after multiple years of heating and cooling, potentially associated with thermal consolidation of the claystone. Yazdani et al. (2019) performed pressure chamber tests to study the effects of elevated temperature on the shaft resistance of an energy pile in soft clay and observed an increased side shear capacity with increased temperature. Yazdani et al. (2021) attributed this increase to an increase in lateral earth pressure because the heating period in the experiments was not sufficient to permit full drainage of the pore water pressures. Different from the previous studies, torpedo piles are typically fully embedded within a soil layer, so heating may lead to an improvement in both the side shear capacity and the upward end bearing capacity. This justifies the need to perform further experiments on the effects of temperature on the pullout capacity of torpedo piles.

This study uses a centrifuge modeling approach developed by Ghaaowd et al. (2018) and Ghaaowd & McCartney (2021) to evaluate the effects of drained heating-cooling cycles on the pullout capacity of torpedo piles embedded in soft clay layers. Centrifuge modeling was used in this study because the pore water pressure generation during undrained heating is sensitive to the initial mean effective stress in the clay layer, and the effective stresses in a centrifuge model clay layer are similar to those in a prototype clay layer. Centrifuge modeling also permits the use of time scaling to simulate the effects of long duration heating-cooling cycles in the field, as diffusive time scales according to $1/N^2$ where N is the g-level (Ng et al., 2020). The Actidyne C61-3 centrifuge at the University of California San Diego was used to perform

four tests on torpedo piles in separate clay layers. The four tests involved installation of self-weight installation of the torpedo pile into the clay layers at a constant displacement rate, heating to different target temperatures (20, 45, 65, and 80 °C), cooling back to ambient temperature of 20 °C, and vertical pullout of the torpedo pile at a constant displacement rate. In addition to presentation of the pullout versus displacement curves for the four tests, T-bar penetration results permit evaluation of the impact of the heating-cooling cycle on the undrained shear strength profiles of the clay layer near the torpedo piles.

2. Materials and methods

2.1 Materials

The soil used in the centrifuge modeling experiments was kaolinite clay obtained from M&M Clays Inc. of McIntyre, Georgia. The liquid limit of the kaolinite clay is around 47% and the plastic limit was 28%, so the clay classifies as CL according to the Unified Soil Classification Scheme (USCS). An isotropic compression test performed by Ghaaowd & McCartney (2021) indicates that the slopes of the normal compression line (λ) and the recompression line (κ) for the clay are 0.080 and 0.016, respectively. The hydraulic conductivity of this kaolinite ranges from 2.8×10^{-9} to 8.2×10^{-9} m/s for void ratios ranging from 1.05 to 1.45, respectively. These values are relatively small indicating that partially drained conditions can be expected during heating of the torpedo pile as shown in Figure 1. Ghaaowd & McCartney (2021) reported that the thermal conductivity of this kaolinite ranged from 1.1 to 1.8 W/m°C for void ratios ranging from 3.0 to 0.8, respectively. Ottawa F-65 sand was used as a drainage layer at the base of the clay layers formed in this study. The grain size of this uniform sand varies from 0.1 mm to 0.5 mm, and the sand classifies as SP accordingly to the USCS. The hydraulic conductivity of the sand varies over a narrow range from 2.2×10^{-3} to 1.2×10^{-3} m/s for the loosest and densest states, respectively (Bastidas, 2016).

2.2 Experimental setup

The centrifuge physical modeling tests were performed using a 50th-scale-model torpedo pile that fabricated from stainless steel, as shown in Figure 2a. Although torpedo piles used in the field often have fins that extend the length of the main pile body for hydrodynamic stability (e.g., Bonfim dos Santos et al., 2004), the scale-model torpedo pile was designed to have a uniform cylindrical body with a sharp tip and fins only on the tail to simplify the heat transfer process from the main body of the torpedo pile by replicating a cylinder heat source. The main body of the scale-model torpedo pile has an outer diameter of 15.75 mm (0.79 m in prototype scale) and a length of 108.6 mm (5.43 m in prototype scale) and is hollow to accommodate a cylindrical heating element. The Firerod

1707 heating element from Watlow Electric Manufacturing, Inc. of St. Louis, MO has a length of 101 mm, a diameter of 12.6 mm, and fits snugly within the main cylindrical body of the torpedo pile. The heating element has a maximum power output of 500 W and was operated in temperature-control mode using feedback from an internal thermocouple connected to a Watlow temperature controller mounted on the centrifuge arm. The tip and the tail of the torpedo pile can be threaded into the main body of the torpedo pile to form the scale model torpedo pile having a total length of 160 mm (8 m in prototype scale). The tail of the torpedo pile incorporates a hole to pass the wires from the heating element and includes a horizontal hole that can be used to attach a cable for installation and pullout of the torpedo pile. The picture of the assembled scale-model torpedo pile is shown in Figure 2b after testing. The area for upward end bearing of the torpedo pile is complex due to the presence of the fins and the tapered tail section connected to the cabling, but it is clear from this picture that clay does interact with the tail. As will be discussed in the analysis section, an equivalent diameter of 15.75 mm equal to that of the main body of the torpedo pile was used to calculate the upward bearing capacity of the torpedo pile to account for these different bearing mechanisms.

A schematic of the container with an integrated loading system used to evaluate the effects of temperature effects on the pullout capacity of torpedo piles in clay is shown in Figure 3(a). The container consists of a cylindrical aluminum tank having an inner diameter of 550 mm, a wall thickness of 16 mm, and a height of 470 mm that resting atop an “O”-ring seal in a groove within a 620 mm-square base plate. The cylindrical

tank is held down to the base plate via four hold-down tabs on the side of the cylinder that fit around 50-mm diameter threaded rods that are threaded into the 50 mm-thick base plate. A 620 mm-square upper reaction plate is mounted on the top of the threaded rods. The upper reaction plate supports stepper motors that are used for loading the torpedo pile (in the center of the container) and a T-bar penetrometer (offset from the center by 100 mm and not shown in Figure 3a and serves as a mounting location for a 100 mm-long linear potentiometer used for tracking pullout displacement. The torpedo pile is connected via the stainless-steel cable to a load cell that is connected to the stepper motor in the center of the upper reaction plate, which permits the pile to be lowered into the clay layer under its self-weight and pulled out vertically after the thermal improvement process. Due to the length restrictions of the stepper motor drive rod within the centrifuge, the initial position of the T-bar was a depth of 60 mm (a prototype scale depth of 3 m) within the clay layer. Accordingly, the insertion and extraction of the T-bar only permitted characterization of the undrained shear strength profile from a depth of 60 mm to a depth of 220 mm (a prototype scale depth of 11 m) at a radial distance of 100 mm. Fortunately, the depth range of the T-bar penetration brackets the position of the torpedo pile prior to pullout. A picture of the container mounted in the centrifuge basket is shown in Figure 3b that shows the locations of the two stepper motors used for installation and extraction of the torpedo pile and T-bar along with the ports in the side of the container for installing sensors at different depths in the clay layer.

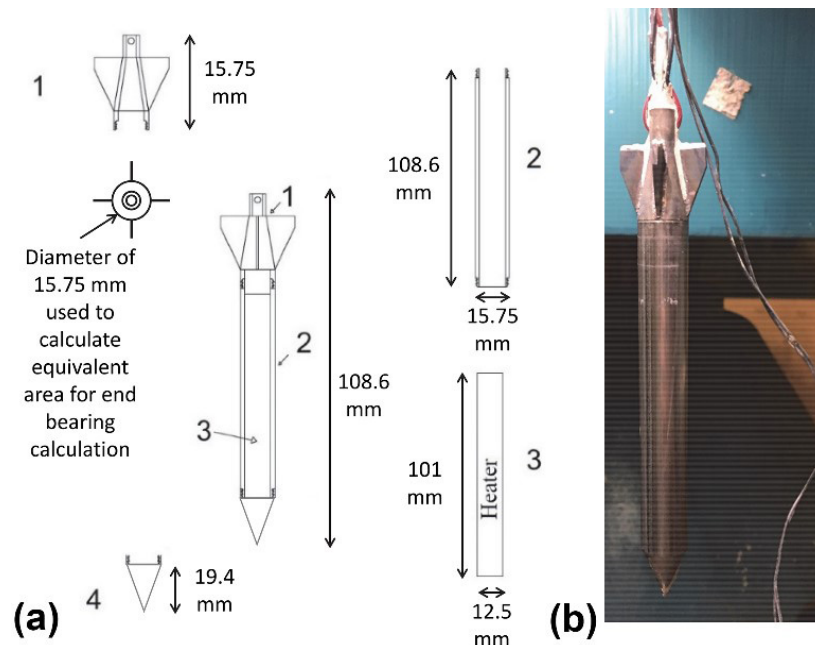


Figure 2. Centrifuge-scale torpedo pile: (a) Schematic showing (1) top cap with fins, (2) body, (3) internal electric resistance heater, (4) pointed tip; (b) picture showing mooring line connection to the top cap of the torpedo pile.

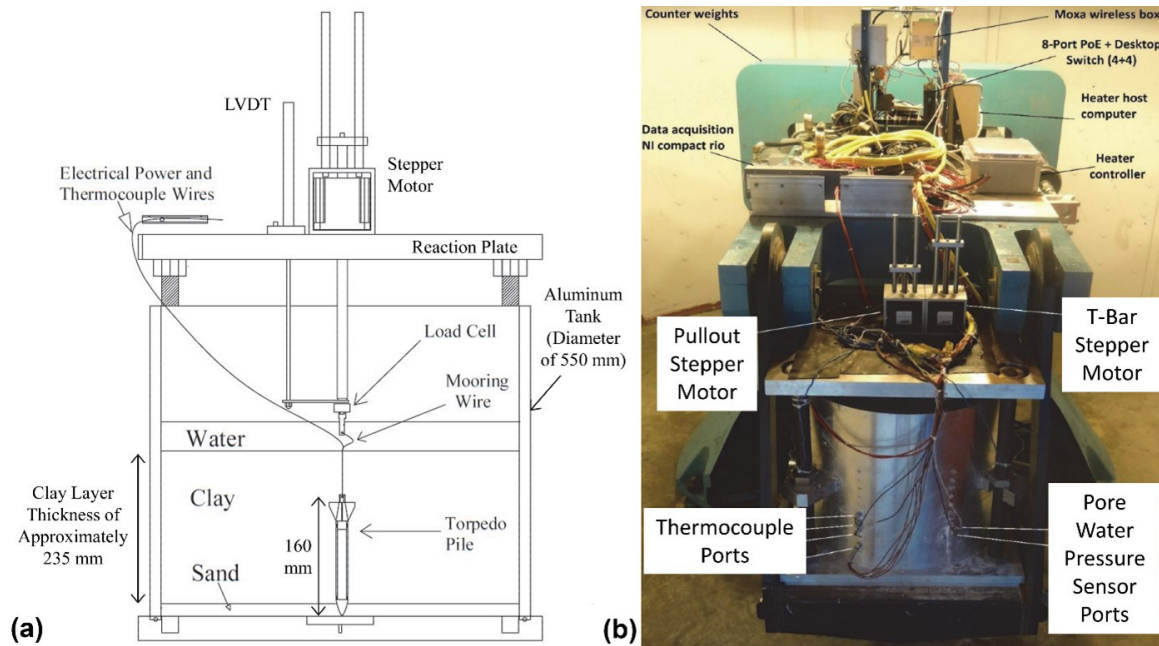


Figure 3. Experimental setup: (a) cross-sectional schematic of the setup showing the installed torpedo pile location; (b) picture of the setup mounted on the centrifuge basket.

2.3 Experimental procedures

The clay layer was prepared by mixing dry kaolinite clay in powder form with water under vacuum to form a slurry having a gravimetric water content of 130% ($2.8 \times LL$). The slurry was carefully poured into the container to avoid air inclusions atop a 20 mm-thick layer of Ottawa sand that acts as a drainage layer. A filter paper and a 50 mm-thick porous stone having the same diameter as the inside of the cylinder were placed atop the clay layer. After 24 hours of self-weight consolidation, dead-weights corresponding to vertical stresses of 2.4, 6.3, and 10.2 kPa were added atop the porous stone in 24-hour increments. The first dead weight included an aluminum disk that helped to distribute the vertical stress of the dead weights atop the porous stone. The vertical stress was then increased to 23.6 kPa using a hydraulic piston that reacted against the upper reaction plate, which was maintained for another 24 hours. After this time, the upper reaction plate was removed, and the hydraulic piston was replaced with the stepper motor assemblies for the foundation and the T-bar. After the 1g consolidation of the clay layers was completed, six type K thermocouples and five miniature Druck PDCR 81 pore water pressure sensors were inserted through the container side wall into the clay layer. The sensor insertion was facilitated by attaching the sensor cable to a thin rod as summarized by Ghaaowd & McCartney (2021). After processing the data from the experiments, it was found that only two of the pore water pressure sensors gave meaningful results (PPT3 and PPT4) and the other pore water pressure sensors had been damaged in an early experiment. Because

the positions of the sensors may change after consolidation in the centrifuge, the final positions of the sensors were verified at the end of the experiment when excavating the clay layer, as summarized in Table 1. Because the sensor locations were slightly different in each experiment as noted in Table 1, the sensors locations are not shown in Figure 3.

The assembled container was then placed inside the centrifuge basket for in-flight self-weight consolidation at 50 g. This procedure was found to produce a normally-consolidated clay layer with an overconsolidated portion near the surface. More details of the soil layer preparation are provided in Ghaaowd & McCartney (2021). During in-flight self-weight consolidation at 50 g, the excess pore-water pressures were monitored using the pore pressure transducers. A typical time series of the pore water pressure during centrifugation was presented in Ghaaowd & McCartney (2021) for a test on an end-bearing energy pile test that confirms that the clay layer reached more than 90% of primary consolidation before moving to the next testing stage. The void ratio at the end of self-weight consolidation in the four different tests was approximately 1.4, while after self-weight consolidation a decrease in void ratio with depth was observed in post-test measurements as will be reported later in the paper. The clay layer thickness in the four experiments after 1g consolidation was approximately 235 mm (11.75 mm in prototype scale), and a thin layer of water was permitted atop the clay layer ranging from $H_w = 40$ to 70 mm. This water layer was connected via a standpipe to a drain at the bottom of the container, so the clay layer was effectively double drained during the duration of the experiment.

Table 1. Sensor locations in the four tests.

Sensor	Test T1		Test T2		Test T3		Test T4	
	r (mm)	Depth (mm)	r (mm)	Depth (mm)	r (mm)	Depth (mm)	r (mm)	Depth (mm)
TC1		Surface	26	225	16	240	11	225
TC3	-	-	36	190	21	205	22	190
TC4	-	-	56	145	26	160	46	145
TC2	-	-	61	160	46	175	31	160
TC5	-	-	91	165	86	180	78	165
TC6	-	-	141	180	135	195	121	180
PPT3	140	36	51	170	46	180	66	180
PPT4	140	36	66	220	66	190	66	160

After stabilization at 50g, the torpedo pile was installed in flight into the sedimented clay layers. Although torpedo piles are typically installed in the field by being dropped through water from a certain depth so that it penetrates at high velocity to a target depth, it was not possible to simulate this high velocity installation approach in the centrifuge. To lead to repeatability between the different experiments and to ensure the verticality of the torpedo pile after installation, the torpedo piles in this study were installed by lowering them under their self-weight into the soft clay using the cable connected to the stepper motor at a model-scale velocity of 0.1 mm/s. While this is a much slower velocity than torpedo piles may experience in the field, it is sufficient to lead to undrained conditions. Using this approach, the pile tip was able to pass through the clay layer and become embedded in the dense sand layer. This penetration depth was confirmed by the position of the stepper motor, and by the fact that the load cell connected to the torpedo pile cable indicated no load and the mooring cable went slack. The torpedo pile was inserted so that the height of clay above the torpedo pile is approximately 94 mm (4.7 m in prototype scale). When the excess pore water pressure generated due to the pile insertion dissipated, the temperature of the heated torpedo pile was increased using the Watlow heat controller until reaching the target temperature at the pile wall. As mentioned, it was important for heating to continue during centrifugation until the soil temperature and pore water pressure stabilized, which typically required 5-10 hours in model scale (520 to 1040 days in prototype scale). However, for consistency in comparison of results all the tests on heated piles involved heating for approximately 30 hours in model scale, which was longer than necessary for thermo-hydraulic equilibrium and corresponds to a total duration of heating in prototype scale is 3125 days or 8.56 years. After this point, the pile was cooled for 10 hours in model scale and was then pulled out at the same velocity as used for installation.

After pullout testing of the pile the T-bar penetrometer, with a T diameter of 14 mm, a T length of 57 mm, and a shaft diameter of 11 mm, was used to measure the undrained shear strength profiles of the clay layers containing the heated and unheated torpedo piles. Insertion of the T-bar into the clay

layer can be used to infer the undrained shear strength of the intact clay layer as a function of depth, while extraction of the T-bar can be used to infer the undrained shear strength of disturbed clay as a function of depth (Stewart & Randolph, 1994). As mentioned, the T-bar was designed to permit model-scale penetrations between 60 and 235 mm and was driven by a second stepper motor at a model-scale velocity of 0.2 mm/s to ensure undrained conditions during insertion and extraction. T-bar penetration tests were performed after pile pullout testing in each clay layer at a radius of 100 mm from the heated and unheated torpedo piles (6.35 pile diameters), which is far enough away to be undisturbed from the pile insertion and extraction based on the pore water pressure measurements, but close enough to be influenced by temperature based on the thermocouple measurements.

3. Results

3.1 Thermo-hydraulic response of the pile and clay layer

Model-scale time histories of temperature at different locations in the four tests are shown in Figure 4. The maximum pile temperatures and maximum changes in pile temperature summarized in Table 2. There were generally 5 stages in each of the tests which are delineated in the figures using vertical dashed lines, including: (I) consolidation of the clay layer during centrifugation; (II) insertion of the torpedo pile under self-weight; (III) heating of the pile and surrounding soil; (IV) cooling of the pile and surrounding soil; and (V) pullout of the pile. In all the tests, there was a slight cooling effect as the centrifuge spun up followed by a slight warming due to centrifuge operation. The average surface temperature of 20 °C in the baseline Test T1 shown in Figure 4a was used as a reference temperature when calculating the changes in pile temperature. In the tests on heated torpedo piles in Tests T2, T3, and T4, the pile temperature rapidly increased to the target temperatures of 45, 65, and 80 °C, and approximately 5-10 hours was required for the temperatures at the different monitoring points in the clay layer to stabilize. After the

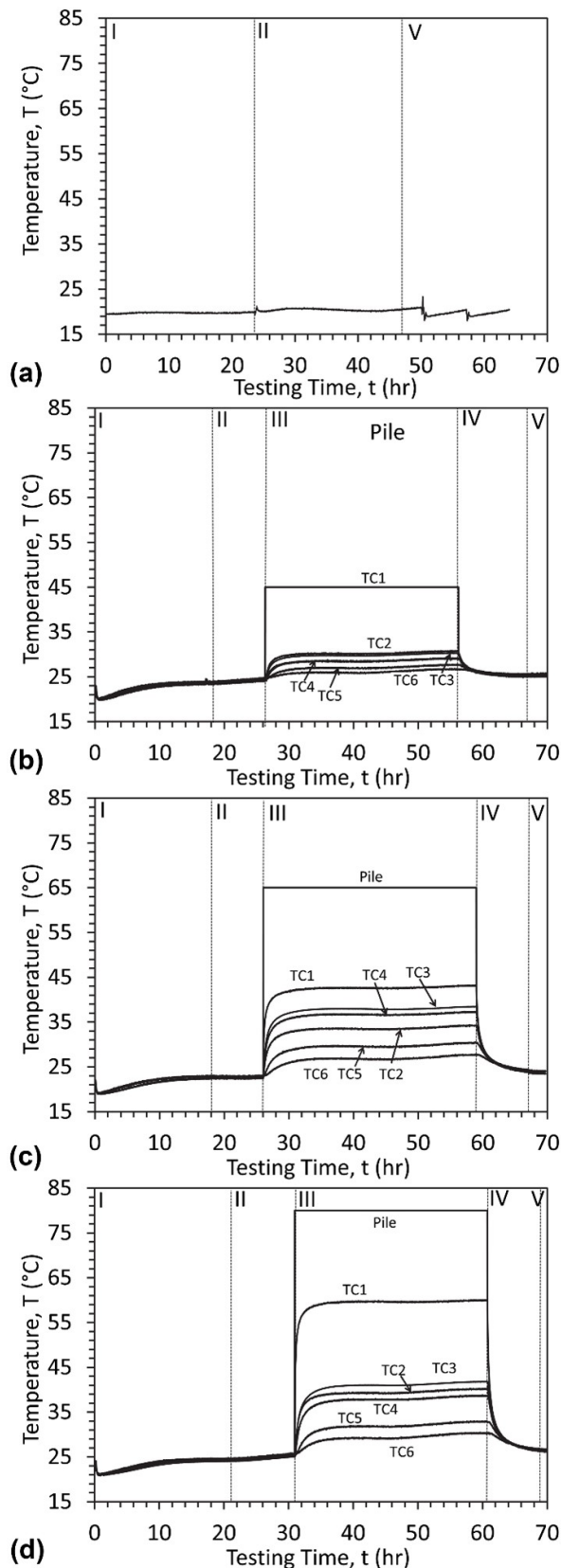


Figure 4. Time series of temperature readings at different radii from the torpedo pile during the five testing stages: (a) test T1 (clay surface only); (b) test T2; (c) test T3; (d) test T4.

approximately 30 hours of heating in each of the tests, cooling back to ambient conditions was achieved in approximately 5 hours even though 10 hours was permitted.

Profiles of temperature with radial location at steady-state conditions, which was selected as a time of 25 hours after the start of heating in Stage (III) are shown in Figure 5. Two observations from these profiles are that the temperature of the clay was nonlinearly distributed with radial location, and that the clay even at locations relatively close to the pile did not approach the temperature of the torpedo pile. In Test T2 the closest thermocouple was 26 mm away from the torpedo pile, while in Tests T3 and T4 there were two thermocouples closer to the pile that indicated a sharp drop-off in temperature. Accordingly, it is likely that a similar sharp drop-off in temperature occurred in the clay near the torpedo pile in Test T2. It is interesting that even when applying a pile temperature of 80 °C (change in pile temperature of 60 °C) that the clay temperature at a model-scale radial location of 11 mm (3.125 mm from the pile) only experienced a change in temperature of 35 °C. This is partly due to the high thermal conductivity of the stainless-steel torpedo pile, which likely permitted upward and downward heat transfer in addition to lateral heat transfer. The implication of this sharp drop-off in the radial temperature distribution around the cylindrical heat source is that the magnitude of the change in pore water pressure in the clay may be smaller than that associated with the full change in pile temperature. While changes in temperature of the clay were observed out to a prototype-scale radial location of more than 7 m (a model-scale radial location 150 mm) or nearly 9.5 pile diameters, the largest changes in temperature were within 2 pile diameters of the torpedo pile. This indicates that the greatest thermal improvement of the clay layer will occur relatively close to the torpedo pile.

Model-scale time series of pore water pressure at two locations in the clay layers are shown in Figure 6. The magnitudes of pore water pressure depend on the

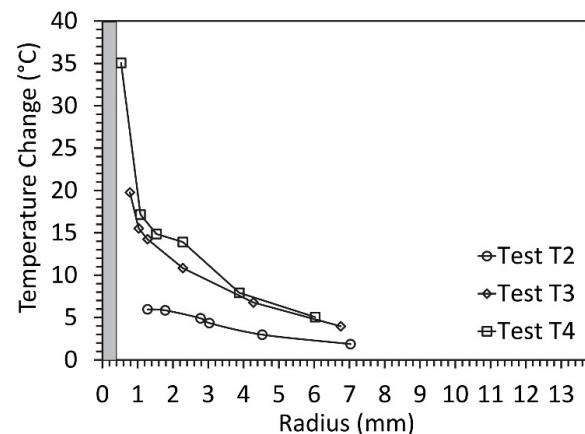


Figure 5. Prototype-scale equilibrium temperature profiles in the three tests on heated torpedo piles.

Table 2. Summary of tests on the torpedo piles after a heating-cooling cycle involving different maximum pile temperatures during centrifugation at $N=50g$.

Test	Pile temperature during heating	Change in pile temperature	Maximum pullout load (prototype scale)	Percent improvement in pile pullout capacity	Min/ave./max. undrained shear strength from T-bar*
	(°C)	(°C)	(kN)	(%)	(kPa)
T1	20	0	-97	-	7.2/12.7/18.2
T2	45	25	-117	19	10.6/14.4/18.2
T3	65	45	-139	42	-
T4	80	60	-153	56	11.6/15.3/19.0

*Defined over the length of the torpedo pile at a radius of 5 m or a distance of 4.6 m from the edge of the torpedo pile (prototype scale).

ponded water height and the actual locations of the pore water pressure sensors as measured at the end of the tests. A decrease in pore water pressure is observed in Stage (I) while the clay layer consolidates in the centrifuge, and a small increase in pore water pressure occurs when the pile is inserted into the clay layer in Stage (II). Some additional consolidation of the clay layer likely occurred in Stage (II) during pile insertion, but this study is not focused on the penetration resistance of the torpedo pile during insertion. During heating in Stage (III), only a very small increase in pore water pressure was observed. During cooling in Stage (IV) a small decrease in pore water pressure was observed, but of a smaller magnitude than that observed during heating. During pullout in Stage (V) a large increase in pore water pressure was observed.

The pore water pressure response during heating is better highlighted in the excess pore water pressure versus the time of heating (model scale) in Figure 7. The maximum increases in pore water pressure in Tests T2, T3, and T4 were 1.5, 2.0, and 2.0 kPa, respectively. The similar excess pore water pressures in Tests T3 and T4 could be explained by the closer location of PPT3 in Test T3 and the similar changes in temperature of the pile at the radial locations of these sensors as shown in the change in temperature profiles in Figure 5. The excess pore water pressures all show a rapid generation followed by dissipation within approximately 5 hours of heating time. The thermal improvement process closer to the pile may have taken a longer duration, which was the reason for the longer model-scale heating duration of 30 hours in the centrifuge tests. Similar to the excess pore water pressure results presented in Ghaaowd & McCartney (2021) for end-bearing energy piles in clay, the magnitudes of excess pore water pressure were less than those obtained using the undrained thermal pressurization model of Ghaaowd et al. (2017), likely due to partial drainage in the centrifuge experiments.

3.2 Torpedo pile pullout response

The prototype-scale pullout load versus displacement curves for the heated and unheated torpedo piles in clay layers having similar initial conditions are shown in Figure 8a.

All four pullout curves start from a self-weight load of 122 kN. An increase in pullout capacity with the increase in maximum pile temperature is observed. The maximum pullout force versus the maximum pile temperature is shown in Figure 8b. A linear trend is observed in this figure, indicating that higher pile temperatures will lead to greater thermal improvement. The difference in pullout capacity for the piles with maximum temperatures of 20 and 80 °C was 56 kN in prototype scale, which corresponds to a relative difference of 58% percent. This is a substantial increase in pullout capacity that indicates that thermal improvement was successful.

The stiffness of the pullout curves in Figure 8a is relatively similar for all four tests, which is a similar observation that that made by Ghaaowd & McCartney (2021) when analyzing tests on end-bearing energy piles in soft clay. It was expected that the increase in undrained shear strength of the clay layer with thermal improvement would also correspond to an increase in stiffness of the clay-pile interface. The similar stiffnesses observed in Figure 8b may have occurred because the heated torpedo piles experienced thermal axial strains in the direction opposite to gravity during heating that may have counteracted the positive effect of the thermal improvement in the stiffness. Further research is needed to understand the effects of thermal improvement on the stiffness response during torpedo pile pullout, but it is clear from these tests that thermal improvement has a positive effect on the magnitude of pullout capacity.

3.3 T-bar penetration test results

The T-bar penetration results for the clay layers with unheated and heated torpedo piles permit evaluation of the effects of cyclic heating-cooling to different temperatures from an initial temperature of 20 °C on the behavior of normally consolidated clay layers. The undrained shear strength profiles for the clay layer at a model-scale distance of 100 mm from the four torpedo piles are shown in Figure 9a. The correlations of Stewart & Randolph (1994) were used to interpret the undrained shear strength profiles from the T-bar penetration results. A problem with the stepper motor in Test T3 prevented a T-bar test from being performed

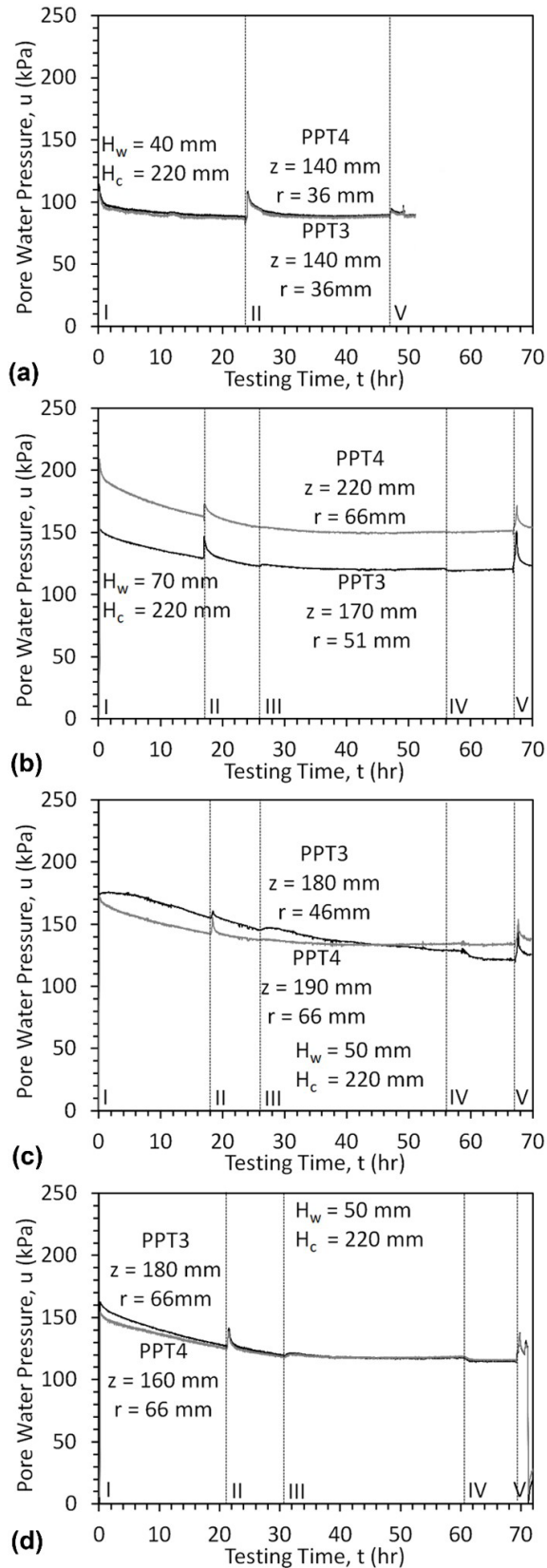


Figure 6. Time series of pore water pressure at different radii from the torpedo pile during the five testing stages: (a) test T1; (b) test T2; (c) test T3; (d) test T4.

after the pile was heated to 65°C , but from the other three tests the T-bar tests indicate an increase in undrained shear strength in the middle section of the clay layer with increasing maximum pile temperature. The changes in clay temperature at a model-scale radial location of 100 mm (a prototype-scale radial location of 5 m) are much smaller than those of the pile as shown in Figure 5, but a clear improvement is still observed at this location. The positive undrained shear strengths during insertion of the T-bar were generally greater than the negative undrained shear strength during extraction

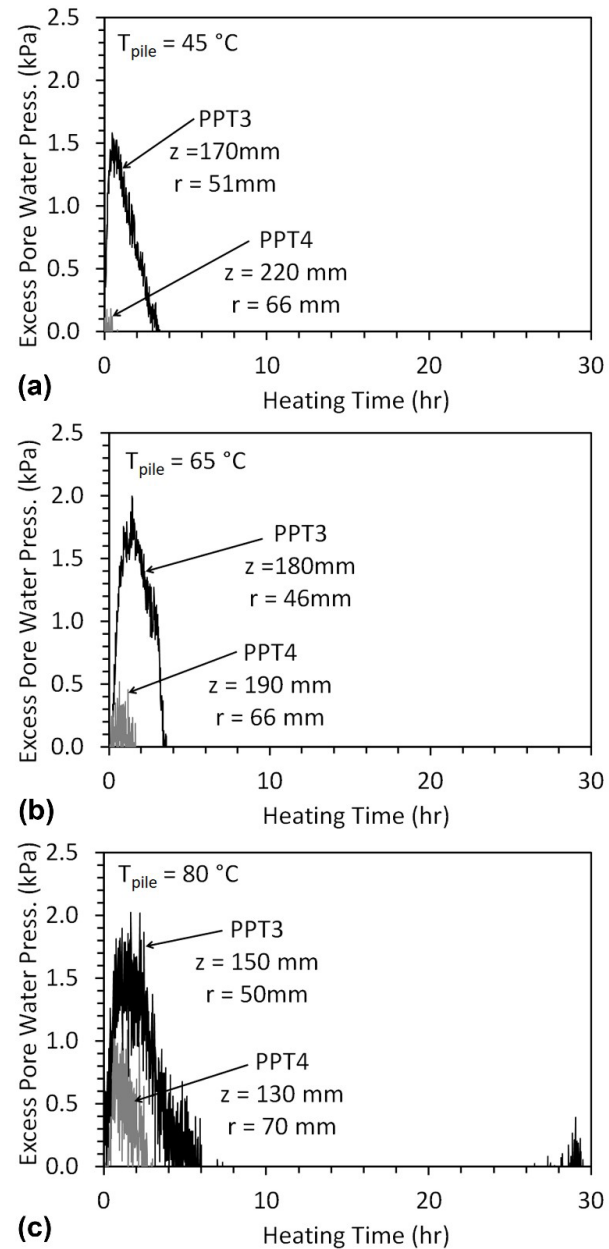


Figure 7. Time series of excess pore water pressure at different radii from the torpedo pile during heating stage: (a) test T2; (b) test T3; (c) test T4.

of the T-bar, but a typical bell-shaped curve was noted in all three tests. The thickness of the sand layer may have been slightly greater in Test T1 which explains the large increase in undrained shear strength at the bottom of the clay layer. The maximum, minimum, and average undrained shear strengths along the length of the torpedo pile obtained from the profiles in Figure 9a are summarized in the last column of Table 2.

At the end of testing, soil samples were obtained at the radial location of the T-bar on the opposite side of the profile. Samples were not obtained from near the center of the profile due as they may not be representative of the conditions after heating due to the disturbance caused by pullout of the torpedo pile. The void ratios inferred from gravimetric water content samples at the end of the tests are shown in Figure 9(b). Lower void ratios are observed in the clay layers that experienced higher temperatures, which correspond well with the increases in the undrained shear strength with temperature inferred from the T-bar penetration tests. While the results from the T-bar and soil samples after

testing cannot be directly correlated with the pullout tests due to the differences in the locations of these measurements, they are good indicators that thermal improvement occurred in the clay layer due to torpedo pile heating.

4. Analysis and comparison with end bearing energy pile pullout

The pullout capacity of torpedo piles Q_{ult} can be estimated using the following equation used by Gilbert et al. (2008) for the pullout of torpedo piles:

$$Q_{ult} = Q_{side} + Q_{end} = \alpha c_{u,average} A_{side} + c_{u,end} N_c d_c s_c A_{end} \quad (1)$$

where Q_{side} is the side shear capacity, Q_{end} is the upward end bearing capacity, α is a side shear reduction factor to account for installation effects, $c_{u,average}$ is the average undrained shear strength along the length of the torpedo pile, A_{side} is the area

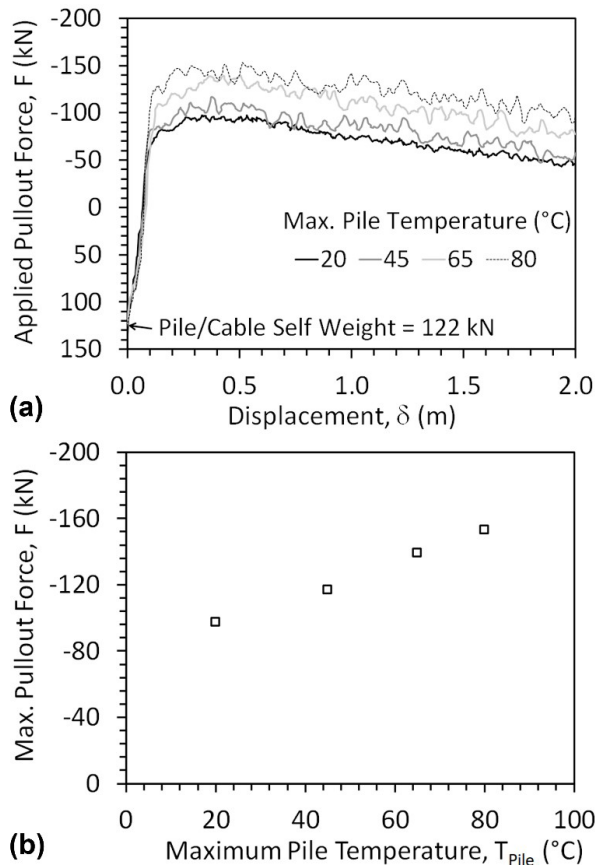


Figure 8. Results from pullout tests on torpedo piles after a heating-cooling cycle involving different maximum pile temperatures: (a) applied pullout force versus displacement curves (prototype scale), (b) pullout capacity as a function of the maximum pile temperature experienced during a heating-cooling cycle.

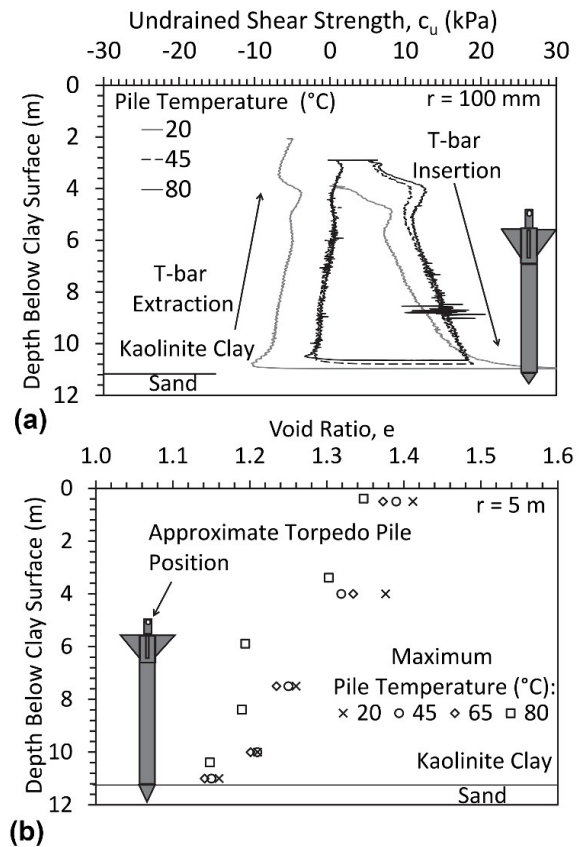


Figure 9. (a) prototype-scale profiles of undrained shear strength measured by the T-bar in three of the four tests on torpedo piles heated to different temperatures (positive values for insertion and negative values for extraction); (b) prototype-scale profiles of void ratio with depth at the same radial location at the T-bar test (5 m in prototype scale or 100 mm in model scale).

Table 3. Analysis of torpedo pile capacity components (prototype scale).

Test	Maximum pullout load	Calculated upward end bearing capacity ¹	Calculated side shear capacity	Back-calculated average undrained shear Strength at pile-clay interface ²
	(kN)	(kN)	(kN)	(kPa)
T1	-97	-31	-66	12.2
T2	-117	-46	-71	13.1
T3	-139	-48	-90	16.7
T4	-153	-51	-102	19.0

¹Calculated assuming an end area corresponding to a circular area corresponding to the fins; ²Calculated assuming a reduction factor of $\alpha = 0.4$

of the sides of the torpedo pile in clay, $c_{u,end}$ is the undrained shear strength at the upper end of the torpedo pile, $N_c d_c s_c$ is the adjusted undrained bearing capacity factor for a deep foundation equal to 9, and A_{end} is the equivalent cross-sectional area of the end of the torpedo pile to account for the taper and presence of the fins as shown in Figure 2a.

Specifically, the value of A_{end} was assumed to be equal to the cross-sectional area of the main body of the torpedo pile for simplicity. The upward end bearing capacity was calculated for each of the piles using the minimum undrained shear strength values from the T-bar tests in Table 2 (which correspond to the level of the upper end of the torpedo pile). The undrained shear strength at the level of the upper end of the pile for Test T3 was assumed to be linearly distributed between values measured at that level in Tests T2 and T3. The calculated upward end bearing capacities are summarized in Table 3, along with the side shear capacities calculated as the difference between the measured ultimate pullout capacity and the calculated upward end bearing capacities. Using the calculated side shear capacity for the torpedo pile tested at room temperature conditions, the average undrained shear strength from the T-bar test in Table 2 (which was assumed to be the same as at the soil-pile interface), and the side area of the pile, a value of α was back-calculated to be 0.4, which represents both a lower interface shear strength than the undrained shear strength of the soil and the effects of installation on the interface shear strength. Gilbert et al. (2008) assumed $\alpha = 1$, but found a consistent overprediction of the pullout capacity indicating that a lower value of α like that used in this study may be appropriate. This same value of α was then used to back-calculate the average undrained shear strength values at the soil-pile interface for each of the tests on the heated torpedo piles, which are summarized in the last column of Table 3. An increase in average undrained shear strength at the soil-pile interface occurred with the increase in maximum pile temperature. The magnitudes are greater than the undrained shear strength values from the T-bar tests measured at a prototype-scale distance of 5 m from the pile and represent the undrained shear strength at the clay-pile interface. While this analysis is simple and could be improved through further testing of physical models, it is helpful to understand the different ways that thermal improvement can enhance the pullout capacity of torpedo piles.

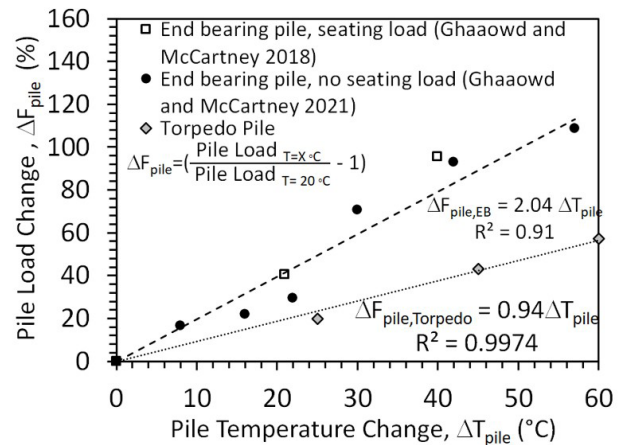


Figure 10. Percent increase in pullout capacity of the torpedo piles in soft clay after in-situ heating to different changes in pile temperature compared with results from end bearing energy piles in soft clay.

A comparison of the percent increase in pullout capacity of the torpedo pile in soft clay with the maximum change in temperature during heating with similar values measured from centrifuge tests on end-bearing energy piles in the same clay layer in centrifuge tests performed by Ghaaowd & McCartney (2018, 2021) is shown in Figure 10. A linear trend is observed for the torpedo piles and the end-bearing energy piles, but the slope of the trend line is steeper for the end-bearing energy piles. The end-bearing energy piles extended through the full length of the clay layer having a similar thickness to the clay layer investigated in this study, so a greater length of clay was improved. In their experiments, thermal improvement only affected the side shear capacity of the piles as the top of the end-bearing energy piles was extending out of the clay layer. Overall, this comparison confirms the feasibility of thermal improvement of the pullout capacity of piles from soft clay in general and emphasizes the importance of the configuration of the energy pile in the clay subsurface when estimating increases in pullout capacity.

5. Conclusions

Torpedo piles in soft clay layers were evaluated at a scale of 1/50 in a geotechnical centrifuge to evaluate the

impacts of a pile heating-cooling cycle on the behavior of the clay layer and the corresponding pullout capacity of the torpedo pile. Measurements of temperature and pore water pressure in the clay layer surrounding the piles supports the hypothesis that thermal consolidation leads to the improvement in shear strength. These measurements also indicate that the zone of influence of the change in temperature is primarily within 2 pile diameters from the heated torpedo pile and that the thermal consolidation process is mostly complete after 500 days in prototype scale (a model-scale time of 5 hours). The undrained shear strength values of the clay layers surrounding the heated-cooled torpedo piles inferred from T-bar penetration tests and from the pile pullout tests were found to be greater than that of a clay layer surrounding an unheated torpedo pile. A reduction in void ratio was also observed at the end of testing for clay layers that had experienced higher temperatures. The pullout capacities of the torpedo piles that had experienced greater changes in temperature during the heating-cooling cycle were greater than that of the unheated torpedo pile. The slopes of the pullout load versus displacement curves were similar, which may be due to the impact of upward displacements associated with thermal expansion of the heated torpedo piles prior to pullout, leading to an initially elastic pullout response for all the torpedo piles. The amount of the improvement in the torpedo pile capacity was found to increase linearly with the maximum change in temperature of the pile, but with a lower slope than that measured for tests on end-bearing energy piles in the same soft clay in previous studies.

Acknowledgements

Support from the University of California San Diego is appreciated. The views in this paper are those of the authors alone.

Declaration of interest

The authors have no conflicts of interest.

Authors' contributions

Ismaail Ghaaowd: conceptualization, Formal Analysis, Methodology. John S. McCartney: conceptualization, Methodology, Supervision, Funding acquisition, Validation, Project administration, Writing – original draft. Fernando Saboya: investigation, Methodology, Resources, – review & editing.

List of symbols

A	Area
c_u	Undrained shear strength
D	Pullout displacement

e	Void ratio
H_w	Height of water above the surface of the clay layer
N	Centrifuge g-level
Q_{ult}	Pullout capacity
T_{pile}	Temperature of the pile
ΔF	Percent change in pile pullout capacity
ΔT	Change in temperature
ΔH	Change in soil layer height
Δu_w	Change in pore water pressure

References

- Abuel-Naga, H.M., Bergado, D.T., Bouazza, A., & Ramana, G.V. (2007a). Volume change behavior of saturated clays under drained heating conditions: experimental results and constitutive modeling. *Canadian Geotechnical Journal*, 44(8), 942-956. <http://dx.doi.org/10.1139/t07-031>.
- Abuel-Naga, H.M., Bergado, D.T., & Lim, B.F. (2007c). Effect of temperature on shear strength and yielding behavior of soft Bangkok clay. *Soil and Foundation*, 47(3), 423-436. <http://dx.doi.org/10.3208/sandf.47.423>.
- Abuel-Naga, H.M., Bergado, D.T., & Bouazza, A. (2007b). Thermally induced volume change and excess pore water pressure of soft Bangkok clay. *Engineering Geology*, 89(1-2), 144-154. <http://dx.doi.org/10.1016/j.enggeo.2006.10.002>.
- Baldi, G., Hueckel, T., & Pellegrini, R. (1988). Thermal volume changes of the mineral-water system in low-porosity clay soils. *Canadian Geotechnical Journal*, 25(4), 807-825. <http://dx.doi.org/10.1139/t88-089>.
- Bastidas, A.M. (2016). *Ottawa F-65 sand characterization* [Ph. D. dissertation]. University of California, Davis.
- Bergentahl, L., Gabrielsson, A., & Mulabdic, M. (1994). Changes in soft clay caused by increases in temperature. In *Proceedings of the 13th International Conference on Soil Mechanics and Foundation Engineering* (pp. 1637-1641), New Delhi.
- Bonfim dos Santos, A., Henriques, C.C.D., & Pimenta, J.M.H.A. (2004). Improvements achieved in the project of FPSO P-50. In *Offshore Technology Conference* (Paper No. OTC 16705), Houston. <http://dx.doi.org/10.4043/16705-MS>.
- Burghignoli, A., Desideri, A., & Miliziano, S. (2000). A laboratory study on the thermomechanical behavior of clayey soils. *Canadian Geotechnical Journal*, 37(4), 764-780. <http://dx.doi.org/10.1139/t00-010>.
- Campanella, R.G., & Mitchell, J.K. (1968). Influence of temperature variations on soil behavior. *Journal of the Soil Mechanics and Foundations Division*, 94(SM3), 709-734. <http://dx.doi.org/10.1061/JSFEAQ.0001136>.
- Cekerevac, C., & Laloui, L. (2004). Experimental study of thermal effects on the mechanical behaviour of a clay. *International Journal for Numerical and Analytical Methods in Geomechanics*, 28(3), 209-228. <http://dx.doi.org/10.1002/nag.332>.
- Ghaaowd, I., & McCartney, J.S. (2018). Centrifuge modeling of temperature effects on

- the pullout capacity of energy piles in clay. In *DFI 43rd Annual Conference on Deep Foundations* (pp. 1-7), Anaheim, CA.
- Ghaaowd, I., & McCartney, J.S. (2021). Centrifuge modeling methodology for energy pile pullout from saturated soft clay. *Geotechnical Testing Journal*, 45(2). <http://dx.doi.org/10.1520/GTJ20210062>.
- Ghaaowd, I., McCartney, J.S., Huang, X., Saboya, F., & Tibana, S. (2018). "Issues with centrifuge modeling of energy piles in soft clays. In *Proceedings of the 9th International Conference on Physical Modeling in Geotechnics: Physical Modelling in Geotechnics* (pp. 1365-1370). London: Taylor & Francis Group.
- Ghaaowd, I., Takai, A., Katsumi, T., & McCartney, J.S. (2017). Pore water pressure prediction for undrained heating of soils. *Environmental Geotechnics*, 4(2), 70-78. <http://dx.doi.org/10.1680/jenge.15.00041>.
- Gilbert, R.B., Morvant, M., & Audibert, J. (2008). *Torpedo piles joint industry project - model torpedo pile tests in kaolinite test beds. Report to minerals management service* (48 p.). Austin: University of Texas.
- Houston, S.L., Houston, W.N., & Williams, N.D. (1985). Thermo-mechanical behavior of seafloor sediments. *Journal of Geotechnical Engineering*, 111(12), 1249-1263. [http://dx.doi.org/10.1061/\(ASCE\)0733-9410\(1985\)111:12\(1249\)](http://dx.doi.org/10.1061/(ASCE)0733-9410(1985)111:12(1249)).
- Maddocks, D.V., & Savvidou, C. (1984). The effect of the heat transfer from a hot penetrator installed in the ocean bed. In *Proceedings of the Symposium on the Application of Centrifuge Modeling to Geotechnical Design*, Craig, Manchester U.K.
- McCartney, J.S., & Murphy, K.D. (2017). Investigation of potential dragdown/uplift effects on energy piles. *Geomechanics for Energy and the Environment*, 10, 21-28. <http://dx.doi.org/10.1016/j.gete.2017.03.001>.
- Ng, C.W.W., Farivar, A., Gomaa, S.M.M.H., & Jafarzadeh, F. (2021). Centrifuge modeling of cyclic nonsymmetrical thermally loaded energy pile groups in clay. *Journal of Geotechnical and Geoenvironmental Engineering*, 147(2), 04021146. [http://dx.doi.org/10.1061/\(ASCE\)GT.1943-5606.0002689](http://dx.doi.org/10.1061/(ASCE)GT.1943-5606.0002689).
- Ng, C.W.W., Shi, C., Gunawan, A., & Laloui, L. (2014). Centrifuge modelling of energy piles subjected to heating and cooling cycles in clay. *Géotechnique Letters*, 4(4), 310-316. <http://dx.doi.org/10.1680/geolett.14.00063>.
- Ng, C.W.W., Zhang, C., Farivar, A., & Gomaa, S.M.M.H. (2020). Scaling effects on the centrifuge modelling of energy piles in saturated sand. *Géotechnique Letters*, 10(1), 57-62. <http://dx.doi.org/10.1680/jgele.19.00051>.
- Pothiraksanon, C., Bergado, D.T., & Abuel-Naga, H.M. (2010). Full-scale embankment consolidation test using prefabricated vertical thermal drains. *Soil and Foundation*, 50(5), 599-608. <http://dx.doi.org/10.3208/sandf.50.599>.
- Samarakoon, R., & McCartney, J.S. (2020). Role of initial effective stress on the thermal consolidation of normally consolidated clays. *E3S Web of Conferences*, 205, 09001. <https://doi.org/10.1051/e3sconf/202020509001>.
- Samarakoon, R., Ghaaowd, I., & McCartney, J.S. (2018). "Impact of drained heating and cooling on undrained shear strength of normally consolidated clay. In *International Symposium on Energy Geotechnical (SEG-2018)* (pp. 243-250), Switzerland.
- Stewart, D., & Randolph, M. (1994). T-Bar penetration testing in soft clay. *Journal of the Geotechnical Engineering Division*, 120(12), 2230-2235. [http://dx.doi.org/10.1061/\(ASCE\)0733-9410\(1994\)120:12\(2230\)](http://dx.doi.org/10.1061/(ASCE)0733-9410(1994)120:12(2230)).
- Takai, A., Ghaaowd, I., McCartney, J.S., & Katsumi, T. (2016). Impact of drainage conditions on the thermal volume change of soft clay. In *GeoChicago 2016: Sustainability, Energy and the Geoenvironment* (pp. 32-41), Chicago. <http://dx.doi.org/10.1061/9780784480137.004>.
- Towhata, I., Kuntiwattanaku, P., Seko, I., & Ohishi, K. (1993). Volume change of clays induced by heating as observed in consolidation tests. *Soil and Foundation*, 33(4), 170-183. http://dx.doi.org/10.3208/sandf1972.33.4_170.
- Uchaipichat, A., & Khalili, N. (2009). Experimental investigation of thermo-hydro-mechanical behaviour of an unsaturated silt. *Geotechnique*, 59(4), 339-353. <http://dx.doi.org/10.1680/geot.2009.59.4.339>.
- Vega, A., & McCartney, J.S. (2015). Cyclic heating effects on thermal volume change of silt. *Environmental Geotechnics*, 2(5), 257-268. <http://dx.doi.org/10.1680/envgeo.13.00022>.
- Yazdani, S., Helwany, S., & Olgun, G. (2019). Investigation of thermal loading effects on shaft resistance of energy pile using laboratory-scale model. *Journal of Geotechnical and Geoenvironmental Engineering*, 145(9), 04019043. [http://dx.doi.org/10.1061/\(ASCE\)GT.1943-5606.0002088](http://dx.doi.org/10.1061/(ASCE)GT.1943-5606.0002088).
- Yazdani, S., Helwany, S., & Olgun, G. (2021). The mechanisms underlying long-term shaft resistance enhancement of energy piles in clays. *Canadian Geotechnical Journal*, 58(11), 1640-1653. <http://dx.doi.org/10.1139/cgj-2019-0236>.
- Zeinali, S.M., & Abdelaziz, S.L. (2021). Thermal consolidation theory. *Journal of Geotechnical and Geoenvironmental Engineering*, 147(1), 04020147. [http://dx.doi.org/10.1061/\(ASCE\)GT.1943-5606.0002423](http://dx.doi.org/10.1061/(ASCE)GT.1943-5606.0002423).

Physical modeling of thermal improvement in normally consolidated and overconsolidated soil

João Alberto Machado Leite¹ , Sérgio Tibana^{2#} 

Article

Keywords

Thermal consolidation
Thermomechanics
Undrained shear resistance

Abstract

Knowledge of the soil-temperature relation and its peculiarities have been widely discussed in Geotechnics. Previous studies show that heated fine-grained soil induces pore pressure, and as a result, the soil exhibits a consolidation effect similar to that of conventional consolidation when pore pressure is dissipated. The outcome of this process depends on soil characteristics such as the overconsolidation ratio and plasticity. Consolidated soil typically induces positive pore pressure while overconsolidated one induces negative pore pressure when heated. The phenomenon described was explored in this study aimed at the thermal consolidation product regarding the decrease in void ratio and consequent increase in undrained shear strength (S_u) of a soil submitted to heating. These aspects were investigated using physical models at 1g gravity field, built on a laboratory scale. The heat source was placed inside a driven torpedo pile model in a medium consisting of a kaolin and metakaolin mixture. The undrained shear strength profile was defined by T-Bar tests involving different effective stresses and consolidation temperatures. The results show that for both mediums (normally consolidated and overconsolidated), undrained shear strength tends to grow proportionally to the temperature variation and permanent volume change is reached after a heating-cooling cycle. On the other hand, undrained shear strength indicates less significant variations for higher overconsolidation ratios.

1. Introduction

The effect of temperature variation on soil properties has long been studied in geotechnics; however, the complex behavior of soils under temperature variation is a barrier to faster development and precise predictions in this area.

Some important applications have propelled geothermal studies, such as nuclear waste disposal (Slovic et al., 1991; Hueckel & Pellegrini, 1992; Delage et al., 2000) and, more recently, energy piles (Mimouni & Laloui, 2014; Chen & McCartney, 2016).

These studies include soil-pile interaction, soil and foundation thermal strains, ultimate pile capacity, and stress and strain development due to temperature variations (Ng et al., 2014, 2015; Murphy et al., 2015; Goode III & McCartney, 2015).

In addition to these practical studies, relevant contributions made by several researchers in theoretical and modeling contexts, such as Campanella & Mitchell (1968), Demars & Charles (1982), Baldi et al. (1988) and Delage et al. (2000), allow better understanding of temperature, physical and mechanical effects and indicate the possibility of thermal consolidation.

This thermal phenomenon is a consequence of clay heating that leads to greater expansion of the water in the system than the soil solid minerals. The expansion difference, combined with the low soil permeability, generates excess of pore pressure. The pore pressure dissipation induced by temperature changes and the consolidation of clays subjected to pressure changes occur in a similar manner (Campanella & Mitchell, 1968).

Normally consolidated soils tend to experience only contraction strains when heated and apparent pre-consolidation stress tends to increase. On the other hand, overconsolidated soils tend initially to experience a rise in volume at low temperatures, followed by contraction at high temperatures. This depends on soil characteristics and the overconsolidation ratio (OCR) (Plum & Esrig, 1969; Baldi et al., 1988; Cui et al., 2000; Laloui & Cekerevac, 2008).

Considering all these aspects, the State University of Norte Fluminense Darcy Ribeiro (UENF) research group has been investigating the effects of temperature change on the improvement of submarine clayey soil properties using physical modeling and special laboratory tests.

The main objective of this paper was to present the results of physical modeling 1g tests carried out at the

[#]Corresponding author. E-mail address: stibana@gmail.com

¹Faculdade CNEC Rio das Ostras, Civil Engineering Laboratory, Rio das Ostras, RJ, Brazil.

²Universidade Estadual do Norte Fluminense Darcy Ribeiro, Civil Engineering Laboratory, Campos dos Goytacazes, RJ, Brazil.

Submitted on October 28, 2021; Final Acceptance on January 11, 2022; Discussion open until May 31, 2022.

<https://doi.org/10.28927/SR.2022.076421>



This is an Open Access article distributed under the terms of the Creative Commons Attribution License, which permits unrestricted use, distribution, and reproduction in any medium, provided the original work is properly cited.

UENF Geotechnical Centrifuge Laboratory. A number of undrained shear strength profiles obtained with T-Bar tests of the physical models were presented.

2. Materials and methods

2.1 Container and instrumentation

Four tests were carried out in a cylindrical container with inner diameter of 45.7 cm and height of 48 cm. A porous stone was placed at the bottom of the container to ensure double drainage and accelerate pore pressure dissipation during consolidation. Vertical load was applied to the top of the model with a perforated steel cap, where small holes allowed drainage from the top. The heat source was an electrical resistor installed inside a 25 cm-high torpedo pile model with an external diameter of 2.5 mm. The same beam used to place the torpedo pile model in the center of the container was used to install 2 rods in which the instrumentation was placed, as illustrated in Figure 1. The rods were positioned at 2 cm and 12 cm from the heat source and used to insert the pore pressure transducers and thermocouples into the model. Table 1 shows the distance and depth of each instrument associated with the rods. The consolidation system consisted of an electric motor coupled to a steel cap with outer diameter smaller than that of the inner container. The motor applied the load, which was recorded by a load cell.

2.2 Mixture of kaolin and metakaolin

A mixture of kaolin (40%) and metakaolin (60%) by weight was prepared with an initial moisture content of $1.5 \times$ liquid limit to be used in the model. Table 2 summarizes the results of the physical properties of the mud. The results presented show that the mixture was a fine mud containing 84.2% silt and clay, and the specific gravity of particles was

2.63. The liquid and plastic limits were 62.5 and 35.7%, respectively. The mixture was prepared in a mixer adapted to apply vacuum during the 30-minute homogenization process.

2.2.1 Model preparation

The homogenized and de-aerated mud was poured into the container and the load application system was installed to consolidate it in tests with overconsolidated models. The normally consolidated model was subjected to its self-weight consolidation.

Three overconsolidated models were prepared, each with final vertical effective stress application of 25, 50 and 100 kPa. Given that at the end of consolidation the effective soil height was insufficient to install the instrumentation and carry out the tests, another layer of sludge was consolidated with the same vertical effective stress. Thus, the steel cap was removed and the instrumentation and torpedo pile were installed.

2.3 Thermal consolidation and undrained shear strength (S_u)

The thermal consolidation of each model was carried out with temperature increases of 30 and 60 °C above ambient

Table 1. Instrument configuration in the containers.

Radial distance from pile (mm)	Depth inside soil (mm)	Thermocouple	PP Transducer
20	45	H11	PP11
	90	H12	PP12
	135	H13	-
120	45	H21	PP21
	90	H22	PP22
	135	H23	-

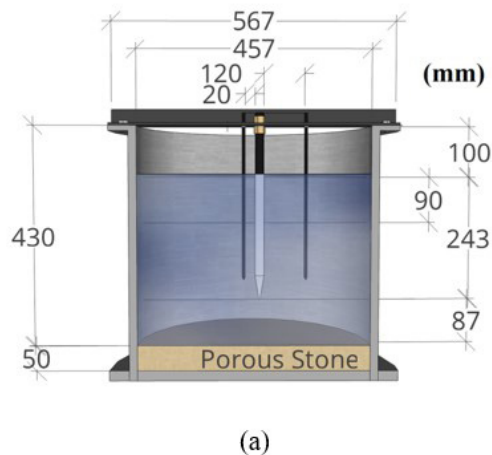


Figure 1. (a) lay-out of the container and instrumentation (b) torpedo and instrumentation installation.

Table 2. Characterization of the kaolin and metakaolin mixture.

	Fine sand (%)	Silt (%)	Clay (%)	G	LL (%)	PL (%)	PI (%)
Mixture	15.7	58.8	25.4	2.63	62.5	35.7	26.7

Table 3. T-bar test details for each stage.

Applied stress (kPa)	Thermal load	Radial distance from the pile (cm)			
		2	5	8	12
0	ΔT 30 °C		X		X
	ΔT 60 °C		X		X
	ΔT 0 °C		X		X
25	ΔT 30 °C				
	ΔT 60 °C	X	X	X	X
	ΔT 0 °C	X	X	X	X
50	ΔT 30 °C		X	X	X
	ΔT 60 °C		X	X	X
	ΔT 0 °C		X	X	X
100	ΔT 30 °C		X	X	
	ΔT 60 °C	X	X	X	
	ΔT 0 °C	X	X	X	

temperature (25 °C). The temperature of the model was increased by turning on the heater. The increase and dissipation of excess pore pressure was monitored by pore pressure transducers. Thus, during each temperature increment and after the heater was turned off and the model cooled, the undrained shear strength profile was determined at different distances from the pile.

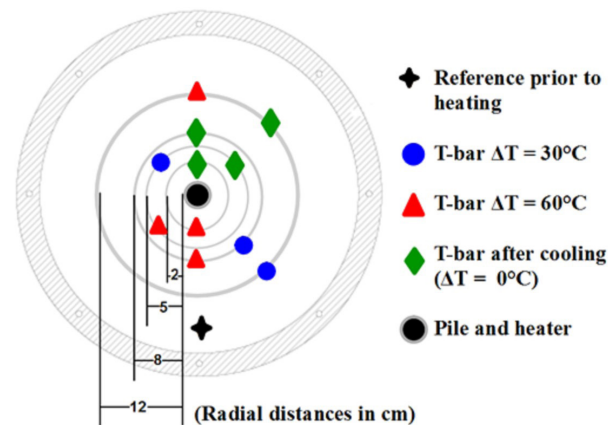
The undrained shear strength profiles of all tests were determined from the mini T-Bar tests. The T-Bar tests were conducted according to Stewart & Randolph (1991). Prior to the thermal consolidation of all the models, a T-bar test was carried out to obtain the initial undrained shear strength profile of each model. These results were used to calculate the S_u gain after thermal consolidation.

A summary of test configurations is presented in Table 3 and Figure 2. Table 3 shows the temperature variations applied ($\Delta T=30$ °C, $\Delta T=60$ °C and $\Delta T=0$ °C) and the distances from the pile where the tests were performed (2, 5, 8 and 12 cm). Each of these tests was compared to the initial reference test, carried out prior to thermal consolidation. Figure 2 illustrates the arrangement and distribution of the tests performed in each heating step as an example of the pattern used for all models.

3. Results and discussions

3.1 Mechanical consolidation

The mechanical consolidation of each container was carried out in steps until the final effective stress was reached. The mechanical consolidation curves of the models are presented

**Figure 2.** Generic T-bar test arrangement showing the number and position of tests conducted for each heating step.

in Figure 3, while Table 4 shows the void ratio development for each stress step of the consolidation. Given the good agreement of the curves, it can be considered that the methodology produced very similar models, suggesting that the undrained shear strength obtained with the T-Bar in each model can be compared. After mechanical consolidation, the steel cap was removed and the torpedo pile with the heater and instrumentation rods installed.

3.2 Thermal consolidation

Figure 4 demonstrates the evolution of temperature over time, showing the temperature of the thermocouples on the surface of the pile, such as those placed at different depths

Table 4. Void ratio variation during mechanical consolidation for different stresses applied to each container.

Total Applied Stress (kPa)	0.00 kPa	2.50 kPa	5.00 kPa	10.00 kPa	25.00 kPa	50.00 kPa	100.00 kPa
0.00	2.48	-	-	-	-	-	-
25.00	2.53	2.24	1.96	1.77	1.61	-	-
50.00	2.47	2.22	2.02	1.70	1.56	1.53	-
100.00	2.46	2.18	2.02	1.78	1.60	1.52	1.40

and distances from the pile, according to Table 1. All the tests started with a T-bar test before any temperature was applied in the model. Next, an increase of 30 °C above room temperature was applied to the heater inside the pile, corresponding to time zero in Figure 4. The temperature of the pile rapidly rose to about 55 °C, as did the soil temperature, increasing more for lower positions in the soil and for distances nearer the heat source, as shown in the curves. After 24 h, the temperature in the system stabilized, and a series of T-bar tests were conducted. A new 30 °C rise was then applied to the heater, reaching a total variation of about 60 °C above ambient temperature. Once again, after 24 h, another series of T-bar tests were carried out, the heater was turned off and the system started to cool down naturally. Finally, after the system had cooled completely, identified by the equalization of all the thermocouples with the ambient temperature, the last series of T-bar tests were performed. This process was followed for all the containers, each with a different stress state.

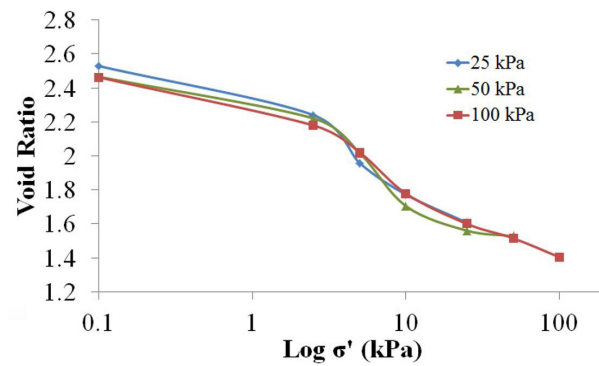
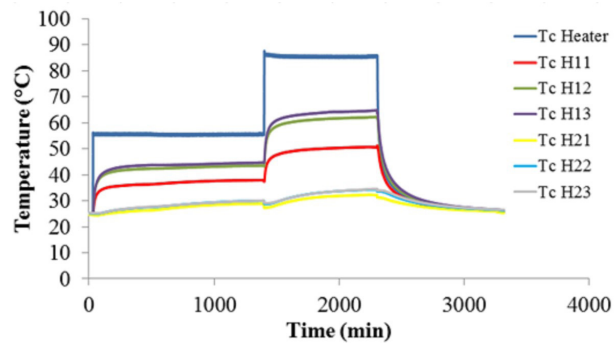
3.3 T-Bar tests

The results showed a close relation between temperature and S_u for clays, where temperature invariably influenced soil response. In normally consolidated tests, which obtained the lowest stress levels, S_u strength gain during and after heating was the most noticeable, especially in the tests conducted during temperature variations. Despite the low S_u magnitude variations in absolute values, they were the most relevant, proportionally to their initial strength.

Overconsolidated soil also showed undrained shear strength variations. In these cases, the noteworthy pattern observed among the different containers consisted of increased strength in the final profile portions, at the greatest soil depths.

This region experienced positive S_u variations for the different overconsolidation levels in the containers and the different distances tested. It is believed that these patterns are a consequence of two common characteristics in the region analyzed: the proximity to the bottom container drainage and the consequence of a more lightly overconsolidated zone at the greatest depths.

In addition, despite exhibiting greater average magnitude variation, the average strength increase for higher overconsolidation levels revealed a smaller percentage variation compared to the initial (reference) strength when compared to the soils with lower overconsolidation levels.

**Figure 3.** Consolidation curves of the overconsolidated models.**Figure 4.** Temperature development over time on thermocouples inserted into the models.

These findings can be better visualized in the following bar graphs (Figures 5 to 8), which compare, among the different consolidation levels, (a) the absolute value of the average S_u variation, and (b) the average S_u variation percentage, for each thermal load applied ($\Delta T=30$ °C and $\Delta T=60$ °C) and for the end of the heating-cooling cycle ($\Delta T=0$ °C). Figures 5, 6, 7 and 8 show the relationships described for distances from the pile surface of 2, 5, 8 and 12 cm, respectively.

An example of the interpretations reported can be extracted from the tests carried out at a distance of 2 cm for containers subjected to 25 and a 100 kPa during consolidation, as shown in Figure 5. For the former, the absolute average S_u increments in the studied region were 7.32 and 1.05 kPa during $\Delta T=60$ °C and after system cooling,

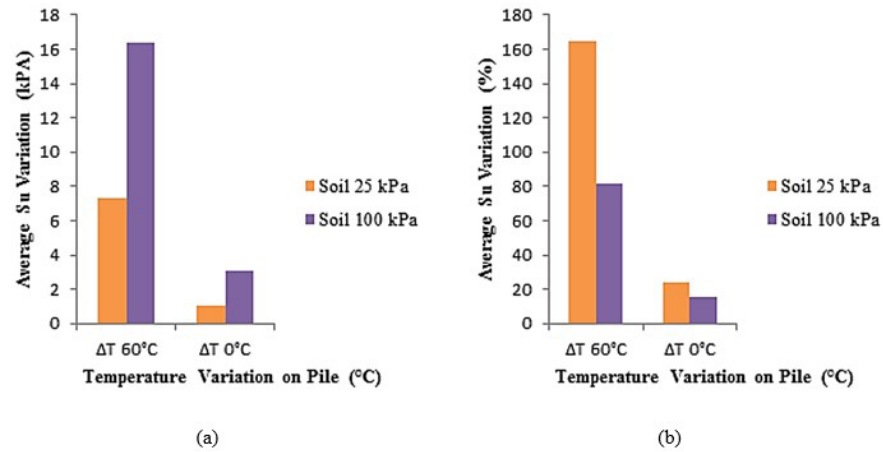


Figure 5. Average S_u variation in (a) absolute values and (b) percentage for the 2 cm test distance.

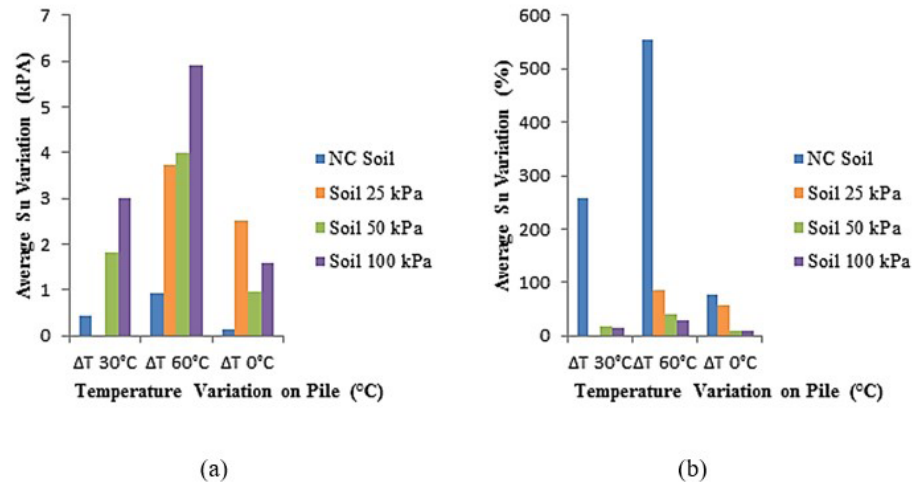


Figure 6. Average S_u variation in (a) absolute values and (b) percentage for the 5 cm test distance.

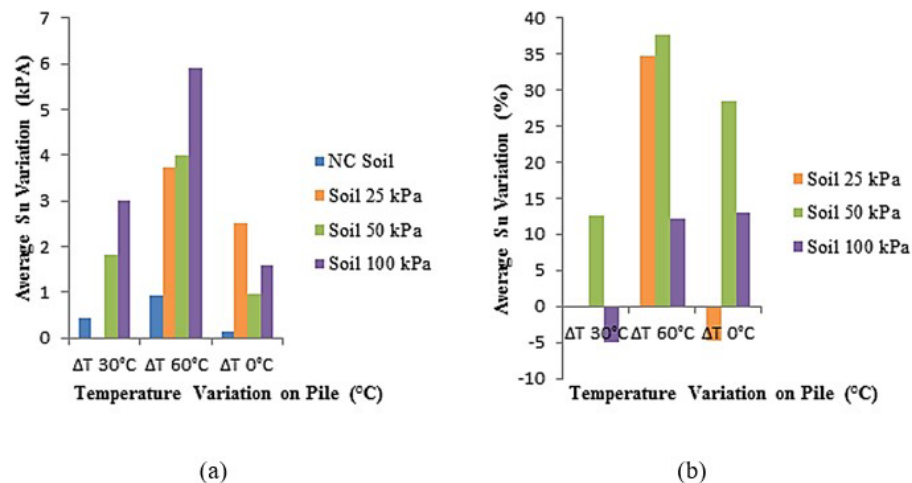


Figure 7. Average S_u average in (a) absolute values and (b) percentage for the 8 cm tests distance.

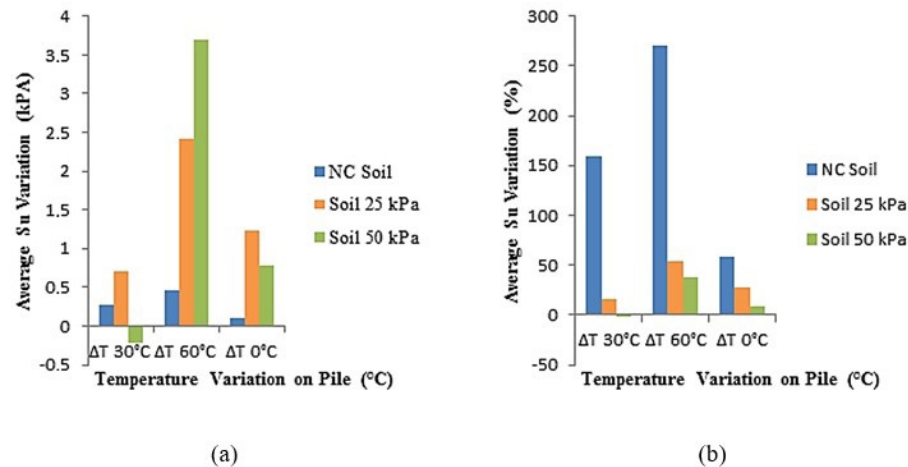


Figure 8. Average S_u variation in (a) absolute values and (b) percentage for the 12 cm test distance.

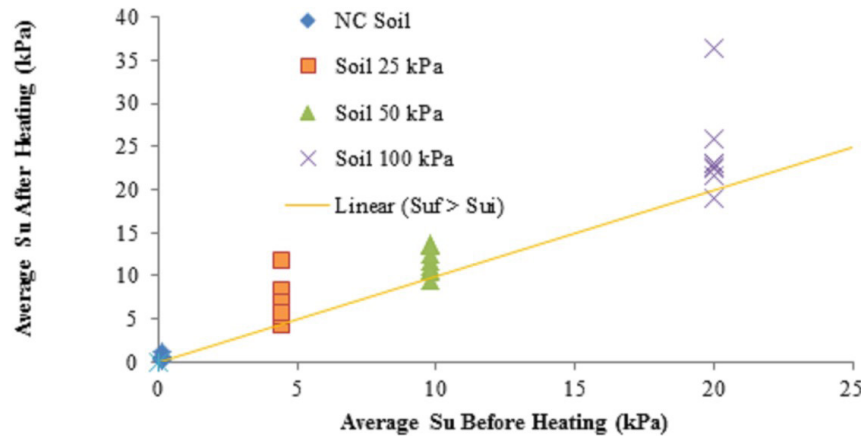


Figure 9. Relation between the average strength of tests under the influence of temperature and the initial average strength prior to heating for different consolidation levels.

respectively, while the average percentage increase for the same situations were 165 and 24%. For the latter container, the absolute average S_u increments were 16.28 and 3.1 kPa, during $\Delta T=60^\circ\text{C}$ and $\Delta T=0^\circ\text{C}$, while the average gains were 82 and 15%.

The graphs show that the highest average S_u variation occurred during heating with a 60°C variation on the pile. Moreover, there was relevant S_u variation even for the furthest distance – 12 cm from the pile surface. Finally, it is important to note that some tests showed negative average strength variation.

A summary of the influence of temperature on the average undrained shear strength of the soils is illustrated in Figure 9. In the figure, all the average S_u variation values are plotted as a function of their initial reference value, prior to heating, for each consolidation level. On the graph, a 45° slope line divides the points with strength gain due to the influence of temperature – those above the line, and with strength loss – those below the line.

4. Conclusions

In general, it can be said that the experimental program achieved the initial goals. Mechanical and thermal consolidation worked very well. The T-Bar tests made it possible to determine the undrained shear strength profiles of the models in the different stages.

Due to the low level of effective stress at 1g, an average undrained shear strength profile was determined, and the efficiency of thermal consolidation evaluated by comparing the average value of each stage against the initial value.

As expected, the normally consolidated and slightly overconsolidated models showed the greatest percentage S_u increase, while the strongly overconsolidated models show that thermal consolidation is less efficient. In addition, results after the heating-cooling cycle reveal some irreversible changes, which is more interesting from a technical standpoint.

Acknowledgements

The authors would like to thank Petrobras for the financial support for this research project. The work described in this article is part of a Term of Cooperation signed between Petrobras and the State University of Northern Fluminense Darcy Ribeiro (UENF), to develop the research project entitled “Optimized Solutions of Fixed Anchorage Points” (Contractual Instrument 0050.0098204.15.9). The first author is grateful to the UENF for the scholarship granted.

Declaration of interest

The authors have no conflicts of interest to declare. All co-authors have observed and affirmed the contents of the paper and there is no financial interest to report.

Authors' contributions

João Alberto Machado Leite: conceptualization, Data curation, Writing – original draft. Sérgio Tibana: conceptualization, Methodology, Supervision, Project administration, Writing – review & editing.

List of symbols

%	percentage;
°C	degrees Celsius;
cm	centimeters;
<i>g</i>	acceleration of gravity;
<i>h</i>	hours;
<i>kPa</i>	kiloPascal;
<i>LL</i>	liquid limit;
<i>mm</i>	millimeters;
<i>NC</i>	normally consolidated;
OCR	over consolidation ratio;
<i>Su</i>	undrained shear strength;
UENF	Universidade Estadual do Norte Fluminense
ΔT	temperature variation;
σ	effective stress.

References

- Baldi, G., Hueckel, T., & Pellegrini, R. (1988). Thermal volume changes of the mineral-water system in low-porosity clay soils. *Canadian Geotechnical Journal*, 25(4), 807-825. <http://dx.doi.org/10.1139/t88-089>.
- Campanella, R.G., & Mitchell, J.K. (1968). Influence of temperature variations on soil behavior. *Journal of the Soil Mechanics and Foundation Engineering Division*, 94(3), 709-734. <http://dx.doi.org/10.1061/JSFEAQ.0001136>.
- Chen, D., & McCartney, J.S. (2016). Parameters for load transfer analysis of energy pile in uniform nonplastic soils. *International Journal of Geomechanics*, 17(7), 1-17. [http://dx.doi.org/10.1061/\(ASCE\)GM.1943-5622.0000873](http://dx.doi.org/10.1061/(ASCE)GM.1943-5622.0000873).
- Cui, Y.J., Sultan, N., & Delage, P. (2000). A thermomechanical model for saturated clays. *Canadian Geotechnical Journal*, 37(3), 607-620. <http://dx.doi.org/10.1139/t99-111>.
- Delage, P., Sultan, N., & Cui, Y.J. (2000). On the thermal consolidation of Boom clay. *Canadian Geotechnical Journal*, 37(2), 343-354. <http://dx.doi.org/10.1139/t99-105>.
- Demars, K.R., & Charles, R.D. (1982). Soil volume changes induced by temperature cycling. *Canadian Geotechnical Journal*, 19(2), 188-194. <http://dx.doi.org/10.1139/t82-021>.
- Goode III, J.C., & McCartney, J.S. (2015). Centrifuge modeling of boundary restraint effects in energy foundations. *Journal of Geotechnical and Geoenvironmental Engineering*, 141(8), 04015034. [http://dx.doi.org/10.1061/\(ASCE\)GT.1943-5606.0001333](http://dx.doi.org/10.1061/(ASCE)GT.1943-5606.0001333).
- Hueckel, T., & Pellegrini, R. (1992). Effective stress and water pressure in saturated clays during heating-cooling cycles. *Canadian Geotechnical Journal*, 29(6), 1095-1102. <http://dx.doi.org/10.1139/t92-126>.
- Laloui, L., & Cekerevac, C. (2008). Non-isothermal plasticity model for cyclic behaviour of soils. *International Journal for Numerical and Analytical Methods in Geomechanics*, 32(5), 437-460. <http://dx.doi.org/10.1002/nag.629>.
- Mimouni, T., & Laloui, L. (2014). Towards a secure basis for the design of geothermal piles. *Acta Geotechnica*, 9(3), 355-366. <http://dx.doi.org/10.1007/s11440-013-0245-4>.
- Murphy, K.D., McCartney, J.S., & Henry, K.S. (2015). Evaluation of thermo-mechanical and thermal behavior of full-scale energy foundations. *Acta Geotechnica*, 10(2), 179-195. <http://dx.doi.org/10.1007/s11440-013-0298-4>.
- Ng, C.W.W., Shi, C., Gunawan, A., & Laloui, L. (2014). Centrifuge modelling of energy piles subjected to heating and cooling cycles in clay. *Geotechnique Letters*, 4(4), 310-316. <http://dx.doi.org/10.1680/geolett.14.00063>.
- Ng, C.W.W., Shi, C., Gunawan, A., Laloui, L., & Liu, H.L. (2015). Centrifuge modelling of heating effects on energy pile performance in saturated sand. *Canadian Geotechnical Journal*, 52(8), 1045-1057. <http://dx.doi.org/10.1139/cgj-2014-0301>.
- Plum, R.L., & Esrig, M.I. (1969). *Some temperature effects on soil compressibility and pore water pressure* (pp. 231-242). Washington: Highway Research Board.
- Slovic, P., Flynn, J., & Layman, M. (1991). Perceived risk, trust, and the politics of nuclear waste. *Science*, 254(5038), 1603-1607. <http://dx.doi.org/10.1126/science.254.5038.1603>.
- Stewart, D.P., & Randolph, M.F. (1991). A new site investigation tool for the centrifuge. In *Proc. International Conference on Centrifuge Modelling – Centrifuge* (pp. 531-538), Boulder.

Numerical study on heat transfer performance of geothermal piles in a Brazilian sandy soil

Caique Roberto de Almeida¹ , Cyro Albuquerque Neto² ,

Cristina de Hollanda Cavalcanti Tsuha³ , Maria Eugenia Gimenez Boscov^{1#} 

Article

Keywords

Geothermal pile
Numerical model
TRT
Air conditioning
Energy consumption

Abstract

The worldwide consumption of electric energy destined for air conditioners, expected to triple by 2050, can be lessened by geothermal piles, which transfer heat from the internal environment of buildings to the subsoil. This paper shows the influence of pile geometry and properties of soil, pile, and pipe materials on the heat transfer of a geothermal pile to the surrounding soil, to support design from the viewpoint of thermal performance optimization. A numerical model was developed with ANSYS CFX 19.2, a high-performance Computational Fluid Dynamics tool, and calibrated using data from a thermal response test performed in a saturated sandy soil in São Paulo, Brazil. A parametric analysis was carried out varying pile length, diameter, and slenderness; soil and pile material conductivities; degree of saturation; fluid inlet temperature; fluid flow rate; and pipe thermal resistance. Results show that the fluid inlet temperature is the most influential parameter on the thermal performance of the pile. Heat transfer grows when geometrical parameters (diameter and length) are increased mainly due to an increase in heat exchange surface area, whereas the normalized heat transfer rate per unit of surface area of the pile is practically unaltered. Higher soil, pipe and pile thermal conductivities improve thermal performance. The degree of saturation increases the thermal conductivity of the soil; however, the effect is not remarkable on the system's thermal performance for saturation degrees higher than 20%. The fluid flow must be turbulent but increases above a certain flow rate do not improve the thermal performance.

1. Introduction

The worldwide use of air conditioners to refrigerate buildings consumed approximately 2,000 TWh of electric energy in 2018, a demand that tripled from 1990 to 2018. By 2050, this number is expected to exceed 6,000 TWh, with the most significant increases occurring in emerging economies with hottest climates (IEA, 2018). This increasing trend is enhanced by climate change (Hernandez Neto, 2020), since rising average temperatures will lead to a significant increase in CDDs (Cooling Degree Days) around the world, though at differing rates across regions: a 1 °C increase in global average temperature by 2050 may lead to an average increase in CDDs of 25% (IEA, 2018). The baseline scenario modeled by the International Energy Agency previews a rise in the number of individual cooling units or systems worldwide from just above 3.4 billion in 2016 to more than 8 billion in

2050 in the residential sector, and from 530 million to over 1.3 billion in the commercial sector (IEA, 2018).

Meanwhile, the worldwide use of geothermal energy increased from 8,664 MW to 70,329 MW between 1995 and 2015. Ground source heat pumps (GSHP) for air conditioning - piles, boreholes, closed or open loop systems - are responsible for 55.3% of the produced geothermal energy, a small contribution to the reduction of electrical energy consumption (IEA, 2018). Heating by geothermal piles started in Europe in 1984 (Brandl, 2006) and had an average increase of 10% per year in the following 20 years (Curtis et al., 2005).

In Brazil, the rise in average family income provided conditions for the ownership of household air conditioners to increase 9.0% per year from 2005 to 2017, consequently more than tripling electricity consumption for air conditioners (EPE, 2018). The electricity consumption for air conditioners

#Corresponding author. E-mail address: meboscov@usp.br

¹Universidade de São Paulo, Department of Structural and Geotechnical Engineering, São Paulo, SP, Brasil.

²Centro Universitário FEI, Department of Mechanical Engineering, São Bernardo do Campo, SP, Brasil.

³Universidade de São Paulo, Department of Geotechnical Engineering, São Carlos, SP, Brasil.

Submitted on October 29, 2021; Final Acceptance on January 17, 2022; Discussion open until May 31, 2022.

<https://doi.org/10.28927/SR.2022.076621>



This is an Open Access article distributed under the terms of the Creative Commons Attribution License, which permits unrestricted use, distribution, and reproduction in any medium, provided the original work is properly cited.

reached 18.7 TWh in 2017 and is predicted to reach 48.5 TWh in 2035.

Brazil is the ninth largest consumer of electrical energy in the world (Pereira et al., 2013). Geothermal energy in Brazil is mainly utilized for BRT (Bathing, Recreation and Tourism), PIS (Potential for Industrial use and Space heating) and TDB (Therapeutic, Drinking and Bathing). The contribution of geothermal energy to the overall Brazilian electrical energy generation, only 0.3% in 2012, is expected to reach 1% by 2040 (IEA, 2016).

In tropical climates, geothermal piles may take advantage of the deep foundations of buildings to dissipate thermal energy in superficial layers of soils (Loveridge & Powrie, 2013). However, research on the efficiency of energy piles to cool internal building temperatures in tropical climates is still limited. In Brazil, interest is still concentrated in the academy and the first case of geothermal piles for building conditioning was implanted in 2020 (Tsuha, 2020).

Some studies analyzed the potential of GSHP technology in Brazilian soils and climate. Morais et al. (2020) carried out a thermal response test (TRT) in a 12-m long geothermal pile of 0.25-m diameter installed in unsaturated lateritic clayey sand in São Carlos (SP), observing that performance was greatly affected by seasonality. Bandeira Neto (2015) tested 12-m long geothermal piles in the same soil, obtaining heat exchange rates by pile length of 79 W.m⁻¹ to 110 W.m⁻¹ for diameters ranging from 0.25 m and 0.50 m. These results were later employed by Orozco (2016) to formulate a numerical model in COMSOL Multiphysics software. Ferreira (2017) performed TRTs in a 12-m long geothermal pile of 0.4-m diameter installed in clayey soil in Campos dos Goytacazes (RJ) and concluded that, despite favorable soil thermal properties, the high undisturbed soil temperature made unfeasible the use of this technology to cool buildings interiors. Morais & Tsuha (2018) conducted a TRT in a 15-m long pile of 0.35-m diameter inserted in a sandy subsoil with high groundwater level (1.9 m below the surface) in São Paulo (SP) to obtain design parameters for the foundations of the CICS Living Lab building, which is the first case of use of geothermal piles in Brazil.

Ozudogru et al. (2014) developed and validated a numerical model of a TRT (0.45-m diameter and 20-m length) in sandy soil using COMSOL Multiphysics software. The adopted hypotheses were: conduction is the process that governs heat transfer in geothermal systems; heat transfer predominantly occurs in the radial direction; and the steel cage hardly influences heat exchange between pile and soil. Thompson III (2013) validated a numerical model based on a TRT performed in a 0.3-m diameter and 25-m geothermal pile in clayey and sandy soils, considering that the circulating fluid is incompressible and initial temperatures equal in the entire geothermal system.

This paper shows the results of numerical simulations carried out to investigate the heat transfer potential of geothermal piles as a function of pile geometry and involved

materials, based on data from the TRT conducted by Morais & Tsuha (2018). The aim is to understand better the thermal performance of a geothermal pile considering local conditions of subsoil and climate.

2. Methods

The numerical model was developed in ANSYS CFX 19.2 Software, a Computational Fluid Dynamics (CFD) tool largely used in industry and in academic Multiphysics projects to solve complex problems with high-performance computing. The transport phenomena of heat transfer and fluid flow are represented by partial differential equations, and the CFX application uses the Finite Volume Method (FVM) as a form of discretization for the equations' solution (Maliska, 2004).

The numerical procedure followed two steps: (i) model validation, using experimental data from a TRT; and (ii) the parametric study, where the influence of the following parameters on pile performance were investigated: length, diameter and slenderness of the pile, pile and soil thermal conductivities, soil degree of saturation, fluid inlet temperature, fluid flow rate and pipe thermal resistance.

3. Experimental data: TRT

The TRT was performed by Morais & Tsuha (2018) on a 0.35-m diameter and 15-m long micropile (filled with grout) with a single U-loop (HDPE pipe with 32 mm external diameter and 26 mm internal diameter) during 10 days in February 2017 (Brazilian summer). 20-m deep prospecting boreholes conveyed a soil profile composed of a thick layer of clayey sand covered by a 2.5-m layer of organic silt-sandy clay, and a borrow 1-m top layer of red to gray silt-sandy clay. The groundwater level depth, which varies from 2 to 4 m along the year, was 1.9 m during the test.

The undisturbed soil temperature was determined prior to the TRT by measuring the circulating water inlet and outlet temperatures without heat input into the system. During the test, a flow rate of $3.52 \times 10^{-3} \text{ m}^3 \times \text{s}^{-1}$ and an applied power of 1,061 W or $70.8 \text{ W} \times \text{m}^{-1}$ (heat rate per unit length of pile) were used. Test results show that the heat rate injected into the pile was practically constant, variations in ambient temperature influenced the circulating fluid, and the geothermal system stabilized after 50 hours. Values obtained using the infinite line source theory were: λ (slope of the average temperature \times log time curve) = 1.99 with correlation coefficient $R^2 = 0.85$, soil thermal conductivity $K = 2.82 \text{ W} \times \text{m}^{-1} \times \text{K}^{-1}$, and soil thermal resistance $rb = 0.13 \text{ m} \times \text{K} \times \text{W}^{-1}$. Table 1 shows the temperatures recorded during the TRT.

Table 1. Measured temperatures during the TRT (Morais & Tsuha, 2018).

TRT measurement	Value
Undisturbed ground temperature (K)	297.33
Average ambient temperature (K)	301.15
Maximum ambient temperature (K)	315.95
Minimum ambient temperature (K)	294.15
T _{in} 50 hours (K)	312.45
T _{out} 50 hours (K)	311.65
T _{in} 100 hours (K)	313.25
T _{out} 100 hours (K)	312.45
T _{in} 200 hours (K)	314.25
T _{out} 200 hours (K)	313.55
Flow rate (m ³ s ⁻¹)	0.66
Average heat power (kW)	1.06

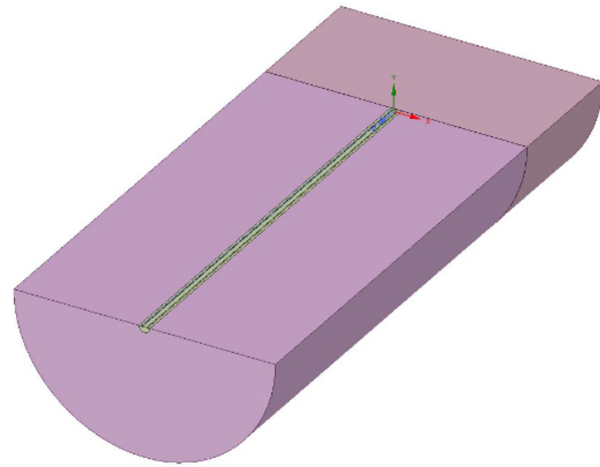
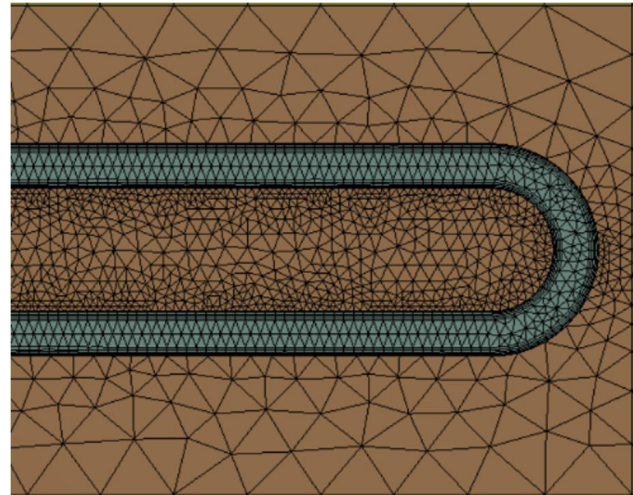
4. Numerical model

4.1 Geometry

The Space Claim module was used to create the geometry of the numerical model. The pile has a diameter of 0.35 m and a length of 15 m. The pipes have an inner diameter of 26 mm and an outer diameter of 32 mm. The bottom of the U loop was placed 10 cm above the pile tip. The steel cage was ignored since it has little influence on the heat exchange processes (You et al., 2017; Ozudogru et al., 2014). The soil was modeled as a continuous medium with cylindrical shape and 3-m radius (approximately 8.5 times the pile diameter), i.e., a distance large enough for the influence of pile heating on the soil to be negligible. Additionally, the model adopted a 3-m thick soil layer below the pile tip. The simulations were performed on a symmetrical half of the problem to decrease computational cost. Figure 1 illustrates the geothermal system geometry in ANSYS CFX.

4.2 Mesh

The mesh was created using the Meshing module. The mesh was refined inside the pipes, where there is circulating fluid, since the phenomena of turbulent water movement and forced convection make the modeling process more complex. The complexity of these phenomena also advises against the simplifying hypothesis of thermal energy flow in preferential directions, a fundamental condition for the choice of hexahedral elements. Therefore, tetrahedral elements, which are suitable for complex geometries such as the bottom of the U-loop, were used for the circulating fluid mesh. Tetrahedral elements also facilitate adjusting the mesh of transition zones compared to hexahedral elements. However, tetrahedral elements with different dimensions in pile and fluid must be matched to keep mesh connectivity

**Figure 1.** Geothermal pile geometry.**Figure 2.** Transition mesh between fluid and grout.

and quality. The Inflation command generates prismatic elements to address connection problems and helps the user in the iterative process of restructuring previously defined tetrahedral elements to obtain adequate transitions. The space delimited by the surfaces of the HDPE pipes has 258,400 nodes and 551,765 elements. Figure 2 shows the mesh in the U-loop region.

Hexahedral elements (which form a mesh with fewer elements and reduce computational cost) were chosen to model the soil surrounding the pile. It is an acceptable choice since they are aligned in the direction of the thermal flow: radial heat transfer is the predominant mode of heat flow in a geothermal pile (Sani et al., 2019). As the surrounding soil mesh approaches the region where heat flow phenomena occur, smaller elements are necessary to guarantee a progressive refinement from the soil to the pile. The surrounding soil geometry has

692,640 nodes and 661,248 elements. Figure 3 illustrates the ground mesh around the pile (XY axis).

Tetrahedral elements were used for the pile as the best configuration to meet the criterium of greater refinement (compared to the surrounding soil), also achieving an adequate transition between surrounding soil (coarser) and fluid mesh (more refined). The pile's central region, between the pipes, was more refined compared to the annular elements between soil and pipes because it is a transition between very refined regions (pipes). For the pile, 270,148 nodes and 1349,839 elements were used. Figure 4 illustrates the pile mesh in three-dimensional view.

For the soil geometry below the pile tip, the mesh should match the soil surrounding the pile and pile element (more refined), therefore, tetrahedral elements were used. Moreover, in this region energy flow does not occur predominantly in the radial direction, which rules out the use of hexahedral elements. The soil geometry below the pile has 50,042 nodes and 260,957 elements. Figure 5 shows the soil mesh at the bottom of the pile.

4.3 Turbulence model

The $k-\varepsilon$ turbulence model was used in the Setup module. This model, commonly used in CFD simulations, is based on two equations representing the turbulent flow properties of

turbulent kinetic energy (kt) and turbulent energy dissipation (εt), responsible for determining the turbulence scale.

4.4 Model validation

The TRT performed by Moraes & Tsuha (2018) was used for the model validation. Three different times during the TRT were simulated; at each time, steady state condition was considered. The comparison was based on measured and simulated temperatures. A good fit in the validation phase indicates that the numerical model is reliable for parametric studies.

The parameters of the grout material were: density of $2400 \text{ kg}\times\text{m}^{-3}$, specific thermal capacity of $1000 \text{ J}\times\text{kg}^{-1}\times\text{K}^{-1}$, and thermal conductivity of $2.0 \text{ W}\times\text{m}^{-1}\times\text{K}^{-1}$. The HDPE pipes were simulated by a surface with a thermal resistance of $0.012 \text{ m}^2\times\text{K}\times\text{W}^{-1}$, calculated from a thickness of 6 mm and a thermal conductivity of $0.5 \text{ W}\times\text{m}^{-1}\times\text{K}^{-1}$ (ABNT, 2003; Orozco, 2016). Water properties at 25°C are: density $997 \text{ kg}\times\text{m}^{-3}$, specific thermal capacity $4181.7 \text{ J}\times\text{kg}^{-1}\times\text{K}^{-1}$, and thermal conductivity $0.6069 \text{ W}\times\text{m}^{-1}\times\text{K}^{-1}$. The thermal conductivity of the soil estimated by the TRT was $2.82 \text{ W}\times\text{m}^{-1}\times\text{K}^{-1}$. The specific thermal capacity of the soil was estimated as $1578.9 \text{ J}\times\text{kg}^{-1}\times\text{K}^{-1}$ based on Lhendup et al. (2014).

The following boundary conditions were applied:

- Time $t = 50 \text{ h}$: fluid inlet temperature 312.42 K , mass flow $0.3363 \text{ kg}\times\text{s}^{-1}$, ambient temperature 310.71 K , heating power 1031.20 W , undisturbed ground temperature 297.33 K (same for the three times);
- Time $t = 100 \text{ h}$: fluid inlet temperature 313.26 K , mass flow $0.3366 \text{ kg}\times\text{s}^{-1}$, ambient temperature 311.16 K , heating power 1083.44 W ;
- Time $t = 200 \text{ h}$: fluid inlet temperature 314.29 K , mass flow rate $0.3663 \text{ kg}\times\text{s}^{-1}$, ambient temperature 313.10 K , heating power 1107.29 W .

Heat is exchanged by natural convection at the top of the geothermal system (adopted convection heat coefficient

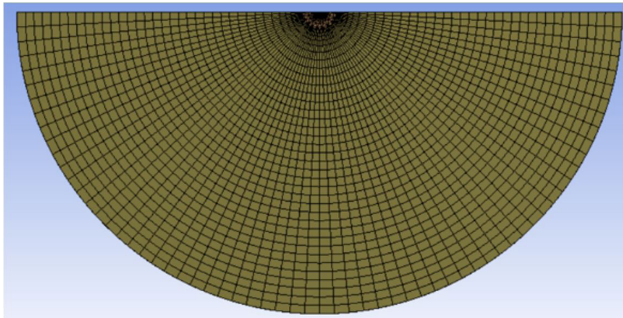


Figure 3. Detail of the soil mesh surrounding the geothermal pile.

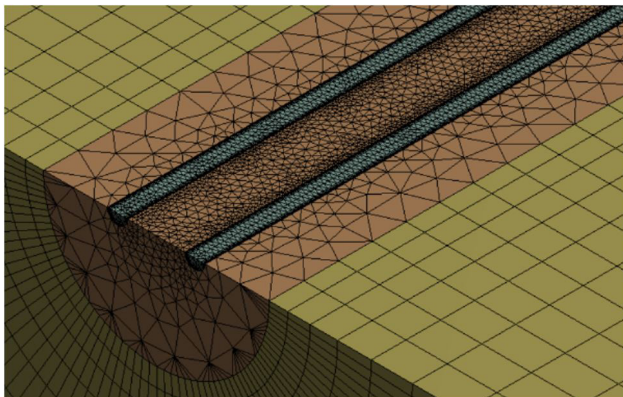


Figure 4. 3D meshes of the pile material, pipes, and soil.

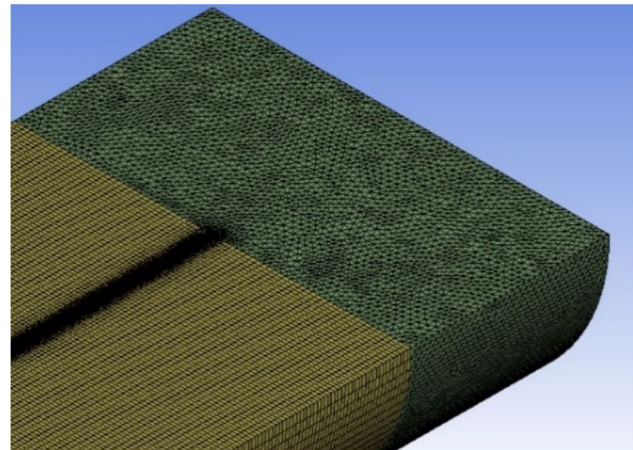


Figure 5. Mesh of the soil geometry below the pile tip.

of $10 \text{ W}\times\text{m}^{-2}\times\text{K}^{-1}$). In the outlet pipes the fluid is assumed to flow at atmospheric pressure. Soil temperature of 297.33 K (undisturbed ground temperature) was adopted for the distance of 3 m from the pile axis and at 3 m below the pile tip. Initially, the pile and soil temperatures are equal. Additionally, the soil limit domain is adiabatic; thus, all phenomena occur within the system composed of fluid, pipes, pile material and soil. Water circulates inside the pipes under turbulent flow conditions, Reynolds number equal to $17,109$.

Table 2 compares experimental and numerical values of outlet temperature for the three times evaluated. The standard deviation for experimental temperatures was calculated considering the temperatures before and after (in a 1-minute interval) those measured at 50 , 100 and 200 h . Combined uncertainty was calculated using Equation 1.

$$u_c^2 = u_i^2 + \sigma^2 \quad (1)$$

where: u_c is the combined uncertainty, u_i is the standard uncertainty (calculated as half of the PT-100 sensors' error limit) and σ is the standard deviation.

The deviations between numerical and experimental outlet temperatures are lower than the error limit of the PT-100 sensors ($\pm 0.5 \text{ K}$). The simulations based on the described parameters and conditions provided consistent numerical results when compared to the experimental results, therefore, the model was considered validated.

Figure 6 shows the values of total heat transfer rate obtained at the interfaces pipe/pile, pile/soil, soil/air and soil limit (radius of 3 m measured from the pile axis). The heat transfer rate at the pile/soil interface increased from 50 h (420.04 W) to 200 h (474.63 W), when the geothermal system stabilizes. This value of total heat transfer rate at the pile/soil interface under stable conditions indicates a relevant potential for thermal energy dissipation. Heat transfer rates at the pipe/pile interface are slightly higher than at the pile/soil interface. The soil limit presents a much higher rate (723.34 W at 200 h), due to the heat absorbed from the environment above the soil/pile system, where the air temperature is 313.1 K . This hypothesis is confirmed by the heat transfer rates at the soil/air interface, equivalent to the difference between the rates at the pipe/pile and soil limit interfaces. This phenomenon was observed in all stages of the parametric study.

Table 2. Combined uncertainty of numerical results.

Time	Experimental outlet temperature (K)	Numerical outlet temperature (K)	Deviation (K)	Combined uncertainty ($\pm\text{K}$)
50	311.7	311.6	0.1	0.3
100	312.5	312.7	-0.2	0.3
150	313.6	313.8	-0.2	0.3

Figure 7 shows the radial distribution of temperatures in a XY plane located at depth 7.5 m and time 200 h . Temperatures decrease as the radial distance from the pile center reaches the soil limit (undisturbed soil temperature = 297.3 K). Figure 8 illustrates the temperature distribution in a XZ plane (located at the pile center). The thermal influence zone's diameter (zone where the temperatures are at least 1 K higher than the undisturbed soil temperature) is 4.55 m .

5. Parametric analysis

The basic scenario for the simulations consisted of the following parameters: 15 m length, 0.35 m diameter, grout thermal conductivity of $2 \text{ W}\times\text{m}^{-1}\times\text{K}^{-1}$, and soil thermal conductivity of $2.82 \text{ W}\times\text{m}^{-1}\times\text{K}^{-1}$.

5.1 Pile length

Pile lengths (L) of 5 , 10 , 15 , 20 , 30 , and 50 m were simulated for a 0.35-m pile diameter. Increase in pile/soil heat exchange area increases the heat transfer rates at the pipe/pile, pile/soil, soil limit and soil/air interfaces (Figure 9a). However, Figure 10b shows that the heat transfer rate normalized by the pile surface area increases by 10% when the pile length increases from 5 to 50 m , but mostly until 20-m length. For piles longer than 20 m , increase in pile

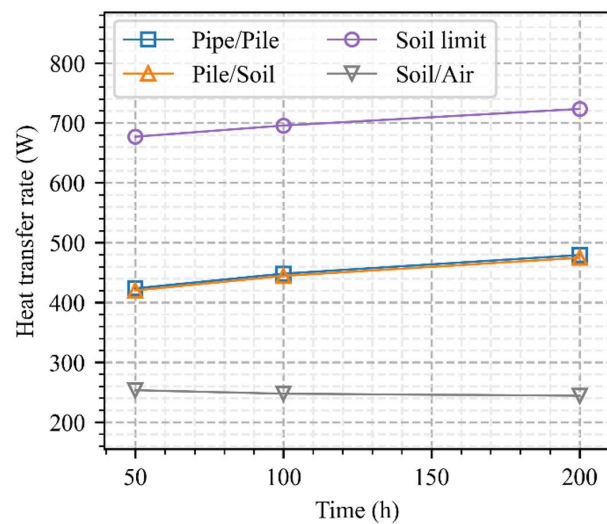


Figure 6. Heat transfer rate as a function of time at interfaces of the geothermal system.

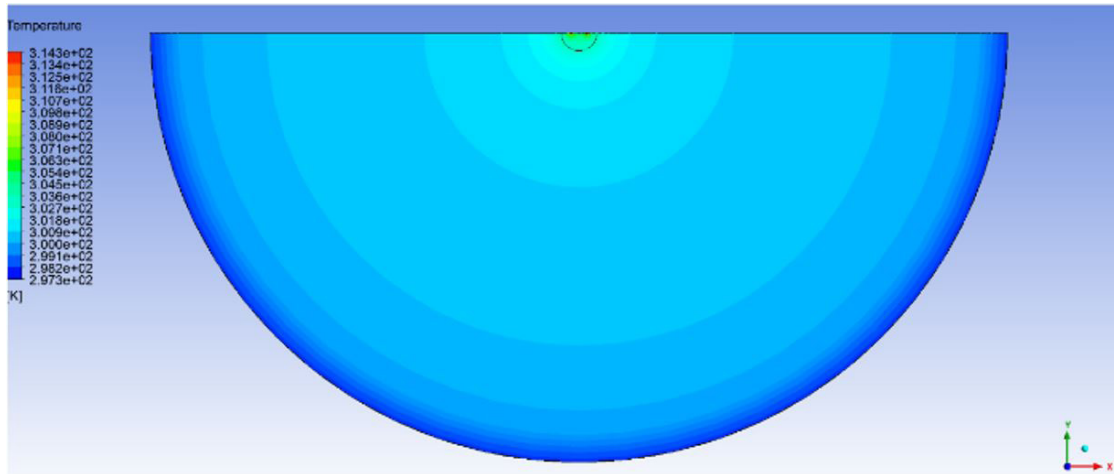


Figure 7. Radial distribution of temperatures in a XY plane at depth 7.5 m, time = 200 h.

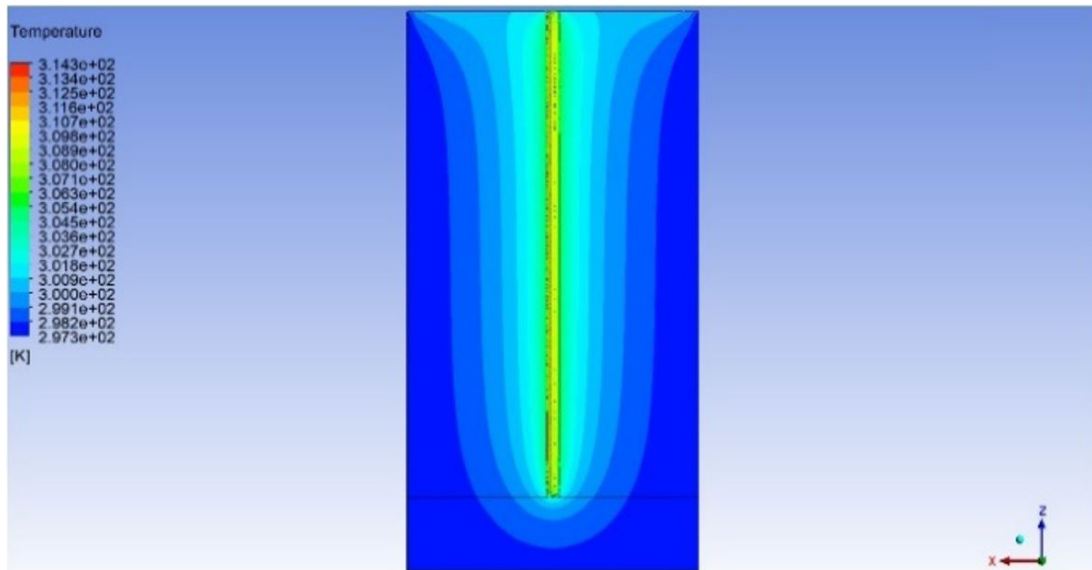


Figure 8. Distribution of temperatures in a XY plane located at the pile center, time = 200 h.

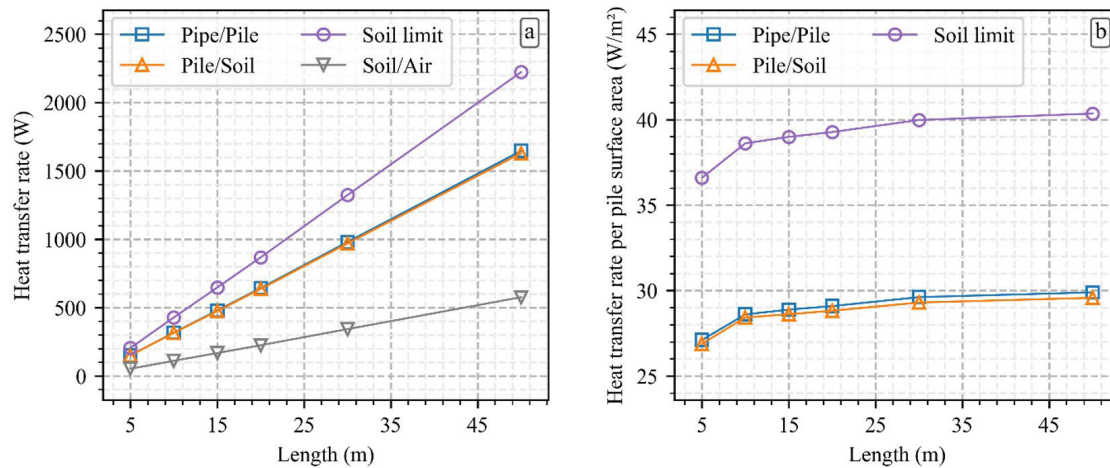


Figure 9. Heat transfer rate vs pile length: (a) total; (b) normalized by pile surface area.

length (consequently in pile surface) provides higher total heat exchanges (Figure 9a) but does not significantly improve the thermal efficiency per unit area.

5.2 Pile diameter

Pile diameters (D) of 0.2 m, 0.35 m, 0.50 m, 0.70 m, 0.90 m, and 1.1 m were simulated for a pile length of 15 m. The increase in diameter (and the consequent increase in the heat exchange area between pile and soil) allows an increase in heat transfer rate at the pipe/pile, pile/soil, soil/air and soil limit interfaces. Figure 10a shows the linear growth of the heat transfer rate with the increase of pile diameter. Figure 10b shows the variation of heat transfer rate normalized by pile surface area as a function of pile diameter. At the pile/soil interface, the normalized heat transfer rate increases by 7% when the diameter increases from 0.2 m to 1.1 m. For pile diameters larger than 0.35 m, the increase in diameter provides

higher heat exchange, but the thermal efficiency of the pile per unit area of surface is little affected.

5.3 Pile slenderness

Pile slenderness index is given by L/D (Rotta Loria & Laloui, 2016). Two series were simulated: (1) varying pile length for a 0.35-m diameter pile, and (2) varying pile diameter of a 15-m long pile. The slenderness indexes for series (1) were: 14.3, 28.6, 42.9, 57.1, 85.7, and 142.9. Increase in the pile/soil heat exchange area causes an increase in total heat transfer rates at the interfaces: the heat transfer rate increases linearly with the pile slenderness index (Figure 11a). The slenderness indexes simulated for series (2) were: 11.8, 14.4, 18.6, 26.0, 37.1, and 65.0. In this case, L/D ratio increases with the decrease of pile diameter; consequently, the reduction of pile/soil heat exchange area causes a reduction of total heat transfer rates at the system

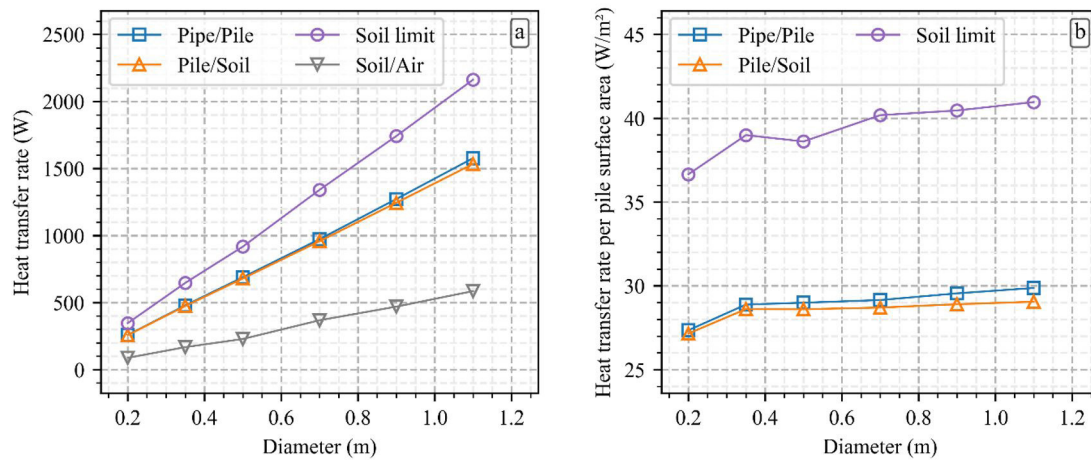


Figure 10. Heat transfer rate vs pile diameter: (a) total; (b) normalized by the pile surface area.

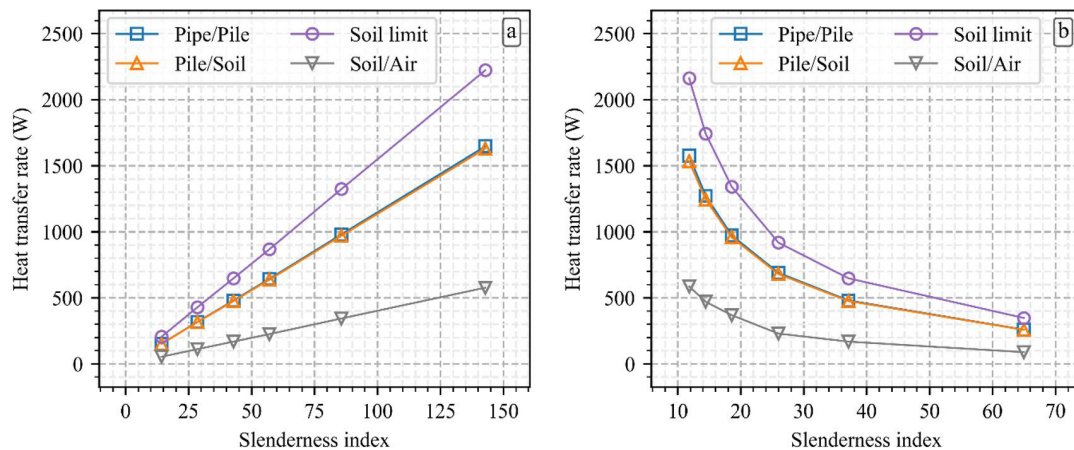


Figure 11. Heat transfer rate vs slenderness: (a) series 1; (b) series 2.

interfaces. Therefore, the heat transfer rate decreases with the increase of the slenderness index for a particular pile length (tending to asymptotes), as shown in Figure 11b. Comparison of Figures 11a and b indicates that the slenderness index is not an adequate indicator for the heat transfer rate of geothermal piles. The pile surface area controls the magnitude of total heat transfer rates. Thus, a particular slenderness index can be related to different values of pile surface area, which would result in different total heat transfer rates.

5.4 Thermal conductivity of the pile material

The grout conductivity varied from $0.17 \text{ W}\times\text{m}^{-1}\times\text{K}^{-1}$ (autoclaved cellular concrete) to $3.85 \text{ W}\times\text{m}^{-1}\times\text{K}^{-1}$ (GAM concrete; Asadi et al., 2018). For pipe/pile, pile/soil and soil limit interfaces, heat transfer rate increases with the increase in grout thermal conductivity, tending to asymptotes (Figure 12). Between the extreme grout thermal conductivity values, the heat transfer rate increased up to 3.6 times at the pile-soil interface. However, thermal conductivities higher than $4 \text{ W}\times\text{m}^{-1}\times\text{K}^{-1}$ apparently will not be accompanied by a further increase in heat transfer rates.

5.5 Soil thermal conductivity

Soil thermal conductivity varied from 0.9 to $3.7 \text{ W}\times\text{m}^{-1}\times\text{K}^{-1}$ - from clay to sandstone, respectively (Lhendup et al., 2014). Heat transfer rate at all interfaces increases with soil thermal conductivity (Figure 13). At the pile-soil interface, the heat transfer rate for sandstone is 2.3 times that for clay.

5.6 Saturation degree

Soil thermal conductivity values for different saturation degrees were based on Sánchez et al. (2015):

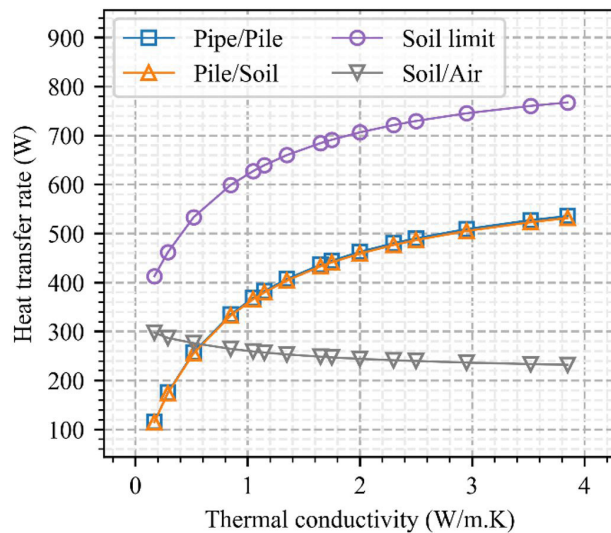


Figure 12. Heat transfer rate vs grout thermal conductivity.

$0.90 \text{ W}\times\text{m}^{-1}\times\text{K}^{-1}$ ($s = 0.015$), $1.35 \text{ W}\times\text{m}^{-1}\times\text{K}^{-1}$ ($s = 0.188$), $1.75 \text{ W}\times\text{m}^{-1}\times\text{K}^{-1}$ ($s = 0.311$), $2.10 \text{ W}\times\text{m}^{-1}\times\text{K}^{-1}$ ($s = 0.480$), $2.40 \text{ W}\times\text{m}^{-1}\times\text{K}^{-1}$ ($s = 0.715$), and $2.65 \text{ W}\times\text{m}^{-1}\times\text{K}^{-1}$ ($s = 1.000$). Heat transfer rates at the interfaces increased with soil saturation until a saturation degree of approximately 20%; further increases in saturation did not cause significant increase in heat transfer rates (Figure 14).

5.7 Fluid inlet temperature

Heat transfer rate increases linearly with the fluid inlet temperature at the pipe/pile, pile/soil and soil limit interfaces (Figure 15): as the fluid inlet temperature increases, the amount of heat injected into the geothermal system and the temperature gradient between the fluid and the rest of the

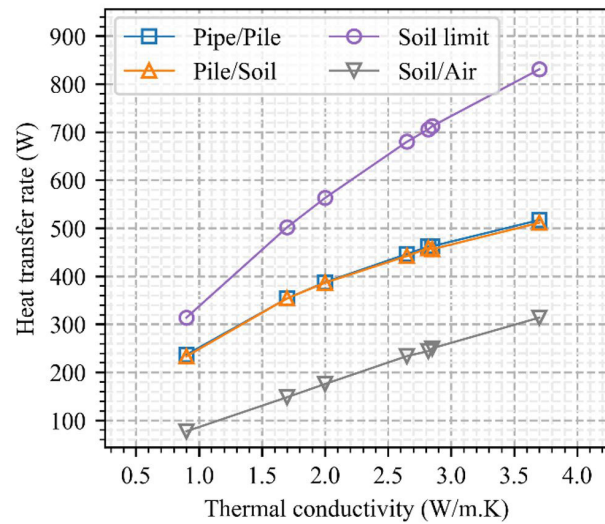


Figure 13. Heat transfer rate vs soil thermal conductivity.

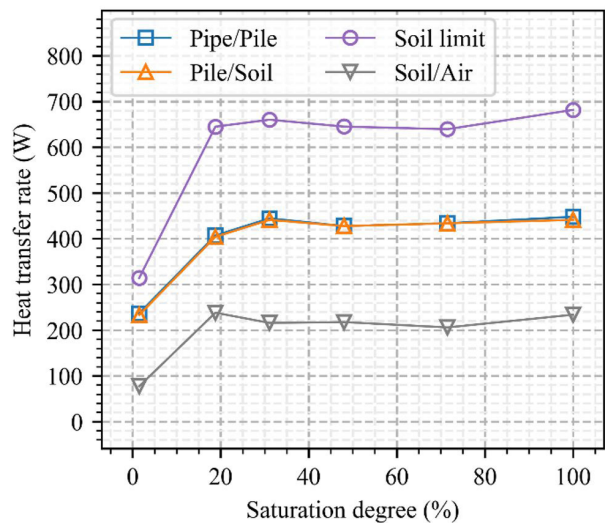


Figure 14. Heat transfer rate vs soil saturation degree.

system also increase. The difference between heat transfer rates at these interfaces decreases with increasing inlet temperature, and for inlet temperatures of approximately 360 K, such differences are lower than 50 K. The proximity among the curves in Figure 15 shows that the thermal exchanges with air in ambient temperature are not relevant as the fluid inlet temperature increases. This can be noticed at the soil/air interface: as the inlet temperatures increase the values of heat transfer rate decrease.

5.8 Fluid flow rate

Heat transfer rate exchanged between pile and soil sharply increases as flow rate increases until a value of approximately $10 \text{ L} \times \text{min}^{-1}$. However, further increases in flow rate do not result in higher heat transfer rates (Figure 16). The increase

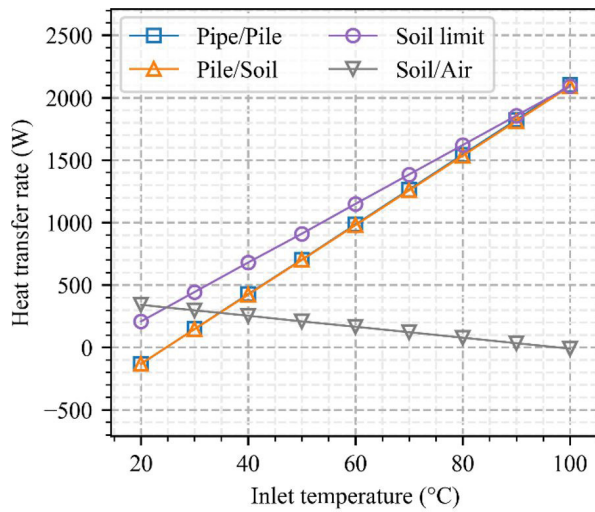


Figure 15. Heat transfer rate vs fluid inlet temperature.

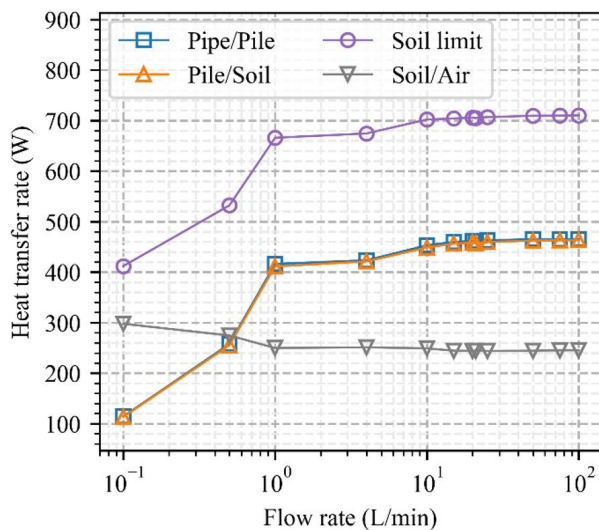


Figure 16. Heat transfer rate vs fluid flow rate.

in heat transfer rate with fluid flow rate can be explained by the relation between the Nusselt number (Equation 2), which represents the gain in terms of heat transfer resulting from the convection/conduction ratio in a fluid, and the Reynolds number (Equation 3). Increasing the velocity of the circulating fluid increases the Reynolds number, which increases the Nusselt number. This process induces greater effectiveness in terms of heat exchange by convection and increases the total heat transfer rates. On the other hand, higher flow rate values decrease the time interval in which the thermal exchanges between the fluid and pipe occur to the point that, in turbulent conditions, the high speeds result in constant heat transfer rates (Figure 16).

$$Nu = \frac{hL_c}{k} \quad (2)$$

where: Nu = Nusselt number, h = coefficient of heat transfer by convection ($\text{W} \times \text{m}^{-2} \times \text{K}^{-1}$), L_c = characteristic length (m), and k = thermal conductivity ($\text{W} \times \text{m}^{-1} \times \text{K}^{-1}$).

$$Re = \frac{uL_c}{\nu} \quad (3)$$

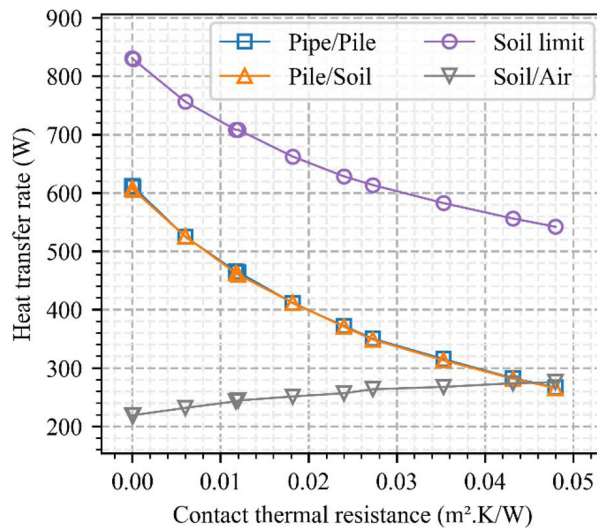
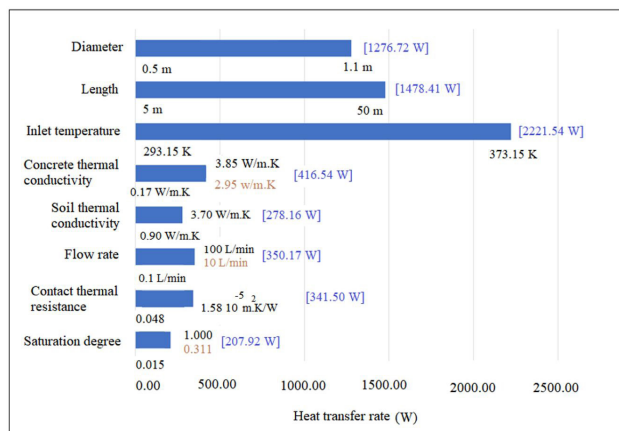
where: Re = Reynolds number, u = flow speed ($\text{m} \cdot \text{s}^{-1}$), L_c = characteristic length (m), and ν = the kinematic viscosity of the fluid ($\text{m}^2 \times \text{s}$).

5.9 Thermal resistance of pipe material

The influence of material and thickness of the pipes on the thermal efficiency of the geothermal pile was investigated by attributing different values of contact thermal resistance at the pipe-pile interface, as presented in Table 3. The increase in thermal contact resistance causes reduction of heat transfer rate values (the greater the thermal contact resistance, the greater is the difficulty imposed on the heat flow), as shown in Figure 17. Materials with higher thermal conductivities provided higher heat transfer rates, such as steel ($R = 0.00012 \text{ m}^2 \times \text{K} \times \text{W}^{-1}$ and $e = 6 \text{ mm}$, with a heat transfer rate 605.10 W at the grout/soil interface). On the other hand, materials with higher thermal contact resistances caused lower heat transfer rates, such as high density polyethylene ($R = 0.048 \text{ m}^2 \times \text{K} \times \text{W}^{-1}$ and $e = 24 \text{ mm}$, with a heat transfer rate of 265.51 W at the grout/soil interface). For null contact thermal resistances at the pipe/pile interface, a heat transfer rate of 607.01 W was obtained, which is the maximum heat transfer rate that the geothermal system could provide under these specified conditions of geometry and materials.

Table 3. Pipe materials and corresponding thermal resistivity.

Material	K (W.m-1.K-1)	e (mm)	R (m2.K.W-1)
PVC	0.17	6	0.0353
HDPE	0.50	3	0.0060
HDPE	0.50	6	0.0120
HDPE	0.50	24	0.0480
HDPE	0.50	12	0.0240
Copper	380	6	1.57895.10-5
Steel	50	6	0.00012
CPVC	0.139	6	0.04317
PEX	0.51	6	0.01176
LDPE	0.33	6	0.01818
Polypropylene	0.22	6	0.02727


Figure 17. Heat transfer rate vs thermal resistance of the pipe.

Figure 18. Heat transfer rate variations per analyzed parameters: maximum and minimum input values of each parameter in black, maximum heat transfer rates in blue, and input values for which heat transfer rates stabilize in brown.

5.10 Synthesis

Heat transfer rates at the pile/soil interface for the parameters evaluated in this study are presented in Figure 18. Fluid inlet temperature, pile diameter and pile length are the parameters that cause the highest increases in heat transfer rates. However, as previously discussed, pile length and diameter do not represent an actual increase in thermal efficiency, as normalized heat transfer rates per unit area are little impacted.

6. Final comments and conclusions

The experimental data from a TRT allowed the validation of a numerical model to analyze the thermal efficiency of a geothermal pile of 0.35-m diameter and 15-m length varying geometry and materials, based on heat transfer at the pipe/pile, pile/soil, soil limit and soil/air interfaces.

Results indicate that the normalized heat transfer rates per unit area do not increase varying pile length and diameter; however, as a consequence of higher heat exchange contact surface, total heat transfer rates increase with larger pile diameters or lengths.

Higher thermal conductivity of pile material results in better heat transfer performance. However, piles with thermal conductivities higher than $2.95 \text{ W} \times \text{m}^{-1} \times \text{K}^{-1}$ did not show a substantial increase in total heat transfer rates. For the pipes, the use of thermally conductive materials and reduction of thickness allow higher thermal exchanges between the circulating fluid and the rest of the geothermal system.

As the fluid inlet temperature increases, the temperature gradient between fluid and soil also increases, resulting in higher thermal efficiency. The fluid must circulate in turbulent regime, however for flow rates higher than $10 \text{ L} \times \text{min}^{-1}$ the values of total heat transfer rate stabilized.

Soil profiles with shallow groundwater levels are a desirable scenario for geothermal piles but heat transfer rates did not increase for saturation degrees higher than 20%. Soils with higher thermal conductivity provide higher total heat transfer rates in the geothermal system; however, subsoil thermal properties are not alterable. On the other hand, pile geometry, pile and pipe materials, and flow rate can be modified to provide an optimized design. Results indicate that there are optimal values of these parameters for the geothermal pile efficiency.

The numerical model also showed that the soil limit interface presents considerably higher heat transfer rates (because of the heat transfer rates provided by the above air temperature), while heat transfer rates at the pipe/pile and pile/soil interfaces are practically coincident, i.e., heat loss in the structural material is negligible.

Finally, numerical modelling of geothermal piles using ANSYS CFX contributed to a better understanding of the heat exchange performance of geothermal piles. Furthermore, numerical models are a powerful, low-cost, and useful tool

to properly design geothermal piles based on relatively few experimental data.

Acknowledgements

The authors are thankful to the Coordination to the Improvement of Higher Education Personnel (CAPES) for the master's scholarship grant number 88888.043643/2013-00.

Declaration of interest

The authors have no conflicts of interest to declare. All co-authors have observed and affirmed the contents of the paper and there is no financial interest to report.

Authors' contributions

Caique Roberto de Almeida: Investigation, Methodology, Formal Analysis, Validation, Writing – original draft. Cyro Albuquerque Neto: Methodology, Formal Analysis, Supervision. Cristina de Hollanda Cavalcanti Tsuha: Data curation. Maria Eugenia Gimenez Boscov: Conceptualization, Methodology, Formal Analysis, Supervision, Writing – review & editing.

List of symbols

h	Coefficient of heat transfer by convection
k	Thermal conductivity
kt	Turbulent kinetic energy
L_c	Characteristic length
u	Flow speed
ϵ_t	Turbulent energy dissipation
ν	Kinematic viscosity
CFD	Computational fluid dynamics
GSHP	Ground source heat pump
HDPE	High density polyethylene
MVF	Finite volumes method
Nu	Nusselt number
Re	Reynolds number
TRT	Thermal response test

References

- Asadi, I., Shafigh, P., Hassan, Z.F.B.A., & Mahyuddin, N.B. (2018). Thermal conductivity of concrete: a review. *Journal of Building Engineering*, 20, 81-93. <http://dx.doi.org/10.1016/j.jobbe.2018.07.002>.
- Associação Brasileira de Normas Técnicas – ABNT. (2003). *ABNT NBR 15220: thermal performance in buildings: terminology, symbols and units*. Rio de Janeiro: ABNT (in Portuguese).
- Bandeira Neto, L.A. (2015). *An experimental study of the thermal response of heat exchanger piles in unsaturated tropical soil* [Master's dissertation, University of São Paulo]. University of São Paulo's repository (in Portuguese). <https://doi.org/10.11606/D.18.2016.tde-08042016-092147>.
- Brandl, H. (2006). Energy foundations and other thermo-active ground structures. *Geotechnique*, 56(2), 81-122. <http://dx.doi.org/10.1680/geot.2006.56.2.81>.
- Curtis, R., Lund, J., Rybach, L., & Hellstrom, G. (2005). Ground source heat pumps: geothermal energy for anyone, anywhere: current worldwide activity. *Proceedings of the World Geothermal Congress* (pp. 24-29), Antalya, Turkey. International Geothermal Association.
- Empresa de Pesquisa Energética – EPE. (2018). Brazilian energy balance 2018. Rio de Janeiro: EPE. Retrieved in October 29, 2021, from <https://www.epe.gov.br/en/publications/publications/brazilian-energy-balance/brazilian-energy-balance-2018>
- Ferreira, M.S. (2017). *Resposta termomecânica de estaca geotérmica* [Master's dissertation, State University of Norte Fluminense]. State University of Norte Fluminense's repository (in Portuguese). <https://uenf.br/posgraduacao/engenharia-civil/dissertacoes-de-mestrado-2017-marina-de-souza-ferreira/>
- Hernandez Neto, A. (2020). Desempenho energético de edificações em cenário de aquecimento global. In *CICS Talks*, São Paulo (in Portuguese). Retrieved in October 29, 2021, from https://www.youtube.com/watch?v=iuGSbz_JQDU
- International Energy Agency – IEA (2016). *Key world energy statistics 2016*. Paris: OECD/IEA. https://doi.org/10.1787/key_energy_stat-2016-en.
- International Energy Agency – IEA (2018). *The future of cooling: opportunities for energy-efficient air conditioning*. Paris: OECD/IEA. Retrieved in October 29, 2021, from <https://www.iea.org/reports/the-future-of-cooling>
- Lhendup, T., Aye, L., & Fuller, R.J. (2014). In situ measurement of borehole thermal properties in Melbourne. *Applied Thermal Engineering*, 73(1), 287-293. <http://dx.doi.org/10.1016/j.applthermaleng.2014.07.058>.
- Loveridge, F.A., & Powrie, W. (2013). Pile heat exchangers: thermal behaviour and interactions. *Proceedings of the Institution of Civil Engineers - Geotechnical Engineering*, 166(2), 178-196. <http://dx.doi.org/10.1680/geng.11.00042>.
- Maliska, C.R. (2004). *Transferência de calor e mecânica dos fluidos computacional* (2a ed.). Rio de Janeiro: LTC (in Portuguese).
- Morais, T.S.O., & Tsuha, C.H.C. (2018). In-situ measurements of the soil thermal properties for energy foundation applications in São Paulo, Brazil. *Izvestiia po Himiia*, 50, 34-41.
- Morais, T.S.O., Tsuha, C.H.C., Neto, L.A.B., & Singh, R.M. (2020). Effects of seasonal variations on the thermal response of energy piles in an unsaturated Brazilian tropical soil. *Energy and Building*, 216, 109971. <http://dx.doi.org/10.1016/j.enbuild.2020.109971>.

- Orozco, H.C. (2016). *Validação do ensaio TRT para estudo paramétrico da troca de calor de uma estaca de energia em um solo tropical* [Master's dissertation, University of Brasília]. Universidade of Brasília's repository (in Portuguese). Retrieved in October 29, 2021, from <https://repositorio.unb.br/handle/10482/21124>
- Ozudogru, T.Y., Olgun, C.G., & Senol, A. (2014). 3D numerical modelling of vertical geothermal heat exchangers. *Geothermics*, 51, 312-324. <http://dx.doi.org/10.1016/j.geothermics.2014.02.005>.
- Pereira, C.D., Lamberts, R. & Ghisi, E. (2013). *Nota técnica referente aos níveis mínimos de eficiência energética de condicionadores de ar no Brasil*. Florianópolis: CB3E – Centro Brasileiro de Eficiência Energética em Edificações (in Portuguese).
- Rotta Loria, A.F., & Laloui, L. (2016). The interaction factor method for energy pile groups. *Computers and Geotechnics*, 80, 121-137. <http://dx.doi.org/10.1016/j.compgeo.2016.07.002>.
- Sánchez, M., Akrouch, G.A., & Briaud, J.L. (2015). An experimental, analytical and numerical study on the thermal efficiency of energy piles in unsaturated soils. *Computers and Geotechnics*, 71, 207-220. <http://dx.doi.org/10.1016/j.compgeo.2015.08.009>.
- Sani, A.K., Singh, R.M., Cavarretta, I., Tsuha, C.H.C., & Bhattacharya, S. (2019). Inlet and outlet pipe heat interaction in a contiguous flight auger (CFA) pile. In: A. Ferrari & L. Laloui (Eds.), *Energy geotechnics SEG 2018* (Springer Series in Geomechanics and Geoengineering). Cham: Springer. http://dx.doi.org/10.1007/978-3-319-99670-7_15.
- Thompson III, W.H. (2013). *Numerical analysis of thermal behaviour and fluid flow in geothermal energy piles* [Master's dissertation, Virginia Polytechnic Institute and State University]. Virginia Tech's repository. Retrieved in October 29, 2021, from <http://hdl.handle.net/10919/24013>
- Tsuha, C.H.C. (2020). Utilização de energia geotérmica superficial na climatização do Edifício CICS Living Lab. In *CICS Talks*, São Paulo (in Portuguese). Retrieved in October 29, 2021, from <https://www.youtube.com/watch?v=Hr4LNMKP3mg>
- You, S., Cheng, X., Yu, C., & Dang, Z. (2017). Effects of groundwater flow on the transfer performance of energy piles: experimental and numerical analysis. *Energy and Building*, 155, 249-259. <http://dx.doi.org/10.1016/j.enbuild.2017.09.023>.

Laboratory experimental and numerical thermal response tests in thermal piles prototypes in tropical soil

Charles Pereira Chaves^{1#} , Juan Deyvson José Camilo da Silva² ,

Renato Pinto da Cunha² , André Luis Brasil Cavalcante² 

Article

Keywords

Energy pile
Numerical simulation
Tropical soil
Thermal piles
Geothermal energy
Thermal chamber calibration

Abstract

This paper provides preliminary results on geothermal energy piles (GEPs) for the thermal climatization of structures founded on the typical tropical unsaturated soil of the central region of Brazil. The research employed a series of prototype simulations of a thermal pile embedded into a calibration chamber with compacted unsaturated soil. It closely simulates the behavior of a (prototype) section from real scale GEPs founded in the geotechnical media of the region, in terms of compactness, mineralogy, water content and thermal variables. One of the on-going thermal tests was numerically simulated with a Multiphysics commercial software to calibrate a model and expand the results to possible scenarios of distinct (laboratory) GEP performance. The analyses will base future simulations of typical foundation layouts for large-scale structures founded on tropical soils of the region to verify the thermal energy efficiency under average operational conditions. Besides the known limitations of this research, still at early stage, an initial assessment was achieved to design shallow geothermal systems for local conditions.

1. Introduction

Greenhouse gas emissions produced by fossil fuels are causing a slow change in the climate's conditions. Air conditioning systems in superstructures demand a considerable amount of the existing carbon-related energy sources, which are non-renewable. Many developed countries have addressed Shallow Geothermal Energy (SGE) as a renewable source of energy worthy of investment and development. SGE refers to the exploitable thermal energy in the shallow subsurface of the earth, using ground source heat pumps to exchange ground heat and provide sustainable energy to superstructures. These energy systems can provide cooling to buildings, helping reduce harmful gas emissions (Brandl, 2006). They can also be useful to agro-industrial structures, possibly to be employed in storage rooms, animal sheds, and other living or working structures largely present within Brazil's Midwest agribusiness frontier.

For instance, storage barns must be refrigerated in this industry to keep crops from germination or deterioration processes, being mostly mainly being used during harvesting season. Other structures that must also be refrigerated are residential living quarters. Feasibility of SGE usage for the region has not yet been assessed. Still, to provide a sustainable

solution, one must initially understand its potential to be implemented into local conditions and know how to design it to provide heat loads usually demanded by common/existing structures.

Hence, this paper focuses on the potential use of energy piles to climatize barns, agricultural, industrial or residential quarters/deposits through the exchange of heat with the typical, mostly unsaturated tropical soil of the Brazilian Midwest region (Figure 1).

The agribusiness in this central region is vital. It competes in a worldwide range, which could initially allow the implementation of clean, sustainable energy systems that are uncommon in Brazil. They are also relatively expensive to implement, given the lack of companies, technology, personnel, and expertise.

As most of the needed energy is supplied from the ground, the SGE system contributes to the cost-saving operation of the superstructure, besides decreasing the release of greenhouse gases into the atmosphere (a critique which is made to large-scale meat producer farms of the Brazilian Midwest regarding methane emissions). Notice that in the COP26, Brazil has compromised itself to cut off all methane emissions by 2050, which is not a simple task.

[#]Corresponding author. E-mail address: charles.chaves@ifgoiano.edu.br

¹Instituto Federal Goiano, Departamento de Engenharia Civil, Rio Verde, GO, Brasil.

²Universidade de Brasília, Departamento de Engenharia Civil e Ambiental, Brasília, DF, Brasil.

Submitted on December 22, 2021; Final Acceptance on January 22, 2022; Discussion open until May 31, 2022.

<https://doi.org/10.28927/SR.2022.078921>



This is an Open Access article distributed under the terms of the Creative Commons Attribution License, which permits unrestricted use, distribution, and reproduction in any medium, provided the original work is properly cited.



Figure 1. Brazilian states and Midwest region: the agribusiness frontier for exportation of commodities.

Nevertheless, there are certain minimum requirements for the installation of SGE systems, as an abundant array of previous publications has already been ascertained in the literature, especially in the last 5 years or so (for instance, Akrouch et al., 2015; Di Donna et al., 2016; Olgun et al., 2017; Salciarini et al., 2017; Rotta Loria et al., 2018; Sani et al., 2019; Sani & Singh, 2020; Bourne-Webb & Bodas Freitas, 2020; Cunha & Bourne-Webb, 2022, among others).

Unsaturated soils are also rarely considered as a thermal medium for heat exchange. However, experience has shown that the SGE system works, besides decreasing heat exchange efficiency (Ahmadipour & Basu, 2016; Akrouch et al., 2016; Sani et al., 2018). It seems, however, that the typical laterized tropical soils of the midwest region of Brazil have special features that may render them more feasible for SGE exploitation, as an abundant presence of iron and aluminum oxides. From pedogenetic aspects of their formation, this mineralogical characteristic increases their overall thermal conductivity (Bandeira Neto, 2015; Orozco, 2016; Sousa Júnior, 2017). Of course, this poses an extra challenge to the design but nevertheless encourages further research in this direction.

Efficiency in SGE systems also depends on other variables. For instance, stable ground temperature over seasons is inevitable for sustainable long-term heat exchange operations. A geothermal heat exchange system is considered balanced when the heating and cooling demand is approximately the same. When the heating or cooling demand is greater than the other, there is a nonsymmetrical energy expense, and the whole system becomes unbalanced. Generally speaking, in

the majority of the Brazilian regions, the operation of ground source heat pump (GSHP) systems would be unbalanced, as the cooling demand might be higher than the heating one throughout the year. Thus, the geotechnical medium can gradually heat up and lose efficiency for thermal storage. In the case of GEPs, the increase in axial stress and strain is observed (Akrouch et al., 2014; Murphy et al., 2015; Abdelaziz & Ozudogru, 2016). This phenomenon can be explained by the difference in the thermal expansion coefficients of the pile and the soil, and end restraints, as demonstrated by Goode III & McCartney (2015). This is certainly another challenge for design.

Therefore, before full application within local geotechnical, environmental and thermal constraints, research must be done to understand how SGE systems can operate daily, either at short and large time frames, considering the existing unsaturated medium local temperatures. So, with prototype tests that simulated a GEP section immersed into a compacted soil “representative” of the region, and thermal variables derived from both laboratory tests and empirical correlations, it was possible to gather information on a “normal” GEP operation that served to calibrate a thermal model for subsequent numerical simulations.

Distinct working scenarios for heat flow production by an isolated energy pile were numerically evaluated by a Multiphysics commercial software, considering several external variables as flow, fluid inlet temperatures, and pipe configurations. Steady-state conditions were assumed in the parametrization, with distinct time frames of heat production.

The exercise proved valuable to grasp an initial understanding of potential capabilities for exploiting thermally active piles into local structures. It is theoretically feasible, experimentally valid, and possibly operational. However, further validation is mandatory to broaden the knowledge to real scale and time conditions.

Energy demand in the region is undoubtedly existent. The sustainable appeal is strong, but the implementation of this technology still depends on other factors yet to be matured, as the availability of technology, design companies and contractors, governmental policies and funding, public awareness, and large-scale experimental research. Actually, lots of research.

2. Materials and methods

2.1 Geothermal properties and geotechnical characterization of the soil

The soil used in this research was collected in the Geotechnical Experimental Field of the University of Brasília (UnB), Darcy Ribeiro Campus located in the Federal District (DF), in August 2019. The reason for the choice of the collection site was due to the fact that the soil collected is characteristic of the entire DF and the vast knowledge

of the geotechnical characteristics of the soil due to the numerous researches developed in this experimental field, which can be cited the works of Guimarães (2002), Silva (2007, 2009), Fuji (2012), Borges (2014), Queiroz (2015), among other works developed in the Graduate program in Geotechnics at UnB.

Table 1 shows, in summary, the main geotechnical parameters obtained in the characterization tests. This is a soil whose specific weight of grains is 27.32 kN/m^3 .

2.2 The prototype and compression soil in the chamber

The prototype was executed and concreted in a compacted soil within the chamber with average soil moisture content of 20%, void ratio of 0.8, porosity of 44%, and dry unit weight of 13.6 kN/m^3 (as shown in Figure 2a). The soil was compacted into 12 sequential layers to simulate “average” conditions of the tropical soil of the Federal District of Brazil, where the University of Brasília geotechnical research site is located (home base of the studies presented here).

The compaction process was carried out by layering with a manual compactor with a $16 \times 16 \text{ cm}^2$ square socket, weight of 10.73 kg, drop height of 27.5 cm, and 513 strokes per layer, evenly distributed over the 12 soil layers. This procedure has enabled a total compaction energy of approximately 2353.6 kN.m/m^3 (24 kgf.cm/cm^3). These specifications allowed the compacted specific weight, density, and other soil

variables to “approach” those conditions found in the field deposit, normally derived via previous laboratory data and parameters estimated by traditional SPT correlations at this site. The chosen soil moisture content was the lower possible in the dry range of the curve that permitted the desired dry unit weight with a homogeneous compaction (Figure 3).

2.3 Thermal parameters of the soil

The parameters of the compacted soil were defined by empirical methods that relate the thermal conductivity (λ_{soil}) and the specific heat capacity (C_p) with geotechnical variables of the layer as porosity, degree of saturation, mineralogy, and granulometric distribution. This was done because thermal tests of the local soil deposit, or the compacted soil samples, have not been performed yet at this stage of the research.

The 1 m of compacted soil layer along the GEP prototype was divided into 12 distinct layers according to compaction procedures carried out during sample preparation. Lu et al.'s (2007) methodology was employed to derive the average thermal conductivity of each layer, considering the thermal conductivities of the minerals that form this soil, the porosity, and the respective degree of saturation of the layers.

The thermal conductivity parameter for each layer is related to the (bulk) thermal conductivity of a laterized soil strata within the first 4 m of the research site (λ_{mineral}), since this is the zone where the soil sample was extracted. Although differences are expected, the superficial soil characteristics from the site, at this depth range, do not change considerably with depth (up to the 8 to 10 m transition zone before the typical regional saprolite of slate).

The mentioned (bulk) variable represents the bulk thermal conductivity of the minerals of this zone, as a whole,

Table 1. Main geotechnical characterization parameters of the tropical soil analyzed.

Parâmetro	WL (%)	WP (%)	IP (%)	G _s	SUCS
	41	24	17	2,76	CL-ML

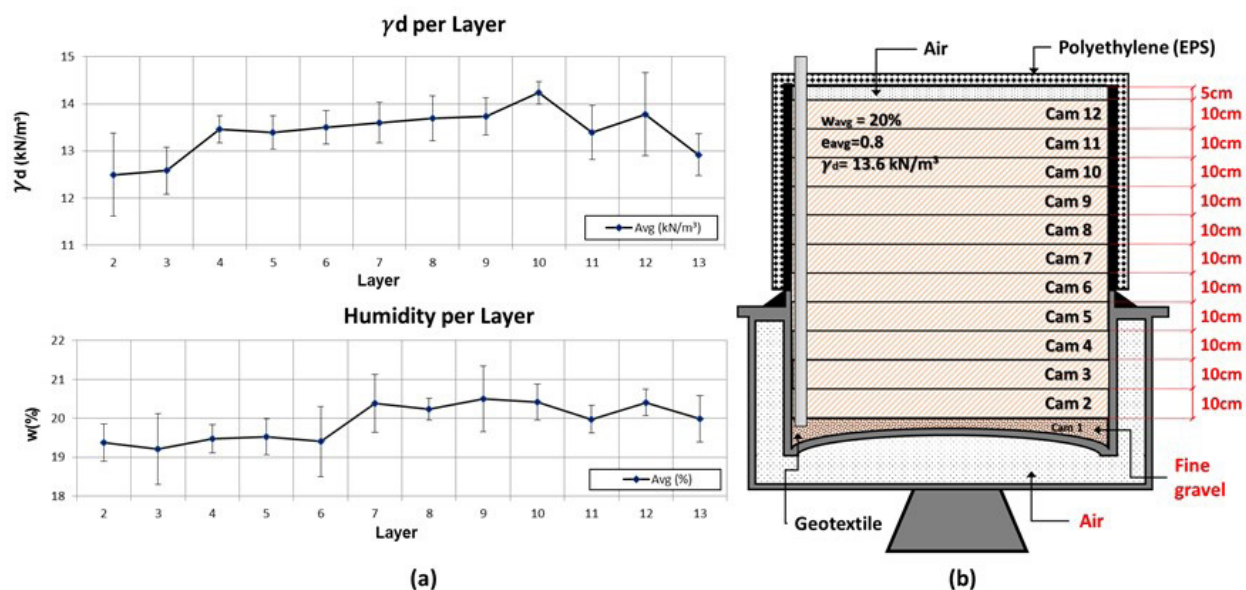


Figure 2. (a) Soil moisture content and dry unit weight distribution per layer; (b) 12 soil layer distribution in the calibration chamber.

in accordance with their relative percentage within the soil mass. This percentage was defined with X-ray diffractometric tests by Rodrigues (2017), i.e., exemplifying, this author has determined the following amounts of minerals for this soil: 34.9% of quartz, 34.6% of gibbsite, 22.1% of kaolinite, 6.6% of hematite, and few (< 1%) percentages of other minerals. A bulk value of 3.94 W/m.K was derived and used in Lu et al.'s (2007) method to estimate each layer's average thermal conductivity (λ).

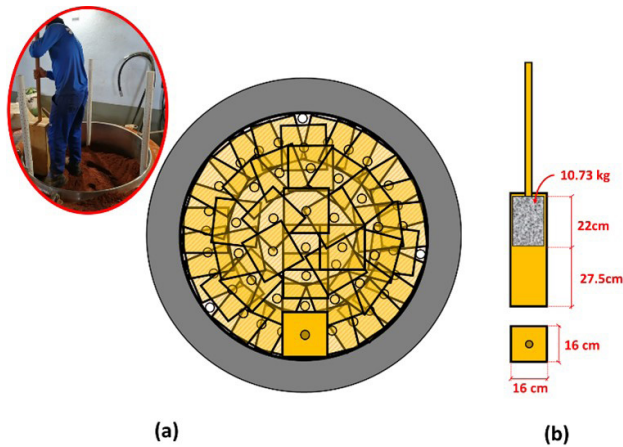


Figure 3. (a) uniformly distribution of compression per layer in the chamber; (b) compactor dimensions and weight.

The specific heat capacity in J/kg.K was derived by the model of Johansen (1975), taking into consideration the dry unit and the specific apparent weight of the soil, the density of the water, the soil water content, and the volumetric heat capacity of the water (as 4.18×10^6 J/m³.K).

2.4 Thermal response test machine and calibration chamber

In order to calibrate the numerical model and to understand the behavior of the GEP prototype under heat exchange conditions, an initial setup test was performed inside a thermally insulated testing chamber (as shown in Figure 4). The dimensions of this cylindrical chamber were 1.1 m in diameter by ~1 m in height.

The developed prototype of the geothermal pile was 1 m long and 20 cm in diameter, with internal HDPE exchanger tubes of 19,05mm in external diameter into an overall 1U loop configuration. The tubes were uniformly distributed along the steel reinforcement cage of the GEP. Thermo sensors were installed at distinct compacted layers surrounding the pile to check the all-around temperature. Those dissipated along the chamber radius at distinct points in the compacted layers (see Figure 5).

Figure 6 shows the basic schematic of the plant of the home-based TRT machine developed by the Arduino platform. It is a closed circuit with water circulation overflow

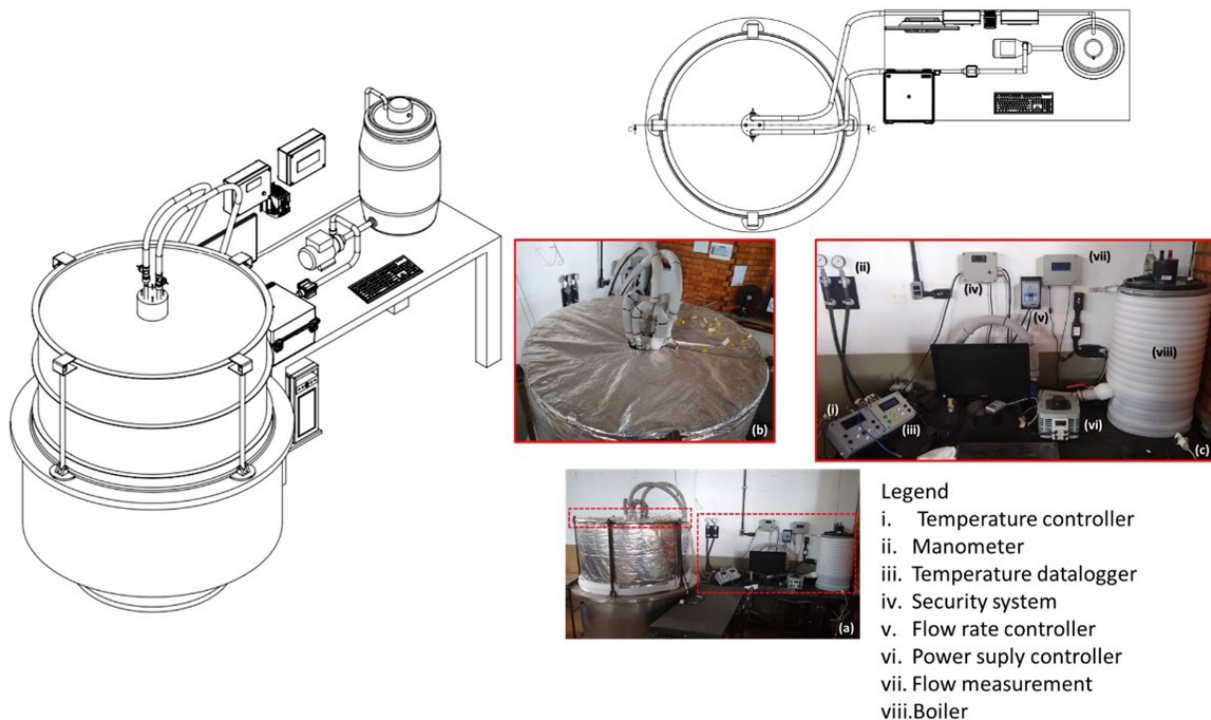


Figure 4. (a) Overview of the thermal response test machine and the calibration chamber. (b) thermal response test machine details, and (c) superior view of the calibration chamber.



1



1

and heating, both controlled in the machine. The flow control was performed by a frequency inverter installed in the pump circuit. The power control was done through a voltage variator coupled with a true RMS Wattmeter.

The inlet and outlet temperatures are collected by a data acquisition system developed by the Arduino platform and the flow measurement system. A safety system was also developed to protect the machine against overheating and eventual power failures.

Figure 7 presents the picture of the U tube configuration of the prototype of the geothermal pile with the thermal couplers installed in the external tube surface and in the pile/soil surface of the bore of the pile.

2.5 Thermal tests in calibration chamber

The thermal response test in the chamber was performed on the prototype of 1U configuration, a constant flow rate of $Q = 3.06$ L/min and electrical power of heating machine

of 150 W, turbulent regime, soil moisture at the beginning of the test was approximately 16.10%, subject to a thermal power of heat exchange of 106 W/m.

The prototype thermal response test results can be seen in Figure 8a and analysis of the test by the linear source method (as shown in Figure 8b).

It is worth noting that the thermal power of heat exchange is relatively high since the average recommendation of heat exchange is between 60 and 80 W/m. In this case, it was chosen to initially analyze a situation of heat exchange at the industrial level.

It is known that the thermal conductivity estimated by the Line Source method is not an accurate estimate for the situation in question since the slenderness of the prototype is well below that recommended by the method to consider an infinite linear source. Therefore, to lessen some of the inaccuracies, a numerical model was calibrated to estimate with greater precision and accuracy the thermal conductivity of the soil analyzed.

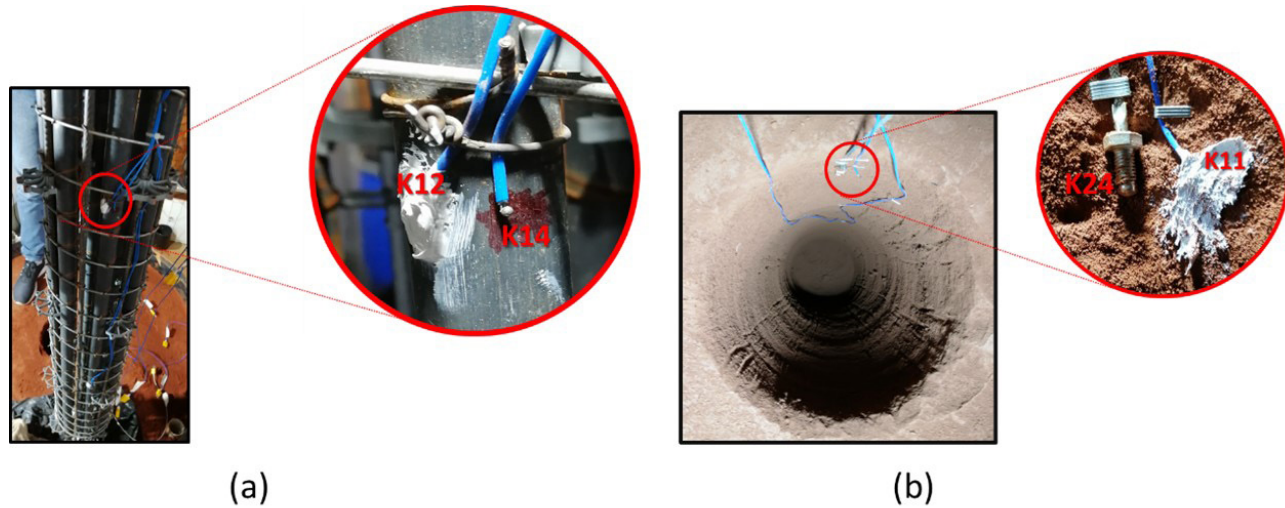


Figure 7. (a) sensors installed on the wall of the prototype pipe before concreting; (b) sensors installed on the wall of the concrete/soil interface of the prototype.

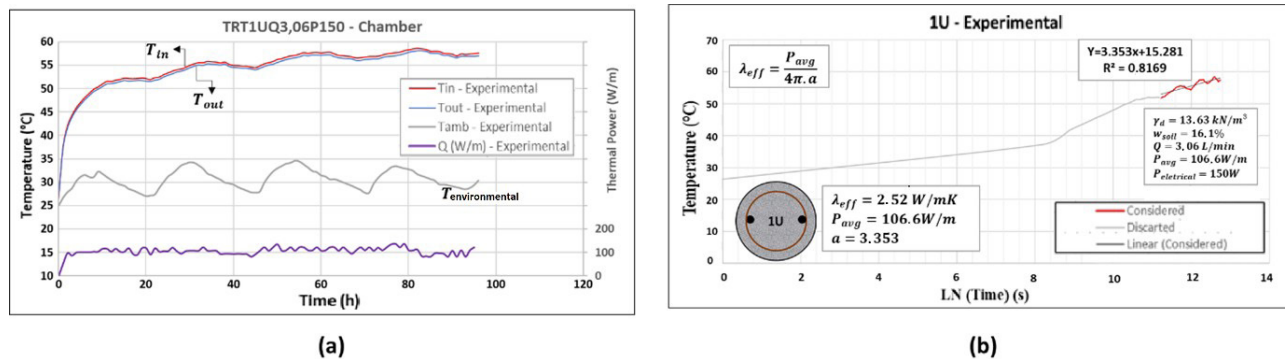


Figure 8. (a) experimental results in the thermal chamber for calibration; (b) analysis results by the infinite linear source method of the TRT test.

During the TRT test, temperature data were collected in space and time from the entire thermal chamber throughout the test. Figure 9 shows the development of the temperature bulb during the trial heating phase of the test.

It can be seen that there was very little temperature increase for test times above 50 h. It was also observed that the temperature bulb reached the chamber walls with border interference.

This situation is not ideal, but a thermal interference of approximately 6 °C of difference in relation to the initial temperature was observed, which can be considered a relatively low variation compared to the maximum temperatures on the wall of the pile (approx. 50 °C).

2.6 Numerical software

Commercial software based on the finite element method, denominated COMSOL Multiphysics v.5.2, was employed in calibration and parametric simulations. It is ideal since it offers specific modules that simulate heat transfer and the flow regime inside the heat exchanger pipes. Moreover, it is quite flexible in terms of boundaries, geometric conditions, and input parameters. It has a friendly output, easy to follow.

For instance, the “heat transfer in solids” module calculated the heat conduction between the concrete pile and surrounding soil. The convective heat between heated fluid and pile wall, or within the circulating system’s fluid, adopted the “non-isothermal pipe flow” module to fully complement the heat phenomena process.

The step-by-step analysis procedure was given by:

- Geometry modeling: in this step, the 3D dimensions of the soil domain, piles, and pipes were specified. The assumed geometry and limits of the model were the same as those used in the experimental test. The soil domain was modeled in a cylindrical shape with a diameter of 1.10 m and height equal to 1.08 m, similar to what was adopted in the lab.

(as in Figure 2). Figure 10 depicts the adopted final mesh of the problem;

- Material properties: in this step, the properties of water, concrete, and soil were specified, as for instance the soil’s specific mass (ρ_{soil}), thermal conductivity (λ_{soil}), and specific heat capacity (C_p), as previously defined in the present paper;
- Non-isothermal pipe flow convection parameters: pipe properties were inputted as shape, internal diameter, wall roughness, and thermal conductivity (λ_{pipe}). The friction factor between inner surface and fluid was estimated with the Colebrook-White equation (Colebrook, 1939), according to COMSOL’s recommendations. Initial values of atm. pipe pressure, fluid inlet/outlet positions, and inlet temperatures around 55 °C at a constant heat rate of 97 W/m were then defined;
- Heat transfer in solids conduction parameters: Initial soil and pile temperatures (T) were given, and eventual variations tried out;
- Mesh configuration: type of element and density. All three types of elements were tested (tetrahedral, prismatic, and hexahedral), and the tetrahedral type was used given its accuracy versus running time. The density of elements has also increased from pipe/pile outwards. The final mesh (Figure 10) respectively adopted 94, 14671, and 22312 elements for pipes, pile, and soil;
- Simulation time: normally of 50 h of system’s flow. Note that the numerical simulations lasted 96 h, beyond the minimum duration recommended by CEN/TC 341 (CEN, 2011).

$$Q_L = C_w \cdot \rho_w \cdot q_{in} \left(\frac{T_{in} - T_{out}}{L_p} \right) \quad (1)$$

where

C_w – specific heat capacity of water (4182 J/kgK);

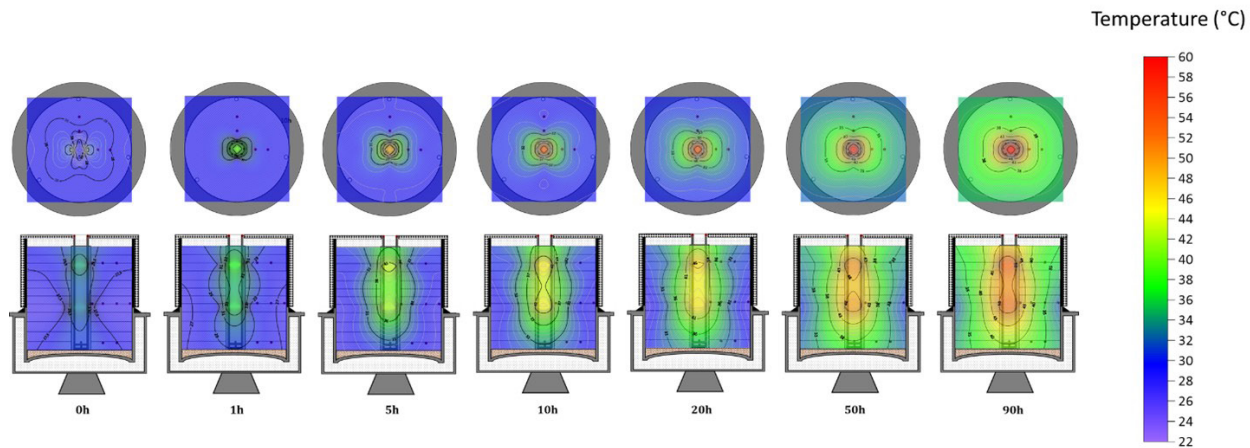


Figure 9. Temperature bulb advancement in the thermal test chamber of prototype 1U-Q3.06-P150.

ρ_w – water density (1000 kg/m³);
 q_{in} – water flow rate (m³/s);
 T_{in} – Inlet temperature (K);
 T_{out} – Outlet temperature (K);
 L_p – Pile length (1 m).

3. Results and discussion

3.1 Calibration of numerical model in thermal chamber

Calibration was performed by inputting previous parameters into the software discretized mesh and running

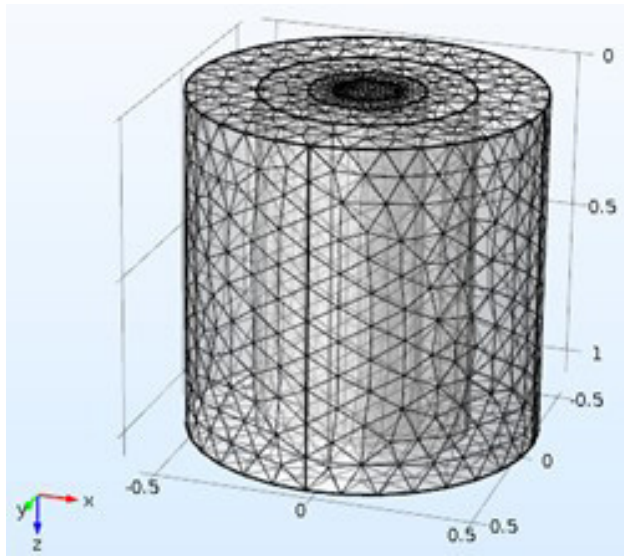


Figure 10. Mesh configuration adopted for numerical analyses.

the problem for 96 h of total time. The initial soil temperature of the chamber was about 29.0 °C, water inflow at 3.06 L/min was also adopted, the experimental heat flux by energy pile was calculated about 105.11 W/m.

During the TRT test, temperature data were collected in space and time from the entire thermal chamber throughout the test. Figure 11a shows the development of the temperature bulb in space and time during the trial heating phase.

Figure 11b shows that for a condition of only 1.0 m lengths, there is considerable boundary influence from the upper and lower ends of the chamber. This has led the analyses in this research to focus on the middle of the prototype, where there are the least possible boundary influence effects in the experiments and results.

The inlet and outlet temperatures of the numerical model were determined linearly, following a linear fit of the data obtained from the experimental tests (as seen in Figure 12).

The calibration was evaluated by comparing the experimental versus simulated thermal energy efficiency ΔT , or inlet/outlet temp at about the same heat flux per meter of the pile. Differences can be seen in in Figure 13.

As it can be clearly noted, the differences between the results were reasonably low, suggesting that the numerical modelling was able to simulate the thermal phenomena reasonably well, besides some minor limitations.

Some of them relate to the boundary conditions of the calibration chamber. Indeed, the boundary was not fully exempt from the pile's thermal influence and from external temperature changes in the laboratory. Moreover, DS1 and K16 temperature sensors (Figure 4) were clearly tampered.

Unfortunately, the chamber was limited in size, and insulation problems were noticed after such tests. Boundary effects are therefore present in both compared results,

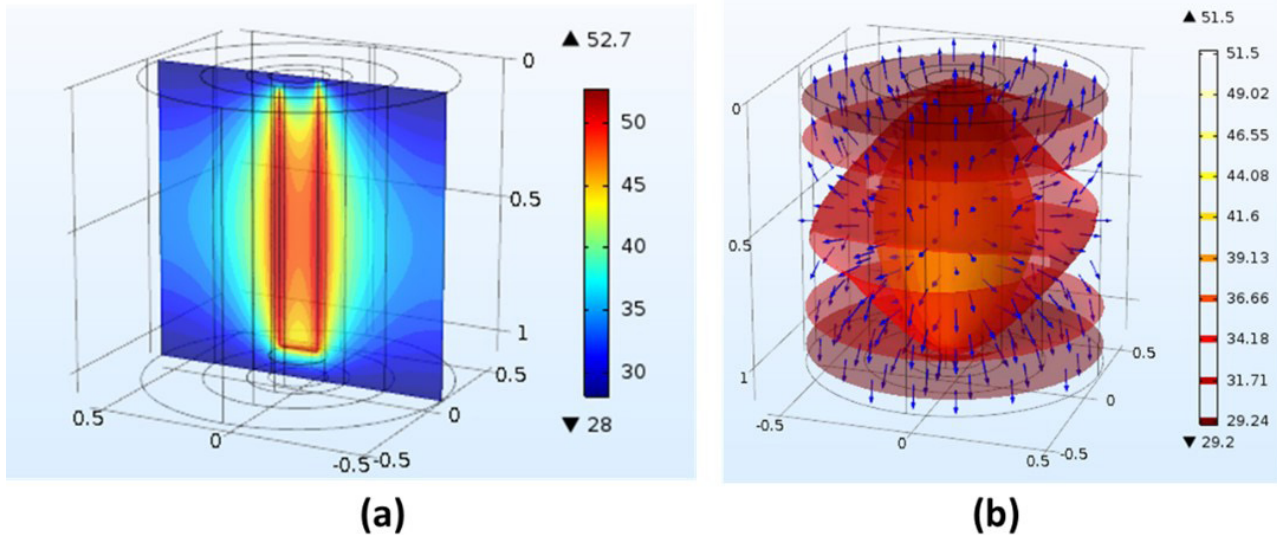


Figure 11. (a) temperature contours (°C) for a longitudinal cross-section of model pile at 96 h of thermal loading; (b) direction of heat flux after 96 h of testing.

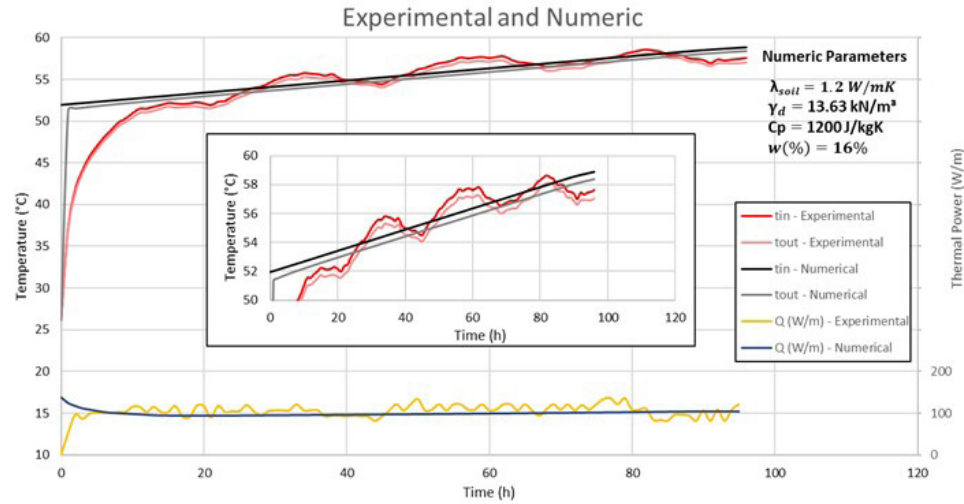


Figure 12. Comparison of experimental and numerical data from model calibration of thermal response test results.

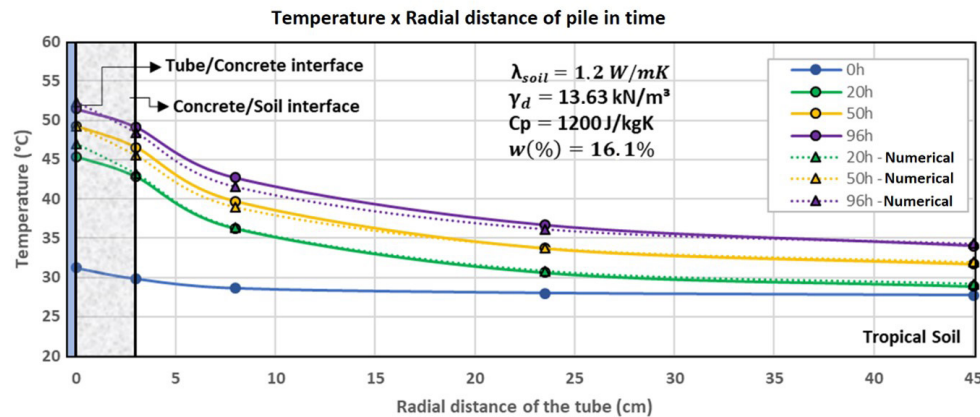


Figure 13. Comparison of experimental and numerical data from model calibration of space and time soil thermal distribution.

which does not invalidate the comparison for most of the chamber sensors (inner section), but must be properly dealt with in future experimental procedures. This aspect will be commented on later.

3.2 Parametric analysis

Numerical simulations were performed for 4 configurations of pipe arrangement in the pile prototype analyzed in the laboratory. From the calibration in 1U (as seen in Figure 11), analyses were performed in three more distinct configurations (2U, 3U, and 4U). In each configuration, the heat flux dissipated by the prototype was verified. The thermal conductivity in each situation was estimated too.

Figure 14 shows the graphs with the results of numerical simulations of the TRT tests for the 4 configurations of the studied prototype. In all configurations, the slope of the temperature line versus the natural logarithm of time remains

constant, not suffering any variation with the configuration of tubes in the pile since the fluid flow rate inside the tubes remained constant in all configurations.

Although it is not ideal for analyzing a TRT with a prototype pile whose slenderness is much lower than that recommended by the standard. For the line source method to be accurate, the analyses were performed in such a way as to show that there is no variation in the slope of the regression line as a function of the configuration, which allows us to see that the variation of the effective conductivity of the prototype in the chamber was dependent only on the thermal flux dissipated in this same apparatus.

Due to the increase in the number of tubes, with the established configurations, the time and length of water circulation in the tube increased, which has allowed the observation of the increase in the inlet and outlet temperature variation in the tube as a function of its configuration. In addition, the heat exchange surface area of the tube increases. Consequently,

the heat flux over the pile increases in the same proportion. This can be seen in Figure 15, which shows the variation between the inlet and outlet temperature of the prototype and the variation of heat dissipated to the ground for the configurations studied in each presented graph.

Observing Figure 16, one can notice a significant increase in the heat flux dissipated in the prototype from 1U to the 2U configurations. Going from 96.76 W/m to 155.63 W/m of heat exchanged an increase of approximately 60.9% in heat exchange from 2U to other configurations (3U and 4U). Moreover, the heat exchange rate increase from 3U to 4U is practically the same (around 14%).

This information becomes quite useful when determining the best cost/benefit of using tubes per pile. For this situation, for instance, increasing the length of 50% of the tube (from 2U to 3U) becomes unfeasible since the gain in the heat exchange rate in the prototype increases to only 13.8%. However, when increasing the length of the tube from 1U to 2U, one notices a considerable gain in the heat exchange rate in the tested prototype analyzed, allowing the perception that the 2U configuration has the best cost-benefit compared to the other simulated scenarios.

This paper showed the thermal behavior of a prototype pile heat exchanger in tropical soil, subjected to different

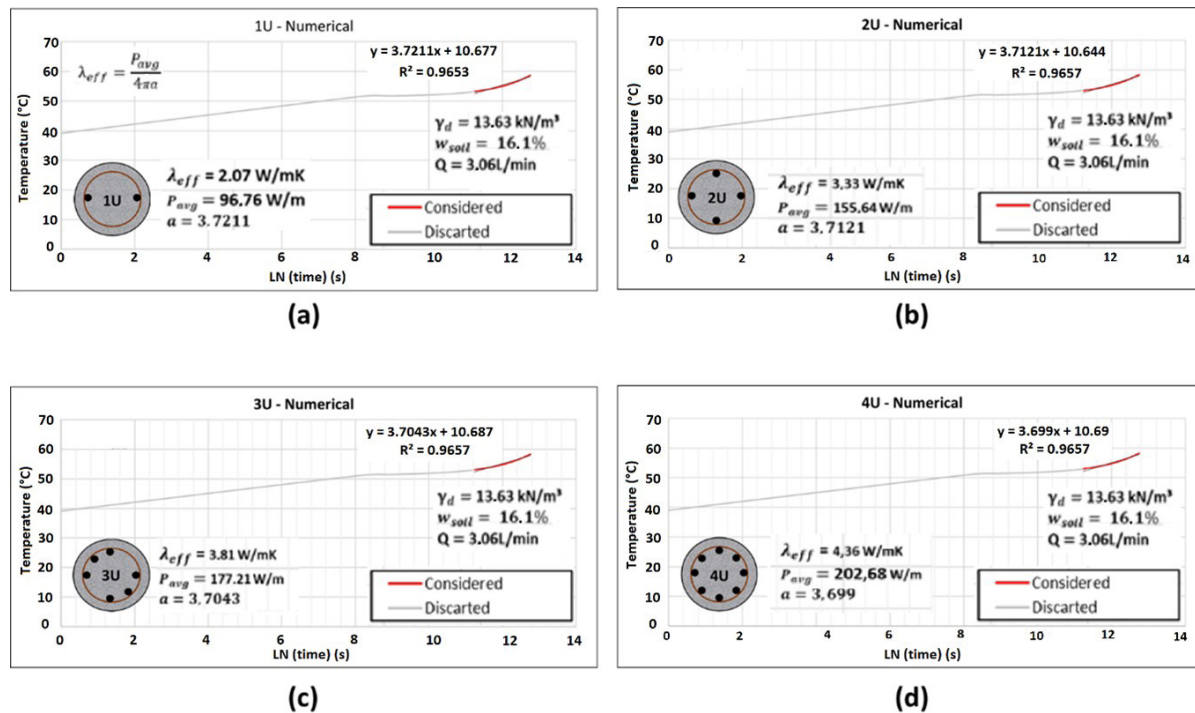


Figure 14. Thermal conductivity analysis by the line source method for configurations: (a) 1U; (b) 2U; (c) 3U; (d) 4U.

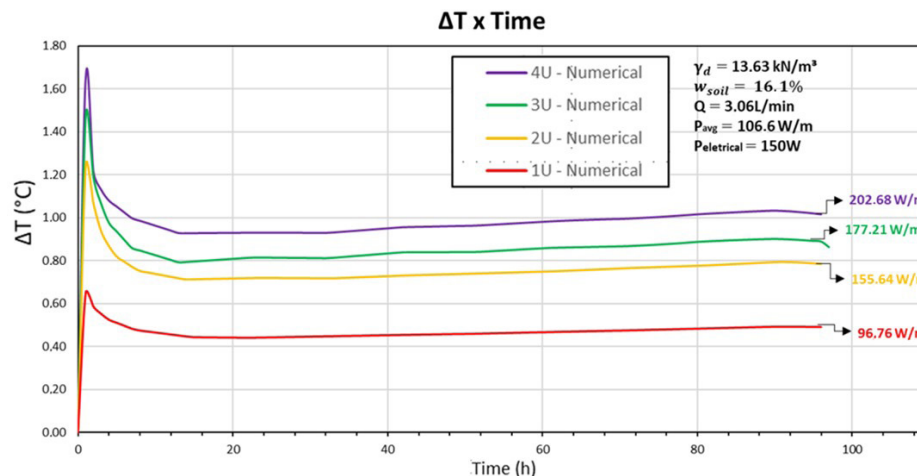


Figure 15. Variation of inlet and outlet water temperature in the prototype with test time.

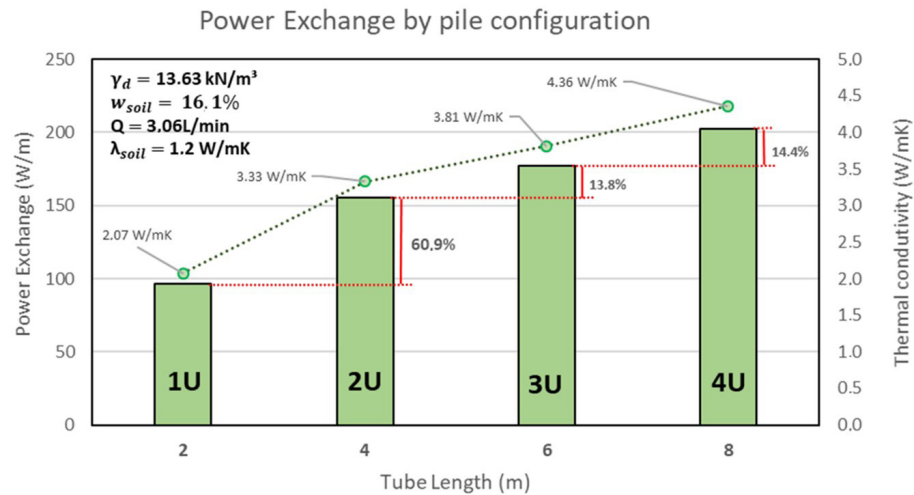


Figure 16. Cost benefit analysis for the best pile configuration analyzed.

configurations. There is still little work in Brazil developed in this line of research, especially in unsaturated tropical soil. This motivated the research groups of the Geotechnical Postgraduate Program of the University of Brasília (GPFees and Geofluxe) to contribute to the development of this field of research nationwide.

4. Conclusions

The paper has provided preliminary results from on-going research that has employed a series of prototype simulations of a thermal pile embedded into a calibration chamber, with compacted unsaturated soil from a laterized deposit. The analyses will hopefully base future simulations of typical foundation layouts for large-scale structures founded on tropical soils of the region. This research is therefore an initial step on this direction.

Based on the analyses performed in this paper, it could be concluded that:

- After 50 h of testing, it is noticed that the regime of temperature increase over time is practically stationary, and the test can be analyzed with the equations from a stationary point of view (as can be seen in Figure 13);
- The angular coefficient derived from the analyses of the TRT simulations is independent of the configurations tried out in this paper. On the other hand, the heat flux dissipated by the prototype on the ground varies considerably depending on the configuration studied, being most efficient in the 2U condition and least efficient in the 3U and 4U configurations;
- The variation of the effective thermal conductivity of the prototype as a function of the pipe configuration in the analyzed heat exchanger pile prototype depends only on the variation of the heat flux

dissipated from the prototype to the ground. This variation is, therefore, independent of the slope of the line source method analysis (as can be seen in Figure 14);

- Increasing the tube contact area increases the heat flux dissipated in the heat exchanger;
- The thermal response machine allowed the successful development of laboratory tests, which made it possible to develop relatively low-cost equipment to be reproduced by the academic community – especially for the special conditions of the soil in the mid-west region of Brazil.

It can be concluded that, besides the known limitations of this on-going research, still at an early stage, an initial assessment was achieved regarding some of the critical parameters to design heat exchanger pipes and piles immersed in the tropical unsaturated soil of the Federal District of Brazil. Perhaps with proper due modifications, the results gathered in this research will be of importance to start designing shallow geothermal systems to exchange heat loads with local superstructures, taking into account the specific local conditions of the region. The development of the whole technology, involving heat pumps, secondary superstructure refrigeration systems, and an integrated design, will eventually follow such initial steps.

Acknowledgements

The authors are grateful to the Geotechnical Graduate Program of the University of Brasília, as well the research group on foundations, in-situ testing, and retaining structures of this same institution (GPFees, <https://rpcunha.wixsite.com/gpfrees>) and the research group on Innovations and Technologies Applied to Environmental Geotechnics (GeoFluxe, <https://geofluxe.com>). They are also indebted to the Instituto Federal Goiano of Rio Verde - GO for all

the structural and administrative support that contributed decisively to the quality of this research. Finally, to both Brazilian sponsorship organizations CNPq and CAPES for all financial aid that allowed the research to go so far.

Declaration of interest

The authors have no conflicts of interest to declare. All co-authors have observed and affirmed the contents of the paper and there is no financial interest to report.

Authors' contributions

Charles Pereira Chaves: conceptualization, Data curation, Visualization, Writing – original draft. Juan Camilo Silva: conceptualization, Data curation, Methodology, Supervision, Validation, Writing – original draft. Renato Pinto da Cunha: Formal Analysis, Funding acquisition, Investigation, Methodology, Project administration, Final Review, Resources, Software. André Luis Brasil Cavalcante: supervision, Validation, Software, Resources, Writing – review & editing.

List of symbols

cm	Centimetres
C_p	Thermal capacity
C_w	Specific heat capacity of water
G_s	Specific gravity of the soil
$HDPE$	High-density polyethylene
IP	Plastic index
J	Joule
K	Kelvin
Kg	Kilogram
L_p	Pile length
m	Linear meter
m^2	Square meter
m^3	Cubic meter
P_{avg}	Thermal power average per meter
$P_{electrical}$	Electrical power
Q	Flow rate
q_{in}	Water flow rate
RMS	Root mean square
$SUCS$	Soil unified classification system
T_{in}	Inlet temperature
T_{out}	Outlet temperature
TRT	Thermal Response Test
W	Watts
WL	Liquid Limit
WP	Plastic Limit
w	Soil moisture content
γ_d	Dry unit weight of the soil
λ_{soil}	Soil thermal conductivity
λ_{pipe}	Thermal conductivity of the pipe





$\lambda_{mineral}$	Mineral thermal conductivity
ΔT	Temperature difference (inlet and outlet)
a	Angular coefficient
ρ_{soil}	specific mass of the soil
ρ_w	Water density
$^{\circ}C$	Celsius degree

References

- Abdelaziz, S., & Ozudogru, T.Y. (2016). Non-uniform thermal strains and stresses in energy piles. *Environmental Geotechnics*, 3(4), 237-252. <http://dx.doi.org/10.1680/jenge.15.00032>.
- Ahmadipour, A., & Basu, P. (2016). Temperature-induced alterations of the shaft and base resistances of a model geothermal pile in dry sand. In *Geo-Chicago 2016: Sustainability and Resiliency in Geotechnical Engineering* (Geotechnical Special Publication, GSP 269, pp. 155-165), Chicago.
- Akrouh, G.A., Sánchez, M., & Briaud, J.L. (2014). Thermo-mechanical behavior of energy piles in high plasticity clays. *Acta Geotechnica*, 9(3), 399-412. <http://dx.doi.org/10.1007/s11440-014-0312-5>.
- Akrouh, G.A., Sánchez, M., & Briaud, J.L. (2015). Effect of the unsaturated soil condition on the thermal efficiency of energy piles In *IFCEE 2015* (Geotechnical Special Publication, GSP 256, pp. 1618-1627), San Antonio, Texas.
- Akrouh, G.A., Sánchez, M., & Briaud, J.L. (2016). An experimental, analytical and numerical study on the thermal efficiency of energy piles in unsat. soils. *Computers and Geotechnics*, 71, 207-220. <http://dx.doi.org/10.1016/j.compgeo.2015.08.009>.
- Bandeira Neto, L.A. (2015). *Experimental study of the thermal response geothermal energy piles foundations in unsaturated soil* [Master's dissertation, São Carlos Engineering School of São Paulo State University]. University of São Paulo's repository (in Portuguese). Retrieved in December 22, 2021, from https://www.teses.usp.br/teses/disponiveis/18/18132/tde-08042016-092147/publico/dissertacao_bandeira.pdf
- Borges, C.R. (2014). *Microstructural study of the hydromechanical behavior of the soil of Brasília-DF* [Master's dissertation, University of Brasília]. University of Brasília's repository (in Portuguese). Retrieved in December 22, 2021, from <https://repositorio.unb.br/handle/10482/17731?mode=full>
- Bourne-Webb, P.J., & Bodas Freitas, T.M. (2020). Thermally-activated piles and pile groups under monotonic and cyclic thermal loading: a review. *Renewable Energy*, 147, 2572-2581. <http://dx.doi.org/10.1016/j.renene.2018.11.025>.
- Brandl, H. (2006). Energy foundations and other thermo-active ground structures. *Geotechnique*, 56(2), 81-122. <http://dx.doi.org/10.1680/geot.2006.56.2.81>.
- CEN/TC 341. (2011). *Geotechnical investigation and testing-geothermal testing-determination of thermal conductivity*

- of soil and rock using a borehole heat exchanger. *Eurocode Standard N525*. CEN, Brussels.
- Colebrook, C.F. (1939). Turbulence flow in pipes, with particular reference to the transition region between the smooth and rough pipe laws. *Journal of the Institution of Civil Engineers*, 11(4), 133-156. <http://dx.doi.org/10.1680/ijoti.1939.13150>.
- Cunha, R.P., & Bourne-Webb, P.J. (2022). A critical review on the current knowledge of geothermal energy piles to sustainably climatize buildings. *Renewable & Sustainable Energy Reviews*, 158, 112072. <http://dx.doi.org/10.1016/j.rser.2022.112072>.
- Di Donna, A., Rotta Loria, A.F., & Laloui, L. (2016). Numerical study of the response of a group of energy piles under different combinations of thermo-mechanical loads. *Computers and Geotechnics*, 72, 126-142. <http://dx.doi.org/10.1016/j.compgeo.2015.11.010>.
- Fuji, L.M.T. (2012). *Study of mixtures of soil, CDW, virgin and hydrated lime for use in road works* [Master's dissertation, University of Brasilia]. University of Brasilia's repository (in Portuguese). Retrieved in December 22, 2021, from <https://repositorio.unb.br/handle/10482/12827>
- Goode III, J.C., & McCartney, J.S. (2015). Centrifuge modeling of end-restraint effects in energy foundations. *Journal of Geotechnical and Geoenvironmental Engineering*, 141(8), 1-13. [http://dx.doi.org/10.1061/\(ASCE\)GT.1943-5606.0001333](http://dx.doi.org/10.1061/(ASCE)GT.1943-5606.0001333).
- Guimarães, R.C. (2002). *Analysis of the properties and behavior of a laterite soil profile applied to the study of the performance of excavated piles* [Master's dissertation, University of Brasilia]. University of Brasilia's repository (in Portuguese).
- Johansen, O. (1975). *Thermal conductivity of soils* [Ph.D. thesis]. University of Trondheim. CRREL Draft Translation 637
- Lu, S., Ren, T., Gong, Y., & Horton, R. (2007). An improved model for predicting soil thermal conductivity from water content at room temperature. *Soil Science Society of America Journal*, 71(1), 8-14. <http://dx.doi.org/10.2136/sssaj2006.0041>.
- Murphy, K.D., McCartney, J.S., & Henry, K.S. (2015). Evaluation of thermo-mechanical and thermal behavior of full-scale energy foundations. *Acta Geotechnica*, 10(2), 179-195. <http://dx.doi.org/10.1007/s11440-013-0298-4>.
- Olgun, C. G., Geyin, M., & Ozudogru, T.Y. (2017). Long-term performance of heat exchanger boreholes at different climatic conditions. In *Geotechnical Frontiers 2017* (Geotechnical Special Publication, GSP 280, pp. 153-164), Orlando, Florida. <https://doi.org/10.1061/9780784480472.016>.
- Orozco, H.C. (2016). *Validation of the TRT for the parametric study of the heat exchange of a geothermal pile in a tropical soil* [Master's dissertation, University of Brasilia]. University of Brasilia's repository (in Portuguese). Retrieved in December 22, 2021, from https://repositorio.unb.br/bitstream/10482/21124/1/2016_HenryCastilloOrozco.pdf
- Queiroz, A.C.G. (2015). *Study of the microstructural behavior of compacted tropical soils* [Master's dissertation, University of Brasilia]. University of Brasilia's repository (in Portuguese). Retrieved in December 22, 2021, from <https://repositorio.unb.br/handle/10482/18299>
- Rodrigues, S.M. (2017). *Mineralogical and microstructural characterization of a weathered profile in Brasilia* [B.Sc. Final Project]. State University of Goiás (in Portuguese).
- Rotta Loria, A.F., Vadrot, A., & Laloui, L. (2018). Analysis of the vertical displacement of energy pile groups. *Geomechanics for Energy and the Environment*, 16, 1-14. <http://dx.doi.org/10.1016/j.gete.2018.04.001>.
- Salciarini, D., Ronchi, F., & Tamagnini, C. (2017). Thermo-hydro-mechanical response of a large piled raft equipped with energy piles: a parametric study. *Acta Geotechnica*, 12(4), 703-728. <http://dx.doi.org/10.1007/s11440-017-0551-3>.
- Sani, A.K., & Singh, R.M. (2020). Response of unsaturated soils to heating of geothermal energy pile. *Renewable Energy*, 147, 2618-2632. <http://dx.doi.org/10.1016/j.renene.2018.11.032>.
- Sani, A.K., Singh, R.M., Amis, T., & Cavarretta, I. (2019). A review on the performance of geothermal energy pile foundation, its design process and applications. *Renewable & Sustainable Energy Reviews*, 106, 54-78. <http://dx.doi.org/10.1016/j.rser.2019.02.008>.
- Sani, A.K., Singh, R.M., Cavarretta, I., & Bhattacharya, S. (2018). Heat storage performance of a pile heat exchanger installed in partially saturated swelling clay. In *Proc. 7th Int. Conf. Unsaturated Soils* (pp. 1-6), Hong Kong.
- Silva, J.P. (2007). *Preliminary studies for the implementation of seepage trenches* [Master's dissertation, University of Brasilia]. University of Brasilia's repository (in Portuguese). Retrieved in December 22, 2021, from <https://repositorio.unb.br/handle/10482/2655>
- Silva, M.T.M.G. (2009). *Methodology for determining parameters for unsaturated soils using tests with known moisture* [Master's dissertation, University of Brasilia]. University of Brasilia's repository (in Portuguese). Retrieved in December 22, 2021, from <https://repositorio.unb.br/handle/10482/7730>
- Sousa Júnior, R.P. (2017). *Parametric study of the thermal response of geothermal pile groups in a tropical soil typical from the Federal District* [Master's dissertation, University of Brasilia]. University of Brasilia's repository (in Portuguese). Retrieved in December 22, 2021, from <https://repositorio.unb.br/handle/10482/31518>

Experimental analysis of improved bearing capacity in offshore foundations due to thermal consolidation

Marina de Souza Ferreira^{1#} , Fernando Saboya Albuquerque Junior¹ ,
Sérgio Tibana¹ , Ricardo Garske Borges² 

Article

Keywords

Offshore foundations
Soft clays
Soil improvement
Physical modeling
Thermal consolidation

Abstract

The anchoring of floating platforms is one of many processes in the oil industry that requires innovative strategies. In this respect, there is interest in developing techniques that improve the shear strength of soft soils in order to increase the bearing capacity of offshore foundations anchored in these soils. Normally consolidated clay soil is known to undergo thermal consolidation when submitted to temperature cycles. The present study aimed to assess the impact of a temperature cycle on soft kaolin clay using a reduced-scale physical model submitted to heating at maximum temperatures of 85 °C and 65 °C, followed by cooling. Variables such as pore pressure, temperature at different soil depths and displacement were monitored during the thermal cycle to better understand the phenomenon. The strength profile before and after heating was determined via T-bar tests conducted in different positions in relation to the heat source. The temperature variation increased the undrained shear strength of the soil directly proportional to the temperature applied and inversely proportional to the radial distance from the heat source, reaching improvements of 123%. In this respect, it is believed that applying a temperature cycle to normally consolidated soft clayey soil can improve the pullout capacity of offshore foundations.

1. Introduction

In terms of fundamental soil mechanical behavior, the relationship between heating and thermal volume changes in clayey soil began to be studied in the 1950s. Finn (1951) conducted laboratory tests to assess the magnitude and rate of consolidation after temperature variations. Later, Campanella & Mitchell (1968) found that when heated, normally consolidated saturated clays initially exhibited increased pore pressure due to the relative difference between the thermal expansion of the soil particles, the solid structure and water. This was followed by thermal consolidation, resulting from the reorganization of contact forces between the soil particles and dissipation of the excess pore pressure caused by the temperature gradient. Since then, researchers have studied the impact of temperature on clayey soils for different purposes.

Baldi et al. (1988) investigated volume changes caused by heating in clays with low porosity and moisture content and observed irreversible shrinking under normally consolidated conditions. Plum & Esrig (1969), Towhata et al. (1993), Cekerevac & Laloui (2004) and Abuel-Naga et al. (2007) also reported shrinkage in normally consolidated clays submitted to heating.

The influence of temperature on the shear strength of clays was demonstrated by Kuntiwattanukul et al. (1995), who heated normally consolidated clays up to 90 °C under drained

conditions and observed an increase in soil stiffness and strength. Trani et al. (2010) heated normally consolidated Bangkok clay up to 90 °C, under drained and undrained conditions, and reported undrained shear strength improvement after one drained heating and cooling cycle. Samarakoon et al. (2018) also found that the undrained shear strength of normally consolidated clays increased when heated under drained conditions, especially after one heating and cooling cycle. Wang & Zhang (2020) assessed thermo-mechanical behavior at the pile-soil interface in soft kaolin clay submitted to temperature variations, using direct shear tests.

As reported by different authors (Houston et al., 1985; Hueckel & Baldi, 1990; De Bruyn & Thimus, 1996; Delage et al., 2000; Cui et al., 2000; Laloui & François, 2009; Di Donna & Laloui, 2015; Coccia & McCartney, 2016; Hong et al., 2016; Zhou & Ng, 2018; Cheng et al., 2020), heating normally consolidated clay increases its shear strength, making this technique particularly appealing in improving the bearing capacity of offshore foundations, where traditional soil improvement methods cannot be applied. Increasing the shear strength of the soil around these foundations enables verticalization of the resulting load and, therefore, fewer mooring lines are needed, which allows for considerable savings at installation of these anchors. Thus, for thermal consolidation to be used as an improvement technique for soft soils, it is important to investigate the influence of a temperature gradient on excess

[#]Corresponding author. E-mail address: marinadesferreira@gmail.com

¹Universidade Estadual do Norte Fluminense Darcy Ribeiro, Department of Civil Engineering, Campos dos Goytacazes, RJ, Brasil.

²CENPES Petrobras Centro de Pesquisa e Desenvolvimento, Rio de Janeiro, RJ, Brasil.

Submitted on November 29, 2021; Final Acceptance on February 4, 2022; Discussion open until May 31, 2022.

<https://doi.org/10.28927/SR.2022.078021>



This is an Open Access article distributed under the terms of the Creative Commons Attribution License, which permits unrestricted use, distribution, and reproduction in any medium, provided the original work is properly cited.

pore pressure, and possible shear strength improvement after its dissipation.

As such, the present study aimed to evaluate a reduced-scale physical model of typical Brazilian marine kaolin clay submitted to maximum temperatures of 65 °C and 85 °C, in order to measure undrained shear strength before and after a heating and cooling cycle with a T-bar penetrometer at different radial distances from the heat source.

2. Materials

The reduced-scale physical model was constructed in a 500 mm-long cylindrical container with an internal diameter of 464 mm, which was filled with a mixture of kaolin and metakaolin soil. A torpedo pile was inserted to serve as a heating element, in addition to pore pressure transducers and thermocouples. The experimental apparatus was placed in a hydraulic press (Figure 1), which applies loads via a controlled electric motor to ensure that the load remains constant throughout the test. A CSR-5000 load cell of 50 kN capacity was used.

Because the soil's response to a temperature gradient depends on its degree of pre-consolidation, an apparatus was needed to maintain constant vertical stress throughout the test without having to remove the top cap for the T-bar tests, ensuring that the soil remained normally consolidated. To that end, a special top cap was designed with holes containing self-tapping screws that could be removed after consolidation to allow the T-bar tests to be performed.

A 250 mm-long hollow pile with an external diameter of 25 mm was used as a foundation element and heat source, fitted with a 750 W heating element 180 mm long and 13 mm wide. Implastec thermal paste was inserted into the element to improve heat transfer between the pile and heating element. The thermal load applied by the heater was controlled to ensure that the temperature within the pile remained constant throughout the experiment.

The heating element, which also serves as a pile, was attached to the center of the top cap, with an instrumentation probe positioned on either side, 30 mm from the heat source, each containing sensors to measure the temperature at three different depths and the pore pressure around the heater (Figure 1). The T-bar tests were conducted through the holes in the cap, which were arranged at radial distances of 30 mm, 88 mm and 153 mm (r/r_{pile} ratio of 2.40, 7.04 and 12.24) from the heat source axis and denominated $R0$, $R1$ and $R2$, respectively.

The experiment was monitored using EPB-PW pore pressure transducers (TE Connectivity), type K thermocouples (Omega TT-K 36-500) and laser displacement sensors (Wenglor CP3MHT80). The locations and nomenclature of the sensors are shown in Figure 2 and Tables 1 and 2, with Table 1 referring to sensors installed on the walls of the container and Table 2 to those on the probe.

In addition to the sensors presented, four thermocouples were installed, two directly above the top cap to measure room temperature ($TC1$ and $TC2$ *AMB*) and two below it to

measure the temperature on the soil surface. Three additional thermocouples were positioned on the surface of the torpedo pile to supply the temperature control system.

T-bar penetrometer tests were performed to obtain the undrained soil shear strength profile. The length and diameter of the penetrometer were 14 and 7 mm, respectively, and undrained shear strength (S_u) was calculated as proposed by Stewart & Randolph (1991):

$$S_u = \frac{F_v}{N_b DL} \quad (1)$$

where F_v is the vertical force during penetration, measured by the strain gauge coupled to the T-bar, N_b is the T-bar factor, and D and L are its diameter and length, respectively.

The soil used in the experiment was a mixture of 40% kaolin and 60% metakaolin (dry weight) and its properties are presented in Table 3.

Table 1. Depth, from the upper surface of the container, and nomenclature of each sensor on the container walls.

	Depth (mm)	Nomenclature
Side 1	200	PP C11
	270	PP C12
	340	PP C13
Side 2	200	PP C21
	270	PP C22
	340	PP C23

Table 2. Depth, from the lower surface of the top cap, and nomenclature of the sensors on the probes.

Pore pressure transducer probes		
	Depth (mm)	Nomenclature
Side 1	125	PP S1
Side 2	125	PP S2
Thermocouple probes		
	Depth (mm)	Nomenclature
Side 1	50	TC S11
	80	TC S12
	110	TC S13
Side 2	50	TC S21
	80	TC S22
	110	TC S23

Table 3. Physical characterization of the kaolin and metakaolin mixture.

Parameter	Value
Liquid limit (%)	45.4
Plastic limit (%)	26.5
Plasticity index (%)	18.9
Specific gravity	2.64
Hygroscopic moisture content (%)	0.64
Colloidal Activity	0.53

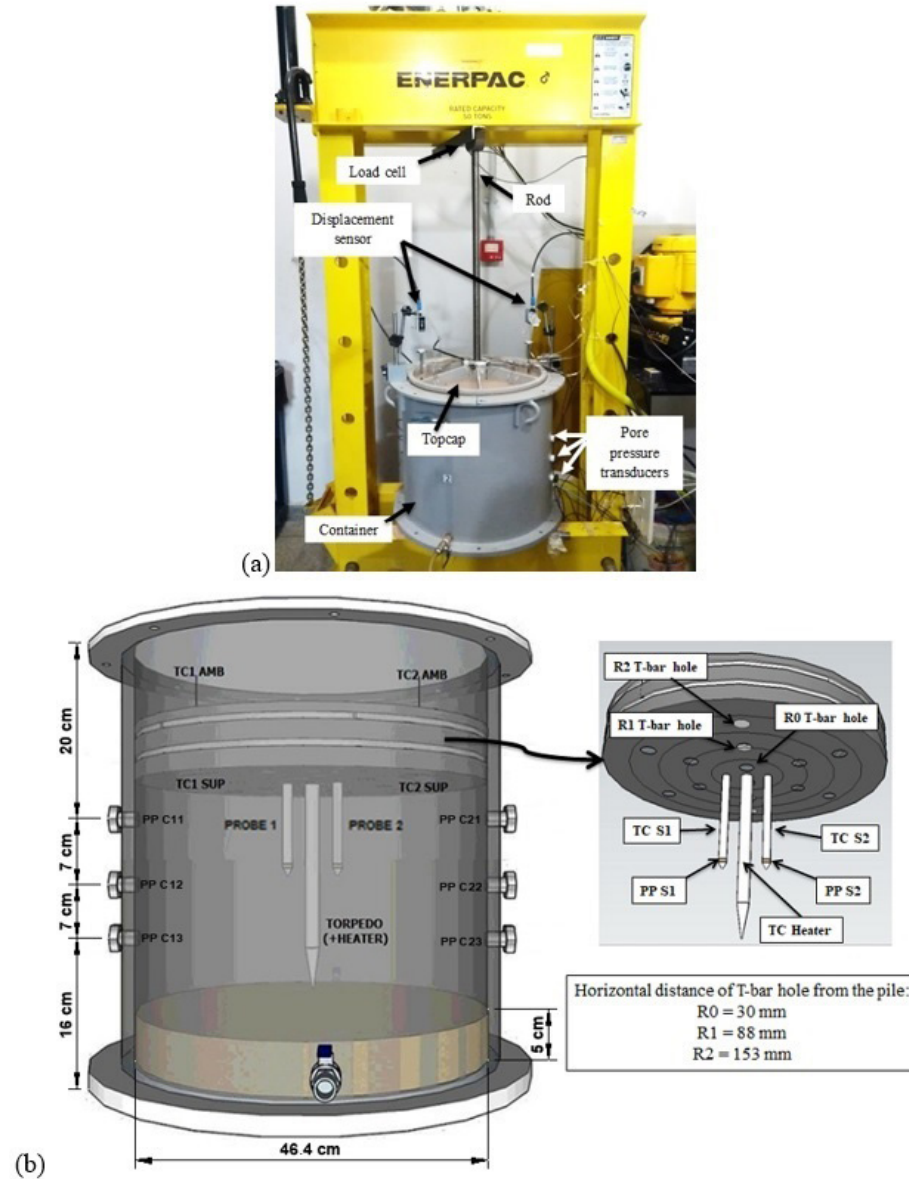


Figure 1. (a) Equipment used to construct the model for testing; (b) Insert of the instruments used in the container and top cap.

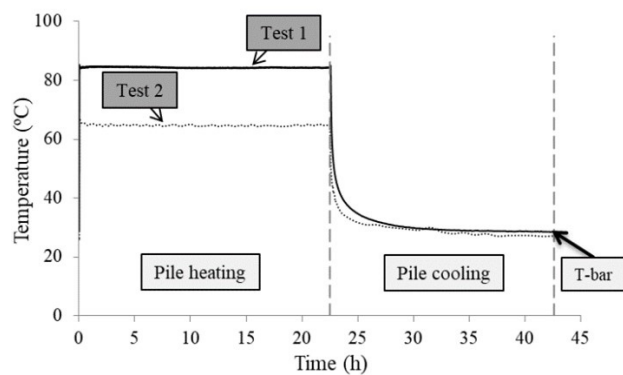


Figure 2. Scheme of stages in tests 1 and 2.

3. Methodology

Two tests were conducted for the present study, each at a different maximum temperature (85 °C and 65 °C), in order to assess the change in soil shear strength after a temperature cycle. The general methodology applied in each test was identical, the heating temperature being the only difference, as presented in Table 4.

3.1 Slurry preparation, mechanical consolidation, and reference T-bar

For slurry preparation, powdered soil was mixed with distilled deaerated water to obtain an approximate moisture

content of 68.1%, followed by homogenization for 30 minutes in a mechanical mixer. Next, the mixture was placed in a vacuum deaerator for 30 minutes to ensure complete saturation and minimize air bubbles.

During mechanical consolidation, loading was performed in stages, applying approximately double the previous load in each stage, with final vertical stress of 50 kPa. The subsequent loads were applied in magnitudes of 5 kPa, 12.5 kPa, 25 kPa and 50 kPa, only once the system had stabilized from the previous stage. Table 5 shows the void ratio (e_f) and moisture (w_f) content after mechanical consolidation, void ratio (e_0) and moisture content (w_0) of the slurry before mechanical consolidation, and the compression index (C_c) in both tests.

These tests made it possible to obtain t_{90} and estimate the coefficient of consolidation (c_v) via Taylor's method (1942) for loads of 12.5 kPa, 25 kPa and 50 kPa, as summarized in Table 6. By determining c_v , the normalized penetration rate of the T-bar penetrometer can be calculated.

At the end of mechanical consolidation, the screws in positions $R1$ and $R2$ on the top cap were removed in order to perform the T-bar test and obtain the undrained shear strength profile of the soil before thermal consolidation, denominated the reference profile. The penetration rate was 16 mm/s, calculated as a function of the c_v of the material, as proposed by Finnie & Randolph (1994).

3.2 Temperature cycle and final T-bar

Heating of the pile began once the undrained shear strength profile (reference) of the soil had been obtained. As previously mentioned, the target temperatures for tests 1 and 2 were 85 °C and 65 °C, respectively. In each test, under constant vertical stress of 50 kPa, the system was allowed to stabilize through dissipation of the excess pore pressure caused by heating. This stage lasted around 22 hours for both tests.

Table 4. Summary of the test stages.

Testing stage	Stage Description
i	Slurry preparation
ii	Consolidation
iii	Reference T-bar
iv	Pile heating
v	Pile cooling
vi	T-bar after temperature cycle

Table 5. Soil moisture content and void ratio before and after mechanical consolidation and compression index for both tests.

Test	e_0	w_0 (%)	e_f	w_f (%)	C_c
1	1.77	68.91	1.24	32.88	0.21
2	1.76	68.72	1.23	32.71	0.17

Following the heating stage, the heater was switched off and the sensors allowed to stabilize by lowering the temperature and pore pressure to the initial values, which took approximately 22 hours. Next, the T-bar tests were conducted at radial distances $R0$, $R1$ and $R2$ for each test, in order to establish a panorama of the change in undrained shear strength with temperature and distance from the heat source. Figure 2 presents the scheme of the stages covered in this item.

4. Results and discussion

4.1 Reference T-bar

Two T-bars were used for each test to obtain the reference strength. For the subsequent strength improvement analyses, the mean between the two reference T-bars for each individual test was used along the entire depth of the model. Thus, given the homogeneity of the soil prepared, the soil in the model was deemed to exhibit this same initial undrained shear strength profile. It is important to underscore that the first 50 mm of soil were disregarded in the analyses because disturbances were observed in this zone, resulting from interaction between the soil surface and the top cap of the container.

The average undrained shear strength profile for each test is shown in Figure 3a. For both tests, strength was greater in the upper section of the model, due to the uneven distribution of the vertical load impacted by possible lateral friction between the wall of the container and the top cap. Additionally, the absolute strength values across the soil depth were used to calculate relative frequency distribution for both tests, as shown in Figure 3b. It should be noted that the mean undrained shear strength was 11.6 kPa and 14.0 kPa for tests 1 and 2, respectively.

4.2 Temperatures

The normalized temperature during heating was calculated based on the fact that the maximum temperatures of 85 °C and 65 °C in tests 1 and 2, respectively, generated approximate respective increases of 55 °C and 39 °C in the pile. To that end, the increase of temperature recorded by each sensor was normalized by the temperature increase of the heating element (dT_{Heater}). The increase of temperature of all the sensors

were calculated by subtracting the temperature registered by the respective sensor (TC) from the room temperature (TC_{AMB}) at the beginning of the test. The curves of temperature increase normalized by the rise in heater temperature for the sensors at different depths, on the soil surface and in the room, are presented in Figure 4.

Regarding normalized temperature increases, the largest increases for the probe sensors located at a radial distance of 3 cm from the pile axis were measured in the sensor closest to the center of the heater, at a depth of 11 cm. The sensors closest to the heater recorded a 40% temperature increase in test 1 and 35% in test 2 in relation to the temperature increase of the pile, whereas the maximum temperature rise in those furthest from the heater, installed on the soil surface, was 21% in test 1 and 10% in test 2. Increases in the remaining sensors were inversely proportional to distance from the heater. There was also a slight increase in the room temperature during the heating stage.

Once the established maximum temperature had been reached, the heating system was switched off and the sensors were allowed to cool naturally until the end of the cooling stage, approximately 20 hours after shutoff.

4.3 Soil response

Undrained heating caused an instantaneous increase in pore pressure in the sensors installed on the probes, which subsequently dissipated after 7 hours (Figure 5) of heating; values are summarized in Table 7. As expected, the increase in pore pressure was greater at higher temperatures.

With respect to deformation, no significant changes in settlement were observed in the displacement sensors in either the heating or cooling stages. However, localized deformation is believed to have occurred in the area around

the heat source, due to the dissipation of excess pore pressure measured during soil heating.

4.4 Undrained shear strength improvement

After application of the temperature cycle, the soil strength profile for the different radial distances from the heat source was obtained via T-bar tests. Strength improvement due to thermal consolidation, expressed in percentage, was calculated by subtracting the mean reference strength from the strength obtained after the temperature cycle (dS_u) and dividing the result by the mean reference strength ($S_{u,ref}$) along the entire depth of the model. This made it possible to obtain a net undrained shear strength improvement profile for each radial distance in each test.

The strength profiles obtained across the soil depth were used to determine the relative frequency distributions of these gains for the different temperatures and radial distances. The histograms showed improvements of 20% to 270% at intervals of 50%.

It should be noted that the strength improvement analyses were interested in two different ways, considering

Table 6. Coefficient of consolidation (c_v) and t_{90} during mechanical consolidation conducted in stages.

Assumed vertical effective stress (kPa)	t_{90} (h)	c_v (cm ² /s)
12.5	12.7	6.7E-03
25.0	11.3	7.2E-03
50.0	6.5	1.2E-02

Table 7. Peak pore pressure due to heating in tests 1 and 2.

Test	Sensor	Maximum pore pressure increase (kPa)	Mean pore pressure increase (kPa)
1	S1	7.77	7.36
	S2	6.94	
2	S1	4.08	4.16
	S2	4.23	

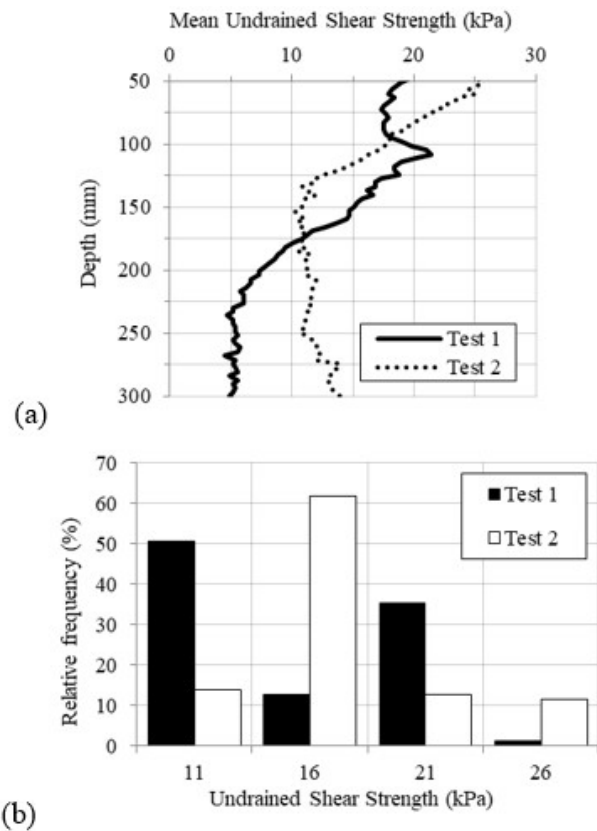


Figure 3. (a) Mean reference undrained shear strength profile for tests 1 and 2; (b) Distribution of relative frequencies for mean reference undrained shear strength along the length of the model, for tests 1 and 2.

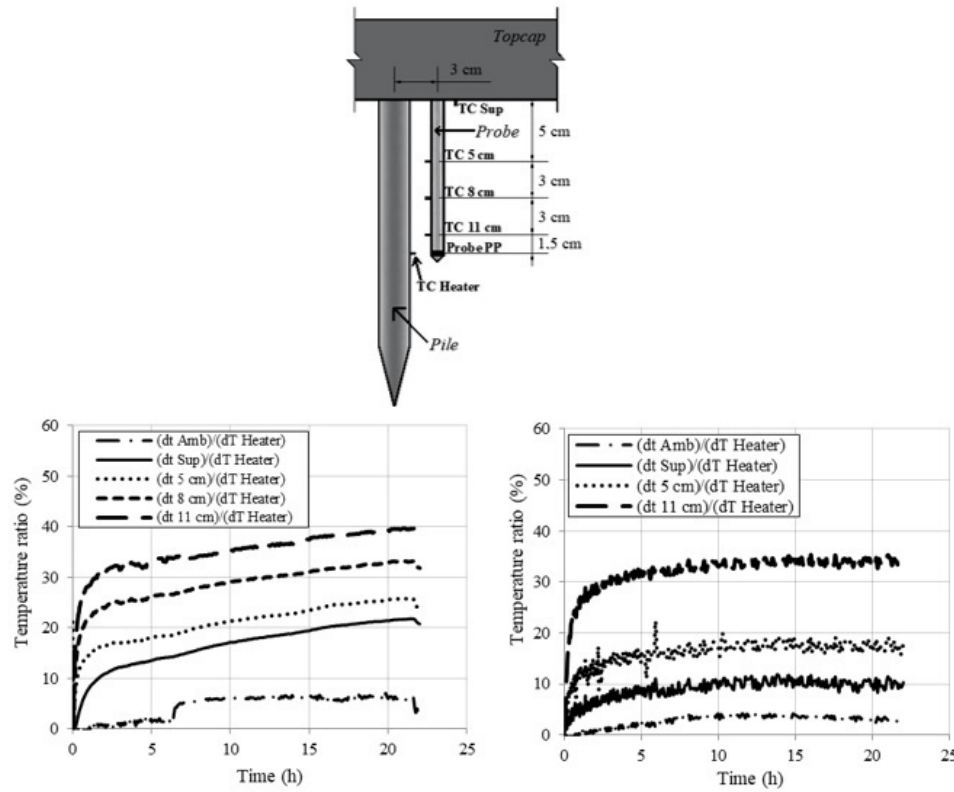


Figure 4. Distribution of temperatures normalized (dt) with time during heating, in tests 1 and 2, respectively.

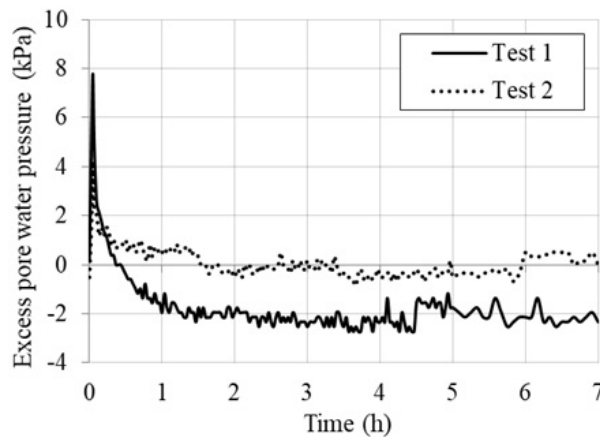


Figure 5. Pore pressure in the probes during the heating stage for tests 1 and 2.

the maximum temperature applied to the soil and in terms of the radial distance of the T-bar from the heat source.

4.4.1 Analysis of shear strength improvement by radial distance

The shear strength improvement profile and its distribution frequency are presented in Figure 6 for radial distances of

30 mm, 88 mm and 153 mm from the heat source in test 1. Mean undrained shear strength was 24.2 kPa, 15.3 kPa and 12.4 kPa for distances $R0$, $R1$ and $R2$, respectively, in test 1, which generated net strength improvements of 123%, 58% and 14% for the respective radial distances. These results indicate that improvement was directly proportional to proximity to the heat source. Additionally, the greatest strength improvements were observed close to a depth of 200 mm for distances $R0$ and $R1$. On the other hand, the T-bar test performed at $R2$ exhibited a more homogeneous improvement profile with depth and less improvement in relation to distances closer to the heat source.

In test 2, the mean undrained shear strength values were 22.8 kPa, 18.9 kPa and 16.6 kPa for $R0$, $R1$ and $R2$, respectively, generating net undrained shear strength improvements of 74%, 36% and 19% with the temperature cycle.

The proportionality between shear strength improvement and proximity to the heat source can once again be observed in the histograms in Figure 7. There is clearly a greater concentration of larger improvements for T-bars closer to the heat-producing pile.

4.4.2 Analysis of improvement according to temperature

Shear strength improvement according to temperature was analyzed by considering each individual radial distance

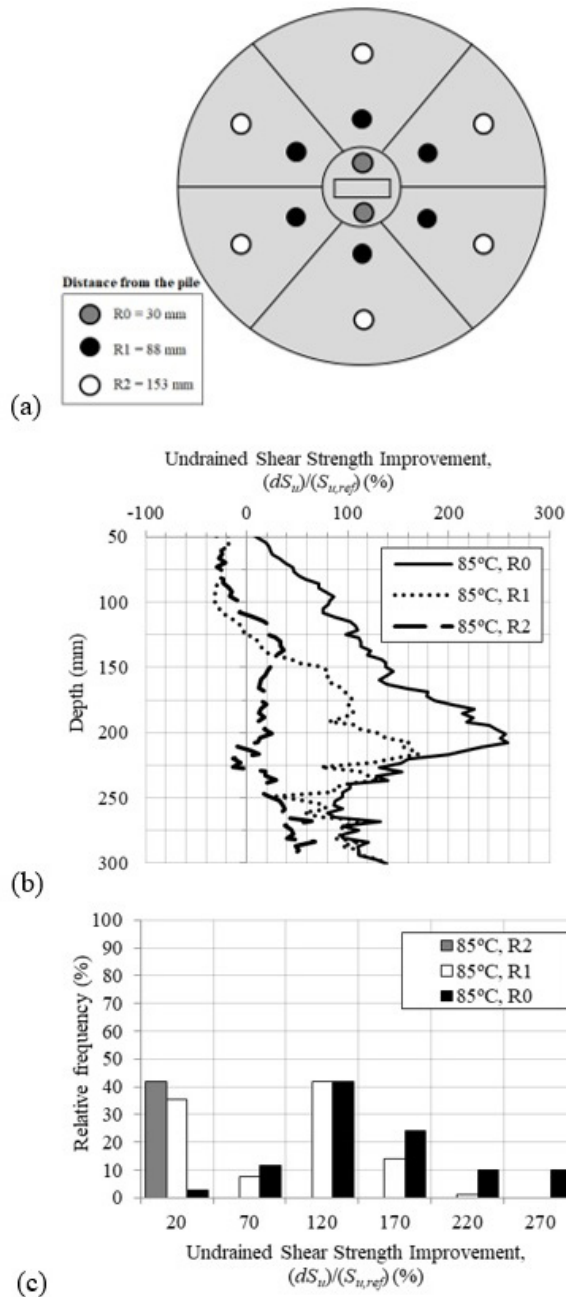


Figure 6. (a) Location of top cap holes in top view; (b) Shear strength improvement profiles at different radial distances for test 1; (c) Distribution of relative frequencies for undrained shear strength improvement at different radial distances for test 1.

and varying the maximum temperatures applied to the soil. The strength improvement calculation was performed by subtracting the strength obtained after the thermal cycle from the reference strength and dividing this value by the reference strength. In addition, the improvement was given in percentage.

For the T-bar closest to the heat source, $R0$, both tests clearly show that increases in strength were directly proportional to the level of heating applied, with average improvements of

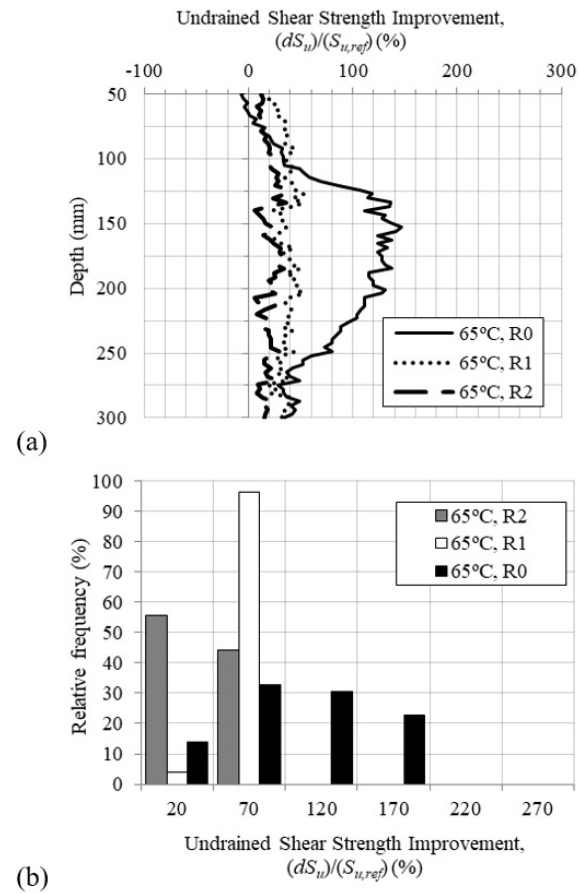


Figure 7. (a) Shear strength improvement profiles at different radial distances for test 2; (b) Distribution of relative frequencies for undrained shear strength improvement at different radial distances for test 2.

123% and 74% for soil heated at 85 °C and 65 °C, respectively (Figure 8). The histograms in Figure 8 reinforce observations of the shear strength improvement profiles, where there is a larger concentration of improvements at higher values for soil heated at the highest temperature.

The shear strength improvement profiles for distance $R1$, 88 mm from the pile axis, are shown in Figure 9 for the different temperatures tested. Once again, greater improvements occurred in soil heated at 85 °C, that is, at this radial distance, increased shear strength is directly proportional to the level of heat applied to the clay.

Figure 10 presents the shear strength improvement profiles and relative histograms at distance $R2$ for the different tests. Based on the different improvement profiles in the Figure 9, the heating level was not relevant for the increase in shear strength at this radial distance.

4.5 Estimating pile pullout capacity

The average values of changes in undrained shear strength made it possible to estimate the pullout capacity of

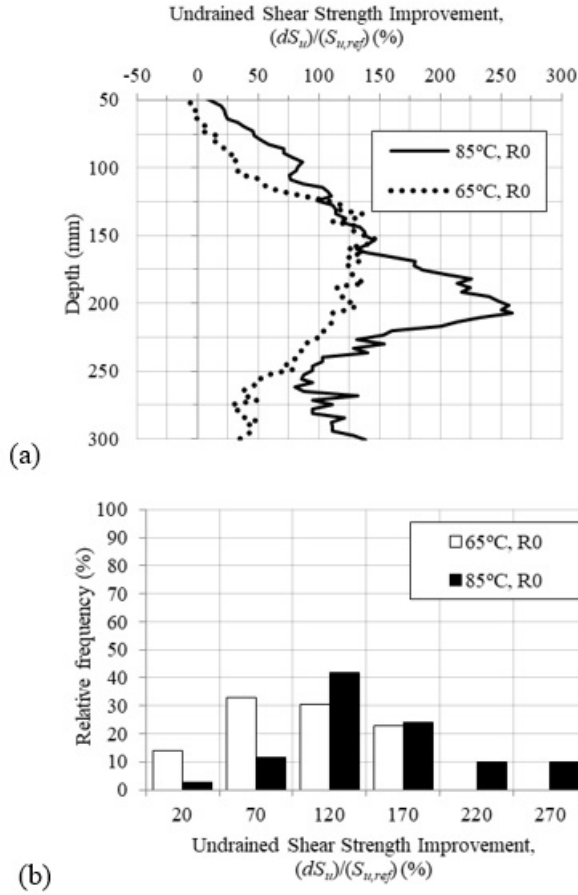


Figure 8. (a) Shear strength improvement profiles obtained at 30 mm (*R0*) from the axis of the heat source for the different tests; (b) Distribution of relative frequencies for undrained shear strength improvement at a radial distance of 30 mm (*R0*) in the different tests.

the pile. To that end, the mean shear strength variation was related to the normalized distance from the heat source for each test, as shown in Figure 11, which exhibits a nonlinear relationship between distance and shear strength variation.

Based on the relationship depicted in Figure 11, shear strength variation at the pile-soil interface and pile pullout capacity before and after the temperature cycle can be estimated, in order to assess the impact of the temperature gradient. To that end, the normalized distance for the pile-soil interface was analyzed and $S_u/S_{u,ref}$ values of 2.63 and 2.00 were found for tests 1 and 2, respectively. Thus, mean undrained shear strength values of 30.6 kPa and 28.1 kPa were recorded at the pile-soil interface for tests 1 and 2, respectively.

Based on shear strength at the interface, the pullout capacity of the pile was estimated using the Alpha method, described by Bai & Bai (2014), with the equation:

$$Q = \alpha S_u A \quad (2)$$

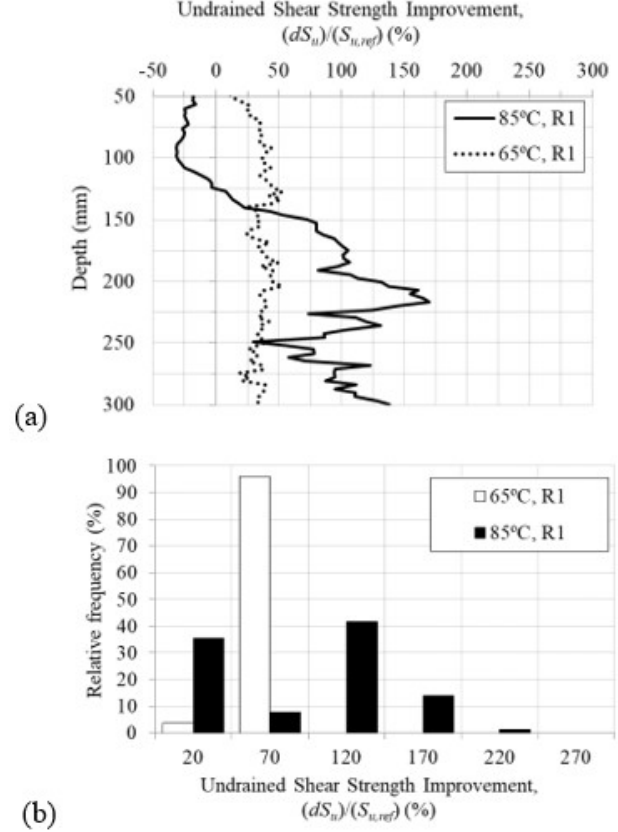


Figure 9. (a) Shear strength improvement profiles obtained at 88 mm (*R1*) from the axis of the heat source for the different tests; (b) Distribution of relative frequencies for undrained shear strength improvement at a radial distance of 88 mm (*R1*) in the different tests.

where Q is pullout capacity, α the cohesion factor, S_u undrained shear strength of the soil and A , the lateral area of the pile. According to the author, the cohesion factor can be calculated as follows:

$$\alpha = 0.608 - 0.123 S_u - \frac{0.274}{S_u^2 + 1} + \frac{0.695}{S_u^3 + 1} \quad (3)$$

with undrained shear strength (S_u) expressed in ksf. In the case of the model, the diameter (13 mm) and length (250 mm) of the pile correspond to an area of 102.1 cm² or 0.0102 m². The calculations for α cohesion factor of pile pullout capacity and net improvement (ΔQ) are presented in Table 8, for strength values before and after thermal treatment.

As demonstrated, there were relevant increases in pile pullout capacity due to the temperature cycle, with net improvement of 132% and 83% in tests 1 and 2, respectively.

The net improvement in pullout capacity was also plotted as a function of the temperature increase experienced by the pile, as shown in Figure 12. The figure also presents data on the reduced-scale physical model tested by Ghaaowd (2018),

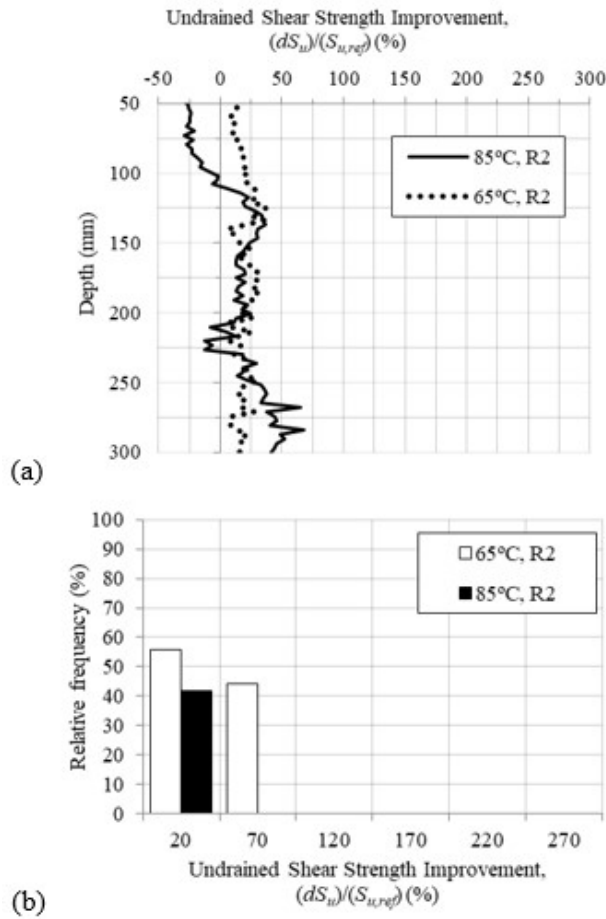


Figure 10. (a) Shear strength improvement profiles obtained 153 mm (R2) from the axis of the heat source for the different tests; (b) Distribution of relative frequencies for undrained shear strength improvement at a radial distance of 153 mm (R2) in the different tests.

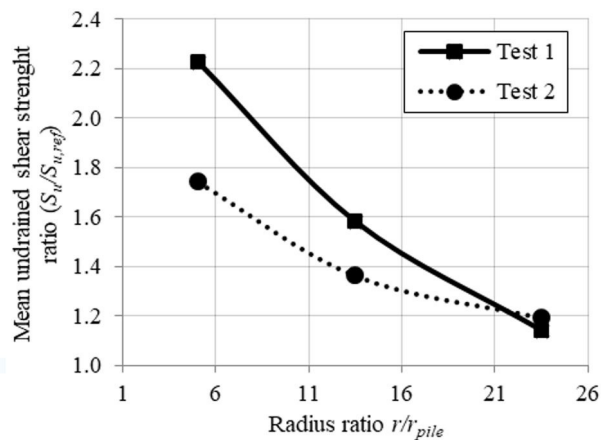


Figure 11. Undrained shear strength after the temperature cycle normalized by the reference shear strength versus distance normalized by the radius of the pile for tests 1 and 2.

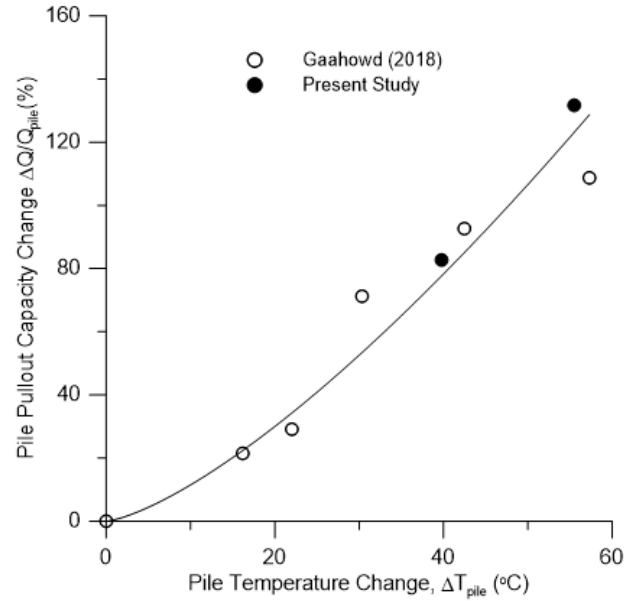


Figure 12. Pile Pullout Capacity Change with induced temperature after thermal consolidation.

Table 8. Estimated pullout capacity of the piles before and after the temperature cycle for tests 1 and 2.

T-bar	S_u (kPa)	α	Q (N)	ΔQ (%)
Reference, Test 1	11.63	1.00	119.33	131.89
Test 1	30.58	0.89	276.71	
Reference, Test 2	14.04	1.00	142.98	82.54
Test 2	28.08	0.91	261.00	

where a miniature torpedo pile was subjected to different temperature cycles in a 50g gravitational field. There is good agreement between the curve obtained from the data in the present study and the data reported by the aforementioned author. It is important to mention that, despite both studies were carried out in different gravity fields, the direct comparison is possible to be made because the variables are expressed in non-dimensional way, which is, in turn, should not be dependent on the scale.

5 Conclusions

Given the need to develop techniques to improve the bearing capacity of offshore foundations in soft clayey soils, the present study aimed to better understand the impact of a temperature cycle on the thermal and mechanical behavior of a soft kaolin clay, using a reduced-scale physical model with a miniature torpedo pile as a heat source, inserted into the soil in question.

Two tests were conducted with reduced-scale models, where soil under constant vertical stress of 50 kPa was submitted to increasing temperatures, reaching maximums of 85 °C and 65 °C, and then cooled. The heating cycle caused consolidation, improving the undrained shear strength of the soil in direct proportion to the temperature level applied and inversely proportional to the radial distance from the heat source. In the T-bar tests closest the pile, at 30 mm, the mean net improvements in undrained shear strength were 123% and 74% for tests 1 and 2, respectively.

Additionally, the pullout capacity of the pile before and after the temperature cycle was estimated, thereby generating net pullout capacity increases of 132% and 83% for tests where the soil was heated at 85 °C and 65 °C, respectively.

As such, we believe that this procedure has considerable potential as an improvement technique for soft soils, in order to increase the bearing capacity of offshore foundations.

Acknowledgements

The Authors are grateful to Petrobras for the financial support of this research (Grant NO SAP: 4600499688, Jur: 0050.0098204.15.9). The first Author is also grateful to the Brazilian Scholarship Agency – CAPES for financing the scholarship during the development of her PhD Thesis).

Declaration of interest

The authors have no conflicts of interest to declare. All co-authors have observed and affirmed the contents of the paper and there is no financial interest to report.

Authors' contributions

Marina de Souza Ferreira: conceptualization, Data curation, Formal analysis, Investigation, Methodology, Validation, Visualization, Writing – original draft, Writing – review & editing. Fernando Saboya Albuquerque Junior: conceptualization, Formal analysis, Methodology, Project administration, Supervision, Writing – review & editing. Sérgio Tibana: conceptualization, Formal analysis, Methodology, Project administration, Supervision. Ricardo Garske Borges: conceptualization, Resources, Funding acquisition, Supervision.

List of symbols

A	Lateral area of the pile
C_c	Compression index
c_v	Coefficient of consolidation
D	T-bar diameter
dS_u	Reference mean strength subtracted from strength after thermal cycle
dT	Temperature variation
e_0	Void ratio of the slurry before mechanical consolidation

e_f	Void ratio of the soil after mechanical consolidation
F_v	Vertical force during T-bar penetration
L	T-bar length
N_b	T-bar factor
PP	Pore pressure transducer
Q	Pullout capacity
r	Radial distance from the center of the pile
$R0$	Nomenclature used to the distance of 30 mm from the center of the pile
r_{pile}	Pile radius
$R1$	Nomenclature used to the distance of 88 mm from the center of the pile
$R2$	Nomenclature used to the distance of 153 mm from the center of the pile
S_u	Undrained shear strength of the soil
$S_{u,ref}$	Reference undrained shear strength of the soil
SI	Side 1 sensor
$S2$	Side 2 sensor
t_{90}	Time to 90% of consolidation
TC	Thermocouple
w_0	Moisture content of the slurry before mechanical consolidation
w_f	Moisture content of the soil after mechanical consolidation
α	Cohesion factor
ΔQ	Net improvement of pile pullout capacity

References







- Abuel-Naga, H.M., Bergado, D.T., & Bouazza, A. (2007). Thermally induced volume change and excess pore water pressure of soft Bangkok clay. *Engineering Geology*, 89(1-2), 144-154. <http://dx.doi.org/10.1016/j.enggeo.2006.10.002>.
- Bai, Q., & Bai, Y. (2014). *Subsea pipeline design, analysis, and installation*. Waltham: Gulf Professional Publishing.
- Baldi, G., Hueckel, T., & Pellegrini, R. (1988). Thermal volume changes of the mineral-water system in low-porosity clay soils. *Canadian Geotechnical Journal*, 25(4), 807-825. <http://dx.doi.org/10.1139/t88-089>.
- Campanella, R.G., & Mitchell, J.K. (1968). Influence of temperature variations on soil behavior. *Journal of the Soil Mechanics and Foundations Division*, 94(3), 709-734. <http://dx.doi.org/10.1061/JSFEAQ.0001136>.
- Cekerevac, C., & Laloui, L. (2004). Experimental study of thermal effects on the mechanical behavior of a clay. *International Journal for Numerical and Analytical Methods in Geomechanics*, 28(3), 209-228. <http://dx.doi.org/10.1002/nag.332>.
- Cheng, W., Hong, P.Y., Pereira, J.M., Cui, Y.J., Tang, A.M., & Chen, R.P. (2020). Thermo-elasto-plastic modeling of saturated clays under undrained conditions. *Computers and Geotechnics*, 125, 103688. <http://dx.doi.org/10.1016/j.compgeo.2020.103688>.

- Coccia, C.J.R., & McCartney, J.S. (2016). Thermal volume change of poorly draining soils II: model development and experimental validation. *Computers and Geotechnics*, 80(SM3), 16-25. <http://dx.doi.org/10.1016/j.compgeo.2016.06.010>.
- Cui, Y.J., Sultan, N., & Delage, P. (2000). A thermomechanical model for saturated clays. *Canadian Geotechnical Journal*, 37(3), 607-620. <http://dx.doi.org/10.1139/t99-111>.
- De Bruyn, D., & Thimus, J.F. (1996). The influence of temperature on mechanical characteristics of Boom clay: the results of an initial laboratory programme. *Engineering Geology*, 41(1-4), 117-126. [http://dx.doi.org/10.1016/0013-7952\(95\)00029-1](http://dx.doi.org/10.1016/0013-7952(95)00029-1).
- Delage, P., Sultan, N., & Cui, Y.J. (2000). On the thermal consolidation of Boom clay. *Canadian Geotechnical Journal*, 37(2), 343-354. <http://dx.doi.org/10.1139/t99-105>.
- Di Donna, A., & Laloui, L. (2015). Response of soil subjected to thermal cyclic loading: experimental and constitutive study. *Engineering Geology*, 190, 65-76. <http://dx.doi.org/10.1016/j.enggeo.2015.03.003>.
- Finn, F. (1951). The effect of temperature on the consolidation characteristics of remolded clay. *ASTM Special Technical Publication*, 126, 65-71. <http://dx.doi.org/10.1520/STP48297S>.
- Finnie, I. M. S., & Randolph, M. (1994). Punch-through and liquefaction induced failure of shallow foundations on calcareous sediments. In *Seventh International Conference on the Behaviour of Offshore Structures* (vol. 1, pp. 217-230), Massachusetts.
- Ghaaowd, I. (2018). *Thermal improvement of the pullout capacity of offshore piles in soft clays* [Doctoral thesis, University of California San Diego]. University of California at San Diego's repository. Retrieved in November 29, 2021, from <https://escholarship.org/uc/item/30z9k89d>
- Hong, P.Y., Pereira, J.M., Cui, Y.J., & Tang, A.M. (2016). A two-surface thermo-mechanical model for saturated clays. *International Journal for Numerical and Analytical Methods in Geomechanics*, 40(7), 1059-1080. <http://dx.doi.org/10.1002/nag.2474>.
- Houston, S.L., Houston, W.N., & Williams, N.D. (1985). Thermo-mechanical behavior of seafloor sediments. *Journal of Geotechnical Engineering*, 111(11), 1249-1263. [http://dx.doi.org/10.1061/\(ASCE\)0733-9410\(1985\)111:11\(1249\)](http://dx.doi.org/10.1061/(ASCE)0733-9410(1985)111:11(1249)).
- Hueckel, T., & Baldi, G. (1990). Thermoplasticity of saturated clays: experimental constitutive study. *Journal of Geotechnical Engineering*, 116(12), 1778-1796. [http://dx.doi.org/10.1061/\(ASCE\)0733-9410\(1990\)116:12\(1778\)](http://dx.doi.org/10.1061/(ASCE)0733-9410(1990)116:12(1778)).
- Kuntiwattanukul, P., Towhata, I., Ohishi, K., & Seko, I. (1995). Temperature effects on undrained shear characteristics of clay. *Soil and Foundation*, 35(1), 147-162. <http://dx.doi.org/10.3208/sandf1972.35.147>.
- Laloui, L., & François, B. (2009). ACMEG-T: soil thermoplasticity model. *Journal of Engineering Mechanics*, 135(9), 932-944. [http://dx.doi.org/10.1061/\(ASCE\)EM.1943-7889.0000011](http://dx.doi.org/10.1061/(ASCE)EM.1943-7889.0000011).
- Plum, R.L., & Esrig, M.I. (1969). Some temperature effects on soil compressibility and pore water pressure. *Highway Research Board*, 103, 231-242.
- Samarakoon, R., Ghaaowd, I., & McCartney, J.S. (2018). Impact of drained heating and cooling on undrained shear strength of normally consolidated clay. In *Energy Geotechnics. SEG 2018* (pp. 243-249). Cham: Springer. https://doi.org/10.1007/978-3-319-99670-7_31.
- Stewart, D. P., & Randolph, M. F. (1991). A new site investigation tool for the centrifuge. In *Proceedings of the International Conference on Centrifuge Modelling* (91, pp. 531-538), Boulder.
- Towhata, I., Kuntiwattanaku, P., Seko, I., & Ohishi, K. (1993). Volume change of clays induced by heating as observed in consolidation tests. *Soil and Foundation*, 33(4), 170-183. http://dx.doi.org/10.3208/sandf1972.33.4_170.
- Trani, L.D.O., Bergado, D.T., & Abuel-Naga, H. (2010). Thermomechanical behavior of normally consolidated soft Bangkok clay. *International Journal of Geotechnical Engineering*, 4(1), 31-44. <http://dx.doi.org/10.3328/IJGE.2010.04.01.31-44>.
- Wang, J., & Zhang, Z. (2020). Experimental studies on thermo-mechanical coupled behavior of pile-clay interface. *IOP Conference Series Earth and Environmental Science*, 455(1), 012113. <http://dx.doi.org/10.1088/1755-1315/455/1/012113>.
- Zhou, C., & Ng, C.W.W. (2018). A new thermo-mechanical model for structured soil. *Geotechnique*, 68(12), 1109-1115. <http://dx.doi.org/10.1680/jgeot.17.T031>.

CASE STUDY

Soils and Rocks
v. 45, n. 1

Thermal design of energy piles for a hotel building in subtropical climate: a case study in São Paulo, Brazil

Letícia Menezes Santos Sá¹ , Alberto Hernandez Neto² ,
Cristina de Hollanda Cavalcanti Tsuha^{1#} , Juliana Pessin¹ ,
Milena Cardoso de Freitas¹ , Thaise da Silva Oliveira Morais¹ 

Case Study

Keywords

Energy piles
Micropile
Steel pile
Continuous flight auger pile

Abstract

The use of shallow geothermal energy through energy piles for the air-conditioning of buildings is increasing worldwide. This type of renewable energy technology is still not utilized in Brazil, where the hot dominating weather regions and the air cooling demand predominate. In this case of unbalanced heat transfer to the ground, the efficiency of the system may decrease with time due to the excessive heat injection into the soil. In order to investigate the possibility of an efficient application of this technology in São Paulo city, a balanced use of the ground for a ground-source heat pump (GSHP) system utilizing energy piles is evaluated in the present paper. Energy foundations were designed to meet the balanced heating and cooling loads (air conditioning and water heating) of a hypothetical business hotel building located in a site at the campus of the University of São Paulo, where thermal response tests (TRTs) were conducted on different types of energy pile. The number of energy piles required to supply the building thermal loads were estimated using the pile heat exchanger modelling software PILESIM 2.1 and compared with an analytical model prediction. The evaluations were done for three different types of pile tested at the site chosen for this study: micropiles, steel pipe, and continuous flight auger (CFA) piles. The results indicate that the ground heat extraction should be considered for the use of GSHP systems with energy piles in air cooling-dominated scenarios similar to the case studied here.

1. Introduction

Over the last twelve years, the consumption of electric energy for air conditioning in Brazilian residences has more than tripled, according to the Brazilian Energy Research Company (EPE, 2018). This growing demand for artificial air cooling causes negative impacts on the cost of electricity and environment. To mitigate this problem, the shallow geothermal energy using ground-source heat pump systems (GSHP) seems to be an environmentally friendly alternative to traditional air conditioning systems.

The GSHP system consists of a ground loop heat exchanger and a heat pump system (Lim et al., 2017), which allows the heat exchange between the ground and ambient temperature for cooling and heating of buildings. This system has been used for many years utilizing deep boreholes as ground heat exchangers; however, the additional cost of drilling deep boreholes has made this technology cost-prohibitive in some situations (Murphy et al., 2015).

An alternative to this problem is the use of deep foundations as ground heat exchangers, commonly known as “energy piles”. Pile foundations, already necessary for structural support, when equipped with geothermal loops can be used for heat exchange operations, exploiting the near-surface geothermal energy (Sutman et al., 2020). Energy piles are constructed with pipe loops attached to the reinforcement cage for circulating heat-carrying fluid to facilitate soil–pile heat transfer.

In this context, heat exchanger piles were installed at the site of the CICS Living Lab, a building being built at the Campus of the University of São Paulo, in the urbane zone of São Paulo city. For this first use of energy foundations in Brazil, thermal response tests (TRTs) were conducted on three different pilot piles, constructed and tested to provide information for the design of the GSHP system that will be used in this building for space air cooling. However, the predominant thermal load demand of buildings in São Paulo is for ambient air cooling; and as mentioned in Zhang & Wei

*Corresponding author. E-mail address: chetsuha@sc.usp.br

¹Universidade de São Paulo, Department of Geotechnical Engineering, São Carlos, SP, Brasil.

²Universidade de São Paulo, Department of Mechanical Engineering, São Paulo, SP, Brasil.

Submitted on November 15, 2021; Final Acceptance on January 17, 2022; Discussion open until May 31, 2022.

<https://doi.org/10.28927/SR.2022.077421>



This is an Open Access article distributed under the terms of the Creative Commons Attribution License, which permits unrestricted use, distribution, and reproduction in any medium, provided the original work is properly cited.

(2012), for cases of unbalanced heating and cooling loads the temperature of underground soil will gradually rise affecting the efficiency of the GSHP system. In cooling-dominated climates this imbalance can lead to an accumulation of heat in the ground, which decreases the coefficient of performance (COP) and increases energy consumption (Martins & Bourne-Webb, 2021).

Different strategies were proposed in previous studies to minimize this problem of heat accumulation of GSHP systems. Hybrid ground-coupled heat pump (GCHP) systems with domestic hot water (DHW) were investigated in Diao et al. (2010) to serve as a supplemental heat rejecter to alleviate the imbalance of ground thermal loads. Akrouh et al. (2020) suggested management strategies to active and/or deactivate groups of piles by zones, to prevent the increase of ground temperatures when dealing with unbalanced thermal loads. Martins & Bourne-Webb (2021) proposed the use of hybrid GSHP-NV systems (where NV means natural ventilation) to decrease cooling load imbalance in cooling-dominated buildings.

Therefore, considering the predominant air cooling demand of buildings in São Paulo city and in Brazilian regions of similar weather conditions, leading over time to an increase of the ground temperature, the current work was proposed to investigate a balanced application of a GSHP system to prevent this problem, by using energy piles for air cooling and to produce hot water daily.

This alternative operation mode of GSHP systems in cooling and heating process (to produce hot water) were investigated to provide a balance of ground temperature in Cui et al. (2008) and in Jalaluddin & Miyara (2012). In this case, the heat extraction from the ground also contributes to the increasing the heat exchange rate in cooling process.

As suggested in Cui et al. (2008), in summer the system can operate in the heating mode for few hours to produce hot water when the cooling need is irrelevant or zero, and in the winter or when the cooling requirement is unnecessary, the main function of the system is to meet the hot water demand.

For the current study, a thermal design of energy piles for a hypothetical business hotel building located at the University of São Paulo campus was carried out using the results of ground thermal parameters and pile thermal resistance obtained from thermal response tests (TRTs) performed on three different types of energy piles at this site. This paper details the simulations procedure and results.

2. Case study description

2.1 Weather and soil conditions

The CICS Living Lab site, assumed for the case simulated in this paper, is located at the University of São Paulo (Figure 1) in São Paulo city (latitude: 23°33'15.8"S; longitude: 46°43'51.2"W), Southeast Region of Brazil, with annual average temperature of approximately 19.3-19.6 °C (maximum 24.9°C-25.2°C and minimum 15.5-15.8°C).

Figure 2 presents the soil profile at the CICS site, the results/ locations of standard penetration tests (SPT tests), and the variation of ground temperature with depth, obtained from temperature sensors installed in CFA piles by Pessin (2021). This figure illustrates the predominance of saturated medium dense slightly clayey sand, from approximately 4 to 16 m deep.

Pessin et al. (2022) determined the groundwater flow velocity of two sandy layers at the CICS site and found the

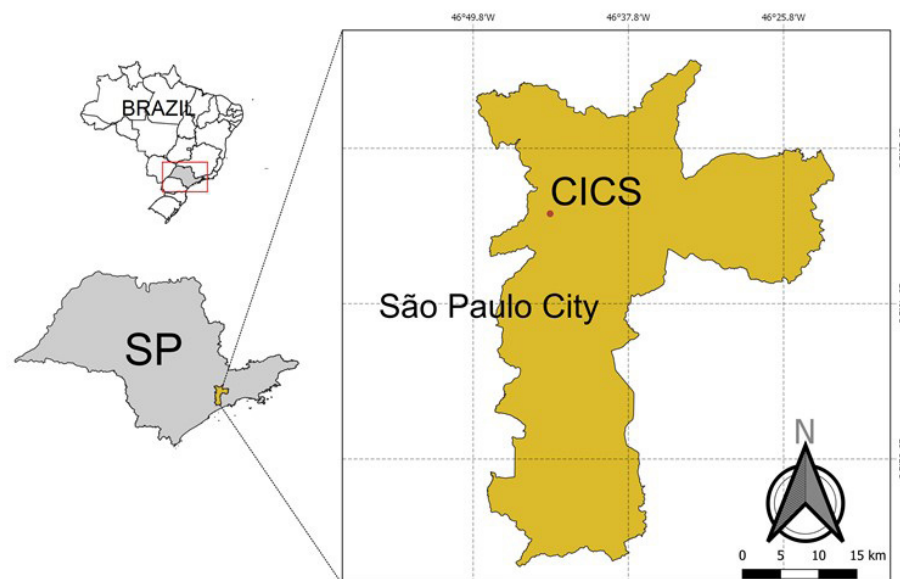


Figure 1. Location of the CICS site.

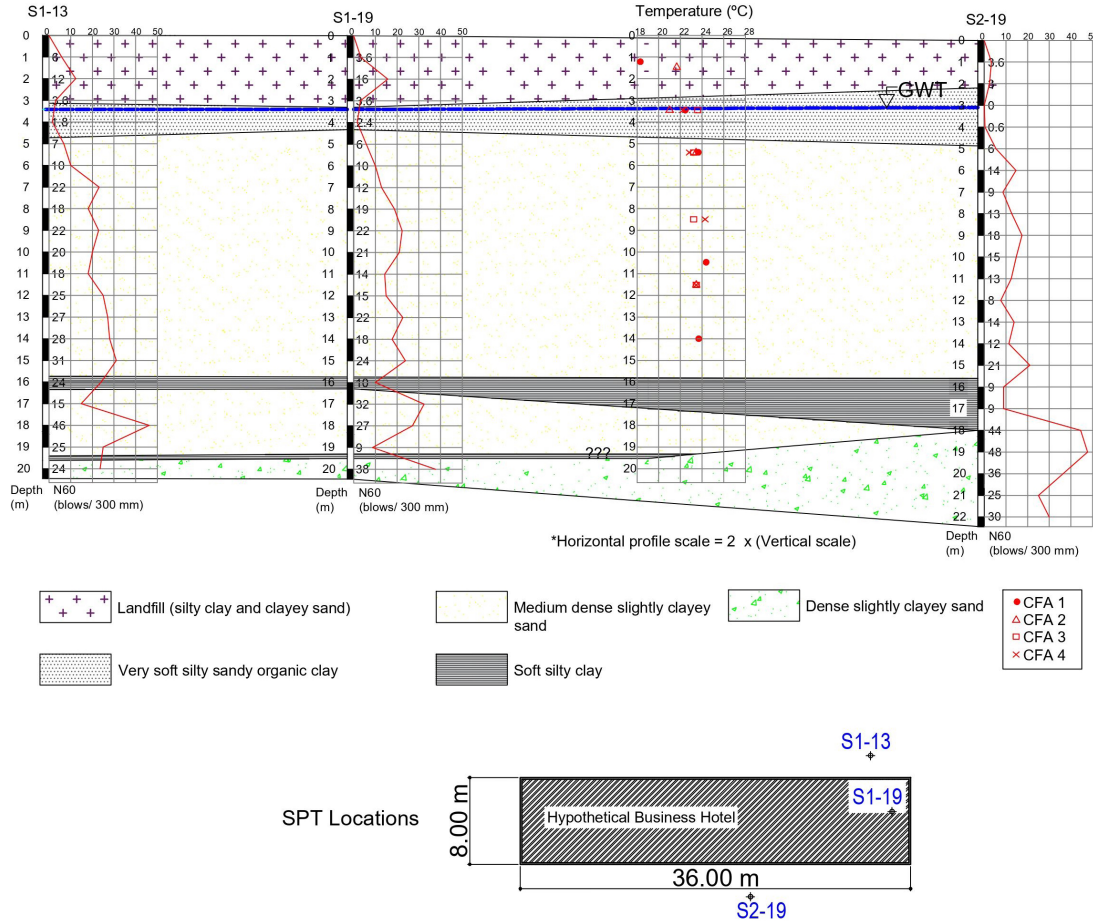


Figure 2. Soil profile, SPT tests results and locations, and ground temperature variations with depth.

Table 1. Characteristics of energy piles.

Type of energy pile	Diameter (m)	Pipe configuration in pile	Average length of piles (m)	Active length ^a of piles (m)
Micropile	0.35	U-shaped pipe	15	15
CFA pile	0.70	Triple-U	15	10.5
Steel pipe pile	0.24 ^b	U-shaped pipe	20	20

^aActive length = pile length equipped with pipes; ^bexternal pipe diameter.

highest values of flow velocity (from 0.05 to 0.2 m/day) for the uniform sand layer from 5 to 6 m deep. For the layer from 10 to 11 m deep, they observed a flow velocity of $\sim 3.3 \times 10^{-4}$ m/day. These values were adopted for the simulation conducted in this work.

2.2 Tested energy piles

Three different types of energy pile, constructed and tested at the CICS site, were assumed for the simulation performed for the hotel building thermal demand presented in this paper (for space cooling and hot water): micropile, continuous flight auger (CFA) pile, and steel pipe pile filled with grout. Figure 3 illustrates the dimensions and installation of the three types of energy pile, and Table 1 describes their

geometrical characteristics. All piles were equipped with loops of high-density polyethylene (HDPE) pipes (inner diameter of 26 mm and outer diameter of 32 mm) for the heat exchange with surrounding soils.

The energy piles showed in Figure 3 were tested in previous investigations. Morais & Tsuha (2018) conducted a thermal response test (TRT) on the energy micropile illustrated in Figure 3a. Later, Pessin (2021) carried out a TRT test on the CFA energy pile (Figure 3b), and Murari (2022) on the steel energy pile (Figure 3c). The details and results of the TRTs performed on these piles are described in these three mentioned studies. TRT tests provide thermal parameters used for simulation of GSHP systems, such as ground effective thermal conductivity, λ_{eff} , and the pile thermal resistance, R_p (Morais, 2019; Park et al., 2019).

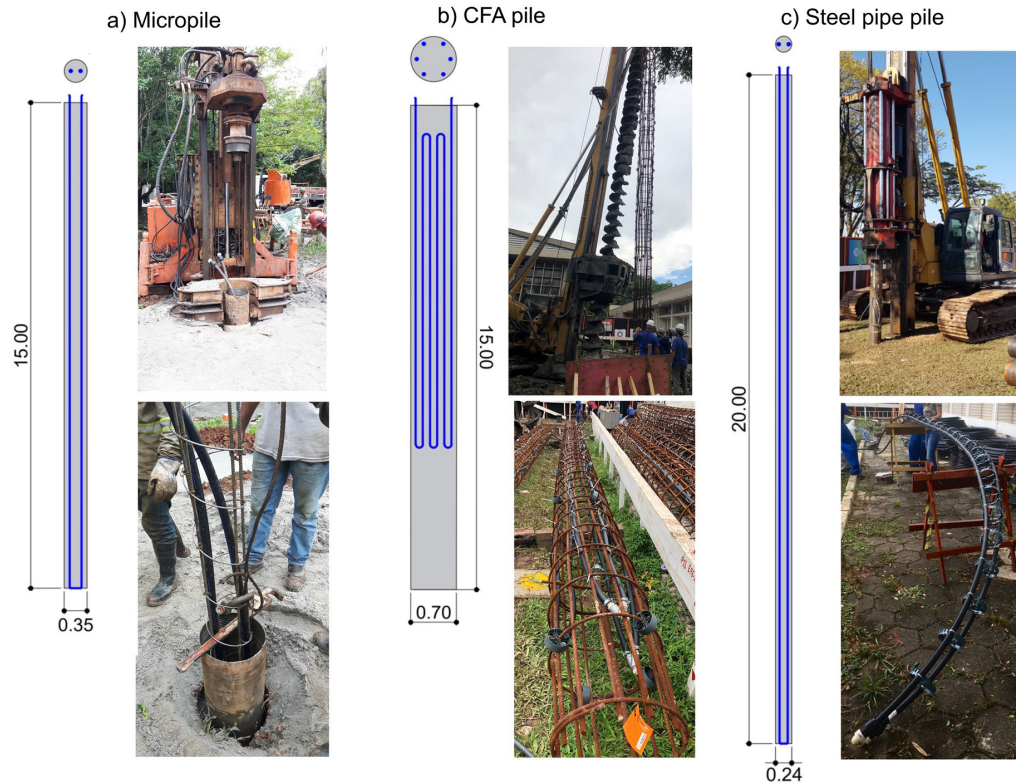


Figure 3. Dimensions and installation of energy piles at the CICS site: (a) micropile; (b) CFA pile; (c) steel pipe pile (dimensions in meters).

TRT is a field experiment for estimating the thermal parameters mentioned above; however, they cannot provide the actual thermal performance of heat exchanger pile in the real operating condition of GSHP systems. For this case, the thermal performance test (TPT) is the most suitable field test to evaluate the thermal performance (Park et al., 2019). Brandl (2013) suggests values of heat exchange rate for the pre-design of energy foundations and feasibility studies; however, for a more reliable estimation of the energy pile performance, a thermal performance test (TPT) was conducted on the CFA energy pile at the CICS site by Pessin (2021), to determine the heat rejection rate of a heat exchanger foundation element during the cooling operation for a building located at the test site.

In a TPT test the inlet fluid (water) temperature is kept constant using a heater system regulated by a temperature controller (You et al., 2014). The heat exchange rate was obtained by monitoring the outlet fluid (water) temperature while maintaining the inlet fluid temperature at approximately 35°C. Further details of the test equipment and experimental procedures can be found in Pessin (2021). As adopted in Park et al. (2016), for this test a mean flow rate of 9.3 l/min (measured by a turbine flowmeter) was used to provide sufficient temperature difference between the inlet fluid and the outlet fluid more than 2 °C. The TPT results are presented in Figure 4. The variation of heat

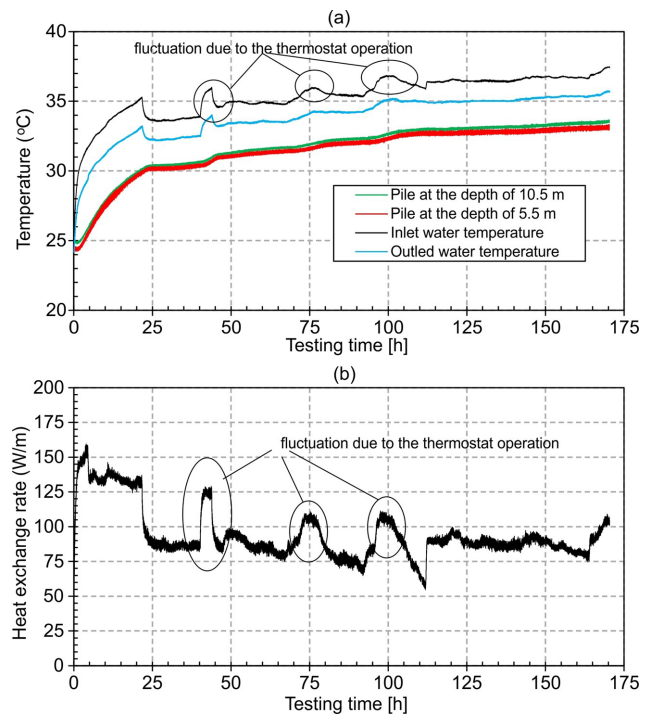


Figure 4. Variation of: (a) the fluid and pile temperatures; (b) of the heat exchange rate of the CFA energy pile over 175 h.

exchange rate (q) showed in this figure was calculated by Equation 1:

$$q = \frac{mc(T_{in} - T_{out})}{L} \quad (1)$$

where, q is the heat exchange rate per pile active length (W/m); T_{in} is the inlet temperature of the fluid (K), T_{out} is the outlet temperature of the fluid (K), m is the flow rate of the fluid (kg s^{-1}), c is the specific heat capacity of the fluid ($\text{J kg}^{-1}\text{K}^{-1}$) and L is the pile active length (m).

Figure 4a shows that after around 110 hours of heat rejection in the ground the pile temperature becomes almost constant. Figure 4b indicates that the heat exchange rate decreases significantly after a few hours and tends to be constant (ignoring the fluctuations caused by the thermostat operation) with a value of approximately 85 W/m. This trend was also observed in a TPT test conducted in You et al. (2014) on a cement-fly ash-gravel (CFG) pile with 420 mm in diameter and 18 m in length.

2.3. Building and GSHP system description

The building considered in this case study is a typical example of a business hotel in São Paulo city, with 20 floors and 12 rooms per floor, as illustrated in Figure 5. The occupancy schedule is defined as most of the occupation occurs from 06:00 PM to 08:00 AM and the main systems (lighting, air conditioning, and water heating) have their main demands on the same period.

Normally, the cooling demand of the building is supplied by a central water-cooling system composed of an electric chiller serving a set of fan coils with one fan coil for each room. The water heating demand of the building is supplied by a central water heating system composed of natural gas water heaters.

As mentioned previously in the text, one of the challenges of using GSHP systems is to balance the cooling and heating loads to control the variation of ground temperature with time. Therefore, the proposed system is composed of a set of heat pumps that provides the cooling and the heating demand for the hotel. Due to the superposition of the heating and cooling demand, it is necessary to include a water heated tank in the system. The temperature of such

tank will be maintained by the set of heat pumps during the day (heat extraction from the ground), when there is a low cooling demand. During the night, the demand of heated water is supplied by the heated water tank and the cooling demand is supplied by the set of heat pumps (heat rejection into the ground).

A simplified schematic of the system for the cooling operation (Figure 6) and heating operation (Figure 7) is presented. To maintain a good efficiency and longer life cycle of the ground source heat pumps, it is important to balance the heating and cooling demand drawn from the ground. For the business hotel, the heating demand is much higher than the cooling demand, which imposes an unbalanced operation. To overcome this problem, the heating demand was split in such way that the heating and cooling demand of the heat pumps are similar to provide a balanced ground load. The remaining heating demand is provided by a set of natural gas water heaters.

3. Simulations using PILESIM 2.1

The program PILESIM 2.1 was used to study the long-term behavior of heat exchanger piles for a hypothetical building at the CICS site. This program was developed to simulate heating and cooling systems with energy piles or multiple borehole heat exchangers (Pahud, 2007). The long-term behavior of the energy piles for the building thermal demand was examined for a period of 20 years. Three different simulations were performed in order to validate the GSHP design for the three different foundation types tested at the CICS site.

3.1 Procedure description

The program PILESIM has been used extensively for the thermal simulation of heat exchanger pile systems. This program uses a modified finite difference method based on a version of the Duct Ground Heat Storage Method (DST) (Fadejev et al., 2017; Hellström, 1991; Martins & Bourne-Webb, 2021; Pahud, 2007) to perform thermal simulations and calculate the heat transfer from the ground to the thermal energy distributed in a building (Pahud, 2007).

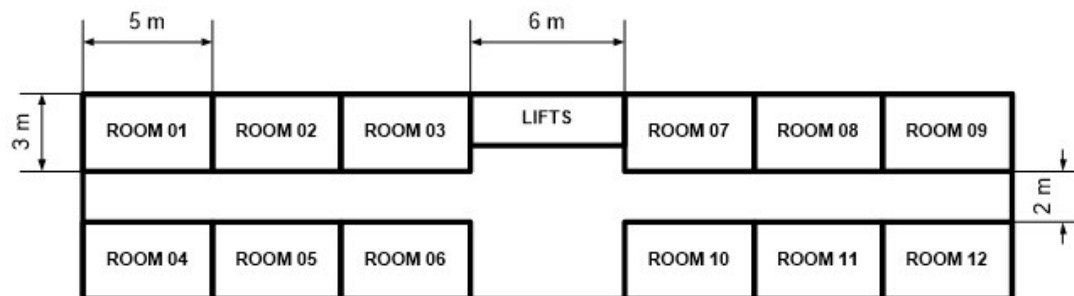


Figure 5. Simplified floor plan of a typical floor of the hotel building.

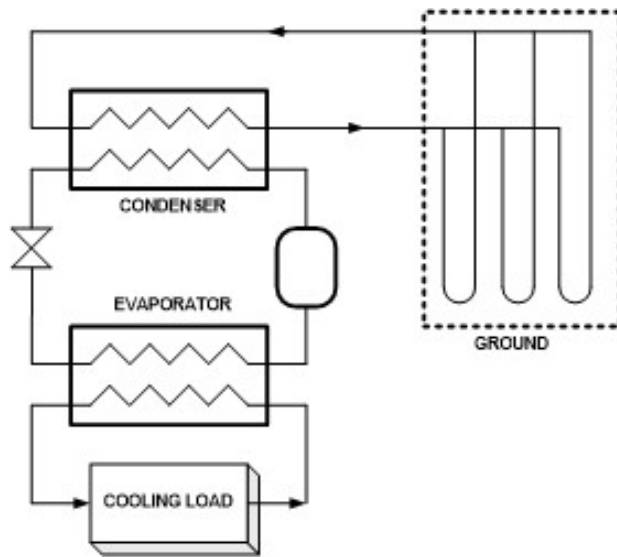


Figure 6. Simplified flow diagram (cooling operation).

The methodology used in this paper is illustrated in Figure 8. The hotel building was modelled using Energy Plus, an open-source tool for whole building simulations (Crawley et al., 2001) coupled with a TMY (Typical Meteorological Year) weather data file for the city of São Paulo. The outputs of such simulations are the hourly profile of the heating and cooling demand of the hotel. The estimated results are introduced as input for the simulations using the program PILESIM 2.1, which provides the thermal performance of energy piles, the thermal loads covered by the geothermal system, the COP values (for heating and cooling operations), the heat extraction and injection rates per meter pile, and the temperature of the ground surrounding the energy piles. This program provides results for each year of operation and over 20 years.

For the simulations using PILESIM 2.1, there are some assumptions that need to be considered for optimal use: (i) a relatively large number of energy piles; (ii) the energy piles

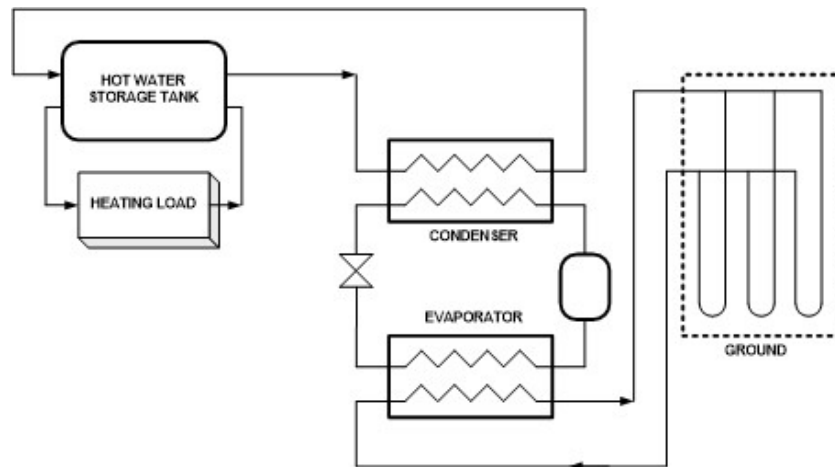


Figure 7. Simplified flow diagram (heating operation).

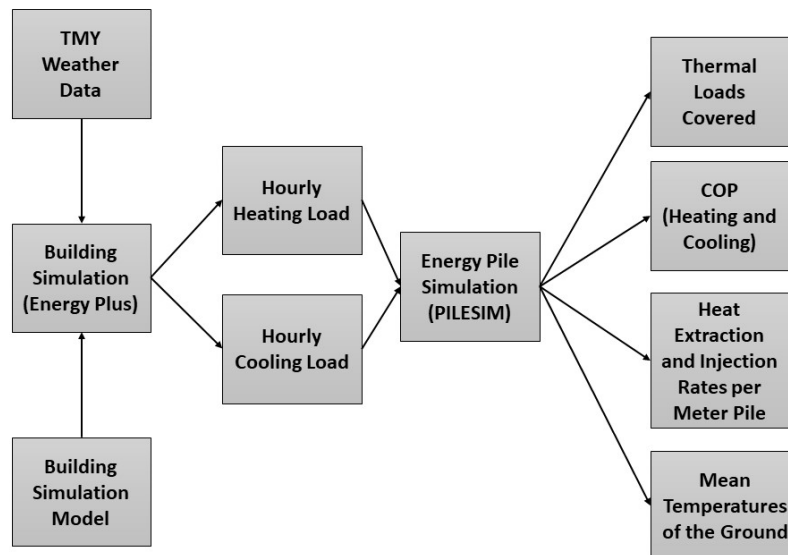


Figure 8. Schematic of the simulation methodology.

should be located in a regular spatial arrangement (a circular or squared area); (iii) the energy piles should have the same active length (Fadejev et al., 2017; Pahud, 2007).

According to the User Manual (Pahud, 2007), the input parameters to define a heat exchanger pile system is grouped in five main categories: (i) ground characteristics; (ii) energy piles parameters; (iii) ground-building interface specifications; (iv) heat pump and cooling machine data; and (v) loading conditions for heating and cooling. Additionally, it is necessary to specify the thermal properties of the soil layers in which the energy piles are installed (up to three layers can be specified). Moreover, it is possible to include the presence of a groundwater flow (if any) and the initial ground temperature before heat exchanges.

The three tested piles and the CICS site described above in the paper were used to characterize the energy foundations and the ground conditions for the simulations. For simplification, based on the soil profile presented in Figure 2, it was assumed that the topsoil layer, from 0 to 4.8 m, consists of a clayey soil with Darcy velocity of groundwater equal to 0 m/day. The second layer, from 4.8 to 10 m, is composed of sandy soil with the Darcy velocity of groundwater equal to 0.125 m/day, average value measured in Pessin et al. (2022) for the layer from 5 to 6 m. The third layer, from 10 to 20 m, is composed of a sandy soil with the Darcy velocity of groundwater equal to 3.3×10^{-4} m/day, based on the results of Pessin et al. (2022).

The soil thermal conductivity (layer from 0 to 20 m depth) for the current simulation was defined equal to 2.7 W/mK, based on the interpretation of the results of TRTs performed on a micropile and a steel pile filled with grout at the CICS site. Morais & Tsuha (2018) obtained a value of ~ 2.8 W/mK from the TRT conducted on a micropile (Figure 3a), and later, Murari (2022) found a value of ~ 2.6 W/mK from the TRT conducted on a steel pile (Figure 3c). The ground volumetric thermal capacity was adopted as 2.4 MJ/m³K, based on the values suggested in Laloui & Rotta Loria (2020). The input parameters for the three types of energy piles evaluated are presented in Table 2. For all simulations, an active pile length (identical to the pile length) of 20 m was defined based on

the driven resistance per pile recorded during steel pipe piles installation at the CICS site. The number of piles were defined in order to provide acceptable results of COP values and of heat rejection rate per meter pile (W/m), as the water heating demand can be complemented by the installation of natural gas water heaters.

For the present simulation it is necessary to include parameters related to the cellar (a non-heated space that separates the heated rooms from the ground below the building) and to the horizontal connected pipes, which are presented in Table 3.

The loading conditions for heating and cooling were obtained through EnergyPlus software for the standard business hotel, as presented in Figure 8. Loading conditions were determined based on heat demand, cold demand, and corresponding temperature levels. The parameters related to the heat pump and cooling machine thermal performances were calculated to ensure the best functioning of the system. A heat pump works with a refrigeration cycle which requires maintaining a higher condensing temperature (50 to 52 °C). To be able to reject the heat from the heat pump condenser, the inlet water temperature in the energy piles should be 45 °C in cooling operation mode. When the heat pump operates in the heating operation mode, the inlet water temperature in the energy piles should be 7 °C. These data were used as input to the simulations using PILESIM 2.1.

A limitation of the PILESIM program is that it only considers continuous cooling/heating operation for six months, and, for the current hotel building evaluated an alternative operation mode was assumed. Therefore, as the alternative operation mode increases the energy pile performance (Cui et al., 2008; Jalaluddin & Miyara, 2012), the results of the current simulation correspond to the most unfavorable operation mode.

3.2 Results

Long-term simulations performed with PILESIM 2.1 provided different results for the three types of heat exchanger piles evaluated. The simulations were carried out

Table 2. Energy piles parameters for simulation with PILESIM 2.1.

	Micropiles	CFA piles	Steel pipe piles
Diameter (m)	0.35	0.70	0.24
Number of piles	180	68	115
Average active length of piles (m)	20	20	20
Pile thermal resistance R_b (K/(W/m)) ^a	0.13	0.04	0.10
Internal pile thermal resistance R_a (K/(W/m)) ^b	0.39	0.40	0.34
Average spacing between piles (m)	1.20	2.10	1.50
Pipe configuration in pile	U-pipe configuration	U-pipe configuration	U-pipe configuration
Pipe number in a cross section of a pile	2	6	2
Pipe inner diameter (mm)	26	26	26

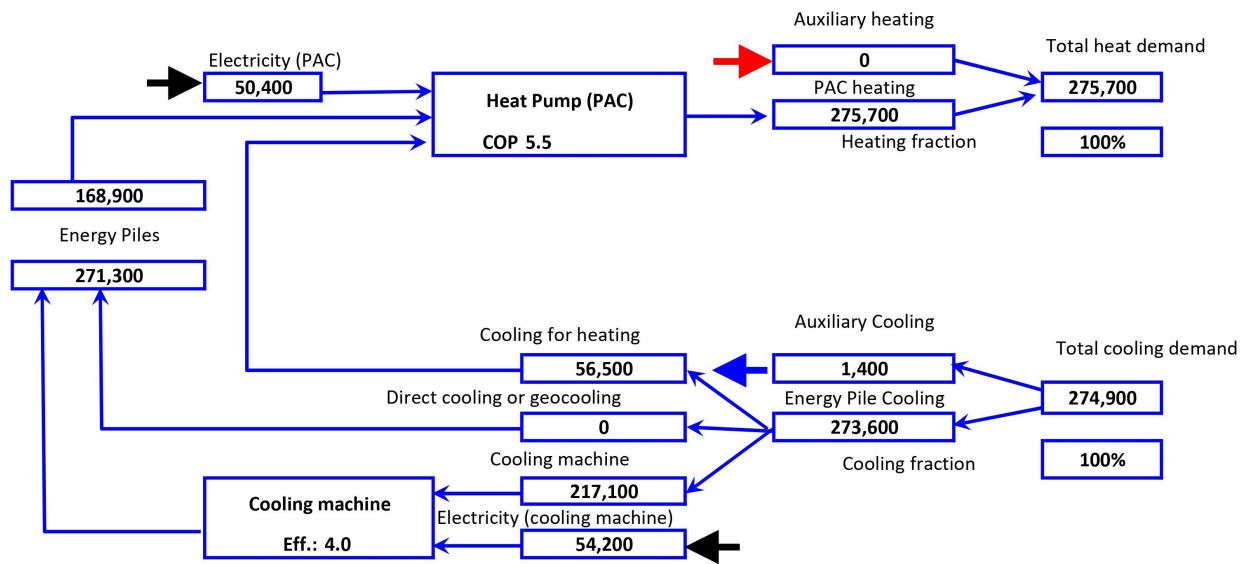
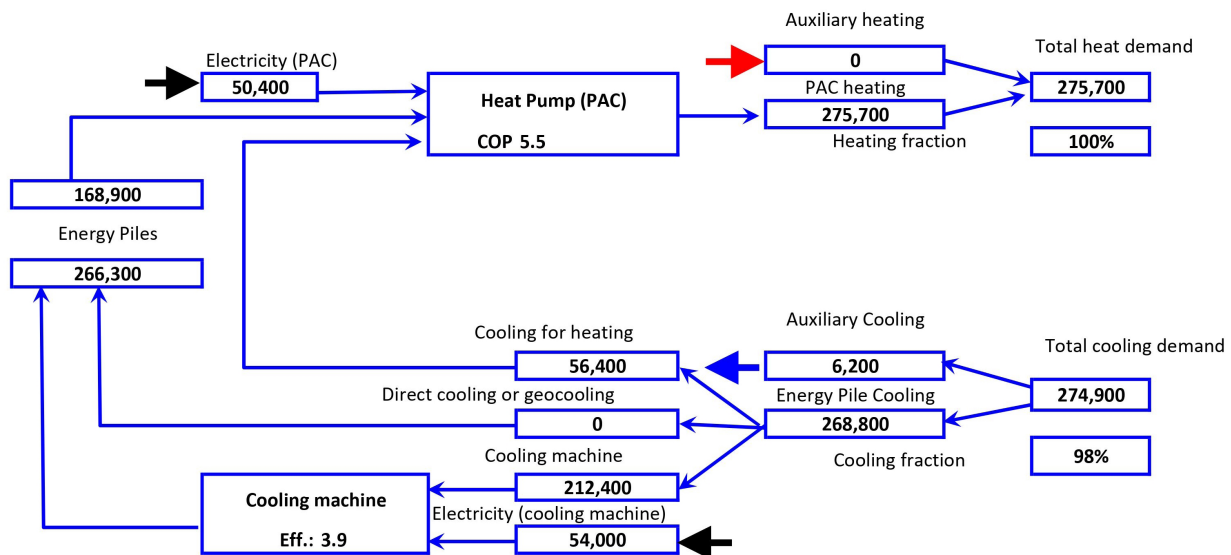
^aValues obtained by Morais & Tsuha (2018), Pessin (2021), and Murari (2022) from the interpretation of TRTs; ^bCalculated by equations suggested in Hellström (1991), assuming an average typical thermal conductivity value for saturated concrete suggested in Loveridge (2012).

Table 3. Interface ground-building parameters.

Interface ground-building parameters	Input values for simulations
Room air temperature in building (°C)	24
Height of the cellar between rooms and ground (m)	0.60
Air change rate in the cellar (1/h)	0.00
Global-room cellar heat transfer coefficient (W/m ² K)	6.70
Insulation thickness between ground and cellar (m)	0.00
Concrete thickness between ground and cellar (m)	0.14
Length of the horizontal pipes on ground (m)	36.00

to predict the thermal behavior of the piles over 20 years. The outputs of the program (mean values for the period of simulation, for all scenarios adopted) are presented in Figures 9, 10 and 11.

The results of Figures 9 to 11 show that the average values of COP during 20 years of heating are the same for the three simulations using different types of piles, and the values of efficiency for the cooling are also similar. Most of the obtained values are within the ranges presented in Brandl (2006), which recommended GSHP systems with COP values ≥ 4 for economic reasons. Only the simulation for steel pipe piles presented a value of 3.9 for the average efficiency of the cooling machine (slightly smaller than the recommended value).

**Figure 9.** System heat balance in kWh/year (period of 20 years) for the system utilizing micropiles.**Figure 10.** System heat balance in kWh/year (period of 20 years) for the system utilizing steel pipe piles.

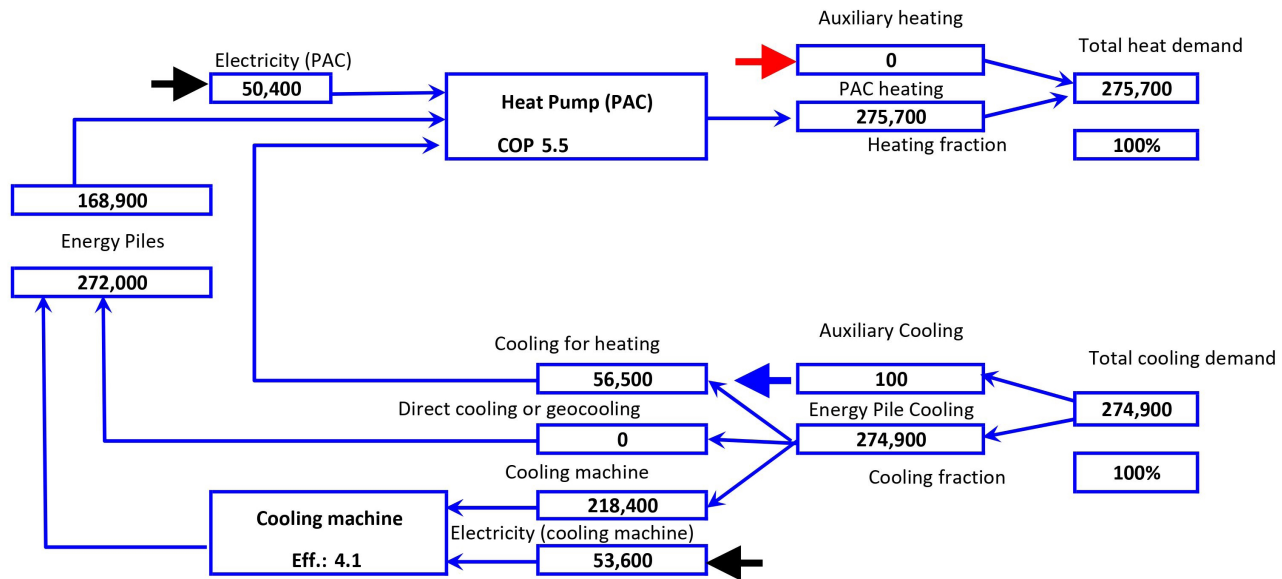


Figure 11. System heat balance in kWh/year (period of 20 years) for the system utilizing CFA piles.

Figures 9 to 11 also indicate the fractions of total heating demand covered by the heat pump and the fraction of the total cooling demand covered by the piles system and cooling machine. For the cases utilizing micropiles and CFA piles, 100% of the heating and cooling energies could be covered by the GSHP system, without the need for power provided by an auxiliary source. For the case with steel energy piles, the heating demand covered by the energy piles is 100%, while for cooling is 98%.

The program also provides results of the variation of the ground temperature during 20 years of operation of the GSHP system (Figure 12). The average initial ground temperature was about 23.8 °C; therefore, Figure 12 indicates an increase of approximately 11 °C in soil temperature after 20 years. This figure also shows that the ground temperature rises and remains practically constant after around 10 years of system operation. On the other hand, this increase does not seem to have affected the system efficiency, as in most cases the COP values are within the recommended range. Figure 12 also shows that the increase of ground temperature is slightly lower for the case of CFA piles. Probably it occurs because the number of piles in this case is reduced compared to the other two cases (Table 2).

On the other hand, as mentioned before in the text, the program PILESIM considers periods of six months of continuous operation (for cooling or heating demand), and the alternative cooling/heating mode proposed for the studied hotel building can alleviate the heat buildup in the surrounding soil. Jalaluddin & Miyara (2012) noted that the alternative operation mode provides a balance of ground temperature around the ground heat exchanger. Therefore, the results shown in Figure 12 correspond to the most critical condition for the ground, by considering a continuous operation mode. Probably

for the hotel building proposed with an alternative operation mode the increase in ground temperature would be lower.

Additionally, the operation of energy foundations will cause temperature changes inside piles inducing additional stresses, which can affect the pile settlement. Therefore, the use an alternative cooling/heating mode appears to be less problematic for the foundation behavior, as in this case the variation of pile temperature would be reduced compared to the case of a continuous operation.

The average values of heat extraction and injection rates per meter of pile during 20 years of simulation are shown in Table 4. The heat injection and extraction rates per meter pile are higher for the CFA piles (larger pile diameter and larger heat exchange surface) and lower for the micropiles. The results for heat injection rates obtained for the cases of CFA and steel pipe piles are in good agreement with the recommendations of Brandl (2013) which suggested values of 40-60 W/m for piles with a diameter smaller than 0.5 m and 35 W/m² for piles with diameter greater than 0.6 m (for the CFA pile case the obtained value of 71 W/m corresponds to ~32 W/m²). For the case of the system using micropiles, the values obtained are slightly lower than the recommended for piles with a diameter smaller than 0.5 m.

Additionally, the heat exchange rate recommended in Brandl (2013) for piles with diameter larger than 0.6 m is slightly lower than the value observed from the TPT test conducted on a CFA pile at the CICS site (Figure 4). Therefore, the suggested heat exchanger rate for the pre-design of energy foundations seems to be adequate for the current case study.

On the other hand, the heat extraction rates per meter pile for heating purposes are much higher compared to those obtained for cooling purposes. The values obtained for CFA piles case (135 W/m) and steel piles case (80 W/m) are

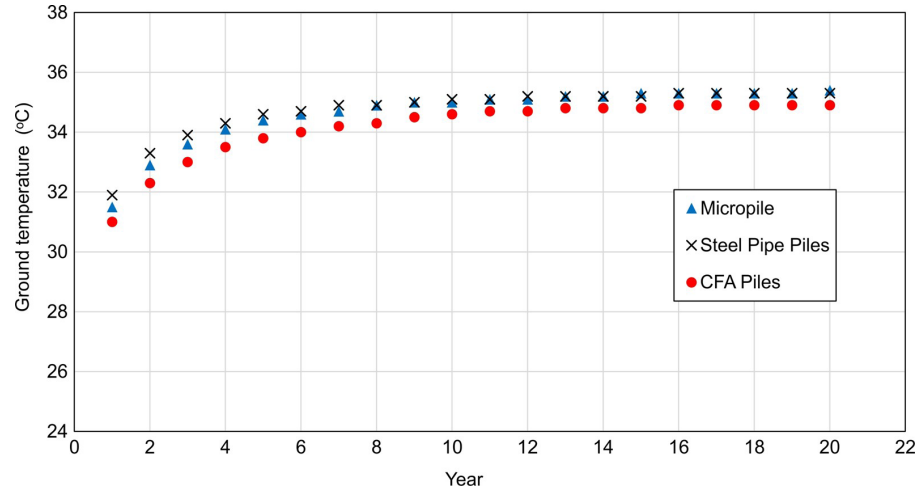


Figure 12. Variation of ground temperature during 20 years of the GSHP system operation.

Table 4. Results of simulations with PILESIM 2.1

	Micropiles	CFA piles	Steel pipe piles
Heat extraction rate per meter pile (W/m)	51	135	80
Heat injection rate per meter pile (W/m)	27	71	42

higher than those recommended by Brandl (2013) mentioned above. As shown in Table 4, only the values obtained for the micropiles case are within the recommended range (51 W/m). However, the main demand for the hotel building in São Paulo city is for space cooling, as the water heating demand can be complemented by other energy sources if the heat extraction using CFA and steel energy piles be not enough to the heating load requirement.

4. Comparison with analytical model

For comparison purposes, another estimation of the necessary length of energy piles for the GSHP system evaluated was done using an analytical model proposed by Ingersoll et al (1954 apud Kavanaugh & Rafferty, 2014). This model is based on the equation for the heat transfer from a cylinder buried in the ground, developed and evaluated in Carslaw & Jaeger (1947 apud Kavanaugh & Rafferty, 2014).

The first parameter that should be defined, besides the heating and cooling loads, is the coefficient of performance of the heat pump. This coefficient considers the efficiency of the heat pump and provides the actual amount of heat that should be rejected or extracted from the ground, as shown in Equations 2 and 3.

$$\frac{q_{cond}}{q_{lc}} = \frac{COP_c + 1.0}{COP_c} \quad (2)$$

where:

q_{cond} : heat pump condenser heat rate to ground [W];

q_{lc} : building cooling load [W];

COP_c : coefficient of performance (cooling mode).

$$\frac{q_{evap}}{q_{lh}} = \frac{COP_h - 1.0}{COP_h} \quad (3)$$

where:

q_{evap} : heat pump evaporator heat rate from ground [W];

q_{lh} : building heating load [W];

COP_h : coefficient of performance (heating mode).

The net annual heat transfer rate (q_a) is evaluated as the average between the q_{cond} and q_{evap} with the full-load hours in cooling ($EFLH_c$) and heating ($EFLH_h$), respectively, as shown in Equation 4.

$$q_a = \frac{q_{cond} \times EFLH_c + q_{evap} \times EFLH_h}{8760} \quad (4)$$

The equation for calculating the ground heat exchanger length for cooling is Equation 5:

$$L_c = \frac{q_a R_{ga} + q_{cond} (R_b + PLF_m R_{gm} + F_{sc} R_{gst})}{t_g - \frac{ELT + LLT}{2} + t_p} \quad (5)$$

The equation for calculating the ground heat exchanger bore length for heating is represented by Equation 6:

$$L_h = \frac{q_a R_{ga} + q_{evap} (R_b + PLF_m R_{gm} + F_{sc} R_{gst})}{t_g - \frac{ELT + LLT}{2} + t_p} \quad (6)$$

where:

F_{sc} : short-circuit heat loss factor between supply and return tubes in bore;

L_c : required bore length for cooling [m];

L_h : required bore length for heating [m];

PLF_m : part-load factor during design month;

q_a : net annual average heat transfer to the ground [W];

R_{ga} : effective thermal resistance to the ground – annual pulse [m.K/W];

R_{gst} : effective thermal resistance to the ground – short pulse [m.K/W];

R_{gm} : effective thermal resistance to the ground – monthly pulse [m.K/W];

R_b : thermal resistance of bore [m.K/W];

t_g : undisturbed ground temperature [°C];

t_p : long-term ground temperature penalty caused by ground heat transfer imbalances [°C];

ELT : heat pump entering liquid temperature [°C];

LLT : heat pump leaving liquid temperature [°C].

The analytical model allows the design of the GSHP system in a simplified way, providing the pile lengths necessary to meet the energy demands. Table 5 presents the outputs of the analytic calculations.

The total pile length and shaft area values provided by the analytical model are similar to those of the simulations using PILESIM 2.1 for the micropiles and CFA piles cases. As illustrated in Table 5 and Figure 13, these values estimated using the program PILESIM 2.1 were 10% higher for the micropiles case and 12% higher for the CFA piles case

compared to the analytical model results. However, for the steel pile case, the values obtained using PILESIM 2.1 are 37% higher compared to those found by the analytical model.

The difference in total shaft area necessary between CFA piles and micropiles shown in Figure 13b can be explained by the difference in relative area ratio between the heat exchanger pipes and the pile shaft area (A_{pipe}/A_{pile}), illustrated in Table 6. During the GSHP system operation, the heat can be extracted or rejected in the ground by circulating a fluid (normally water) through the heat exchanger pipes. As presented in Table 6, for the CFA pile case the pipe area is 27% of the pile shaft area (ground contact area), while for the micropile case is only 18%. Therefore, a higher ground contact area (shaft area) is necessary for the micropile evaluated in this paper.

On the other hand, for the steel pipe pile case the relative area ratio is 27%, equal to the CFA pile case, and the necessary shaft area is around 60% of the value obtained for the CFA pile (see Table 5). Therefore, these results indicate that the relative area ratio is not the only influential parameter on the energy pile performance, and that the thermal performance is not directly proportional to the pile shaft diameter (for piles with the same values of A_{pipe}/A_{pile}).

The estimation of the pile shaft area needed to meet the required design pile load capacity for the hotel building simulated is not considered in the current evaluation of energy pile systems. For a conventional foundation design, the shaft resistance capacity for piles is proportional to the shaft area for a particular pile type. However, the results of

Table 5. Analytical model vs. PILESIM results.

Results	Analytical model			PILESIM program		
	Micropiles	CFA piles	Steel pipe piles	Micropiles	CFA piles	Steel pipe piles
Total pile length (m)	3249.5	1209.4	1676.2	3600	1360	2300
Total pile shaft area (m ²)	3573.0	2659.6	1263.8	3958.4	2990.8	1734.2

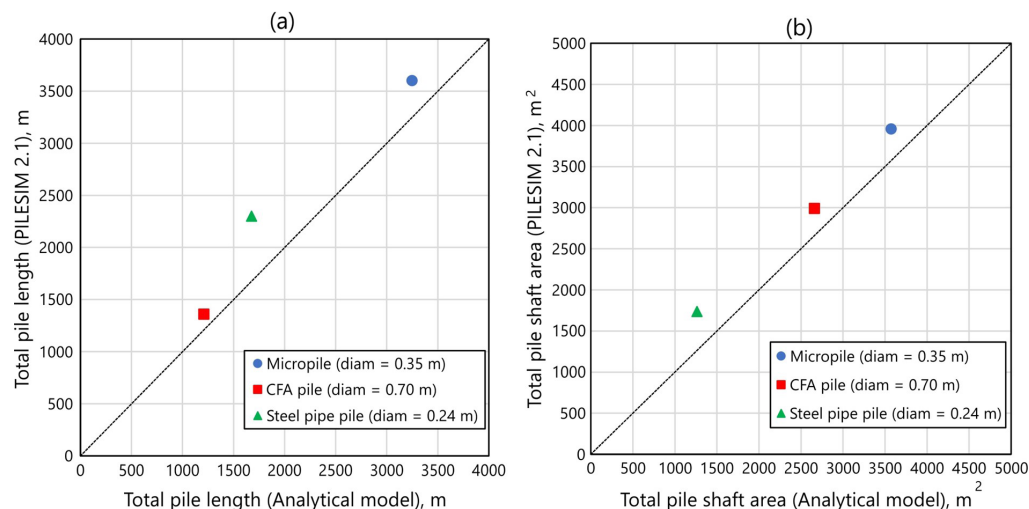


Figure 13. Results of (a) total needed pile length; (b) shaft area.

Table 6. Relative area ratio between the heat exchanger pipes and the pile shaft area (A_{pipe}/A_{pile}).

	Micropiles	CFA piles	Steel pipe piles
Pile shaft diameter (m)	0.35	0.70	0.24
Pipe external diameter (m)	0.032	0.032	0.032
Pipe number in a cross section of a pile	2	6	2
A_{pipe}/A_{pile}	0.18	0.27	0.27

needed shaft area to meet the thermal loads of a building shown in Figure 13 are independent of pile type (or installation procedure), while for the foundation design the values of unit skin friction (and needed shaft area) vary according to the pile type.

For a more economical application of energy pile systems, the total pile length (or shaft area) needed to meet the thermal loads should be lower than those needed to support the building mechanical loads. If the total pile length necessary for energy purposes is higher than the requirement for the foundation design, additional heat exchanger boreholes can be used to complement the building thermal demand.

5. Conclusions

The number and length of energy piles needed to meet the thermal loads demand of a hypothetical business hotel in São Paulo city were estimated using the program PILESIM 2.1 and by an analytical model. For the simulations, the ground and energy pile characteristics assumed were obtained from different studies carried out on the CICS site, located at the University of São Paulo campus. The simulations were carried out considering a continuous operation of the GSHP system; however, in the proposed case these systems operate in alternative operation mode, which increases the energy pile system performance as observed in previous studies.

The performance results obtained for the GSHP system using three different types of energy piles, considering the most unfavorable operation mode, show the feasibility of this technology in São Paulo city for a balanced demand of heating and cooling loads. However, further numerical and experimental studies are necessary to investigate the pile heat transfer in alternative operation modes for the climatic condition evaluated, to incentive the implementation of this renewable energy technology in regions of hot or warm climates.

Acknowledgements

The authors acknowledge the financial support given by TUPER S/A, the Center for Innovation in Sustainable Construction, CICS/USP, the National Council for Scientific and Technological Development - CNPQ for the financial support (Process 310881/2018-8), the State of São Paulo Research Foundation - FAPESP (Process 2014/14496-0),

and the Coordination of Improvement of Higher Education Personnel – CAPES (for granting the doctoral scholarship of the first author).

Declaration of interest

The authors declare that they have no financial interests or personal relationships that could have appeared to influence the study reported in this paper.

Authors' contributions

Leticia Menezes Santos Sá: conceptualization, Methodology, Formal analysis, Writing – original draft preparation. Alberto Hernandez Neto: formal analysis, Conceptualization, Writing - review & editing. Cristina de Hollanda Cavalcanti Tsuha: supervision, Funding acquisition, Writing - review & editing. Juliana Pessin: data curation, Writing - review & editing. Milena Cardoso de Freitas: data curation, Writing - review & editing. Thaise da Silva Oliveira Morais: Data curation, Writing - review & editing.

List of symbols

c	Specific heat capacity of the fluid
CFA	Continuous flight auger
$CICS$	Sustainable Construction Innovation Center
COP	Coefficient of Performance of the heat pump
COP_c	Coefficient of performance (cooling mode)
COP_h	Coefficient of performance (heating mode)
ELT	Heat pump entering liquid temperature
EPE	Energy Research Company
F_{sc}	Short-circuit heat loss factor between supply and return tubes in bore
$GSHP$	Ground source heat pump
$HDPE$	High density polyethylene
L	Pile depth
L_c	Required bore length for cooling
L_h	Required bore length for heating
LLT	Heat pump leaving liquid temperature
m	Flow rate of the fluid
PLF_m	Part-load factor during design month
q	Heat exchange rate per pile depth
q_a	Net annual average heat transfer to the ground
q_{cond}	Heat pump condenser heat rate to ground
q_{evap}	Heat pump evaporator heat rate from ground
q_{lc}	Building cooling load
q_{lh}	Building heating load
R_a	Internal thermal resistance of pile
R_b	Thermal resistance of the heat exchanger borehole/pile
R_{ga}	Effective thermal resistance to the ground – annual pulse
R_{gm}	Effective thermal resistance to the ground – monthly pulse

R_{gst}	Effective thermal resistance to the ground – short pulse
SPT	Standard Penetration Test
t	Time
t_g	Undisturbed ground temperature
T_{in}	Inlet temperature of the fluid
T_{out}	Outlet temperature of the fluid
t_p	Long-term ground temperature penalty caused by ground heat transfer imbalances
TPT	Thermal performance test
TRT	Thermal response test
TMY	Typical Meteorological Year
λ	Soil thermal conductivity
λ_{eff}	Subsoil effective thermal conductivity

References



- Akrouch, G.A., Sánchez, M., & Briaud, J.L. (2020). Thermal performance and economic study of an energy piles system under cooling dominated conditions. *Renewable Energy*, 147, 2736-2747. <http://dx.doi.org/10.1016/j.renene.2018.11.101>.
- Brandl, H. (2006). Energy foundations and other thermo-active ground structures. *Géotechnique*, 56(2), 81-122. <http://dx.doi.org/10.1680/geot.2006.56.2.81>.
- Brandl, H. (2013). Thermo-active ground-source structures for heating and cooling. *Procedia Engineering*, 57, 9-18. <http://dx.doi.org/10.1016/j.proeng.2013.04.005>.
- Crawley, D.B., Lawrie, L.K., Winkelmann, F.C., Buhl, W.F., Huang, Y.J., Pedersen, C.O., Strand, R.K., Liesen, R.J., Fisher, D.E., Witte, M.J., & Glazer, J. (2001). EnergyPlus: creating a new-generation building energy simulation program. *Energy and Building*, 33(4), 319-331. [http://dx.doi.org/10.1016/S0378-7788\(00\)00114-6](http://dx.doi.org/10.1016/S0378-7788(00)00114-6).
- Cui, P., Yang, H., & Fang, Z. (2008). Numerical analysis and experimental validation of heat transfer in ground heat exchangers in alternative operation modes. *Energy and Building*, 40(6), 1060-1066. <http://dx.doi.org/10.1016/j.enbuild.2007.10.005>.
- Diao, N., Cui, P., Liu, J., & Fang, Z. (2010). R&D of the ground-coupled heat pump technology in China. *Frontiers of Energy and Power Engineering in China*, 4(1), 47-54. <http://dx.doi.org/10.1007/s11708-009-0080-3>.
- Empresa de Pesquisa Energética – EPE (2018). *Uso de ar condicionado no setor residencial brasileiro: perspectivas e contribuições para o avanço em eficiência energética* (Nota Técnica EPE 030/2018). Retrieved in October 20, 2021, from https://www.epe.gov.br/sites-pt/publicacoes-dados-abertos/publicacoes/PublicacoesArquivos/publicacao-341/NT%20EPE%20030_2018_18Dez2018.pdf
- Fadejev, J., Simson, R., Kurnitski, J., & Haghighat, F. (2017). A review on energy piles design, sizing and modelling. *Energy*, 122, 390-407. <http://dx.doi.org/10.1016/j.energy.2017.01.097>.
- Hellström, G. (1991). *Ground heat storage: thermal analyses of duct storage systems*. Lund University. Retrieved in October 20, 2021, from <http://search.proquest.com/docview/303983441?accountid=14357>
- Jalaluddin, & Miyara, A. (2012). Thermal performance investigation of several types of vertical ground heat exchangers with different operation mode. *Applied Thermal Engineering*, 33-34(1), 167-174. <http://dx.doi.org/10.1016/j.applthermaleng.2011.09.030>.
- Kavanaugh, S., & Rafferty, K. (2014). *Geothermal heating and cooling: design of ground-source heat pump systems*. Atlanta: ASHRAE.
- Laloui, L., & Rotta Loria, A.F. (2020). *Analysis and design of energy geostructures: theoretical essentials and practical application*. London: Academic Press.
- Lim, H., Kim, C., Cho, Y., & Kim, M. (2017). Energy saving potentials from the application of heat pipes on geothermal heat pump system. *Applied Thermal Engineering*, 126, 1191-1198. <http://dx.doi.org/10.1016/j.applthermaleng.2017.04.086>.
- Loveridge, F. (2012). *The thermal performance of foundation piles used as heat exchangers in ground energy systems* [Doctoral thesis, University of Southampton], University of Southampton's repository. Retrieved in October 20, 2021, from [http://eprints.soton.ac.uk/348910/1.hasCoversheetVersion/F Loveridge eThesis FINAL.pdf](http://eprints.soton.ac.uk/348910/1.hasCoversheetVersion/F%20Loveridge%20eThesis%20FINAL.pdf)
- Martins, N.R., & Bourne-Webb, P.J. (2021). Hybridization of heat pump systems with natural ventilation to improve energy efficiency in cooling dominated buildings. *Renewable Energy and Environmental Sustainability*, 6, 33. <http://dx.doi.org/10.1051/rees/2021032>.
- Morais, T.S.O. (2019). *Comportamento térmico e termomecânico de fundações por estacas trocadoras de calor em solos não saturados em região de clima subtropical* [Doctoral thesis]. São Carlos School of Engineering, University of São Paulo (in Portuguese).
- Morais, T.S.O., & Tsuha, C.H.C. (2018). In-situ measurements of the soil thermal properties for energy foundation applications in São Paulo, Brazil. *Bulgarian Chemical Communications*, 50, 34-41.
- Murari, M.C.F. (2022). *Estudo do uso de fundações por estacas tubulares metálicas para energia geotérmica superficial em solo arenoso saturado* [Unpublished doctoral thesis]. São Carlos School of Engineering, University of São Paulo, Brazil (in Portuguese).
- Murphy, K.D., McCartney, J.S., & Henry, K.S. (2015). Evaluation of thermo-mechanical and thermal behavior of full-scale energy foundations. *Acta Geotechnica*, 10(2), 179-195. <http://dx.doi.org/10.1007/s11440-013-0298-4>.
- Pahud, D. (2007). *PILESIM2 user manual*. Switzerland: Istituto Sostenibilità Applicata Ambiente Costruttivo.
- Park, S., Lee, S., Lee, D., Ahn, D., & Choi, H. (2019). Effect of thermal interference on energy piles considering various configurations of heat exchangers. *Energy and*

- Building*, 199, 381-401. <http://dx.doi.org/10.1016/j.enbuild.2019.07.008>.
- Park, S., Lee, S., Lee, D., Lee, S.S., & Choi, H. (2016). Influence of coil pitch on thermal performance of coil-type cast-in-place energy piles. *Energy and Building*, 129, 344-356. <http://dx.doi.org/10.1016/j.enbuild.2016.08.005>.
- Pessin, J. (2021). *Estudo experimental do desempenho de fundações por estacas hélice contínua trocadoras de calor em solo arenoso saturado* [Doctoral thesis]. São Carlos School of Engineering, University of São Paulo (in Portuguese).
- Pessin, J., Tsuha, C. de H.C., Giacheti, H.L., & Riyis, M.T. (2022). Avaliação experimental do fluxo de água subterrânea para projetos de sistemas geotérmicos por estacas trocadoras de calor. In *Anais do 20º Congresso Brasileiro de Mecânica dos Solos e Engenharia Geotécnica*, Campinas (in Portuguese).
- Sutman, M., Speranza, G., Ferrari, A., Larrey-Lassalle, P., & Laloui, L. (2020). Long-term performance and life cycle assessment of energy piles in three different climatic conditions. *Renewable Energy*, 146, 1177-1191. <http://dx.doi.org/10.1016/j.renene.2019.07.035>.
- You, S., Cheng, X., Guo, H., & Yao, Z. (2014). In-situ experimental study of heat exchange capacity of CFG pile geothermal exchangers. *Energy and Building*, 79, 23-31. <http://dx.doi.org/10.1016/j.enbuild.2014.04.021>.
- Zhang, W.Y., & Wei, J. (2012). Analysis on the soil heat accumulation problem of ground source heat pump system in high temperature and high humidity areas. *Energy Procedia*, 14, 198-204. <http://dx.doi.org/10.1016/j.egypro.2011.12.917>.

REVIEW ARTICLES

Soils and Rocks
v. 45, n. 1

Thermo-hydro-mechanical behaviour of partially saturated fine-grained soils in the context of energy geostructures

Amirhossein Hashemi^{1#} , Melis Sutman¹ 

Article

Keywords

Thermo-hydro-mechanical behaviour
Partial saturation
Temperature variations
Matric suction
Energy geostructures

Abstract

The multi-physical phenomena, particularly water content and temperature variations, governing the behaviour of soils should be considered in the design and analysis of the energy geostructures. Soil temperature and water content variations impose a significant risk on the stability and serviceability of existing and future geostructures. Although potential failure modes, impacts at a system scale, and the response of saturated soils to thermal loads are previously discussed, interpretation of the thermo-hydro-mechanical behaviour of partially saturated soils in the context of energy geostructures is not thoroughly investigated. In this regard, this paper brings together the experimental data from several laboratory investigations to attain a comprehensive understanding of the partially saturated fine-grained soils response under thermo-hydro-mechanical loading, which plays a vital role in the analysis of the soil behaviour and energy geostructures in contact with them. In this paper, the effect of thermal loading in different matric suctions and hydraulic loading at different temperatures on soil preconsolidation stress, water content variation, thermal and hydraulic conductivities, and compression indexes are studied. Furthermore, soil thermal deformation is studied in detail for different overconsolidation ratios and matric suctions.

1. Introduction

Though the thermo-hydro-mechanical (THM) behaviour of fully saturated soils is studied to an adequate level, several emerging problems in geotechnical and geo-environmental engineering pose multi-physics problems involving non-isothermal processes in unsaturated soils. The massive challenge of climate change has been highlighted since the industrial era due to the huge rise in greenhouse gas emissions (IPCC, 2014). The emissions are known as the root cause of few significant issues such as global warming, fluctuations in the groundwater level, and variations in precipitation patterns (Karl et al., 2009). As part of the mitigation strategy to face the challenge of climate change, energy geostructures are known as an efficient approach towards developing sustainable and environmentally friendly technologies to meet space heating-cooling needs while serving as structural supports (Laloui & Sutman, 2020). The importance of studying the THM behaviour of partially saturated soil is further highlighted by the coupled variations in temperature and water content of the surrounding soil within the context of energy geostructures.

Fundamental knowledge achieved in the framework of seasonal air temperature variations affecting the top layer of soils, variations in temperatures of soil samples obtained from different depths of the ground and their transportation to the laboratories (Burghignoli et al., 2000), long-term laboratory tests related to buried cables (Abdel-Hadi & Mitchell, 1981), heat storage (Slegel & Davis, 1977) or nuclear waste storage (Houston et al., 1985; McGinley, 1983) in the past several decades has formed the bedrock of the progress in this field. However, most of the studies in the field of partially saturated soils have been conducted at ambient temperature. Therefore, the effect of temperature variations on their behaviour is yet to be fully understood.

To address issues arising due to the employment of energy geostructures, obtaining experimental data on the thermo-mechanical behaviour of partially saturated soils, developing and quantitatively validating constitutive models, and finally employing them to predict the soil response are of paramount importance. In this regard, the THM behaviour of soils is studied at an adequate level to assist engineers in using available constitutive models for fully saturated conditions. In this paper, one step forward, a review of the thermo-hydro-mechanical behaviour of partially saturated

[#]Corresponding author. E-mail address: amirhossein.hashemi@hw.ac.uk

¹Heriot-Watt University, School of Energy, Geoscience, Infrastructure and Society, Edinburgh, UK

Submitted on November 1, 2021; Final Acceptance on January 24, 2022; Discussion open until May 31, 2022.

<https://doi.org/10.28927/SR.2022.076821>



This is an Open Access article distributed under the terms of the Creative Commons Attribution License, which permits unrestricted use, distribution, and reproduction in any medium, provided the original work is properly cited.

soils is presented, which includes the synthesis of the latest experimental outcomes in this field. Nonetheless, in order to develop a general framework, extensive studies are still required to investigate the effect of further phenomena such as heating and cooling cycles, anisotropy, thermal fatigue, the time dependence of the impact of the thermal cycles, initial void ratio (Laloui et al., 2014; Vega & McCartney, 2014; Coccia & McCartney, 2016), and coupled transfer of water and heat via porous media.

Throughout this paper, the experimental data has been normalised by the ones obtained at room temperature and lowest matric suction (i.e., reference temperature and reference matric suction), water content or degree of saturation, or porosity, to emphasise the influence of temperature and suction variations. Furthermore, all the stress/suction units are presented in kPa, unit weights in kN/m^3 , and temperature units in $^{\circ}\text{C}$, unless otherwise stated.

2. Effects on soil characteristics

The thermal and mechanical history of the fine-grained soils plays a significant role in determining the temperature impact on shear strength and deformation. However, due to the influence of matric suction on soil behaviour, as well as the coupled nature of temperature and water content variations, this phenomenon becomes more complicated for unsaturated samples. In this regard, the impact of temperature and matric suction variations on preconsolidation stress and soil water content deserves a thorough evaluation through available experimental evidence.

2.1 Preconsolidation stress

There are only a few studies to examine the concurrent effects of matric suction and temperature variations on preconsolidation stress. Figure 1a shows the variation of effective preconsolidation stress by changes in matric suction. In this figure, the x-axis is normalised by matric suction equal to 50 kPa, which is selected to provide a reasonable range for the entire data set. The general trend shows that preconsolidation stress increases with increasing matric suction. This phenomenon is mainly associated with matric suctions above the air-entry value, as the degree of saturation does not change considerably until air-entry matric suction is exceeded (Salager et al., 2008; Uchaipichat & Khalili, 2009).

Salager et al. (2008) observed that for the lower values of matric suction, the rate of increase in preconsolidation stress with matric suction is higher, although the maximum imposed matric suction was limited to 300 kPa. On the other hand, the experimental data from the literature show continuous hardening with increasing matric suction (Lloret et al., 2003; Jotisankasa, 2005; Blatz et al., 2005; Tang et al., 2008; Mun & McCartney, 2014). Alsherif & McCartney (2016) proposed the power-law model to address this issue, by which the suction hardening effect on preconsolidation

stress is estimated for the entire suction range. The model was successfully validated against literature data sets.

Figure 1b shows changes in effective preconsolidation stress by temperature where effective preconsolidation stress is observed to decrease with temperature for a fixed matric suction, and the rate of decrease is higher for the lower temperature values (Abuel-Naga et al., 2007a; Salager et al., 2008). In this regard, Eriksson (1989) observed that, for the temperature range of 5°C to 55°C , effective preconsolidation stress asymptotically reached a fixed value with increasing temperature. Contrarily, an initial decrease of preconsolidation stress was followed by an eventual increase for the temperature range of 30°C to 70°C in the study of Saix et al. (2000). However, the data in their study was analysed employing the net stress framework for samples with a matric suction of 4.9 kPa. The leading cause of this trend is believed to be thermal softening due to the thermal loading of normally consolidated soils (Romero et al., 2003) counteracting hardening due to hydraulic loading (Khosravi et al., 2020). For instance, the sample with higher matric suction shows higher effective preconsolidation stress during thermal loading (i.e., the effect of thermal softening becomes less prominent with increasing matric suction). However, the rate of effective preconsolidation stress evolution with temperature is observed to be suction-independent (François et al., 2007). Conversely, the rate of effective preconsolidation stress evolution with matric suction is observed to be either thermally dependent (Laloui et al., 2014) after the reinterpretation of Uchaipichat & Khalili (2009) data sets or independent (François et al., 2007).

In this regard, Alsherif & McCartney (2016) argued that the effect of temperature and matric suction on effective preconsolidation stress is, in fact, path-dependent according to the two series of experiments carried out with the same matric suction and temperature which were applied in the opposite orders. In one of these experiments, matric suction was first increased to 291 MPa, followed by heating up to 64°C (ST path). The second one was first heated up to 64°C , and then the matric suction was increased up to 317 MPa (TS path). After mechanical loading, it was observed that the specimen exposed to high matric suction before temperature increase showed higher effective preconsolidation stress. Thus, it was concluded that thermal hardening might happen depending on the succession order of thermal and hydraulic loading. Another example of the stress path dependency is virtual preconsolidation due to cyclic temperature variations before mechanical loading, similar to creep-deformation (Burghignoli et al., 2000; Sultan et al., 2002; Abuel-Naga et al., 2007b).

Alongside matric suction and temperature, Tidfors & Sällfors (1989) introduced clay content and the depositional environment as determining factors affecting preconsolidation stress where soils with higher activity experience more reduction in preconsolidation stress due to temperature increase (Laloui et al., 2014).

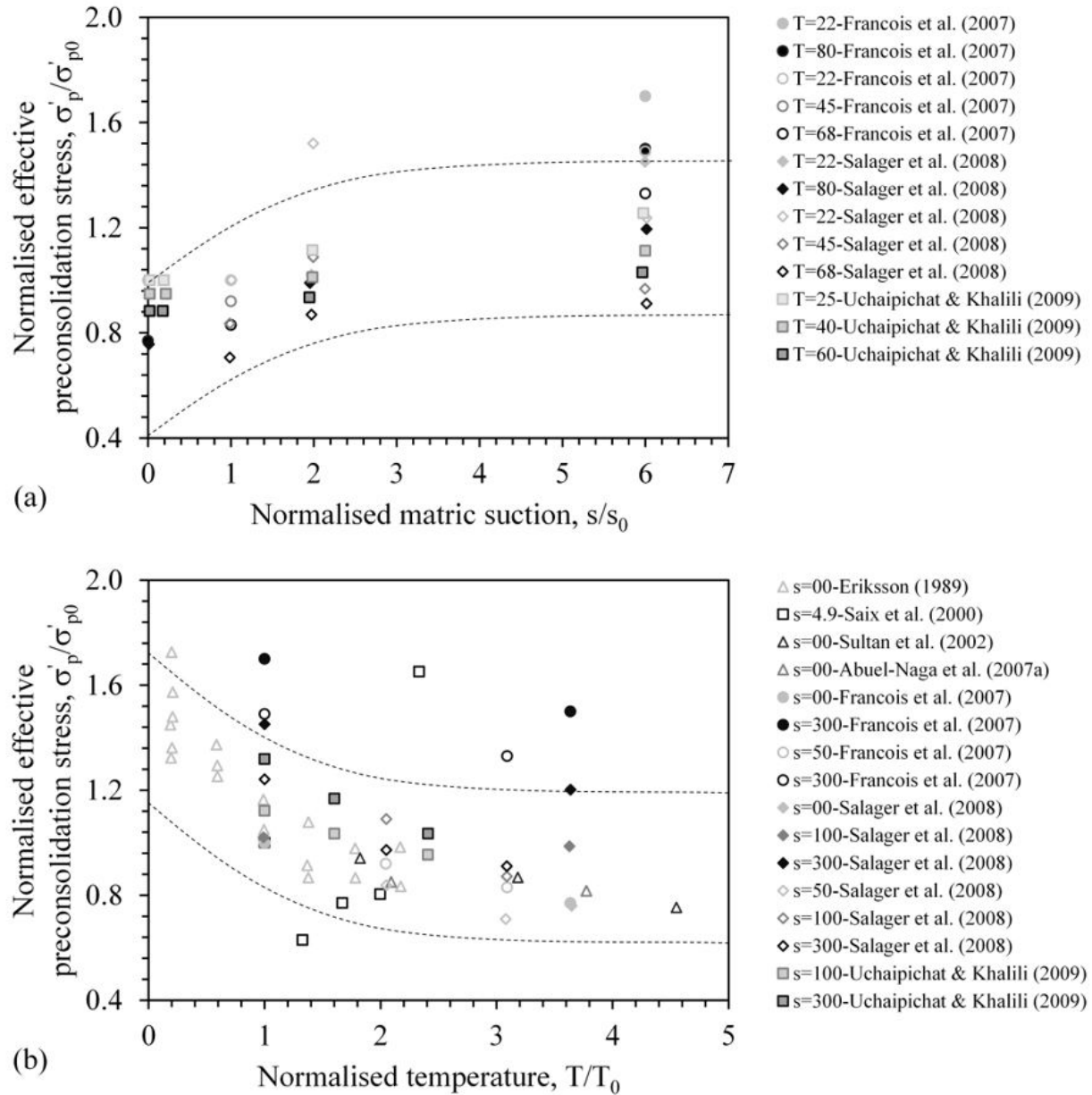


Figure 1. Evolution of preconsolidation stress with (a) matrix suction (b) temperature.

2.2 Water content

Hydraulic processes near and beneath the ground surface can cause unsaturated conditions around energy geostructures during construction or service life, affecting shear strength and volume change behaviour. As shown in Figure 2a, the soil water content decreases with increasing matrix suction (Olson & Langfelder, 1965; Krahn & Fredlund, 1972; Rao & Revanasiddappa, 2000). However, in low matrix suctions before the air-entry value, the rate of change in water content is low and becomes more pronounced with increasing matrix

suction, which continues until the residual water content is reached. Furthermore, considering the tests performed at two different temperatures (Romero et al., 2001), it can be observed that in the lower range of matrix suction and lower dry densities, the influence of elevated temperature on the water content evolution during hydraulic loading is more pronounced.

A comparison of samples with varying densities reveals a more evident change in water content due to increments in matrix suction for loose samples. The role of the water regimes in soil pores can be considered a fundamental mechanism

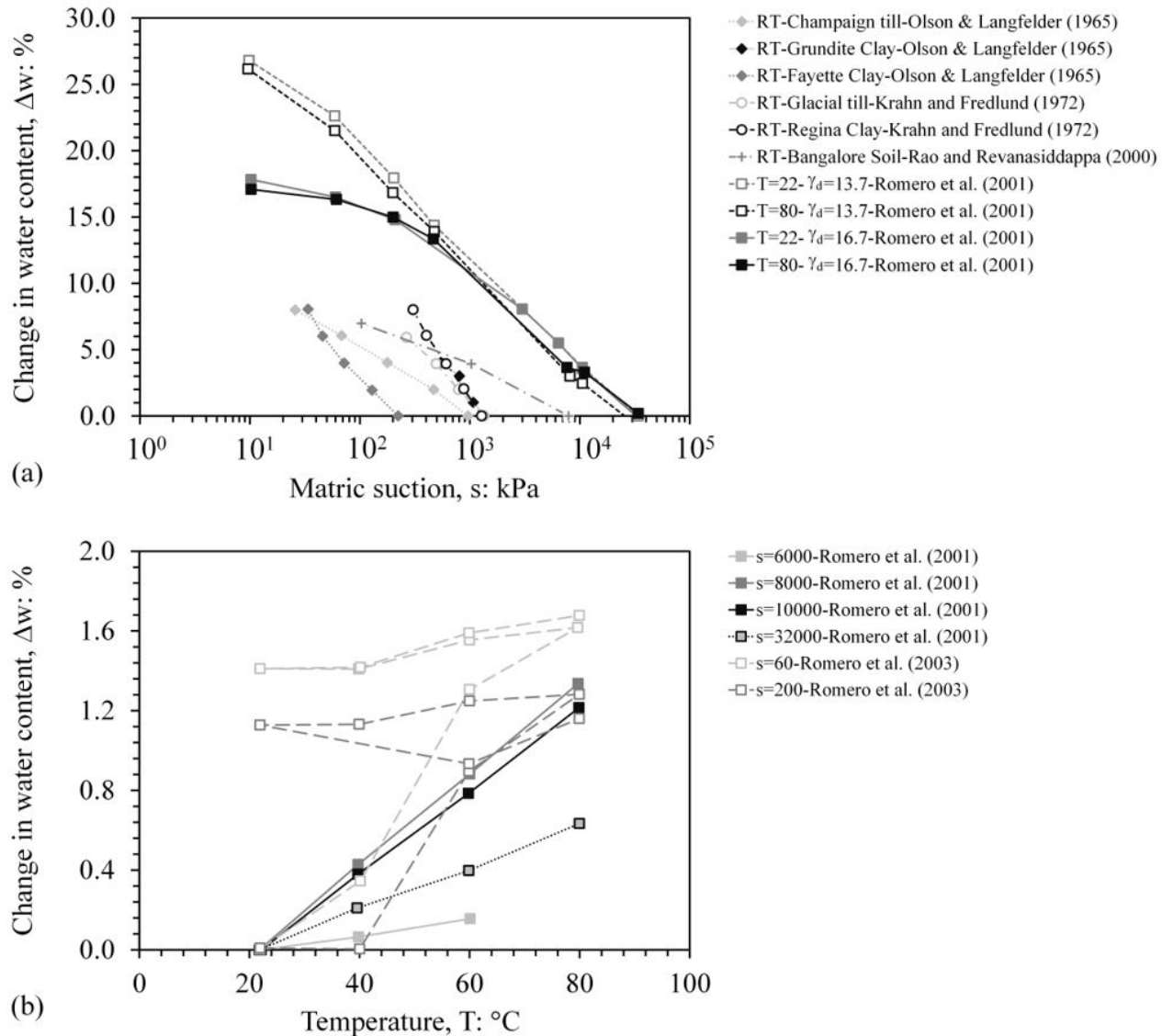


Figure 2. Changes in water content during (a) hydraulic loading (b) thermal loading.

to explain this phenomenon. In clayey soils, pores can be divided into two distinct classes: (i) an interlamellar space and an interparticle porosity between connected clay clusters (where absorbed water is located), and (ii) an interaggregate space between aggregates where free water exists (Laloui & Loria, 2019; Houhou et al., 2020). Soil pores become smaller by increasing soil dry density through compaction or by increasing the mechanical load. The water regime in the pores, thus, changes from free water to adsorbed water even at low suction values, reducing the amount of water drained from the sample due to hydraulic loading or elevated temperatures. However, adsorption is regulated at high matric suction, and the dry unit weight of the soil does not significantly affect the soil-water retention capacity (Romero et al., 2001; Garakani et al., 2018).

Figure 2b shows the amount of water drained due to thermal loading, which clearly increases with increasing temperature for relatively high suction values (i.e., 6000–32000 kPa). On the other hand, for suction values of 60 kPa and 200 kPa, no significant amount of water was drained out of the specimen when thermally loaded up to 40 $^{\circ}\text{C}$, after which a considerable increase in the drainage rate was observed (Romero et al., 2003). This phenomenon was associated with a lack of appreciable volumetric change until reaching 40 $^{\circ}\text{C}$ by pointing out an apparent overconsolidation effect, which disappeared during the tests performed at higher suctions.

The effect of thermal loading on soil water content can be explained considering two fundamental driving mechanisms. First, as the thermal expansion rate of pore water is around seven to ten times that of most soil particles, thermal loading

results in differential expansion of pore water and solids, urging excess water to drain out of the soil (Vega & McCartney, 2014). Furthermore, as the temperature rises, the viscosity of the pore fluid decreases, promoting the water drainage. Thus, lower water content is expected for a heated sample. However, heating appears to have a less pronounced effect on the degree of saturation, which can be attributed to the thermally-induced collapse of the soil skeleton, particularly in normally consolidated soils (Coccia & McCartney, 2016). Thus, the degree of saturation can be considered an essentially temperature-independent parameter, only slightly decreasing with increased temperature (Coccia & McCartney, 2016). The impact of thermal loading on the deformation behaviour of soils is further discussed later in Section 3.

3. Effects on volumetric behaviour

The serviceability of energy geostructures as structural support is governed by the thermal volume change behaviour of soils, which is a complex phenomenon due to an interplay between temperature, suction, and stress history. A review and synthesis of available experimental evidence on the thermal deformation of soils with different stress histories and matric suction, as well as temperature and matric suction impacts on compression indexes are presented in the following section.

3.1 Volumetric deformation

In the framework of the thermo-hydro-mechanical behaviour of soils, it is essential to predict soil deformation to mitigate displacement affecting serviceability during the

life of a structure or a natural deposit. Many experiments are conducted, and variables such as stress history (François et al., 2007), thermal history, recent stress history, heating period, and constant high-temperature phases (Burghignoli et al., 2000), the time elapsed between the end of primary consolidation of the last applied mechanical load and the start of the thermal load (Campanella & Mitchell, 1968), soil type (Coccia & McCartney, 2016), plasticity index (Sultan et al., 2002; Sutman, 2013), and anisotropy (Laloui et al., 2014) are introduced as determining parameters affecting soil volumetric behaviour.

In Figure 3, the thermal axial strain per 1 °C temperature increase is plotted against *OCR* for fine-grained soils in different matric suctions. Similar to the response of saturated soils to thermal loading (Baldi et al., 1988; Graham et al., 2001; Cekerevac & Laloui, 2004; Abuel-Naga et al., 2005; Vega & McCartney, 2014; Di Donna & Laloui, 2015), overconsolidated partially saturated soils undergo dilation, while normally consolidated specimens contract, which is further investigated in Figure 4 (Saix, 1991).

Three factors are considered as fundamental driving mechanisms behind the volumetric response of soils during thermal loading. (i) The rearrangement of particles explaining the irreversible component of contractive strain, which is associated with the reduction in the preconsolidation stress during heating, leaving the normally consolidated soils in an unstable state (Laloui et al., 2014). This effect mainly depends on the properties of the soil structure, and its rate is considered to be pore water pressure-independent (Campanella & Mitchell, 1968). Furthermore, it is observed by Burghignoli et al. (2000) that the volume reductions occur at a virtually constant porosity during cooling and

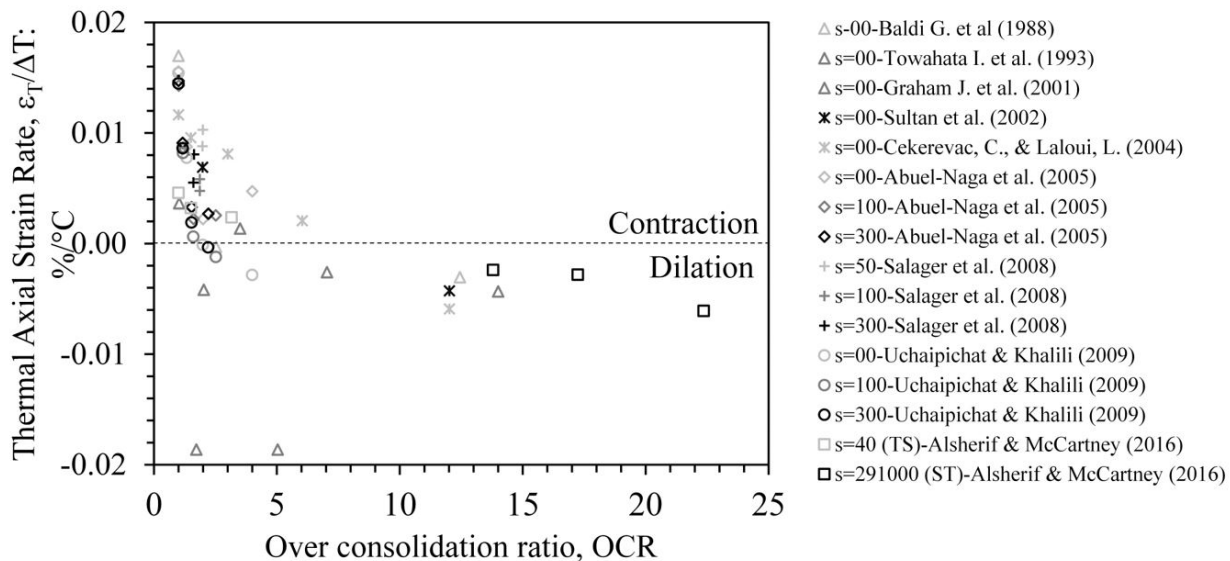


Figure 3. Effect of suction and overconsolidation ratio on thermal axial strain during thermal loading.

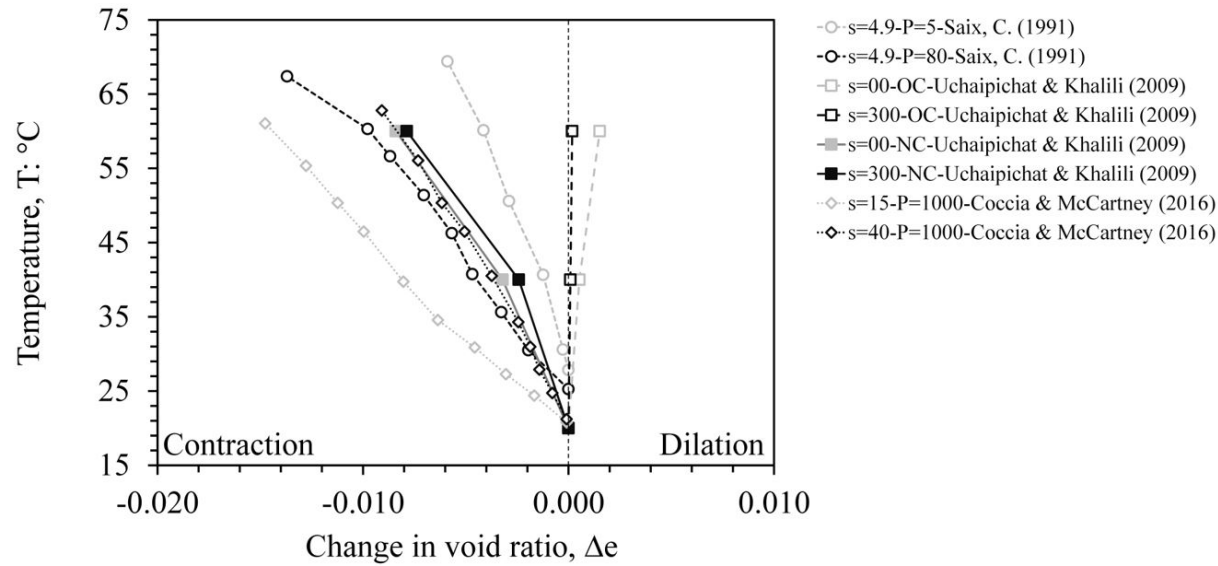


Figure 4. Changes in void ratio during thermal loading.

subsequent low-temperature state. Thus, there is no significant rearrangement of particles that may be an explanation for elastic contraction during cooling.

On the other hand, as an explanation for the reversible expansive strains, (ii) expansion of soil components, clay minerals, and pore water, and (iii) the increase in repulsive forces between clay particles undergoing thermal loading, which results in an increase in inter-particle spacing are proposed (Campanella & Mitchell, 1968; Laloui et al., 2014; Coccia & McCartney, 2016). The irreversible contraction component dominates for normally consolidated clays, while the reversible expansion component dominates for highly overconsolidated clays.

It is evident in Figures 3 and 4 that the tendency of highly overconsolidated soils to expand and normally consolidated to contract is common for both saturated and partially saturated soils. However, the associated volumetric strains are evidently smaller for partially saturated soils, compared to the saturated ones. This phenomenon can be attributed to the dependence of apparent preconsolidation stress on temperature and suction variations, where the yield surface tends to shrink with increasing temperature and expand with increasing suction, as previously presented in this paper. Thus, considering the soils initially on or close to the yield surface, the expansion of the yield surface with suction causes an increase in the thermo-elastic expansive portion of volumetric strains at the initiation of the heating phase, leading to an overall decrease in thermo-plastic contractive volumetric strains. On the other hand, a decrease in the thermo-elastic expansion of highly overconsolidated soils with increasing suction is also observed in Figure 4. This

behaviour can be associated with the increase in effective stress being greater than that of the apparent preconsolidation stress, which leads to a reduction in the overconsolidation ratio and, thus, to lower thermo-elastic volumetric strains (Uchaipichat & Khalili, 2009).

In between the previously presented conditions, there exists an intermediate one in which temperature increase of highly overconsolidated samples will exhibit an initial elastic expansion within the yield surface, which is followed by a plastic contraction once the yield surface is reached, as the temperature is increased further (Sultan et al., 2002). For instance, in experiments conducted by Cekerevac & Laloui (2004), overconsolidated kaolinite ($OCR = 12$), exhibits contraction after the temperature reaches 50 °C during thermal loading. The extent of the reversible expansion/irreversible contraction parts of deformation due to the thermal loads depends on soil type, plasticity, and OCR . The temperature at which the transition occurs between thermal expansion and contraction increases with OCR (Sultan et al., 2002). Thus, even heavily overconsolidated soils may contract at high temperatures if the yield surface is reached (François & Laloui, 2008).

Considering the response of soils to cyclic thermal loads, a comparatively limited amount of additional contraction is observed for saturated soils during successive cycles (Campanella & Mitchell, 1968; Sultan et al., 2002; Vega & McCartney, 2014). The effect of thermal creep and the subsequent strain hardening are introduced as the underlying mechanisms for this response (Campanella & Mitchell, 1968; Burghignoli et al., 2000). It can also be explained by the fact that the yield surface shrinks, and irreversible plastic strains

develop as temperature increases. The development of plastic strains leads to strain hardening and, thus, swelling of the yield surface (Sultan et al., 2002). As the yield surface expands in the subsequent thermal cycles, the soil remains within the yield loci and thus undergoes reversible strains (Hueckel & Baldi, 1990). However, cyclic stabilisation and the effects of thermal creep may still cause an additional minor amount of contraction (Campanella & Mitchell, 1968).

3.2 Deformation parameters

It is generally accepted that the compression index is independent of the stress ratio provided that the ratio between deviatoric stress and generalised mean effective stress is kept constant (Salager et al., 2008). To investigate this, the evolution of the compressibility index with matric suction and temperature are presented in this section. The data sets are categorised regarding the employed device, where “O”, “I”, and “TR” stand for Oedometer, Isotropic cell, and Triaxial cell, respectively.

Compressibility index variations with matric suction and temperature are shown in Figure 5 and 6, respectively. As observed in Figures 5a and 6a, swelling and compression indexes decrease as matric suction increases for data analysed in the framework of net stress (Romero et al., 2003; Tang et al., 2008; Salager et al., 2008; Uchaipichat & Khalili, 2009). This behaviour can be attributed to the lower thermo-elastic volumetric strain leading to lower values of compression indexes, as discussed in the previous section. However, the experimental data analysed in the context of effective stress shows a negligible matric suction effect on the evolution of the compressibility index (François et al., 2007; Salager et al., 2008).

Temperature effects on compressibility indexes are investigated in Figure 5b and 6b, where no specific trend is identified in saturated (Finn, 1952; Campanella & Mitchell, 1968; Di Donna & Laloui, 2015) and unsaturated conditions (Saix et al., 2000; Abuel-Naga et al., 2007c; Tang et al., 2008; Uchaipichat & Khalili, 2009; Coccia & McCartney, 2016). However, Romero et al. (2003) stated that in contrast with the swelling index, which is insensitive to temperature variations, the compression index increases slightly with increasing temperature for data analysed in the framework of net stress.

4. Effects on thermal and hydraulic conductivity

The extent to which the soil at the vicinity of energy geostructures is influenced by their operation highly depends on the thermal and hydraulic conductivities. Furthermore, the operation of energy geostructures is associated with a change in surrounding soil temperature and water content. Therefore, the evolution of thermal and hydraulic conductivities with

temperature and water content of the soil is investigated in the following section.

4.1 Thermal conductivity

An understanding of how heat is transferred through the porous soil media is of high importance in fields of studies such as geothermal energy resources (White, 1973), radioactive waste disposal (Li et al., 2013), energy geostructures (Laloui & Sutman, 2019), soil science, and agriculture meteorology (Lu et al., 2007; Nikolaev et al., 2013). The three practical heat transfer mechanisms in unsaturated soils are conduction through particle-to-particle contacts, convection via water-vapour flow, and phase changes or latent heat transfer (Lu & Dong, 2015). Factors such as soil mineralogy (Brigaud & Vasseur, 1989), grain size distribution (Chen, 2008; Yun & Santamarina, 2008), soil structure (Chen, 2008), porosity (Brigaud & Vasseur, 1989; Tarnawski et al., 2011), water content (Hiraiwa & Kasubuchi, 2000; Lu & Dong, 2015), particle shape, cementation (Dong et al., 2015), and temperature (Sakaguchi et al., 2007; Nikolaev et al., 2013) are introduced as determining parameters affecting thermal conductivity of soils. Both intrinsic physical properties of each phase of soils and the environmental variation of each phase determine the thermal properties of the soil (Dong et al., 2015). Hence, it is necessary to consider properties and the volumetric fraction of each phase, as well as the medium geometry, to predict the thermal conductivity of the overall medium (Yun & Santamarina, 2008).

Figure 7a shows that the thermal conductivity increases significantly by increasing the degree of saturation. Generally, the thermal conductivity evolution with degree of saturation can be divided into three stages: (i) a slight increase as the degree of saturation increases to the permanent wilting point, (ii) a significant increase as the degree of saturation increases further to the field capacity, and (iii) a slight increase or decrease near the saturation (Nikolaev et al., 2013; Lu & Dong, 2015). The thermal conductivity evolution with degree of saturation in silty and clayey soils is smoother than in sandy soils, without distinct inflection points (Dong et al., 2015).

At a low degree of saturation, the thermal conductivity of the soil increases gradually since the water only coats the soil particles, and the pores between the soil particles are filled with air. At the permanent wilting point, the water menisci are formed and become gradually interconnected. The water fills the gaps between the soil particles resulting in a significant expansion of the heat transfer paths through the water film connecting the particles where conductive heat transfer occurs (solid-water-solid conduction) (Nikolaev et al., 2013; Lu & Dong, 2015). Variations in thermal conductivity at high degrees of saturation are small, as further changes in the size of occluded air bubbles do not effectively change the paths of conductive heat transfer (Nikolaev et al., 2013; Lu & Dong, 2015).

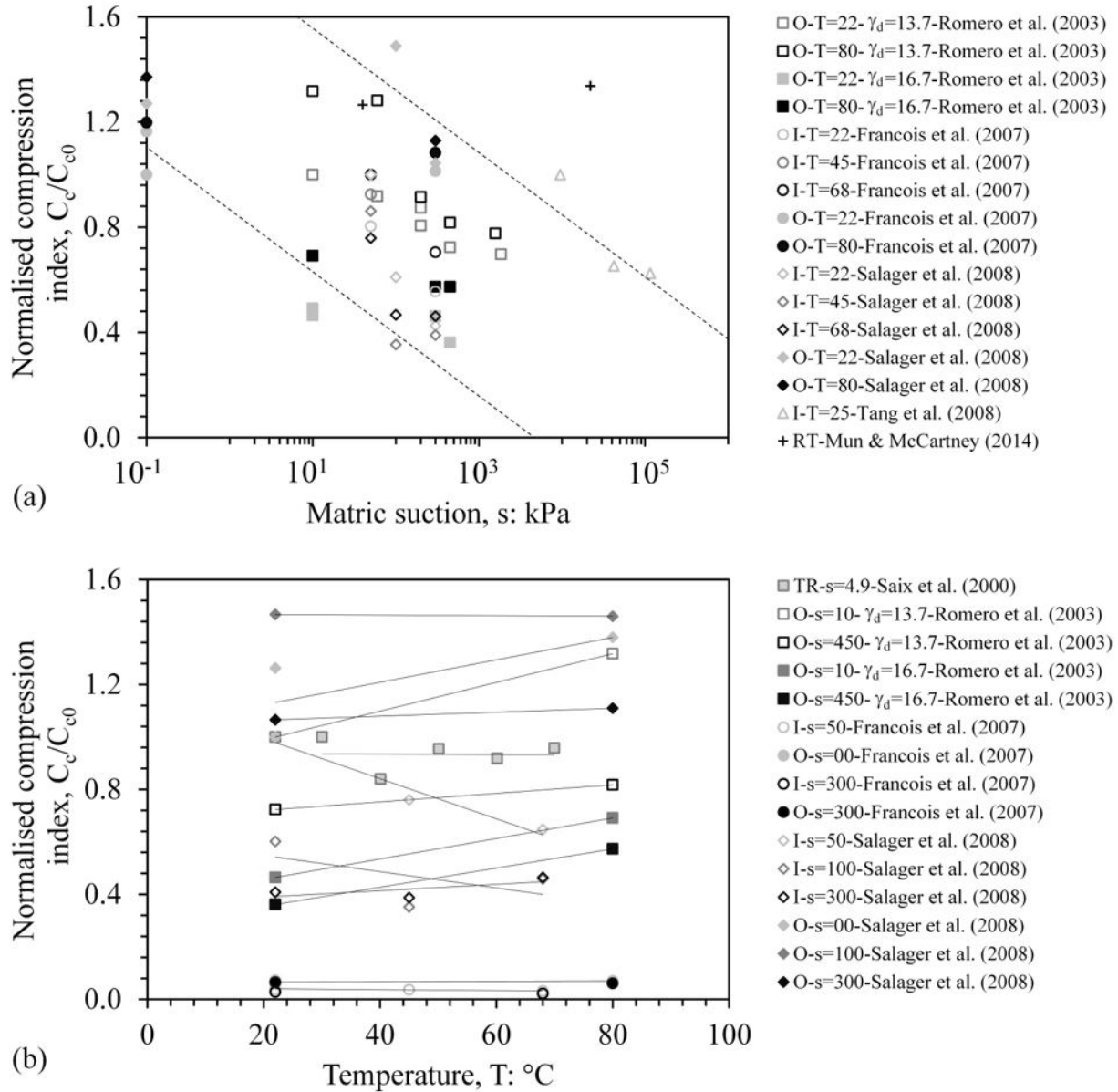


Figure 5. Changes in swelling index with (a) matric suction (b) temperature.

Latent heat transfer due to vapor migration is more pronounced in higher temperatures, which leads to an apparent thermal conductivity higher than the one through pure heat conduction. Therefore, it can be observed that the evolution of thermal conductivity with degree of saturation is not affected by temperature change when the soil temperature is increased up to the room temperature (RT). Nevertheless, when the temperature is increased further, thermal conductivity varies sharply with degree of saturation. Moreover, it can be observed from Figure 7a that for tests carried out at high temperatures (e.g., 72–75 °C), there exists a degree of saturation above which the thermal conductivity ceases to increase further.

In fact, it can be observed from the tests on Ottawa sand by Nikolaev et al. (2013) that when the specimens were heated to 72 °C, even a slight decrease in thermal conductivity occurred after a certain degree of saturation. This phenomenon was reported to be caused by the formation of small air pockets surrounded by soil particles and water, which hinder the water vapour movement and thus result in a decrease in heat transfer due to minimal mass transfer (Nikolaev et al., 2013; Lu & Dong, 2015).

The evolution of thermal conductivity with porosity is presented in Figure 7b. Although a distinct decrease of thermal conductivity with porosity is observed for all

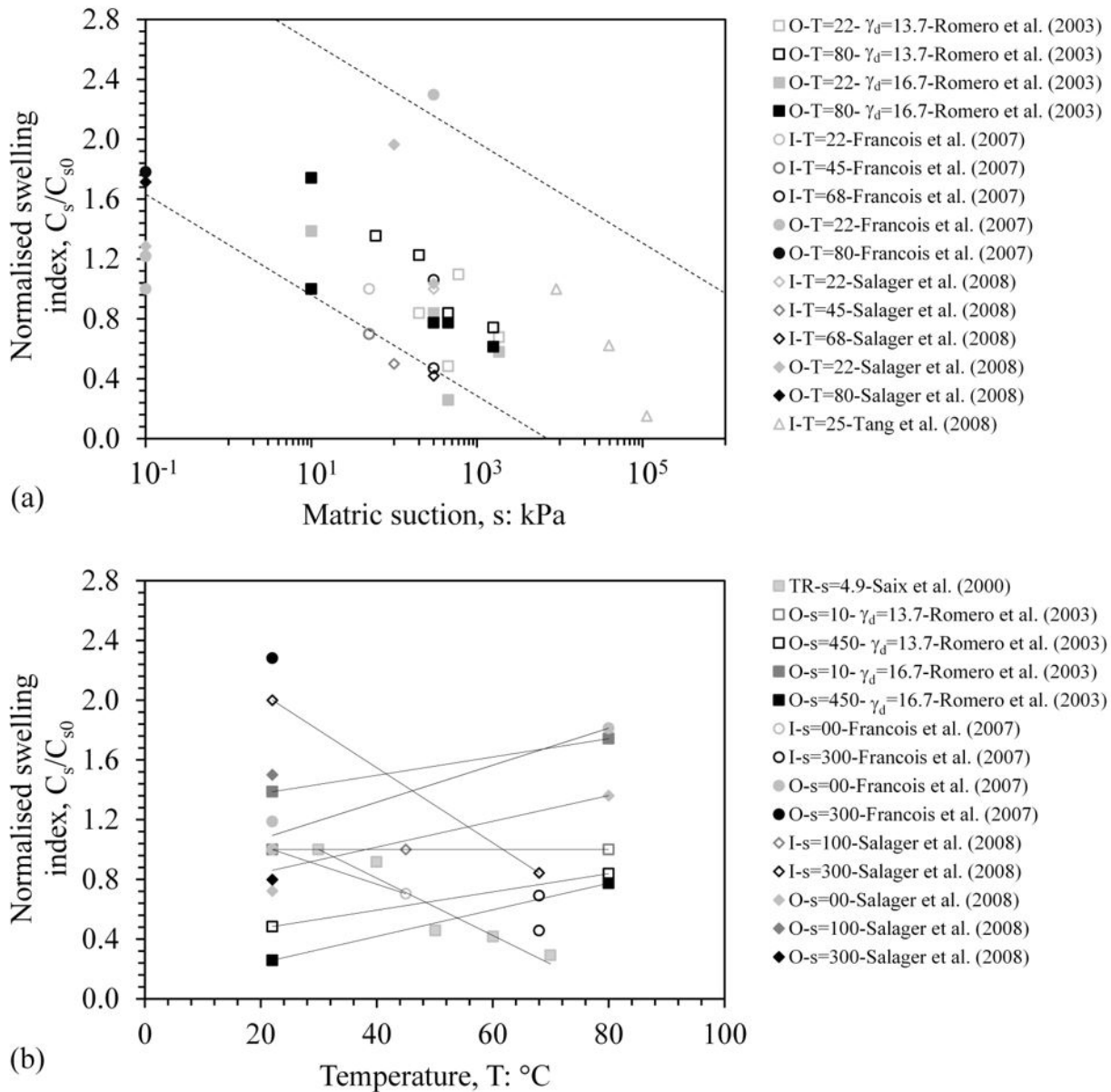


Figure 6. Changes in compression index with (a) matric suction (b) temperature.

specimens, the trend becomes more evident in dry specimens compared to the saturated ones (Johansen, 1977). This is due to the fact that the main pathways for thermal conduction between dry soil grains are limited to grain contact points, which are restricted as the porosity increases (Chen, 2008). Nevertheless, for saturated soils, a higher porosity implies more water available in soil pores, facilitating solid-water-solid heat conduction and thus resulting in a less severe reduction in thermal conductivity due to porosity increments (Tarnawski et al., 2011).

The effect of temperature variations on thermal conductivity is shown in Figure 8. In the dry condition,

as shown in Figure 8a, the thermal conductivity generally increases when the temperature increases. On the other hand, Figure 8b indicates contradictory trends for the thermal conductivity variation with temperature, considering saturated soils. For instance, both increasing and decreasing trends can be observed comparing two distinct thermally loaded saturated Ottawa sand specimens (Tarnawski et al., 2009; Nikolaev et al., 2013).

As previously mentioned, the thermal conductivity of any mixture is related to the thermal properties of each phase; thus, the temperature impact on each soil component should be considered to explain the overall thermal conductivity

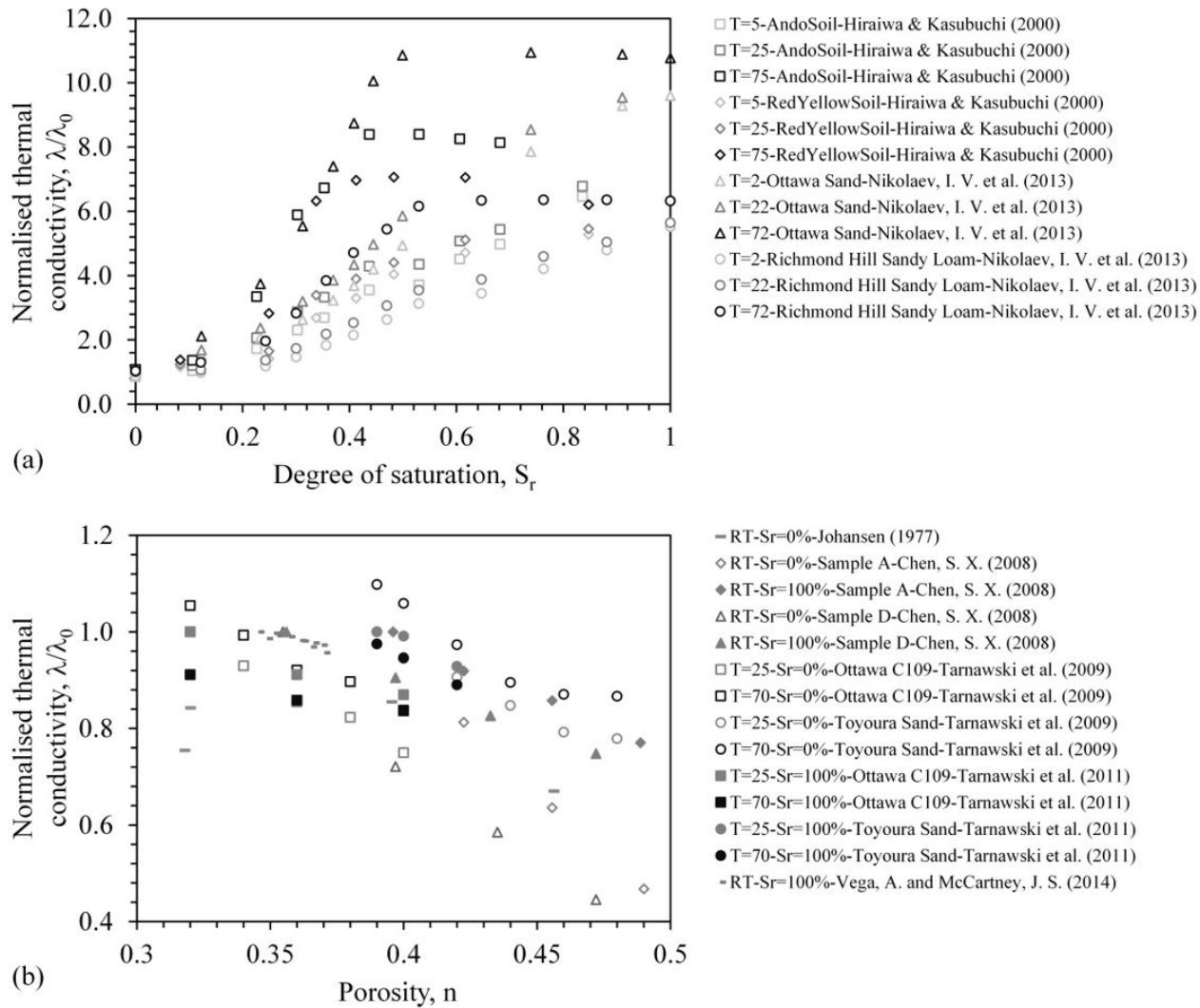


Figure 7. Evolution of thermal conductivity with (a) degree of saturation (b) porosity.

evolution with temperature (Sakaguchi et al., 2007; Gens, 2010). The thermal conductivity of soil minerals, except feldspar, decreases with increasing temperature, while water and air thermal conductivities are inversely temperature-dependent parameters at least for the temperature range of 0-100 °C (Farouki, 1981). The soil porosity intrinsically controls the function of each thermally impacted soil component in the thermal conductivity determination. The presence of water and air in the pore space not only affects the overall thermal conductivity due to their individually temperature-dependent nature but also due to the water and air acting as insulators for soil grains. Therefore, the higher the porosity, the less pronounced is the effect of temperature increase on soil grains in terms of thermal conductivity reduction. Furthermore, the heat conduction through the water and air between solid particles decreases (reduction of thermal bridges), while the transfer of latent heat increases (liquid-

island theory) as temperature increases (Sakaguchi et al., 2007). However, the soil skeleton collapse due to thermal loading, particularly considering normally consolidated soils, enhances heat conduction.

In the dry state, the factors enhancing thermal conductivity surpass the decreasing ones and lead to an increase in thermal conductivity with temperature, as shown in Figure 8a. Nonetheless, a reduction in thermal conductivity with increasing temperature is reported for low volumetric water content (θ) Toyoura sands, i.e., $\theta \leq 0.07$ (Sakaguchi et al., 2007). The decrease in conduction with increasing temperature, which overcomes the increase in the transfer of latent heat, was considered a potential reason behind this phenomenon by the authors. However, experiments performed on the mixture of Toyoura sand and kaolinite show an increasing trend of thermal conductivity during thermal loading (Sakaguchi et al., 2007). The reason

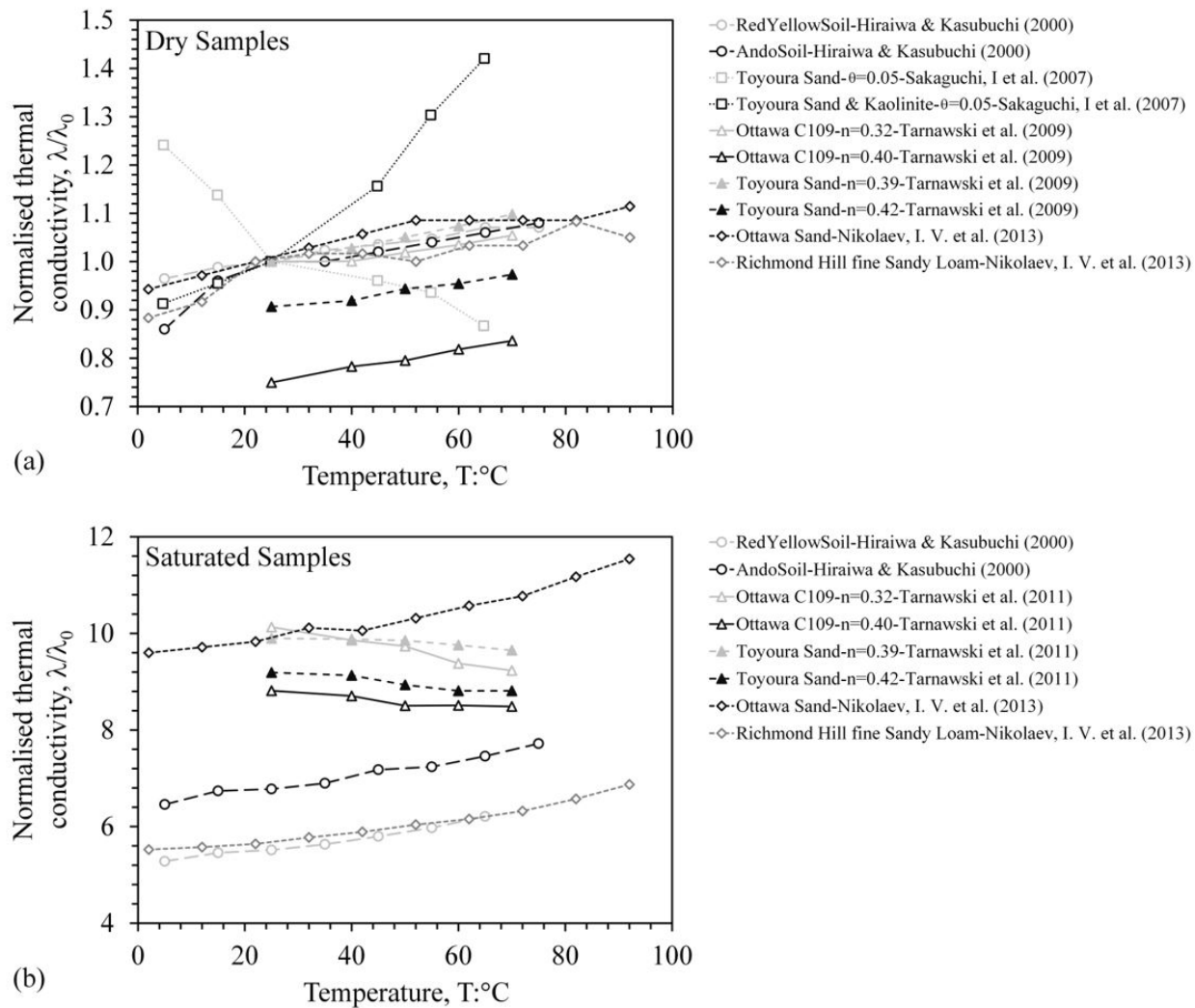


Figure 8. Evolution of thermal conductivity with temperature for (a) dry samples (b) saturated samples.

is associated with the added kaolinite, which not only has higher thermal conductivity than air and water but also enhances the thermal bridges, especially in the nearly dry state (Farouki, 1981; Sakaguchi et al., 2007).

In the saturated state, regarding the lower insulating capability of water compared to air, Tarnawski et al. (2011) found a decreasing trend in thermal conductivity variation with temperature for saturated Ottawa and Toyoura sand. For the higher porosity specimen, there was more water and less temperature impact on the thermal conductivity of the quartz and thus less reduction in soil thermal conductivity for the Ottawa sand. However, other studies performed on Ottawa sand, or the other soils, suggest that increasing thermal conductivity components dominate over the decreasing ones when loaded thermally (Hiraiwa & Kasubuchi, 2000; Nikolaev et al., 2013).

4.2 Hydraulic conductivity

Hydraulic conductivity of soils depends on the number of parameters such as mineral composition, soil density, fluid properties (e.g., viscosity and chemistry), and temperature (Ye et al., 2013). Water presence in soil pores facilitates water movement leading to higher hydraulic conductivity, as shown in Figure 9a. It is also evident that temperature increments result in higher hydraulic conductivity (Constantz, 1982). However, this trend is not observed for Norfolk sandy loam soil, where hydraulic conductivity was measured at different points in a Lucite flow cell (Hopmans & Dane, 1986).

In this regard, Figure 9b shows a clear trend of increase in hydraulic conductivity with temperature for fully saturated specimens (Towhata et al., 1993; Cho et al., 1999). The temperature impact on the matric potential, the

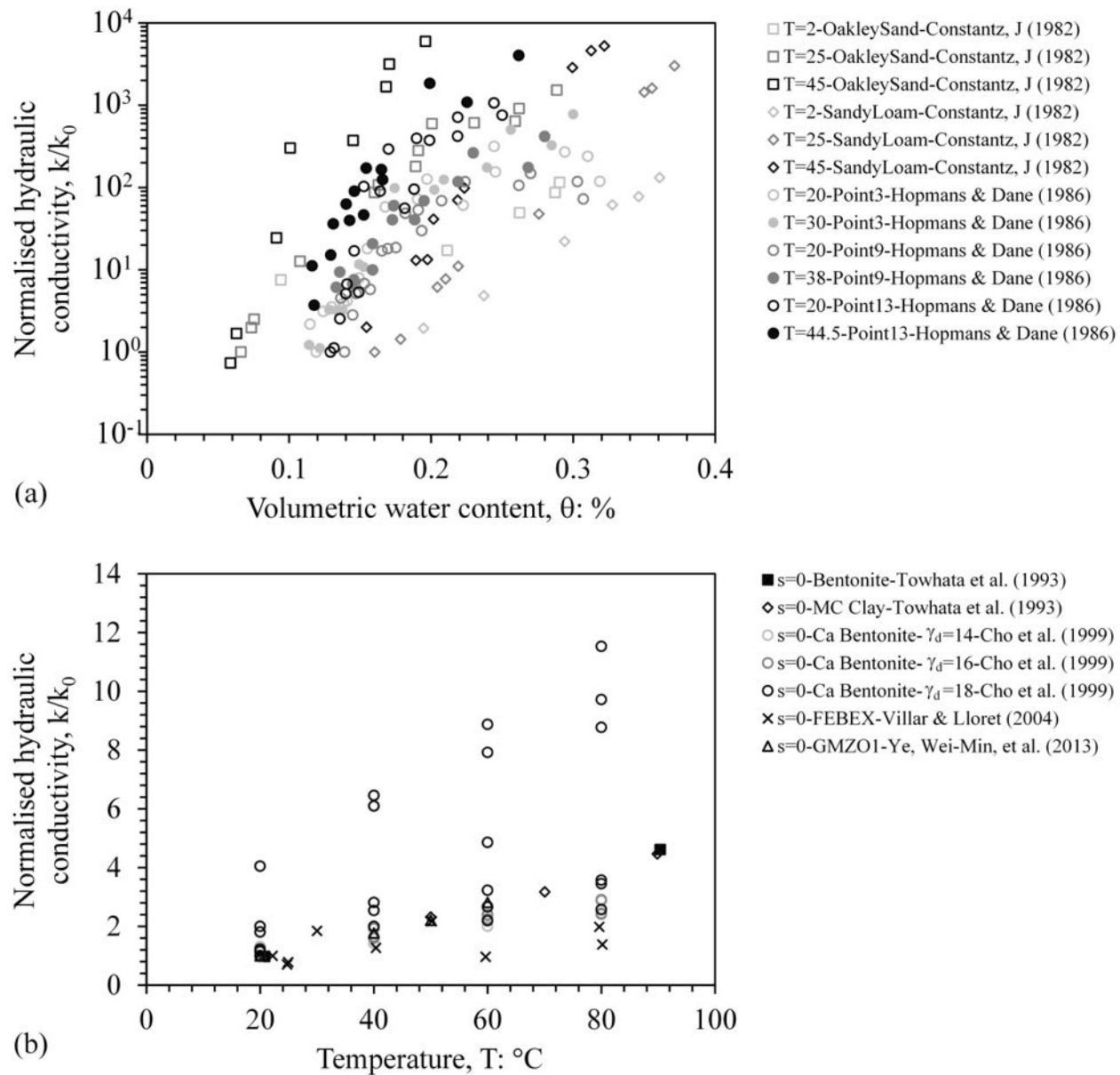


Figure 9. Evolution of hydraulic conductivity with (a) temperature (b) volumetric water content.

surface tension of the soil water, and the diffuse double-layer thickness are all considered fundamental driving mechanisms behind the temperature-sensitivity of hydraulic conductivity (Constantz & Murphy, 1991). Moreover, a decrease in water viscosity with increasing temperature leads to higher hydraulic conductivity (Hopmans & Dane, 1986; Constantz & Murphy, 1991; Delage et al., 2000). Although the temperature dependence of the viscosity of soil water may vary from that of free water (Constantz & Murphy, 1991; Romero et al., 2001), heating is also associated with the movement of high-density adsorbed water to large pores, increasing the proportion of free water in the porous (inter-aggregate) channels (Villar & Lloret, 2004). This phenomenon can be considered as

an increase in temperature enlarging the effective water flow crossing area (Ye et al., 2013). Finally, fabric changes and redistribution of pores due to thermal loading are also inherently considered as responsible for changes in hydraulic conductivity (Romero et al., 2001).

5. Conclusions

It is of paramount importance to investigate the THM behaviour of soils to gain insight into the multi-physical phenomena that govern the behaviour of energy geostructures such as energy piles. Thermal and hydraulic variations can be considered among the most notable phenomena affecting

the surrounding soils. Although temperature variations do not directly lead to adverse effects compared to hydraulic loading, they still govern or modify coupled processes, such as soil shrinkage. Therefore, the thermal behaviour is primarily studied to reveal the response of fine-grained soils to temperature variations, as granular soils are known to have an elastic response to thermal loads. In this regard, the results of the laboratory investigations carried out in the context of unsaturated soils are gathered to obtain comprehensive knowledge of soil response to THM loading within the framework of energy geostructures. Some of the conclusions drawn from the laboratory testing campaigns are as follows:

- The history of soils is preserved in their structure, considering the stress and other environmental changes that have occurred since their deposition, and has a significant impact on the strength and deformation characteristics. The preconsolidation stress is a critical factor in predicting the consolidation settlement of existing and future structures. Although preconsolidation stress is a stress path dependent parameter under THM loading, clear trends in its response to temperature and matric suction variations can be deduced for results analysed in the framework of effective stress. As evidenced by existing experimental studies, an increase in temperature tends to reduce the effective preconsolidation stress due to thermal softening. On the other hand, a rise in matric suction increases effective preconsolidation stress, at least for matric suctions higher than the air-entry value;
- Water content affects the volumetric behaviour of soils to a great extent. The water content of soils surrounding energy geostructures is susceptible to change due to their thermal functioning or a change in groundwater level. As water content decreases, desiccation cracks and shrinkage become more probable. On the other hand, excess pore water pressure is generated with a higher groundwater level, leading to lower effective stress and thus lower shear strength. In this regard, water content variation with temperature and matric suction is studied, and a much higher drainage rate is noticed during hydraulic loading compared to temperature increase. Nonetheless, the amount of water drained under hydraulic loading for fine-grained soils is determined by the dry density and temperature of the soils. For matric suctions less than the residual value, as the adsorbed water portion of the dense specimens is higher than the one of loose samples, more water will be retained in a sample with higher density. However, adsorption governs the retention mechanism in higher suctions, and thus the density effect disappears afterwards. Furthermore, as temperature increases, the viscosity of free water decreases, and the water content decreases even before the hydraulic loading begins. Thus, tests conducted at higher temperatures show less water content variation during hydraulic loading;
- Soil deformation is one of the most critical issues threatening the serviceability of infrastructures. Land subsidence and soil shrinkage due to temperature increase on the one hand and swell or collapse behaviour due to change in the degree of saturation on the other, are common failure modes that could affect the surrounding soil of the energy geostructures. In fact, the function of energy geostructures can exacerbate those failure modes. For instance, water drains out of the soil as heat is transferred to the surrounding soil via the energy geostructures, increasing the suction stress and thus the effective stress. As a result, the overburden pressure exceeds the bearing capacity of the soil, resulting in land subsidence. For fine-grained soils, normally consolidated ones undergo contraction while highly overconsolidated soils dilate when loaded thermally. Factors such as stress path may, however, change the dilative behaviour in overconsolidated soils. (i) Particle rearrangement, (ii) expansion of soil components, and (iii) repulsive forces between clay particles are factors that contribute to the volumetric response of soils. The results also show that compressibility indexes are somehow temperature independent, though they decrease with increasing matric suction;
- As thermal conductivity increases, fluctuations in temperature due to operation of energy geostructures occur in greater extent, and hence thermal loads have a more significant impact on the soil media. Both water content and temperature variation control the thermal conductivity of soils. The thermal conductivity generally increases with the degree of saturation. For tests conducted at temperatures above 70 °C, an initial increase is followed by an eventual decrease, although the extent of temperature increase is well above the expected variations within the framework of energy geostructures. Enhanced solid-water-solid thermal conduction is introduced as the primary cause of thermal conductivity variation with increasing degree of saturation. However, in the case of thermal conductivity evolution with temperature, contradictory trends are observed. The measured data indicates that thermal conductivity may increase with temperature while decreasing trends are also observed in near dry state and saturated conditions. Thus, associating a single mechanism is not sufficient to fully describe this phenomenon,

which requires considering each phase property and the medium geometry variation with temperature;

- The experimental evidence on hydraulic conductivity shows that it increases with a rise in temperature or water content. The matric potential, the surface tension of the soil water, the diffuse double-layer thickness, and pore redistribution plays a paramount role in hydraulic conductivity variation with temperature.

In summary, projected changes in the temperature and water content of the soils surrounding energy geostructures may lead to significant changes in soil behaviour. Although individual changes in soil properties can pose their own challenges assuming a single driver, the compounding effect of multiple drivers and the influence of variation of soil properties on each other can be more significant and escalate the failure possibility. The extent of soils impacted by THM loading will increase as thermal and hydraulic conductivity increases. The water content and soil temperature will change to a greater extent, leading to a more significant change in the preconsolidation stress, affecting deformation characteristics and soil strength to a greater extent.

Declaration of interest

The authors have no conflicts of interest to declare that are relevant to the content of the paper.

Authors' contributions

Amirhossein Hashemi: conceptualization, data curation, writing – original draft. Melis Sutman: supervision, writing – review & editing.

List of symbols

C_c	compression index
C_{co}	reference compression index
C_s	swelling index
C_{so}	reference swelling index
e	void ratio
k	hydraulic conductivity
k_0	reference hydraulic conductivity
n	porosity
OCR	overconsolidation ratio
p	net confining stress
s	matric suction
s_0	reference matric suction
S_r	degree of saturation
T	absolute temperature
T_0	absolute temperature
w	gravimetric water content
γ_d	soil dry density
ε_T	thermal axial strain

ε_v	volumetric strain
θ	volumetric water content
λ	thermal conductivity
λ_0	reference thermal conductivity
p	preconsolidation stress
p_0	reference preconsolidation stress
σ_v	vertical stress

References











- Abdel-Hadi, O.N., & Mitchell, J.K. (1981). Coupled heat and water flows around buried cables. *Journal of Geotechnical and Geoenvironmental Engineering*, 107(11), 1461-1487. <http://dx.doi.org/10.1061/AJGEB6.0001203>.
- Abuel-Naga, H.M., Bergado, D.T., & Bouazza, A. (2007a). Thermally induced volume change and excess pore water pressure of soft Bangkok clay. *Engineering Geology*, 89(1-2), 144-154. <http://dx.doi.org/10.1016/j.enggeo.2006.10.002>.
- Abuel-Naga, H.M., Bergado, D.T., & Lim, B.F. (2007b). Effect of temperature on shear strength and yielding behavior of soft Bangkok clay. *Soil and Foundation*, 47(3), 423-436. <http://dx.doi.org/10.3208/sandf.47.423>.
- Abuel-Naga, H.M., Bergado, D.T., Bouazza, A., & Ramana, G. (2007c). Volume change behaviour of saturated clays under drained heating conditions: experimental results and constitutive modeling. *Canadian Geotechnical Journal*, 44(8), 942-956. <http://dx.doi.org/10.1139/t07-031>.
- Abuel-Naga, H., Bergado, D., Soralump, S., & Rujivipat, P. (2005). Thermal consolidation of soft Bangkok clay. *Lowland Technology International Journal*, 7(1), 13-22.
- Alsherif, N.A., & McCartney, J.S. (2016). Yielding of silt at high temperature and suction magnitudes. *Geotechnical and Geological Engineering*, 34(2), 501-514. <http://dx.doi.org/10.1007/s10706-015-9961-x>.
- Baldi, G., Hueckel, T., & Pellegrini, R. (1988). Thermal volume changes of the mineral-water system in low-porosity clay soils. *Canadian Geotechnical Journal*, 25(4), 807-825. <http://dx.doi.org/10.1139/t88-089>.
- Blatz, J., Anderson, D., Graham, J., & Siemens, G. (2005). Evaluation of yielding in unsaturated clays using an automated triaxial apparatus with controlled suction. In T. Schanz (Ed.), *Unsaturated soils: experimental studies*. Berlin: Springer. http://dx.doi.org/10.1007/3-540-26736-0_22.
- Brigaud, F., & Vasseur, G. (1989). Mineralogy, porosity and fluid control on thermal conductivity of sedimentary rocks. *Geophysical Journal International*, 98(3), 525-542. <http://dx.doi.org/10.1111/j.1365-246X.1989.tb02287.x>.
- Burghignoli, A., Desideri, A., & Miliziano, S. (2000). A laboratory study on the thermomechanical behaviour of clayey soils. *Canadian Geotechnical Journal*, 37(4), 764-780. <http://dx.doi.org/10.1139/t00-010>.

- Campanella, R.G., & Mitchell, J.K. (1968). Influence of temperature variations on soil behavior. *Journal of the Soil Mechanics and Foundations Division*, 94(3), 709-734. <http://dx.doi.org/10.1061/JSFEAQ.0001136>.
- Cekerevac, C., & Laloui, L. (2004). Experimental study of thermal effects on the mechanical behaviour of a clay. *International Journal for Numerical and Analytical Methods in Geomechanics*, 28(3), 209-228. <http://dx.doi.org/10.1002/nag.332>.
- Chen, S.X. (2008). Thermal conductivity of sands. *Heat and Mass Transfer*, 44(10), 1241-1246. <http://dx.doi.org/10.1007/s00231-007-0357-1>.
- Cho, W., Lee, J., & Chun, K. (1999). The temperature effects on hydraulic conductivity of compacted bentonite. *Applied Clay Science*, 14(1-3), 47-58. [http://dx.doi.org/10.1016/S0169-1317\(98\)00047-7](http://dx.doi.org/10.1016/S0169-1317(98)00047-7).
- Coccia, C.J.R., & McCartney, J.S. (2016). Thermal volume change of poorly draining soils I: critical assessment of volume change mechanisms. *Computers and Geotechnics*, 80, 26-40. <http://dx.doi.org/10.1016/j.compgeo.2016.06.009>.
- Constantz, J. (1982). Temperature dependence of unsaturated hydraulic conductivity of two soils 1. *Soil Science Society of America Journal*, 46(3), 466-470. <http://dx.doi.org/10.2136/sssaj1982.03615995004600030005x>.
- Constantz, J., & Murphy, F. (1991). The temperature dependence of ponded infiltration under isothermal conditions. *Journal of Hydrology*, 122(1-4), 119-128. [http://dx.doi.org/10.1016/0022-1694\(91\)90175-H](http://dx.doi.org/10.1016/0022-1694(91)90175-H).
- Delage, P., Sultan, N., & Cui, Y.J. (2000). On the thermal consolidation of Boom clay. *Canadian Geotechnical Journal*, 37(2), 343-354. <http://dx.doi.org/10.1139/t99-105>.
- Di Donna, A., & Laloui, L. (2015). Response of soil subjected to thermal cyclic loading: experimental and constitutive study. *Engineering Geology*, 190, 65-76. <http://dx.doi.org/10.1016/j.enggeo.2015.03.003>.
- Dong, Y., McCartney, J.S., & Lu, N. (2015). Critical review of thermal conductivity models for unsaturated soils. *Geotechnical and Geological Engineering*, 33(2), 207-221. <http://dx.doi.org/10.1007/s10706-015-9843-2>.
- Eriksson, L. (1989). Temperature effects on consolidation properties of sulphide clays. In *Proc. 12th International Conference on Soil Mechanics and Foundation Engineering* (pp. 2087-2090), Rio de Janeiro.
- Farouki, O.T. (1981). *Thermal properties of soils*. Hanover: US Army Corps of Engineers - Cold Regions Research and Engineering Lab. <http://dx.doi.org/10.21236/ADA111734>.
- Finn, F. (1952). The effect of temperature on the consolidation characteristics of remolded clay. In *Proc. Symposium on Consolidation Testing of Soils* (pp. 65-71), Atlantic City. ASTM International. <http://dx.doi.org/10.1520/STP48297S>.
- François, B., & Laloui, L. (2008). ACMEG-TS: a constitutive model for unsaturated soils under non-isothermal conditions. *International Journal for Numerical and Analytical Methods in Geomechanics*, 32(16), 1955-1988. <http://dx.doi.org/10.1002/nag.712>.
- François, B., Salager, S., El Youssofi, M., Ubals Picanyol, D., Laloui, L., & Saix, C. (2007). Compression tests on a sandy silt at different suction and temperature levels. In *Proc. Computer Applications in Geotechnical Engineering - Geo-Denver 2007* (pp. 1-10), Denver, Colorado. ASCE. [https://doi.org/10.1061/40901\(220\)11](https://doi.org/10.1061/40901(220)11).
- Garakani, A.A., Haeri, S.M., Cherati, D.Y., Givi, F.A., Tadi, M.K., Hashemi, A.H., Chiti, N., & Qahremani, F. (2018). Effect of road salts on the hydro-mechanical behavior of unsaturated collapsible soils. *Transportation Geotechnics*, 17, 77-90. <http://dx.doi.org/10.1016/j.trgeo.2018.09.005>.
- Gens, A. (2010). Soil-environment interactions in geotechnical engineering. *Geotechnique*, 60(1), 3-74. <http://dx.doi.org/10.1680/geot.9.P.109>.
- Graham, J., Tanaka, N., Crilly, T., & Alfaro, M. (2001). Modified Cam-Clay modelling of temperature effects in clays. *Canadian Geotechnical Journal*, 38(3), 608-621. <http://dx.doi.org/10.1139/t00-125>.
- Hiraiwa, Y., & Kasubuchi, T. (2000). Temperature dependence of thermal conductivity of soil over a wide range of temperature (5-75 C). *European Journal of Soil Science*, 51(2), 211-218. <http://dx.doi.org/10.1046/j.1365-2389.2000.00301.x>.
- Hopmans, J., & Dane, J. (1986). Temperature dependence of soil hydraulic properties. *Soil Science Society of America Journal*, 50(1), 4-9. <http://dx.doi.org/10.2136/sssaj1986.03615995005000010001x>.
- Houhou, R., Sutman, M., Sadek, S., & Laloui, L. (2020). Microstructure observations in compacted clays subjected to thermal loading. *Engineering Geology*, 287, 105928. <http://dx.doi.org/10.1016/j.enggeo.2020.105928>.
- Houston, S.L., Houston, W.N., & Williams, N.D. (1985). Thermo-mechanical behavior of seafloor sediments. *Journal of Geotechnical Engineering*, 111(11), 1249-1263. [http://dx.doi.org/10.1061/\(ASCE\)0733-9410\(1985\)111:11\(1249\)](http://dx.doi.org/10.1061/(ASCE)0733-9410(1985)111:11(1249)).
- Hueckel, T., & Baldi, G. (1990). Thermoplasticity of saturated clays: experimental constitutive study. *Journal of Geotechnical Engineering*, 116(12), 1778-1796. [http://dx.doi.org/10.1061/\(ASCE\)0733-9410\(1990\)116:12\(1778\)](http://dx.doi.org/10.1061/(ASCE)0733-9410(1990)116:12(1778)).
- Intergovernmental Panel on Climate Change – IPCC (2014). *Climate change synthesis report: contribution of working groups I, II and III to the Fifth Assessment Report of the Intergovernmental Panel on Climate Change*. Geneva: IPCC.
- Johansen, O. (1977). *Thermal conductivity of soils*. Hanover: US Army Corps of Engineers - Cold Regions Research and Engineering Lab.
- Jotisankasa, A. (2005). *Collapse behaviour of a compacted silty clay*. London: University of London.
- Karl, T.R., Melillo, J.M., Peterson, T.C., & Hassol, S.J. (2009). *Global climate change impacts in the United States*. New York: Cambridge University Press.
- Khosravi, A., Hashemi, A., Ghadiriannari, S., & Khosravi, M. (2020). Variation of small-strain shear modulus of unsaturated silt under successive cycles of drying and

- wetting. *Journal of Geotechnical and Geoenvironmental Engineering*, 146(7), 04020050. [http://dx.doi.org/10.1061/\(ASCE\)GT.1943-5606.0002275](http://dx.doi.org/10.1061/(ASCE)GT.1943-5606.0002275).
- Krahn, J., & Fredlund, D. (1972). On total, matric and osmotic suction. *Soil Science*, 114(5), 339-348. <http://dx.doi.org/10.1097/00010694-197211000-00003>.
- Laloui, L., & Loria, A.F.R. (2019). *Analysis and design of energy geostructures: theoretical essentials and practical application*. London: Academic Press.
- Laloui, L., & Sutman, M. (2019). Energy geostructures: a new era for geotechnical engineering practice. In *Proc. XVII European Conference on Soil Mechanics and Geotechnical Engineering* (pp. 1-15), Reykjavik. IGS – Icelandic Geotechnical Society. <https://doi.org/10.3207/5/17ECSMGE-2019-1106>.
- Laloui, L., & Sutman, M. (2020). Experimental investigation of energy piles: from laboratory to field testing. *Geomechanics for Energy and the Environment*, 27, 100214. <http://dx.doi.org/10.1016/j.gete.2020.100214>.
- Laloui, L., Olgun, C., Sutman, M., McCartney, J., Coccia, C., Abuel-Naga, H., & Bowers, G. (2014). Issues involved with thermoactive geotechnical systems: characterization of thermomechanical soil behavior and soil-structure interface behavior. *DFI Journal-The Journal of the Deep Foundations Institute*, 8(2), 108-120. <http://dx.doi.org/10.1179/1937525514Y.0000000010>.
- Li, D., Sun, X., & Khaleel, M. (2013). Comparison of different upscaling methods for predicting thermal conductivity of complex heterogeneous materials system: application on nuclear waste forms. *Metallurgical and Materials Transactions A, Physical Metallurgy and Materials Science*, 44(1), 61-69. <http://dx.doi.org/10.1007/s11661-012-1269-3>.
- Lloret, A., Villar, M.V., Sanchez, M., Gens, A., Pintado, X., & Alonso, E. (2003). Mechanical behaviour of heavily compacted bentonite under high suction changes. *Geotechnique*, 53(1), 27-40. <http://dx.doi.org/10.1680/geot.2003.53.1.27>.
- Lu, N., & Dong, Y. (2015). Closed-form equation for thermal conductivity of unsaturated soils at room temperature. *Journal of Geotechnical and Geoenvironmental Engineering*, 141(6), 04015016. [http://dx.doi.org/10.1061/\(ASCE\)GT.1943-5606.0001295](http://dx.doi.org/10.1061/(ASCE)GT.1943-5606.0001295).
- Lu, S., Ren, T., Gong, Y., & Horton, R. (2007). An improved model for predicting soil thermal conductivity from water content at room temperature. *Soil Science Society of America Journal*, 71(1), 8-14. <http://dx.doi.org/10.2136/sssaj2006.0041>.
- McGinley, J.M. (1983). *The effects of temperature on the consolidation process of saturated fine-grained soils* [Unpublished MSc thesis]. University of Colorado, Boulder.
- Mun, W., & McCartney, J. S. (2014). Compression behavior of unsaturated clay under high stresses. In *Proc. Geo-characterization and Modeling for Sustainability - Geo-congress 2014* (pp. 1443-1452), Atlanta. ASCE. <https://doi.org/10.1061/9780784413272.141>.
- Nikolaev, I.V., Leong, W.H., & Rosen, M.A. (2013). Experimental investigation of soil thermal conductivity over a wide temperature range. *International Journal of Thermophysics*, 34(6), 1110-1129. <http://dx.doi.org/10.1007/s10765-013-1456-5>.
- Olson, R.E., & Langfelder, L.J. (1965). Pore water pressures in unsaturated soils. *Journal of the Soil Mechanics and Foundations Division*, 97(4), 127-150. <http://dx.doi.org/10.1061/JSFEAQ.0000753>.
- Rao, S.M., & Revanasiddappa, K. (2000). Role of matric suction in collapse of compacted clay soil. *Journal of Geotechnical and Geoenvironmental Engineering*, 126(1), 85-90. [http://dx.doi.org/10.1061/\(ASCE\)1090-0241\(2000\)126:1\(85\)](http://dx.doi.org/10.1061/(ASCE)1090-0241(2000)126:1(85)).
- Romero, E., Gens, A., & Lloret, A. (2001). Temperature effects on the hydraulic behaviour of an unsaturated clay. In D.G. Toll (Eds.), *Unsaturated soil concepts and their application in geotechnical practice* (pp. 311-332). Dordrecht: Springer.
- Romero, E., Gens, A., & Lloret, A. (2003). Suction effects on a compacted clay under non-isothermal conditions. *Geotechnique*, 53(1), 65-81. <http://dx.doi.org/10.1680/geot.2003.53.1.65>.
- Saix, C. (1991). Consolidation thermique par chaleur d'un sol non saturé. *Canadian Geotechnical Journal*, 28(1), 42-50. <http://dx.doi.org/10.1139/t91-005>.
- Saix, C., Devillers, P., & El Youssefi, M. (2000). Eléments de couplage thermomécanique dans la consolidation de sols non saturés. *Canadian Geotechnical Journal*, 37(2), 308-317. <http://dx.doi.org/10.1139/t99-112>.
- Sakaguchi, I., Momose, T., & Kasubuchi, T. (2007). Decrease in thermal conductivity with increasing temperature in nearly dry sandy soil. *European Journal of Soil Science*, 58(1), 92-97. <http://dx.doi.org/10.1111/j.1365-2389.2006.00803.x>.
- Salager, S., François, B., Youssefi, M.S.E., Laloui, L., & Saix, C. (2008). Experimental investigations of temperature and suction effects on compressibility and pre-consolidation pressure of a sandy silt. *Soil and Foundation*, 48(4), 453-466. <http://dx.doi.org/10.3208/sandf.48.453>.
- Slegel, D.L., & Davis, L. (1977). Transient heat and mass transfer in soils in the vicinity of heated porous pipes. *Journal of Heat Transfer*, 99(4), 540-541. <http://dx.doi.org/10.1115/1.3450739>.
- Sultan, N., Delage, P., & Cui, Y. (2002). Temperature effects on the volume change behaviour of Boom clay. *Engineering Geology*, 64(2-3), 135-145. [http://dx.doi.org/10.1016/S0013-7952\(01\)00143-0](http://dx.doi.org/10.1016/S0013-7952(01)00143-0).
- Sutman, M. (2013). Temperature effects on soil behavior in relation to ground-sourced bridge deck deicing systems. In *Proc. Transportation Research Board 92nd Annual Meeting* (pp. 1-8), Washington DC.

- Tang, A.M., Cui, Y.J., & Barnel, N. (2008). Thermo-mechanical behaviour of a compacted swelling clay. *Geotechnique*, 58(1), 45-54. <http://dx.doi.org/10.1680/geot.2008.58.1.45>.
- Tarnawski, V.R., Momose, T., Leong, W., Bovesecchi, G., & Coppa, P. (2009). Thermal conductivity of standard sands. Part I. Dry-state conditions. *International Journal of Thermophysics*, 30(3), 949-968. <http://dx.doi.org/10.1007/s10765-009-0596-0>.
- Tarnawski, V.R., Momose, T., & Leong, W. (2011). Thermal conductivity of standard sands II. Saturated conditions. *International Journal of Thermophysics*, 32(5), 984-1005. <http://dx.doi.org/10.1007/s10765-011-0975-1>.
- Tidfors, M., & Sällfors, G. (1989). Temperature effect on preconsolidation pressure. *Geotechnical Testing Journal*, 12(1), 93-97.
- Towhata, I., Kuntiwattanaku, P., Seko, I., & Ohishi, K. (1993). Volume change of clays induced by heating as observed in consolidation tests. *Soil and Foundation*, 33(4), 170-183. http://dx.doi.org/10.3208/sandf1972.33.4_170.
- Uchaipichat, A., & Khalili, N. (2009). Experimental investigation of thermo-hydro-mechanical behaviour of an unsaturated silt. *Geotechnique*, 59(4), 339-353. <http://dx.doi.org/10.1680/geot.2009.59.4.339>.
- Vega, A., & McCartney, J.S. (2014). Cyclic heating effects on thermal volume change of silt. *Environmental Geotechnics*, 2(5), 257-268. <http://dx.doi.org/10.1680/envgeo.13.00022>.
- Villar, M.V., & Lloret, A. (2004). Influence of temperature on the hydro-mechanical behaviour of a compacted bentonite. *Applied Clay Science*, 26(1-4), 337-350. <http://dx.doi.org/10.1016/j.clay.2003.12.026>.
- White, D.E. (1973). Characteristics of geothermal resources. In P. Kruger & C. Otte (Eds.), *Geothermal energy resources, production, stimulation* (pp. 69-94). Stanford: Stanford University Press.
- Ye, W.M., Wan, M., Chen, B., Chen, Y., Cui, Y., & Wang, J. (2013). Temperature effects on the swelling pressure and saturated hydraulic conductivity of the compacted GMZ01 bentonite. *Environmental Earth Sciences*, 68(1), 281-288. <http://dx.doi.org/10.1007/s12665-012-1738-4>.
- Yun, T.S., & Santamarina, J.C. (2008). Fundamental study of thermal conduction in dry soils. *Granular Matter*, 10(3), 197-207. <http://dx.doi.org/10.1007/s10035-007-0051-5>.

Site characterization for the design of thermoactive geostructures

Ana Vieira^{1#} , Maria Alberdi-Pagola² , Marco Barla³ , Paul Christodoulides⁴ ,
Georgios Florides⁴ , Alessandra Insana³ , Saqib Javed⁵ , João Maranhã¹,
Dejan Milenic⁶ , Iulia Prodan⁷ , Diana Salciarini⁸ 

Review Article

Keywords

Shallow geothermal energy
Thermoactive geostructures
Site thermal characterization
Undisturbed ground temperature
Thermal conductivity

Abstract

This paper addresses the topic of site characterization for the design of Shallow Geothermal Energy (SGE) systems, namely of thermoactive geostructures, which are geotechnical structures, such as piles, retaining walls and tunnel linings, also used as heat exchangers as part of closed-loop SGE systems. Such solutions, being increasingly adopted for buildings' and infrastructures' heating and/or cooling, are considered sustainable and cost effective. For the design of the primary circuit of the SGE system, which is embedded within the superficial soil layers, a comprehensive knowledge of the ground condition at the site is mandatory. This includes the evaluation of the energy features and whether the system can provide the required energy needs during the operational period, as well as the verification of the structural and geotechnical safety and functionality requirements. The site characterization for SGE systems involves different stages, from desk studies to detailed characterization, including in-situ trials, laboratory testing of undisturbed soil samples and the study of possible interferences. The specific aspects that will be addressed are: (i) the assessment of the site undisturbed ground temperature and its hydrogeological features; (ii) the thermal and thermomechanical characterization of the different soil layers; (iii) the investigation of the ground-heat exchanger thermal resistance; (iv) the collection of information related to the environmental constraints and to potential interferences among multiple users, which are related to the service life of the structure. The overall aim is to ensure a proper design of the SGE system for guaranteeing its sustainability in the long term.

1. Introduction

The need for adoption of renewable energy systems is increasing every year especially in the context of CO₂ emissions and climate change issues. Shallow Geothermal Energy (SGE) represent sustainable solutions for ensuring easy access to renewable energy for heating and cooling of buildings and infrastructure. Their performance is dependent on many factors, with site characterization being one of the most relevant. Proper use of piles and other buried concrete structures, such as retaining walls and tunnels, not only for geotechnical and structural purposes, but also for heat exchange, relies on an adequate and well-planned thermal characterization

of the site. The use of the ground as a thermal reservoir is the conceptual basis of SGE functioning.

The design of the primary circuit of an SGE system involves both energy and geotechnical aspects (Figure 1). Adequate knowledge of the ground conditions for SGE systems allows determining whether the ground can fulfil the energy demand of the structure or infrastructure to be served (e.g.: Brandl, 2006; Barla & Di Donna, 2018; Loveridge et al., 2020) and if the structural and geotechnical integrity of the geostructure is affected due to the additional stresses and strains induced by the cyclic temperature changes (Laloui et al., 2014; Rotta Loria & Laloui, 2017; Insana, 2020; Insana et al., 2020). Also, the soil thermal

[#]Corresponding author. E-mail address: avieira@lnec.pt

¹National Laboratory for Civil Engineering, Geotechnics Department, Lisbon, Portugal.

²Centrum Pæle A/S & cp test a/s, Vejle, Denmark.

³Politecnico di Torino, Department of Structural, Building and Geotechnical Engineering, Torino, Italy.

⁴Cyprus University of Technology, Faculty of Engineering and Technology, Limassol, Cyprus.

⁵Lund University, Division of Building Services, Lund, Sweden.

⁶University of Belgrade, Department of Hydrogeology, Belgrade, Serbia.

⁷Technical University of Cluj-Napoca, Department of Structures, Cluj-Napoca, Romania.

⁸Università degli Studi di Perugia, Department of Civil and Environmental Engineering Department, Perugia, Italy.

Submitted on February 8, 2022; Final Acceptance on February 21, 2022; Discussion open until May 31, 2022.

<https://doi.org/10.28927/SR.2022.001022>



This is an Open Access article distributed under the terms of the Creative Commons Attribution License, which permits unrestricted use, distribution, and reproduction in any medium, provided the original work is properly cited.

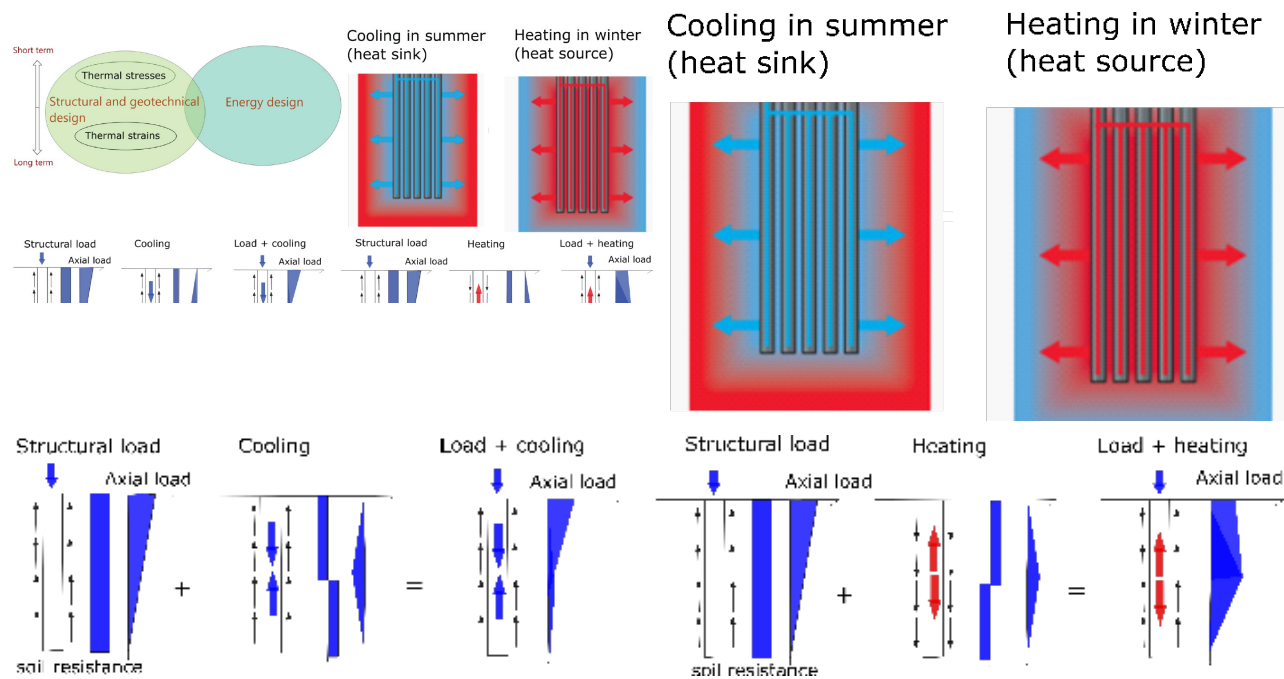


Figure 1. Main design aspects of a primary circuit of an SGE system (a); energy design (b); geotechnical and structural design (c) (Yang et al., 2017).

characteristics and the hydrogeological setting, are decisive factors in the generation of a permanent thermal plume which might affect the long-term energy efficiency of the system. An illustrative example of the consequences (over- or under-sizing a geothermal system) of an inappropriate subsurface characterization, based on a study of more than 1000 SGE systems installed in Germany, was provided by Blum et al. (2011). Hence, for the good performance and functioning of these systems, reliable parameters are needed in the design based on sufficient site investigation.

To reach the first objective of a SGE system proper design, i.e., to guarantee the energy needs, a detailed thermal characterization of the affected soil/ground layers is needed. Yet the evaluation of soil thermal properties is not generally considered during routine site investigation and, thus, additional characterization studies are necessary. Also, the thermal resistance of the thermoactive geostructure must be evaluated, as it affects its heat exchange with the surrounding ground and thus the entire system energy efficiency. The second objective, i.e., to guarantee structural and geotechnical integrity, depends on the geostructure and soil thermo-mechanical behaviour and on their interaction, with particular emphasis in their thermal expansion relative difference and the geostructure support conditions.

The level of detail of site characterization for SGE depends on the design stage and on the importance of the system. In general, two stages can be considered for site characterization: (i) a preliminary stage, which occurs at the planning phase (conceptual design), where the geological and hydrogeological conditions are investigated, and a first

estimate of thermal parameters is provided, checking the feasibility of the system based on the expected building of infrastructure energy demand; (ii) a detailed characterization stage at the scale of the SGE, where the final ground design parameters are established.

The thermal efficiency of SGE (closed-loop) depends mainly on heat transfer by conduction, however, the groundwater flow can also have a significant impact on heat transfer by advection, particularly for coarse grained soil and high seepage velocities (Fan et al., 2007; Insana & Barla, 2020). For this latter case, an enhancement of the heat transfer process is generally achieved. Values of hydraulic conductivity of the soil greater than around 10^{-5} m.s^{-1} may induce significant effects in heat transfer (Hellström, 1991). Other less relevant thermal processes, dependent on soil granulometry and degree of saturation are heat radiation, thermal redistribution of moisture, and free convection in the air (Farouki, 1981).

Since 2000, some countries have published specific recommendations about the design and construction of energy geostructures, with a particular focus on energy piles, which also include site investigation specifications (GSHPA, 2012). Previous studies just related to the topic of ground characterization within the scope of SGE design were presented, for example, by Loveridge et al. (2017), Vieira et al. (2017) and Laloui & Rotta Loria (2020).

The current paper is based on an initial study developed by the authors between 2015 and 2019, in the framework of the COST Action TU1405 (GABI: European network for shallow geothermal energy applications in buildings and

infrastructures), Working Group 1: Soil thermal characterization. It provides a review on the site characterization stages for the evaluation of thermal, hydrogeological and mechanical parameters and the involved methods in the context of SGE applications, from desk studies to laboratory and in-situ testing of soil samples. Also, a brief reference is made to environmental constraints and to the information needed to evaluate potential interferences among multiple users.

2. Preliminary design assessment

During the feasibility or planning stage of a SGE project, a preliminary estimation of the initial conditions and of the thermal properties of the soil on site should be carried out. As the main aim in the preliminary design assessment is to understand the feasibility and the economic convenience of the SGE system, the geotechnical aspect is not dealt with. The most significant aspects for the characterization of the ground thermal behaviour for SGE applications include: (i) the undisturbed ground temperature; (ii) the ground thermal conductivity; (iii) the ground volumetric heat capacity; (iv) the thermal resistance of the ground heat exchanger (GHE); and (v) the groundwater flow (Rees, 2016). At this initial stage, these aspects can be estimated based on geological mapping, analysis of relevant projects, expert judgement and qualified guesswork.

Undisturbed ground temperature T_0 [K] is the average temperature of the ground surrounding a GHE prior to its operation. It determines the initial condition of the geothermal system and its operating temperature limits. The heat transfer between the GHE and the surrounding ground is driven by their relative temperature difference. The thermal conductivity λ [$\text{W}\cdot\text{m}^{-1}\cdot\text{K}^{-1}$] is the ability of the ground to conduct heat, while the volumetric heat capacity $\rho \cdot c_p$ [$\text{J}\cdot\text{m}^{-3}\cdot\text{K}^{-1}$] (being c_p [$\text{J}\cdot\text{kg}^{-1}\cdot\text{K}^{-1}$] the heat capacity and ρ [$\text{J}\cdot\text{kg}\cdot\text{K}^{-3}$] the density) is the capacity of the ground to store heat. The ratio between the last two properties yields the thermal diffusivity α [$\text{m}^2\cdot\text{s}^{-1}$]. Ground with higher thermal conductivity yields larger heat transfer rates and recovers more rapidly from thermal depletions and thermal build-ups. The thermal resistance R_{GHE} [$\text{K}\cdot\text{m}\cdot\text{W}^{-1}$] of the GHE is the effective thermal resistance between the heat carrier fluid circulating in the pipes and the edge of the geostructure in contact with the surrounding ground. A low value of thermal resistance means enhanced heat transfer inside the GHE, which, in turn, means a GHE with a smaller size and lower installation costs.

A simple rule for the evaluation of the undisturbed ground temperature is that the average yearly temperature at bellow a depth of about 10 m is 1°C higher than the average yearly air temperature (SIA, 2005). Such information can be considered enough for a first sizing of the SGE system and can be further confirmed through specific in-situ measurements.

The ground thermal conductivity, which is the most important parameter in the evaluation of the energy efficiency of a SGE is affected by several factors, such as the water

content, the solid particle composition and spatial arrangement and the porosity. λ increases with water content, due to the replacement of air, a poor heat conductor by, water which is a much better one (Figure 2). The values of this parameter vary in-depth through the different soil layers, however averaged values are initially estimated based on different approaches. Specific maps are available online and in the literature for several regions (e.g.: Ditlefsen et al., 2014; Ramstad et al., 2015; Geothermische Screeningstool, 2017). An example is the Thermomap project (ThermoMap, 2013) that provides 10-m average thermal conductivity values for Europe (Figure 3), based on an exhaustive compilation of available data. These maps provide a useful tool for planning, often integrating additional and relevant information, such as climatic data an protected zones. Still, the maps do not explicitly account for local site effects and specific conditions. In fact, they have been developed by assigning the available thermal property data to similar lithological units, thus extrapolating site-level information to whole regions. Alternatively, the initial estimate of the ground thermal conductivity and ground volumetric heat capacity can also be obtained from published data on thermal properties of soils, provided that the geological setting of the considered area is known. Ranges of values of thermal conductivity and volumetric heat capacity of soils and other materials can be found in the literature (Farouki, 1981; VDI, 2010). Some indicative values are shown in Table 1.

Another important parameter to consider when dealing with SGE systems is the thermal resistance of the GHE. R_{GHE} can be simply expressed as the ratio of the temperature difference between the heat carrier fluid and the ground and the applied heat flux. R_{GHE} depends on the number of pipes and their geometric arrangement and the physical properties of the GHE elements. A key factor in this regard is the thermal conductivity of the material between the heat exchanger pipes and the surrounding ground. As for borehole heat exchangers

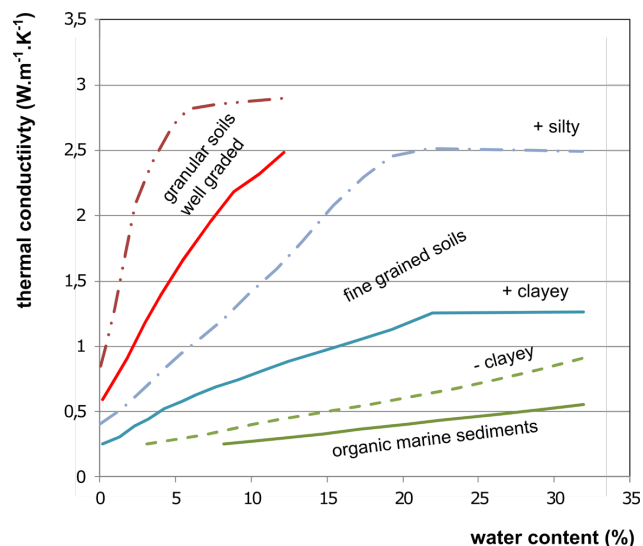


Figure 2. Relation between thermal conductivity and water content for different soils. Adapted from Reiffsteck et al. (2015).

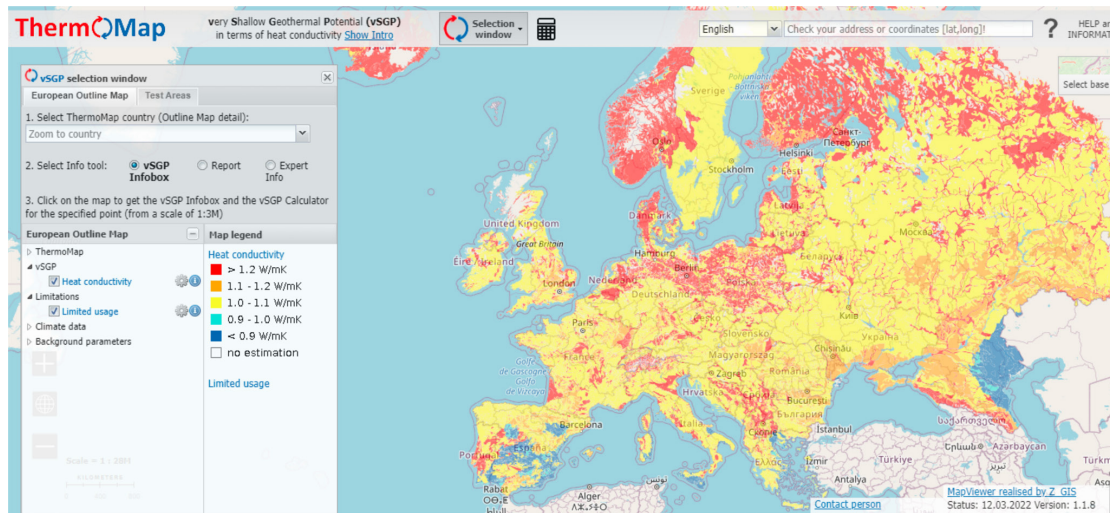


Figure 3. Very Shallow Geothermal Potential (vSGP) in terms of heat conductivity of unconsolidated underground up to 10 m depth (ThermoMap, 2013).

Table 1. Thermal properties of different types of soils and other materials, from (VDI, 2010).

Material	Thermal conductivity λ [$\text{W}\cdot\text{m}^{-1}\cdot\text{K}^{-1}$]		Volumetric heat capacity ρ_p [$\text{MJ}\cdot\text{m}^{-3}\cdot\text{K}^{-1}$]	
	Dry	Saturated	Dry	Saturated
Clay	0.4-1.0	1.1-3.1	1.5-1.6	2.0-2.8
Sand	0.3-0.9	2.0-3.0	1.3-1.6	2.2-2.8
Gravel	0.4-0.9	1.6-2.5	1.3-1.6	2.2-2.6
Air	0.02		0.0012	
Water	0.59		4.15	
Concrete	0.9-2.0		1.8	

(BHEs), there are several publications in the literature providing calculation formulas for the thermal resistance of different energy geostructures, such as energy piles (Loveridge & Powrie, 2014; Claesson & Javed, 2020), tunnel linings (Shafagh et al., 2020) and diaphragm walls (Shafagh & Rees, 2019).

Although for BHEs, Javed et al. (2019) suggested a method to design the whole system based on estimation approaches (without using any in-situ testing) and carried out a sensitivity analysis of the design if such an approach is used. A similar strategy could be implemented for other SGE systems including energy geostructures.

Flowing groundwater can provide significant additional heat transfer by advection in SGE systems (Claesson & Hellström, 2000; Rotta Loria et al., 2015; Di Donna & Barla, 2016; Di Donna et al., 2020), its impact on geothermal system performance differs, depending also on the ground use, i.e., on the thermal needs of the building. The groundwater flow can be beneficial for ground source systems that do not rely on seasonal storage, since it would recharge the heat faster or would remove the heat away (Laloui & François, 2009; Ma & Grabe, 2010; Suryatriyastuti, 2013; Loveridge et al., 2017; Epting et al., 2020; Insana & Barla, 2020). According to SIA (2005), the seasonal heat storage becomes unfeasible when Darcy's velocity exceeds 0.5-1 m/day. Hence, the

geological and/or hydrogeological surveys of each region should be consulted to obtain meaningful information.

Finally, if no additional information is available, it may be acceptable to make an evaluation of the likely energy output based on "rules of thumb" and design charts to assess the feasibility and viability of the geothermal system. Heat extraction rates, expressed as power per meter or per square meter of heat exchanger have been proposed for piles (Brandl, 2006), for tunnels (Di Donna et al., 2020; Insana & Barla, 2020) and for diaphragm walls and slabs (Loveridge et al., 2017).

3. Detailed design characterization

3.1 Thermal parameters and initial conditions

For the final design, the undisturbed ground temperature should be determined in-situ, if possible. A comprehensive review of the available approaches is presented in Vieira et al. (2017). The measurements can be taken by either the downhole temperature logging or the fluid circulation method. In the downhole temperature logging method, the temperature distribution along the borehole depth can be measured by means of a downhole temperature sensing system. A simple or weighted average of the measured temperature values can then be used to approximate the undisturbed ground

temperature. Various downhole temperature measurements systems, including wired temperature sensors, submersible wireless probes, and fiber optics, among others, can be used. Elsewise, the undisturbed ground temperature can be determined by circulating the fluid through a closed-loop GHE without heating or cooling the fluid and measuring the exit temperature of the fluid leaving the GHE.

In addition to undisturbed ground temperature, the thermal properties of the ground can be determined by means of semi-empirical models based on the relative proportions of soil phases and by in-situ or laboratory techniques. Based on the geotechnical characterization of the ground layers, thermal conductivity and specific heat can be estimated on the basis of the relative proportions and soil phases solid, liquid and gaseous phase. Several expressions can be found in the literature, assuming different distributions and geometric arrangements (e.g.: Dong et al., 2015), with the parallel and serial configurations providing, respectively, a lower and an upper bound for thermal conductivity. According to Rees et al. (2000), the weighted geometric mean configuration was found to be adequate by several researchers for a large variety of soils. According to it, soil thermal conductivity is:

$$\lambda = \lambda_s \chi_s \lambda_w \chi_w \lambda_a \chi_a \quad (1)$$

where $\lambda_s, \lambda_w, \lambda_a$ are, respectively, the thermal conductivity of solid, water and air, and $\chi_s = 1 - n$, $\chi_w = n S_r$ and $\chi_a = n(1 - S_r)$ the respective volumetric fractions, n the porosity and S_r the saturation ratio.

As regards the heat capacity of soils, as it is not a directional variable, it can be obtained by adding the heat

capacities of the different constituents based on to their volumetric fractions. For example by:

$$c_p = \chi_s c_s + \chi_w c_w + \chi_a c_a \quad (2)$$

where c_s, c_w, c_a are, respectively, the heat capacity of solid, water and air phases.

The Thermal Response Test (TRT) (Gehlin, 2002) is an in-situ test executed in an already built GHE, which yields the thermal conductivity of the surrounding soil, the GHE thermal resistance and the initial undisturbed temperature (Figure 4). In a TRT heat is injected into the ground at a constant rate in a borehole heat exchanger and the temperature change of the circulating fluid is monitored. Due to its simplicity of design, control and implementation, it is the preferred method for estimating thermal properties. The TRT, originally conceived for vertical BHEs (Spitler & Gehlin, 2015), has been extended to energy piles (GSHPA, 2012; Loveridge et al., 2014). For energy piles, the principle of the test remains the same as for BHEs, yet longer times are usually required to overcome the thermal inertia of the concrete pile. According to Alberdi-Pagola et al. (2018) for 30×30 cm² square piles, 60 hours test durations are required, while for wider piles, according to GSHPA (2012) and Loveridge et al. (2014), at least 100 hours are required. Further recommendations are given in GSHPA (2012).

The main challenge with energy pile TRT arises when interpreting the observed data. Appropriate models need to be used to yield reliable estimates. The models applied (analytical, empirical or numerical) need to account for the length and cross-section of the piles (Alberdi-Pagola et al., 2018), and, therefore, frequently, tailored models, such as the

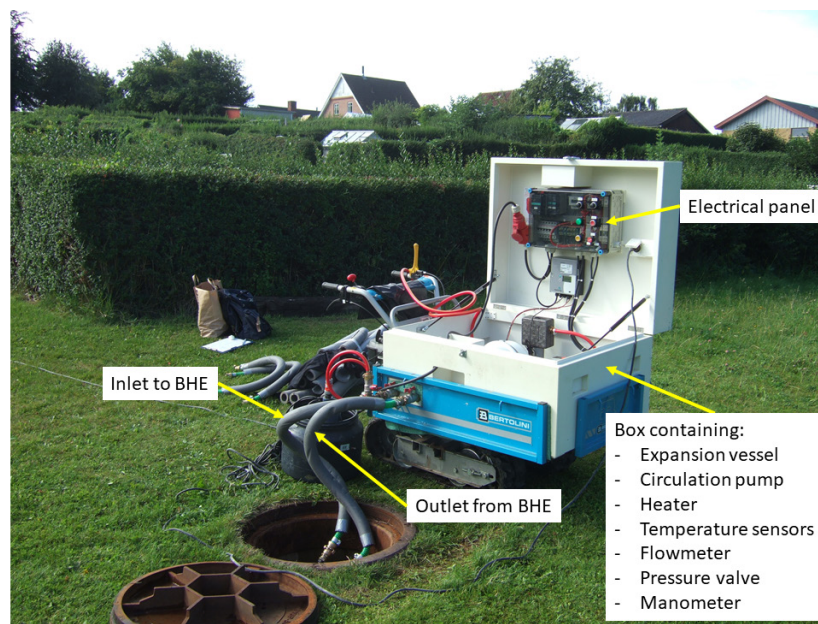


Figure 4. Example of a TRT performed in a 18 m BHE in Denmark, Jutland. From Alberdi-Pagola (2018).

ones proposed in Alberdi-Pagola et al. (2018) and Loveridge & Powrie (2013), are required.

The thermal conductivity of the ground and the thermal resistance of the GHE, which, as said, can be obtained from the TRT data, have counterbalancing effects on the design; using the experimentally determined values of both parameters mitigates some of the error that would occur if only the ground conductivity value estimated from the test was used for the design (Javed et al., 2011). It is still, however, recommended to separately calculate the thermal resistance value of the GHE to control the experimentally determined value. It is recommended that the thermal resistance be determined using the Multipole method (Claesson & Hellström, 2011), which is an analytical method that can be used for any number of arbitrarily placed pipes in a composite region with remarkable accuracy.

TRT measurements can be affected when sufficiently high groundwater flow occurs. The enhanced heat transfer caused by groundwater advection yields a higher effective thermal conductivity of the soil. The advantage of the TRT is that it gives an effective ground conductivity, which already includes the effect of groundwater flow. However, to uncouple the conduction and advection effects, it is recommended to perform a stepwise analysis or to use a moving line source solution when dealing with this type of data (Diao et al., 2004; Sanner et al., 2007). Further hydrogeological effects will be treated later.

Occasionally, TRT has also been used to estimate the volumetric heat capacity of soils. Wagner & Clauser (2005) used synthetic TRT data to perform parameter estimation varying the thermal conductivity and the volumetric heat capacity of the soil in a finite difference model. Moreover, Christodoulides et al. (2016) proposed a methodology for the computation of the ground thermal diffusivity, the volumetric heat capacity and the thermal resistance of a GHE. The methodology was based on the actual parameters used in a TRT experiment and the line source model. However, Austin (2000) suggests that volumetric heat capacity values estimated from standard TRT are not always acceptable. Therefore, it is recommended to assign a volumetric heat capacity value based on the knowledge of the existing soil and treat it as a known value. This assumption will not have a significant impact on the final estimation of the thermal conductivity of the soil. Although less common as they are less easy to perform, in-situ tests can be also used to determine the specific heat capacity of soils by realizing pits of about 1.5 m below the ground surface, in and around the SGE plant (Oladunjoye & Sanuade, 2012).

It is difficult to determine the ground thermal conductivity and the GHE thermal resistance from TRTing of energy geostructures other than energy piles and this is not, therefore, common practice. However, some authors perform thermal performance tests to determine the efficiency of energy geostructures, such as for energy slabs (Lee et al., 2021), energy walls (Di Donna et al., 2017) and tunnel linings

(Barla et al., 2019). Note that these tests do not provide information about the ground properties. Furthermore, when dealing with energy tunnels and diaphragm walls, an important role on heat transfer processes that can crucially affect thermal performance is also played by the climate inside the excavation (Bourne-Webb et al., 2016; Dornberger et al., 2020; Ma et al., 2021). Therefore, a good understanding of the expected airflow temperature and velocity is also suggested.

The characterization of the ground thermal parameters can also be carried out by laboratory tests. There is a large number of different types of tests, some of them standardized. The main advantages of laboratory tests is that they are quick, relatively inexpensive and allow a better control of the boundary conditions, however they do not consider the real field conditions and several determinations are required to obtain representative values of the thermal properties, due to the ground heterogeneity and variability. Nevertheless, in contrast or in complement to TRT, the thermal conductivity of the different soils layers involved can be estimated.

Laboratory techniques for the determination of ground thermal properties, can be divided into steady-state and transient techniques. In the first type a permanent heat flux must be established in the soil sample, whilst in the second, the evaluation of thermal conductivity is performed during the modulated heating up process. As a consequence, transient time or frequency domain methods enable quicker measurement of thermal conductivity as they do not need to wait for a steady-state to be reached. The comparison between test results by using these different approaches suggests some influence of the soil granulometry and saturation conditions; that is the effect of longer test duration in steady-state methods might induce water migration within the sample and larger heat losses which will likely to affect the measurements.

The selection of the most suitable method depends on the type of soil or rock. Typical laboratory tests devices include the needle probe, the transient plane heat source and the thermal cell. The guarded hot plate and the thermal needle probe have been standardized to determine the thermal conductivity for rocks and soils, respectively (ASTM, 2014, 2016). The latter could also be taken to the field.

The comparison of results using different testing procedures also gives an important insight with regard to their capabilities and limitations. For instance, Popov et al. (1999) compared the thermal needle probe, the divided bar and the optical scanning techniques to measure rock samples. Also, the transient plane source technique has shown consistent results when used to measure clayey and sandy soils in Alberdi-Pagola et al. (2018).

As discussed several factors and sources of errors affect the measurement of thermal conductivity. Loveridge et al. (2017) have noted that thermal conductivity values measured in-situ by TRT are systematically higher than those obtained by laboratory tests (Figure 5). These differences can be attributed to different factors such as the sampling disturbance, the water migration within the sample, the in-situ stress and

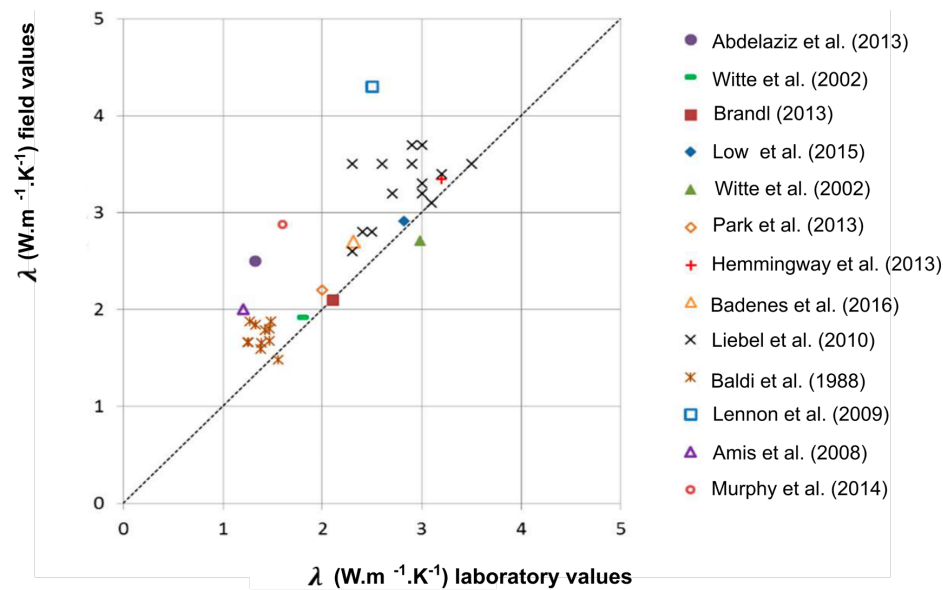


Figure 5. Comparison between conductivity values derived from laboratory and field tests. Adapted from Loveridge et al. (2017) and Vieira et al. (2017).

flow conditions and scale effects, and might influence the SGE design.

3.2 Hydrogeological parameters

Designing SGE systems requires a multidisciplinary approach and a deep understanding of the ground conditions among which the hydrogeological ones play a critical role to ensure the planned thermal efficiency (e.g.: for heat recovery and storage) in a sustainable way.

The most important hydrogeological aspects for the design of thermoactive geostructures are: (i) the geological profile; (ii) the effective porosity of the ground, which will mainly influence the thermal and hydraulic properties of the soil/rock mass; (iii) the horizontal soil/rock hydraulic conductivity; (iv) the vertical to horizontal hydraulic conductivity anisotropy ratio; (v) the groundwater flow characteristics in terms of piezometric levels, seasonal oscillations (especially for very shallow energy geostructures), hydraulic gradient and ground water flow predominant direction with respect to the SGE (particularly those with an important longitudinal extension, as in the case of tunnels or diaphragm walls). The latter will mainly influence seepage velocity, energy yield, heat storage capacity, time to steady state recovery during intermittent operation and features of the possible thermal plume.

The geological profile needs to be defined based on specific geotechnical investigations (continuous boreholes drillings with collection of samples), whose number increases when dealing with linear structures, such as energy tunnels. Effective porosity can be evaluated according to granulometric curves or, if unavailable, from literature data based on the type of soil/rock. The hydraulic conductivity anisotropy

ratio depends on the soil layers stratification, which may lead to a higher horizontal conductivity compared to the vertical one. Back-analyses of in-situ pumping tests can be performed to evaluate such parameter. Phreatic surface location and seasonal oscillation, as well as, groundwater direction and hydraulic gradient can be evaluated based on available maps of isopiezometric curves and on specific in-situ measurements of groundwater level on existing or new piezometer wells in different times of the year.

For the assessment of hydraulic conductivity, in-situ tests can be performed to improve the reliability of models, such as slug tests, push/pull (Klepikova et al., 2016), heat storage experiments (Palmer et al., 1992), heat tracer tests (Macfarlane et al., 2002) or other specific tests (e.g.: Kuo & Liao, 2012). However, these conventional approaches often rely on a global measure and generally lack the spatial coverage required to characterize the heterogeneity of the subsurface. The complementary use of spatially distributed information with geophysical methods or distributed temperature sensing (DTS), which provide spatial information on the subsurface with greater coverage than boreholes and a greater vertical resolution, has increased in the past years (Hermans et al., 2014) and allows to better investigate the heterogeneity of the geology and the groundwater flow. Fujii et al. (2009) used optical fiber sensors to record vertical temperature profiles in two bedrock case studies in Japan and related the results with local geological and groundwater information identifying active groundwater flow.

Efficient recovery of thermal energy stored in the aquifer is only possible in specific hydrogeological conditions such as low natural gradients (Hermans et al., 2018). In addition to the cited characteristics, the heterogeneity of aquifers,

whether located in bedrock or in alluvial plain, makes the efficiency of SGE difficult to predict, due to its influence on groundwater flow and the spatial distribution of hot and cold groundwater plumes (Sommer et al., 2013, 2014). For this reason, a methodology was proposed with specific reference to energy tunnels, that have the particularity to be long linear structures crossing a city for several kilometers, as in the case of urban tunnels (Baralis et al., 2020; Barla et al., 2021). The idea is to subdivide the tunnel path into a number of sections that are characterized by a specific set of hydrogeological and also thermal parameters, so that the study can be performed with reference to such characteristic sections.

Globally, the presence and magnitude of groundwater flow is crucial for the SGE system sustainable long-term behavior. If the flow is high enough, winter extraction mode will be decoupled from summer injection mode (SIA, 2005). Moreover, in case of winter-only operation, groundwater flow will enhance thermal recharge and make an ad hoc thermal recharge useless. It helps dissipating the induced by

geothermal activity thermal changes, which take the form of a thermal plume from upstream to downstream. The shape and the amplitude of the thermal plume depend on the thermal change induced by the SGE which is determined by the building or infrastructure energy demand, on the ground thermal properties and on the water flow velocity. As regards the groundwater flow, high velocity may imply a long and thin thermal plume with a moderate intensity. Inversely, a moderate velocity causes a short and large thermal plume with a decreasing intensity with distance. Figure 6 shows examples of thermal plumes related to the groundwater flow velocity.

The development of models able to simulate heat flow and transport within the subsurface and account for uncertainties related to the subsurface is a challenging and time-consuming task (Baralis, 2020). It often relies on many uncertain parameters involved in heat flow and transport such as hydraulic conductivity, porosity, thermal conductivity or volumetric heat capacity, their associated

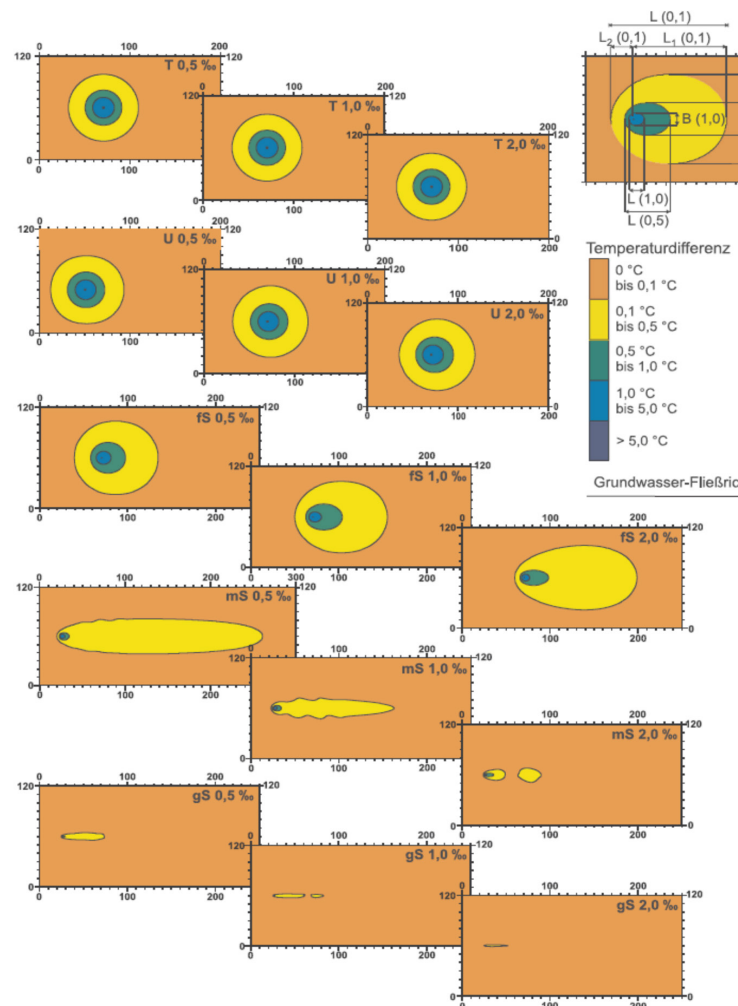


Figure 6. Development of thermal plume according to permeability (5 values, increasing from top to bottom) and hydraulic gradient (0,5%, 1% and 2%) (BRGM, 2012).

spatial heterogeneity and external inputs (e.g.: aquifer recharge or boundary conditions) (Hermans et al., 2018). In many cases, the lack of available data leads the modeler to consider homogeneous layered conceptual models (Lo Russo & Civita, 2009; Nam & Ooka, 2010; Kim et al., 2010; Yapparova et al., 2014) but bears the risk of making poorly-based decisions. As a counter-example, in the case study presented by Radioti et al. (2017), the authors showed that through a long term TRT experiment in heterogeneous geology with very low groundwater flow, the bedrock heterogeneity and the air temperature variations were not critical for a SGE system modeling.

3.3 Thermo-mechanical parameters

The design of thermoactive geostructures (energy piles, diaphragm walls or tunnel linings) must ensure that the geotechnical and structural limit states are not exceeded due to the additional stresses and strains resulting from the temperature changes imposed by their use as heat exchangers. Yet this analysis requires a few additional ground geotechnical parameters, and an understanding of how they are affected by the temperature changes, apart from those for typical ground-structure design.

The principal soil parameters needed for current geotechnical design are related to soil deformability, strength, in-situ stress state, stress history, overconsolidation ratio (OCR) and water regime. Numerous reference texts and standards are available for that issue (e.g.: Look, 2007) with particular reference to Eurocode 7 – Geotechnical Design. The supplementary information required for SGE system design, apart from that of the geostructure itself (concrete or grout thermal expansion coefficient), mainly refers to the ground thermal volumetric behavior, by means of the thermal expansion coefficient of soil, and whether there is a meaningful change of the geotechnical parameters with temperature, i.e., soil non-isothermal behaviour.

Typically, the range of temperature changes imposed in the ground by the operation of a thermoactive geostructure is relatively modest (Knellwolf et al., 2011), mostly $\pm 20^\circ\text{C}$ (Loveridge et al., 2017). Moreover, the major changes occurring in the soil are rather localized and act seasonally under a large wavelength. For these reasons, a significant change in soil geotechnical parameters under SGE operational temperature is not expected (Brandl, 2006; Loveridge et al., 2017; Insana, 2020). Nonetheless, this aspect should be considered depending on the site-specific conditions, the climatic conditions, the complexity of the project, the expected thermal demand and on the characteristics of the thermoactive geostructure.

The mechanical effect of the seasonal thermal loads in the thermoactive geostructure depends on its interaction with the surrounding ground (e.g.: Cekerevac & Laloui, 2004; Di Donna & Laloui, 2015). A comprehensive review of the main features of soil thermo-mechanical behavior

related to the operation of SGE and the main trends observed in the geotechnical parameters' evolution is described in Laloui et al. (2014). Some of this trends are as follows:

- the volumetric change depends on the loading history of soils; normally consolidated clays contract and highly overconsolidated clays dilate when heated under isotropic and drained conditions (Figure 7); normally consolidated clays show an irreversible volume change whereas highly overconsolidated clays show mostly and reversible behavior (Baldi et al., 1988; Hueckel & Baldi, 1990);
- cyclic effects have been observed in drained tests (Burghignoli et al., 1992; Vega & McCartney, 2015), small continued thermally induced changes in volume were registered after the first heating-cooling cycle;
- the effect of temperature changes on the shear strength of the soil still remains to be a subject of controversy, although a significant number of studies has been performed on this issue, some studies report that temperature increase strengthens clay, while there are many experimental results which show that an increase in temperature can slightly reduce the soil shear strength; a variety of factors might be the cause of this discrepancy, such as the soil type, mineralogy, overconsolidation ratio, drainage conditions during heating and shearing;
- oedometer test results (Campanella & Mitchell, 1968) show that the compressibility curves at different temperatures have the same slope, with lower void ratios occurring at higher temperatures; i.e. the preconsolidation pressure decreases with increasing temperature, but the compression index remains unchanged, this behavior has been confirmed by other researchers.

As above-mentioned, the temperature increase of clayey soils in normally consolidated conditions can lead

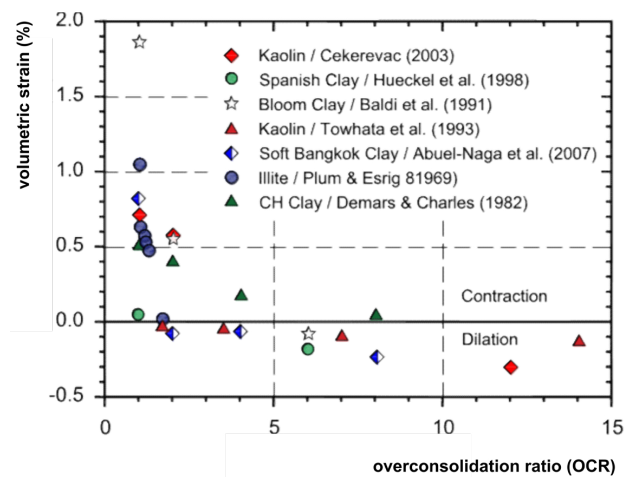


Figure 7. Effect of temperature change and OCR on volume change of saturated clays for $\Delta T 520-40^\circ\text{C}$. Adapted from Laloui et al. (2014).

to a decrease in the soil yield surface, which might induce a volumetric decrease and the occurrence of irreversible strains. This effect generally referred to as thermal compaction requires the use of thermoplastic constitutive soil models to be accounted for (e.g.: Laloui et al., 2014). These possible additional strains, namely in thermoactive floating piles, should be evaluated with adequate numerical modelling (Vieira & Maranhã, 2016). According to (Loveridge et al., 2017) the construction of geostructures in this soil conditions is more challenging

Laloui et al. (2014) also addressed the issue of the evaluation of the temperature variation at the soil/pile interface, referring the fact that stresses induced by temperature variations can be possibly neglected however, this aspect should be further validated and the maximum allowable temperature swing should be considered in the standards.

The soil volumetric expansion is of particular importance, due to its interaction effect with the concrete structure (Loveridge et al., 2017). The relative expansion between the geostructure concrete and the surrounding soil together with the geostructure constrained conditions are determining factors in the stresses and strains induced both in the concrete and in the soil. They also affect the deformation of groups of energy piles and the thermally induced deformation of the soil (Rotta Loria & Laloui, 2017).

The thermo-mechanical volumetric behavior of soil is complex due to its highly non-linear and irreversible stress-strain behavior and to its multiphase constitution. It is not possible to define a simple thermal volumetric soil thermal expansion coefficient (Mitchell, 1993) as it depends on several aspects related to the soil constitution, to the in-situ conditions (effective stresses, pore water pressure, permeability and drainage conditions) and the imposed thermal loads. However, due to the difficulty in assessing this parameter, and for simplification, a constant value is generally considered. Typical values for solid grains range from 1×10^{-5} to 3.4×10^{-5} [$^{\circ}\text{C}^{-1}$] (Delage, 2013), whilst the thermal expansion coefficient of water is 27×10^{-5} [$^{\circ}\text{C}^{-1}$]. Due to the higher value of water thermal volumetric expansion positive pore pressures can be generated during heating in clayey soils, which results in the reduction of soil effective stress. This effect is more pronounced in fully saturated conditions, decreasing significantly for reduced degrees of saturation due to the presence of air in the pores. To account for this effect, numerical modeling of the overall soil/structure system must be carried out.

The evaluation of soil thermal expansion coefficient in drained or undrained conditions depends on the rate of the thermal loading applied to the ground and soil permeability. It is assumed that, in most situations, a drained expansion should be assessed due to the slow rate of thermal loading in SGE. Globally, there is a lack of information in what concerns to the quantification of soil thermal expansion and further research is needed.

3.4 Interferences and environmental constraints

To improve the understanding of a SGE system and guarantee the service life of the geostructure, the site characterization demands further to consider possible environmental influences and influencers. Indeed, potentially, the reservoir can be used by multiple users such as other geothermal or anthropogenic activities and, subsequently, interactions can occur if a thermal plume goes through the geothermal zone of influence of another structure, giving rise to what is commonly called Thermally Affected Zone (TAZ) (Barla et al., 2020). Such condition changes the initial state of another structure with an input of a new source of energy, causing an increase or decrease in the performance of the geothermal system. The lower performance can occur when the new source of heat causes a reduction of the geothermal potential of the structure. Indeed, during summer, the geothermal buildings inject heat in the ground and cause an increase of its temperature. If the ground is already heated by another source, the injected heat decreases. It leads to a decrease of the coefficient of performance (COP) of the heat pump and increases the risk of thermal drift (Figure 8).

Hence, a thorough survey of the installations and of potential interferences must be performed, registering the presence of (Baralis, 2020; Spitler et al., 2021):

- Neighboring installations, as well as their operating features, i.e.,
 - o Open-loop systems (Aquifer Thermal Energy Storage, ATES) or
 - o Closed-loop systems (BHEs, thermoactive geostructures, etc.);
- Groundwater wells (and their interference with thermoactive geostructures and vice versa);
- City underground structures and linear infrastructures (buildings' deep basements, which could have an impact on the subsurface due to heat buildup/leakage, cables, roads and rail tunnels, metro lines, district heating networks, sewage network, buried foundations, car parking);
- Community spatial plan (future investments and projects).

However, the relevance of the above information is inversely proportional to the ease of retrieval, such as in the case of neighboring installations, especially when specific national or regional inventories are lacking. Therefore, the collection of the needed information is not an easy task at all.

For a comprehensive assessment of the initial state, besides the thermal and geotechnical design procedures, the following environmental constraints should be considered specifically for thermoactive geostructures:

- Multi-layered groundwater systems;
- Main groundwater bodies and their type (confined and artesian);

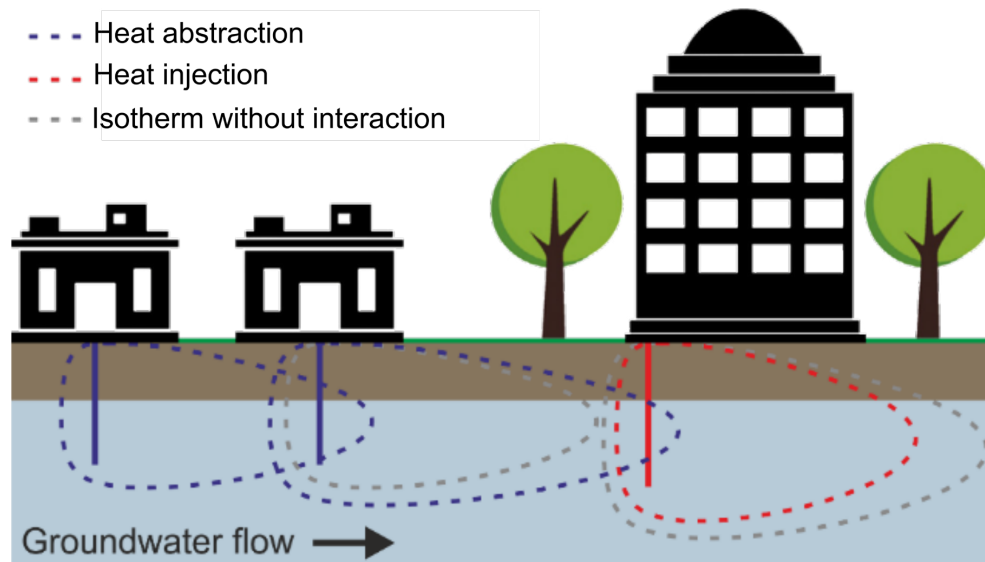


Figure 8. Schematic of interference of geothermal use in urban areas (Rivera et al., 2015).

- Neighboring sensitive buildings (mechanically influenced by thermoactive geostructure) and infrastructure;
- Polluted areas (contaminated soil, legacy pollution);
- Sensitive ecosystems (e.g.: NPWS, 2000): thermoactive geostructures may induce thermal disturbance to ecosystems (Briellmann et al., 2011), as well as impact on groundwater quality caused by induced changes to physicochemical and microbial processes;
- Surface water bodies.

4. Conclusions

For the design of Shallow Geothermal Energy (SGE) systems design service life, namely of thermoactive geostructures, a comprehensive knowledge of the ground conditions at the site is mandatory in order to ensure its energy efficacy and the non-exceedance of its structural and geotechnical limit states. The key aspects involved with site characterization were addressed in this paper, identifying the following main conclusions:

- The site characterization for shallow geothermal systems involves different stages, from desk studies to detailed characterization, including in-situ trials and laboratory testing of undisturbed soil samples;
- A preliminary design assessment represents the first step and requires the estimation of the initial conditions and the thermal properties of the soil on site, including the undisturbed ground temperature, the ground thermal conductivity, the ground volumetric heat capacity, the thermal resistance of the ground heat exchanger and the existence of a groundwater flow;
- The detailed characterization, which is needed at a later stage of the design, includes improved

characterisation of the ground mainly based of TRT, identification of the hydrogeological conditions at the site and the thermo-mechanical aspects. In addition to detailed characterization and in-situ testing, correct interpretation of the tests and influencing factors is also an important aspect that needs to be considered. It is at this stage that the evaluation of the energy features, and the extent to which the system can provide the required energy needs during the operational period, is to be conducted as well as the verification of the structural and geotechnical safety and functionality requirements;

- An additional aspect to be addressed is the identification of possible interferences, collecting information related to the environmental constraints and to existing users in the field.

The use of ground as a thermal reservoir has also brought new challenges in what concerns to its thermal characterization and modelling. Although significant knowledge has been gained in recent years further research and experience is needed. Proper input parameters in the design of thermoactive geostructures will impact the further steps in the implementation of these systems and finally their performance during exploitation. Design of these systems needs to be performed in an integrated multidisciplinary manner. Thermoactive geostructures do represent an innovative part of the SGE systems providing a series of advantages that make them a sustainable and feasible solution for both implementation and exploitation perspectives. The variety of geostructures that can be thermally activated makes of these systems very good solutions for ensuring renewable energy sources for heating and cooling especially in urban dense built environments.

Acknowledgements

The authors gratefully acknowledge Transport and Urban Development COST Action TU1405—European Network for Shallow Geothermal Energy Applications in Buildings and Infrastructures (GABI; www.foundationgeotherm.org).

Declaration of interest

The authors declare no conflict of interest.

Authors' contributions

This manuscript was initiated in the aim of Working Group 1 of COST Action TU1405 activities. Ana Vieira coordinated its realization in collaboration with Maria Alberdi-Pagola, Marco Barla, Paul Christodoulides, Alessandra Insana and Iulia Prodan forming an editorial group which has worked closely together in the final production stages and constitute the main authors of the manuscript. All authors provided technical, theoretical and practical support and approved the final version.

References

- Alberdi-Pagola, M. (2018). *Design and performance of energy pile foundations* [Doctoral thesis]. Aalborg University.
- Alberdi-Pagola, M., Poulsen, S.E., Loveridge, F., Madsen, S., & Jensen, R.L. (2018). Comparing heat flow models for interpretation of precast quadratic pile heat exchanger thermal response tests. *Energy*, 145, 721-733. <http://dx.doi.org/10.1016/j.energy.2017.12.104>.
- ASTM D4612-16. (2016). *Standard test method for calculating thermal diffusivity of rock and soil*. ASTM International, West Conshohocken. Retrieved in October 4, 2018, from <https://www.astm.org/Standards/D4612.htm>
- ASTM D5334-14. (2014). *Standard test method for determination of thermal conductivity of soil and soft rock by thermal needle probe procedure*. ASTM International, West Conshohocken. <https://doi.org/10.1520/D5334-14>.
- Austin, W.A. (2000). Development of an in-situ system and analysis procedure for measuring ground thermal properties. *ASHRAE Transactions*, 106(1), 365-379.
- Baldi, G., Hueckel, T., & Pellegrini, R. (1988). Thermal volume changes of the mineral-water system in low-porosity clay soils. *Canadian Geotechnical Journal*, 25(4), 807-825. <http://dx.doi.org/10.1139/t88-089>.
- Baralis, M. (2020). *Optimisation of geothermal resources in urban areas* [Doctoral thesis]. Politecnico di Torino.
- Baralis, M., Barla, M., Bogusz, W., Di Donna, A., Ryżyński, G., & Żeruć, M. (2020). Geothermal potential of the NE extension Warsaw (Poland) metro tunnels. *Environmental Geotechnics*, 7(4), 282-294. <http://dx.doi.org/10.1680/jenge.18.00042>.
- Barla, M., & Di Donna, A. (2018). Energy tunnels: concept and design aspects. *Underground Space*, 3(4), 268-276. <http://dx.doi.org/10.1016/j.undsp.2018.03.003>.
- Barla, M., Baralis, M., Insana, A., Aiassa, S., Antolini, F., Vigna, F., Azzarone, F., & Marchetti, P. (2021). On the thermal activation of Turin metro Line 2 tunnels. In *International Conference of the International Association for Computer Methods and Advances in Geomechanics* (pp. 1069-1076), Turin, Italy. https://doi.org/10.1007/978-3-030-64518-2_127.
- Barla, M., Di Donna, A., & Baralis, M. (2020). City scale analysis of subsoil thermal conditions due to geothermal exploitation. *Environmental Geotechnics*, 7(4), 306-316. <http://dx.doi.org/10.1680/jenge.17.00087>.
- Barla, M., Di Donna, A., & Insana, A. (2019). A novel real-scale experimental prototype of energy tunnel. *Tunnelling and Underground Space Technology*, 87, 1-14. <http://dx.doi.org/10.1016/j.tust.2019.01.024>.
- Blum, P., Campillo, G., & Kölbl, T. (2011). Techno-economic and spatial analysis of vertical ground source heat pump systems in Germany. *Energy*, 36(5), 3002-3011. <http://dx.doi.org/10.1016/j.energy.2011.02.044>.
- Bourne-Webb, P.J., Bodas Freitas, T.M., & Costa Gonçalves, R.A. (2016). Thermal and mechanical aspects of the response of embedded retaining walls used as shallow geothermal heat exchangers. *Energy and Building*, 125(C), 130-141. <http://dx.doi.org/10.1016/j.enbuild.2016.04.075>.
- Brandl, H. (2006). Energy foundations and other thermo-active ground structures. *Geotechnique*, 56(2), 81-122. <http://dx.doi.org/10.1680/geot.2006.56.2.81>.
- BRGM. (2012). *Impacts potentiels de la géothermie très basse énergie sur le sol, le sous-sol et les eaux souterraines: synthèse bibliographique*. Retrieved in October 4, 2018, from http://oai.afbiodiversite.fr/cindocoai/download/PUBLI/179/1/2012_028.pdf_3877Ko
- Brielmann, H., Lueders, T., Avramov, M., Griebler, C., Schreglmann, K., Ferraro, F., & Bayer, P. (2011). *Shallow geothermal energy usage and its potential impacts on groundwater ecosystems*. Retrieved in October 4, 2018, from <http://www.springerlink.com/openurl.asp?genre=journal&issn=1430-483X>
- Burghignoli, A., Desideri, A., & Miliziano, S.A. (1992). Deformability of clays under non-isothermal conditions. *Rivista Italiana di Geotecnica*, 4/92, 227-236.
- Campanella, R.G., & Mitchell, J.K. (1968). Influence of temperature variations on soil behavior. *Journal of the Soil Mechanics and Foundations Division*, 94(3), 709-734. <http://dx.doi.org/10.1061/JSFEAQ.0001136>.
- Cekerevac, C., & Laloui, L. (2004). Experimental study of thermal effects on the mechanical behaviour of a clay. *International Journal for Numerical and Analytical Methods in Geomechanics*, 28(3), 209-228. <http://dx.doi.org/10.1002/nag.332>.
- Christodoulides, P., Florides, G., & Pouloupatis, P. (2016). A practical method for computing the thermal properties

- of a Ground Heat Exchanger. *Renewable Energy*, 94, 81-89. <http://dx.doi.org/10.1016/j.renene.2016.03.035>.
- Claesson, J., & Hellström, G. (2000). Analytical studies of the influence of regional groundwater flow by on the performance of borehole heat exchangers. In *Proceedings: TERRASTOCK 2000*, Stuttgart, Germany. Retrieved in October 4, 2018, from [http://portal.research.lu.se/portal/en/publications/analytical-studies-of-the-influence-of-regional-groundwater-flow-by-on-the-performance-of-borehole-heat-exchangers\(e78f00aa-0d99-4611-850e-c9037ef13d10\)/bibtex.html](http://portal.research.lu.se/portal/en/publications/analytical-studies-of-the-influence-of-regional-groundwater-flow-by-on-the-performance-of-borehole-heat-exchangers(e78f00aa-0d99-4611-850e-c9037ef13d10)/bibtex.html)
- Claesson, J., & Hellström, G. (2011). Multipole method to calculate borehole thermal resistances in a borehole heat exchanger. *HVAC & R Research*, 17(6), 895-911. <http://dx.doi.org/10.1080/10789669.2011.609927>.
- Claesson, J., & Javed, S. (2020). Explicit multipole formula for the local thermal resistance in an energy pile-the line-source approximation. *Energies*, 13(20), 5445. <http://dx.doi.org/10.3390/en13205445>.
- Delage, P. (2013). On the thermal impact on the excavation damaged zone around deep radioactive waste disposal. *Journal of Rock Mechanics and Geotechnical Engineering*, 5(3), 179-190. <http://dx.doi.org/10.1016/j.jrmge.2013.04.002>.
- Di Donna, A., & Barla, M. (2016). The role of ground conditions and properties on the efficiency of energy tunnels. *Environmental Geotechnics*, 3(4), 214-224. <http://dx.doi.org/10.1680/jenge.15.00030>.
- Di Donna, A., & Laloui, L. (2015). Response of soil subjected to thermal cyclic loading: experimental and constitutive study. *Engineering Geology*, 190, 65-76. <http://dx.doi.org/10.1016/j.enggeo.2015.03.003>.
- Di Donna, A., Cecinato, F., Loveridge, F.A., & Barla, M. (2017). Energy performance of diaphragm walls used as heat exchangers. *Geotechnical Engineering*, 170(3), 232-245. <http://dx.doi.org/10.1680/jgeen.16.00092>.
- Di Donna, A., Loveridge, F., Piemontese, M., & Barla, M. (2020). The role of ground conditions on the heat exchange potential of energy walls. *Geomechanics for Energy and the Environment*, 25, 100199. <http://dx.doi.org/10.1016/j.gete.2020.100199>.
- Diao, N., Li, Q., & Fang, Z. (2004). Heat transfer in ground heat exchangers with groundwater advection. *International Journal of Thermal Sciences*, 43(12), 1203-1211. <http://dx.doi.org/10.1016/j.ijthermalsci.2004.04.009>.
- Ditlefsen, C., Sørensen, I., Slott, M., & Hansen, M. (2014). Estimating thermal conductivity from lithological descriptions: a new web-based tool for planning of ground-source heating and cooling. *Geological Survey of Denmark and Greenland*, 31, 55-58. <http://dx.doi.org/10.34194/geusb.v31.4660>.
- Dong, Y., McCartney, J.S., & Lu, N. (2015). Critical review of thermal conductivity models for unsaturated soils. *Geotechnical and Geological Engineering*, 33(2), 207-221. <http://dx.doi.org/10.1007/s10706-015-9843-2>.
- Dornberger, S.C., Rotta Loria, A.F., Zhang, M., Bu, L., Epard, J.-L., & Turberg, P. (2020). Heat exchange potential of energy tunnels for different internal airflow characteristics. *Geomechanics for Energy and the Environment*, 100229. In press. <http://dx.doi.org/10.1016/j.gete.2020.100229>.
- Epting, J., Baralis, M., Künze, R., Mueller, M.H., Insana, A., Barla, M., & Huggenberger, P. (2020). Geothermal potential of tunnel infrastructures – development of tools at the city-scale of Basel, Switzerland. *Geothermics*, 83, 101734. <http://dx.doi.org/10.1016/j.geothermics.2019.101734>.
- Fan, R., Jiang, Y., Yao, Y., Shiming, D., & Ma, Z. (2007). A study on the performance of a geothermal heat exchanger under coupled heat conduction and groundwater advection. *Energy*, 32(11), 2199-2209. <http://dx.doi.org/10.1016/j.energy.2007.05.001>.
- Farouki, O.T. (1981). *Thermal properties of soils*. U.S. Army Corps of Engineers, Hanover. <http://dx.doi.org/10.21236/ADA111734>.
- Fujii, H., Okubo, H., Nishi, K., Itoi, R., Ohya, K., & Shibata, K. (2009). An improved thermal response test for U-tube ground heat exchanger based on optical fiber thermometers. *Geothermics*, 38(4), 399-406. <http://dx.doi.org/10.1016/j.geothermics.2009.06.002>.
- Gehlin, S. (2002). *Thermal response test: method development and evaluation* [Doctoral thesis]. Luleå University of Technology.
- Geothermische Screeningstool. (2017). Retrieved in October 4, 2018, from <http://tool.smartgeotherm.be/geo/alg>
- GSHPA. (2012). *Thermal pile: design, installation & materials standards*. Ground Source Heat Pump Association, Milton Keynes. Retrieved in February 8, 2022, from http://www.gshp.org.uk/pdf/GSHPA_Thermal_Pile_Standard.pdf
- Hellström, G. (1991). *Ground heat storage: thermal analyses of duct storage systems. I. Theory* (Vol. 1). Department of Mathematical Physics, University of Lund, Lund. Retrieved in February 8, 2022, from <http://books.google.dk/books?id=Ox6lRwAACAAJ>
- Hermans, T., Nguyen, F., Klepikova, M., Dassargues, A., & Caers, J. (2018). Uncertainty quantification of medium-term heat storage from short-term geophysical experiments using Bayesian evidential learning. *Water Resources Research*, 54(4), 2931-2948. <http://dx.doi.org/10.1002/2017WR022135>.
- Hermans, T., Nguyen, F., Robert, T., & Revil, A. (2014). Geophysical methods for monitoring temperature changes in shallow low enthalpy geothermal systems. *Energies*, 7(8), 5083-5118. <http://dx.doi.org/10.3390/en7085083>.
- Hueckel, T., & Baldi, G. (1990). Thermoplasticity of saturated clays: experimental constitutive study. *Journal of the Geotechnical Engineering Division*, 116(12), 1778-1796. [http://dx.doi.org/10.1061/\(ASCE\)0733-9410\(1990\)116:12\(1778\)](http://dx.doi.org/10.1061/(ASCE)0733-9410(1990)116:12(1778)).
- Insana, A. (2020). *Thermal and structural performance energy tunnels* [Doctoral thesis]. Université Paris-Est, Politecnico di Torino.
- Insana, A., & Barla, M. (2020). Experimental and numerical investigations on the energy performance of a thermo-

- active tunnel. *Renewable Energy*, 152, 781-792. <http://dx.doi.org/10.1016/j.renene.2020.01.086>.
- Insana, A., Barla, M., & Sulem, J. (2020). Energy tunnel linings thermo-mechanical performance: comparison between field observations and numerical modelling. *E3S Web of Conferences*, 205, 6008. <http://dx.doi.org/10.1051/e3sconf/202020506008>.
- Javed, S., Ørnes, I.R., Myrup, M., & Dokka, T.H. (2019). Design optimization of the borehole system for a plus-Energy kindergarten in Oslo, Norway. *Architectural Engineering and Design Management*, 15(3), 181-195. <http://dx.doi.org/10.1080/17452007.2018.1555088>.
- Javed, S., Spitler, J.D., & Fahlén, P. (2011). An experimental investigation of the accuracy of thermal response tests used to measure ground thermal properties. *ASHRAE Transactions*, 117(1), 13-21.
- Kim, E.J., Roux, J.J., Rusaouen, G., & Kuznik, F. (2010). Numerical modelling of geothermal vertical heat exchangers for the short time analysis using the state model size reduction technique. *Applied Thermal Engineering*, 30(6-7), 706-714. <http://dx.doi.org/10.1016/j.applthermaleng.2009.11.019>.
- Klepikova, M., Wildemeersch, S., Hermans, T., Jamin, P., Orban, P., Nguyen, F., Brouyère, S., & Dassargues, A. (2016). Heat tracer test in an alluvial aquifer: field experiment and inverse modelling. *Journal of Hydrology*, 540, 812-823. <http://dx.doi.org/10.1016/j.jhydrol.2016.06.066>.
- Knellwolf, C., Peron, H., & Laloui, L. (2011). Geotechnical analysis of heat exchanger piles. *Journal of Geotechnical and Geoenvironmental Engineering*, 137(10), 890-902. [http://dx.doi.org/10.1061/\(ASCE\)GT.1943-5606.0000513](http://dx.doi.org/10.1061/(ASCE)GT.1943-5606.0000513).
- Kuo, C., & Liao, H. (2012). The feasibility of using circulating groundwater as renewable energy sources for air-conditioning in Taipei basin. *Renewable Energy*, 39(1), 175-182. <http://dx.doi.org/10.1016/j.renene.2011.07.046>.
- Laloui, L., & François, B. (2009). ACMEG-T: soil thermoplasticity model. *Journal of Engineering Mechanics*, 135(9), 932-944. [http://dx.doi.org/10.1061/\(ASCE\)EM.1943-7889.0000011](http://dx.doi.org/10.1061/(ASCE)EM.1943-7889.0000011).
- Laloui, L., & Rotta Loria, A. (2020). *Analysis and design of energy geostructures*. Academic Press, London.
- Laloui, L., Olgun, C.G., Sutman, M., McCartney, J.S., Coccia, C.J., Abuel-Naga, H.M., & Bowers, G.A. (2014). Issues involved with thermoactive geotechnical systems: characterization of thermomechanical soil behavior and soil-structure interface behavior. *Journal of the Deep Foundations Institute*, 8(2), 108-120. <http://dx.doi.org/10.1179/1937525514Y.0000000010>.
- Lee, S., Park, S., Won, J., & Choi, H. (2021). Influential factors on thermal performance of energy slabs equipped with an insulation layer. *Renewable Energy*, 174, 823-834. <http://dx.doi.org/10.1016/j.renene.2021.04.090>.
- Lo Russo, S., & Civita, M.V. (2009). Open-loop groundwater heat pumps development for large buildings: a case study. *Geothermics*, 38(3), 335-345. <http://dx.doi.org/10.1016/j.geothermics.2008.12.009>.
- Look, B. (2007). Geotechnical investigation and design tables. In R.W. Sarsby & A.J. Felton (Eds.), *Balkema: Proceedings and Monographs in Engineering, Water and Earth Science* (Vol. 91). Taylor & Francis, London.
- Loveridge, F., & Powrie, W. (2013). Temperature response functions (G-functions) for single pile heat exchangers. *Energy*, 57(0), 554-564. <http://dx.doi.org/10.1016/j.energy.2013.04.060>.
- Loveridge, F., & Powrie, W. (2014). G-functions for multiple interacting pile heat exchangers. *Energy*, 64, 747-757. <http://dx.doi.org/10.1016/j.energy.2013.11.014>.
- Loveridge, F., Brettmann, T., Olgun, C.G., & Powrie, W. (2014). Assessing the applicability of thermal response testing to energy piles. In *Proceedings of the Global Perspective on Sustainable Execution of Deep Foundation Works*, Sweden.
- Loveridge, F., Low, J., & Powrie, W. (2017). Site investigation for energy geostructures. *Quarterly Journal of Engineering Geology and Hydrogeology*, 50(2), 158-168. <http://dx.doi.org/10.1144/qjegh2016-027>.
- Loveridge, F., McCartney, J.S., Narsilio, G.A., & Sanchez, M. (2020). Energy geostructures: a review of analysis approaches, in situ testing and model scale experiments. *Geomechanics for Energy and the Environment*, 22, 100173. <http://dx.doi.org/10.1016/j.gete.2019.100173>.
- Ma, C., Di Donna, A., Dias, D., & Zhang, J. (2021). Numerical investigations of the tunnel environment effect on the performance of energy tunnels. *Renewable Energy*, 172, 1279-1292. <http://dx.doi.org/10.1016/j.renene.2021.03.104>.
- Ma, X., & Grabe, J. (2010). Efficiency Increase of soil heat exchangers due to groundwater flow and air injection. In *Proceedings of the World Geothermal Congress 2010*, Bali, Indonesia.
- Macfarlane, A., Förster, A., Merriam, D., Schrötter, J., & Healey, J. (2002). Monitoring artificially stimulated fluid movement in the Cretaceous Dakota aquifer, Western Kansas. *Hydrogeology Journal*, 10(6), 662-673. <http://dx.doi.org/10.1007/s10040-002-0223-7>.
- Mitchell, J.K. (1993). *Fundamentals of soil behavior*. Wiley, Hoboken. Retrieved in February 8, 2022, from https://books.google.dk/books?id=aw_Gpm_SWJAC
- Nam, Y., & Ooka, R. (2010). Numerical simulation of ground heat and water transfer for groundwater heat pump system based on real-scale experiment. *Energy and Building*, 42(1), 69-75. <http://dx.doi.org/10.1016/j.enbuild.2009.07.012>.
- NPWS. (2000). *Natura 2000*. Retrieved in February 8, 2022, from <https://www.npws.ie/faq/natura2000>
- Oladunjoye, M.A., & Sanuade, O.A. (2012). Thermal diffusivity, thermal effusivity and specific heat of soils in Olorunsogo Powerplant, southwestern Nigeria. *International Journal of Research and Reviews in Applied Sciences*, 13(2), 502-521.
- Palmer, C.D., Blowes, D.W., Frind, E.O., & Molson, J.W. (1992). Thermal energy storage in an unconfined aquifer: 1. Field Injection Experiment. *Water Resources Research*, 28(10), 2845-2856. <http://dx.doi.org/10.1029/92WR01471>.
- Popov, Y.A., Pribnow, D.F.C., Sass, J.H., Williams, C.F., & Burkhardt, H. (1999). Characterization of rock thermal

- conductivity by high-resolution optical scanning. *Geothermics*, 28(2), 253-276. [http://dx.doi.org/10.1016/S0375-6505\(99\)00007-3](http://dx.doi.org/10.1016/S0375-6505(99)00007-3).
- Radioti, G., Sartor, K., Charlier, R., Dewallef, P., & Nguyen, F. (2017). Effect of undisturbed ground temperature on the design of closed-loop geothermal systems: a case study in a semi-urban environment. *Applied Energy*, 200, 89-105. <http://dx.doi.org/10.1016/j.apenergy.2017.05.070>.
- Ramstad, R.K., Midttømme, K., Liebel, H.T., Frengstad, B.S., & Willemoes-Wissing, B. (2015). Thermal conductivity map of the Oslo region based on thermal diffusivity measurements of rock core samples. *Bulletin of Engineering Geology and the Environment*, 74(4), 1275-1286. <http://dx.doi.org/10.1007/s10064-014-0701-x>.
- Rees, S. (2016). *Advances in ground-source heat pump systems*. Woodhead Publishing, Duxford. <http://dx.doi.org/10.1016/B978-0-08-100311-4.09001-4>.
- Rees, S.W., Adjali, M.H., Zhou, Z., Davies, M., & Thomas, H.R. (2000). Ground heat transfer effects on the thermal performance of earth-contact structures. *Renewable & Sustainable Energy Reviews*, 4(3), 213-265. [http://dx.doi.org/10.1016/S1364-0321\(99\)00018-0](http://dx.doi.org/10.1016/S1364-0321(99)00018-0).
- Reiffsteck, P., Couaillier, M., & Grandjean, G. (2015). Validation d'un système de classification thermique des sols. In *Journées Nationales de Géotechnique et de Géologie de l'Ingénieur JNGG2014*, Beauvais.
- Rivera, J.A., Blum, P., & Bayer, P. (2015). Analytical simulation of groundwater flow and land surface effects on thermal plumes of borehole heat exchangers. *Applied Energy*, 146, 421-433. <http://dx.doi.org/10.1016/j.apenergy.2015.02.035>.
- Rotta Loria, A.F., & Laloui, L. (2017). *Impact of thermally induced soil deformation on the serviceability of energy pile groups* (pp. 421-428). Springer, Cham. http://dx.doi.org/10.1007/978-3-319-52773-4_50.
- Rotta Loria, A.F., Di Donna, A., & Laloui, L. (2015). Numerical study on the suitability of centrifuge testing for capturing the thermal-induced mechanical behavior of energy piles. *Journal of Geotechnical and Geoenvironmental Engineering*, 141(10), 4015042. [http://dx.doi.org/10.1061/\(ASCE\)GT.1943-5606.0001318](http://dx.doi.org/10.1061/(ASCE)GT.1943-5606.0001318).
- Sanner, B., Mands, E., Sauer, M., & Grundmann, E. (2007). Technology, development status, and routine application of Thermal Response Test. In *Proceedings of the European Geothermal Congress 2007* (Vol. 30), Unterhaching, Germany.
- Shafagh, I., & Rees, S.J. (2019). Analytical investigations into thermal resistance of diaphragm wall heat exchangers. In *Proceedings of the European Geothermal Congress*, The Hague, The Netherlands.
- Shafagh, I., Rees, S., & Loveridge, F. (2020). Investigations into thermal resistance of tunnel lining heat exchangers. *E3S Web of Conferences*, 205, 06006. <http://dx.doi.org/10.1051/e3sconf/202020506006>.
- SIA. (2005). *Utilisation de la chaleur du sol par des ouvrages de fondation et de soutènement en béton: guide pour la conception, la réalisation et la maintenance*. Société Suisse des Ingénieurs et des Architectes, Zurich. Retrieved in October 1, 2018, from <http://books.google.dk/books?id=KiSommer>.
- Sommer, W., Valstar, J., van Gaans, P., Grotenhuis, T., & Rijnaarts, H. (2013). The impact of aquifer heterogeneity on the performance of aquifer thermal energy storage. *Water Resources Research*, 49(12), 8128-8138. <http://dx.doi.org/10.1002/2013WR013677>.
- Sommer, W.T., Doornenbal, P.J., Drijver, B.C., van Gaans, P.F.M., Leusbrock, I., Grotenhuis, J.T.C., & Rijnaarts, H.H.M. (2014). Thermal performance and heat transport in aquifer thermal energy storage. *Hydrogeology Journal*, 22(1), 263-279. <http://dx.doi.org/10.1007/s10040-013-1066-0>.
- Spitler, J.D., & Gehlin, S.E.A. (2015). Thermal response testing for ground source heat pump systems: an historical review. *Renewable & Sustainable Energy Reviews*, 50, 1125-1137. <http://dx.doi.org/10.1016/j.rser.2015.05.061>.
- Spitler, J.D., Mitchell, M.S., & Gehlin, S. (2021). Use of cross g-functions to calculate interference between ground heat exchangers used in ground-source heat pump systems. In *Proceedings World Geothermal Congress 2*, Reykjavik, Iceland.
- Suryatriyastuti, M. (2013). *Numerical study of the thermoactive piles behavior in cohesionless soils*. Retrieved in October 1, 2018, from <https://www.researchgate.net/publication/259829225>.
- ThermoMap. (2013). *ThermoMap MapViewer*. Retrieved in October 1, 2018, from <http://geoweb2.sbg.ac.at/thermomap/>.
- VDI 4640. (2010). *Thermal use of the underground. Part 1: Fundamentals, approvals, environmental aspects*. Berlin.
- Vega, A., & McCartney, J.S. (2015). Cyclic heating effects on thermal volume change of silt. *Environmental Geotechnics*, 2(5), 257-268. <http://dx.doi.org/10.1680/envgeo.13.00022>.
- Vieira, A., & Maranhã, J.R. (2016). Thermoplastic analysis of a thermoactive pile in a normally consolidated clay. *International Journal of Geomechanics*, 17(1), 04016030. [http://dx.doi.org/10.1061/\(ASCE\)GM.1943-5622.0000666](http://dx.doi.org/10.1061/(ASCE)GM.1943-5622.0000666).
- Vieira, A., Alberdi-Pagola, M., Christodoulides, P., Javed, S., Loveridge, F., Nguyen, F., Cecinato, F., Maranhã, J., Florides, G., Prodan, I., Van Lysebetten, G., Ramalho, E., Salciarini, D., Georgiev, A., Rosin-Paumier, S., Popov, R., Lenart, S., Poulsen, S.E., & Radioti, G. (2017). Characterisation of ground thermal and thermo-mechanical behaviour for shallow geothermal energy applications. *Energies*, 10(12), 2044. <http://dx.doi.org/10.3390/en10122044>.
- Wagner, R., & Clauser, C. (2005). Evaluating thermal response tests using parameter estimation for thermal conductivity and thermal capacity. *Journal of Geophysics and Engineering*, 2(4), 349-356. <http://dx.doi.org/10.1088/1742-2132/2/4/S08>.
- Yang, H., Memon, S.A., Bao, X., Cui, H., & Li, D. (2017). Design and preparation of carbon based composite phase change material for energy piles. *Materials*, 10(4), 391. <http://dx.doi.org/10.3390/ma10040391>.
- Yapparova, A., Matthäi, S., & Driesner, T. (2014). Realistic simulation of an aquifer thermal energy storage: effects of injection temperature, well placement and groundwater flow. *Energy*, 76, 1011-1018. <http://dx.doi.org/10.1016/j.energy.2014.09.018>.



The Ground is our Challenge

MAIN ACTIVITY AREAS

Consultancy, Supervision and Training

- Earth Retaining Structures
- Special Foundations
- Ground Improvement
- Foundations Strengthening and Underpinning
- Façades Retention
- Tunnels and Underground Structures
- Slope Stability
- Geological and Geotechnical Investigation
- Demolition

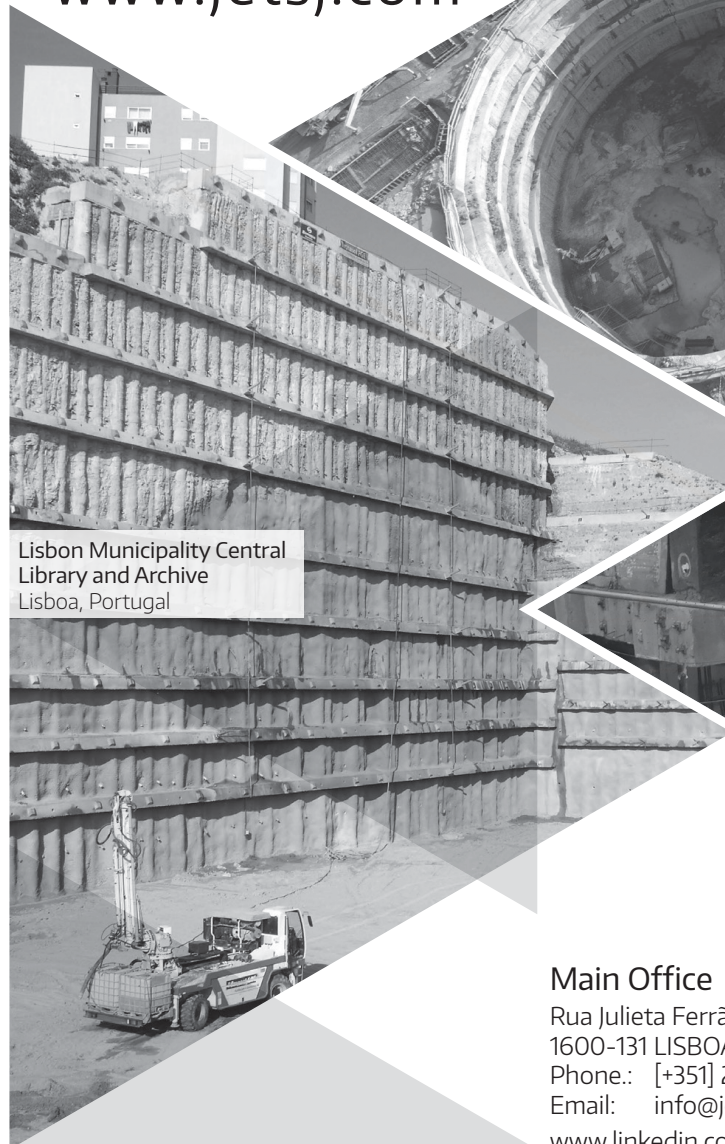
www.jetsj.com



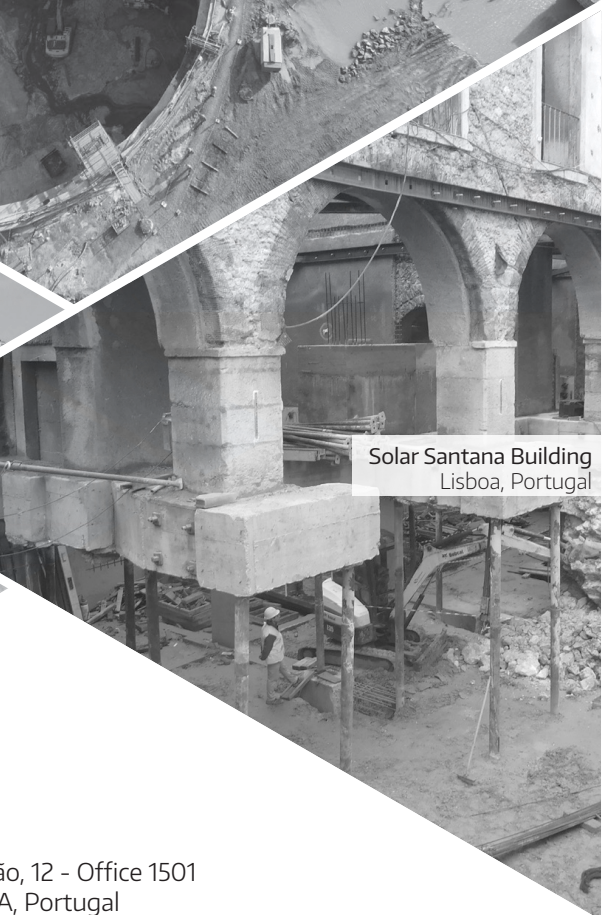
Tool Plazas P2 and P3
Santa Catarina, Brazil



Mining Shaft
Kamsar, Guiné



Lisbon Municipality Central
Library and Archive
Lisboa, Portugal



Solar Santana Building
Lisboa, Portugal

Main Office

Rua Julieta Ferrão, 12 - Office 1501

1600-131 LISBOA, Portugal

Phone.: [+351] 210 505 150 / 51

Email: info@jetsj.com

www.linkedin.com/company/jetsj-geotecnia-lda/



- > **Prospecção Geotécnica**
Site Investigation
- > **Consultoria Geotécnica**
Geotechnical Consultancy
- > **Obras Geotécnicas**
Ground Treatment-Construction Services
- > **Controlo e Observação**
Field Instrumentation Services and Monitoring Services
- > **Laboratório de Mecânica de Solos**
Soil and Rock Mechanics Laboratory

Certificada ISO 9001 por



Parque Oriente, Bloco 4, EN10
2699-501 Bobadela LRS
Tel. 21 995 80 00
Fax. 21 995 80 01
e.mail: mail@geocontrolo.pt
www.geocontrolo.pt


Geocontrolo
Geotecnia e Estruturas de Fundação SA

BELGO GABION. THE BEST CHOICE TO INCREASE YOUR CONSTRUCTION QUALITY.



Belgo Geotech provides steel solutions, for geotechnical applications, to the market. Our products include **gabions**, **rockfall mesh**, **Dramix®** steel fibers, **galvanized pannels** and **meshes for rock support** and **reinforcement systems**, **PC Strand for cable bolts** and **thread bars**. We also offer qualified technical support to meet all of your project's needs. **Our geotechnics feature the strength of steel.**



Learn more at: belgogeotech.com.br

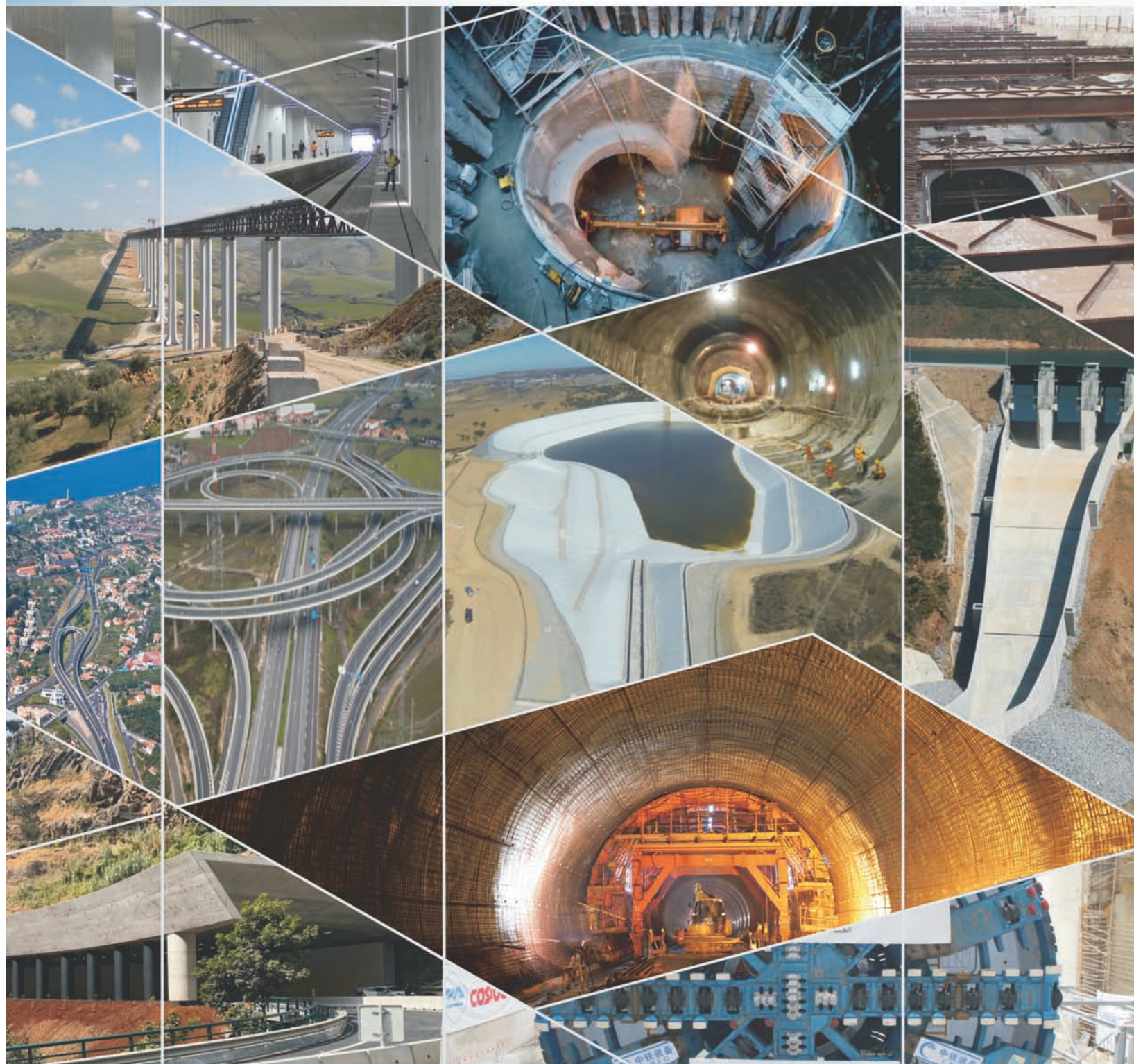
BELGO
GeoTech

Belgo Bekaert Arames

ArcelorMittal

BEKAERT
better together

BUILDING THE WORLD, BETTER



Engineering and Architectural Consultancy

Geology, Geotechnics, Supervision of Geotechnical Works
Embankment Dams, Underground Works, Retaining Structures
Special Foundations, Soil Improvement, Geomaterials



MEMBER OF

TPF - CONSULTORES DE ENGENHARIA E ARQUITETURA, S.A.

www.tpf.pt

40
years

DF+, YOUR TRUST FIRST

GEOLOGICAL, GEOTECHNICAL
ENGINEERING AND WATER
RESOURCES SOLUTIONS FOR THE
MINING SECTOR AND OTHERS.



DF+ IS A COMPANY WITH A FOCUS ON THE MINERAL SECTOR AND MORE THAN 15 YEARS OF EXPERIENCE. WE OPERATE IN ALL PHASES OF A PROJECT, FROM FEASIBILITY STUDIES AND PROJECT DEVELOPMENT TO TECHNICAL MONITORING OF CONSTRUCTION AND MINE CLOSURE.

JOIN OUR SOCIAL NETWORKS TO
KNOW MORE ABOUT OUR SERVICES.



AVE BARÃO HOMEM DE MELO, 4554 - 5th floor
ESTORIL, BELO HORIZONTE/MG

+55 31 2519-1001

comercial@dfmais.eng.br



DF+ GEOTECHNICAL ENGINEERING
AND WATER RESOURCES

PIONEERING AND INNOVATION

SINCE 1921

 **TEIXEIRA DUARTE**
ENGENHARIA E CONSTRUÇÕES, S.A.

PORT FACILITY CONSTRUCTION
NACALA - MOZAMBIQUE



Building a better world.
teixiraduarteconstruction.com



Safety is our nature

SISTEMAS DE ALERTA E MONITORAMENTO

Sistemas de Alerta e Alarme

Ideal para identificação de agentes
deflagradores e monitoramento de
eventos

Rua Visconde de Pirajá, 82 | Ipanema
22410-003 | Rio de Janeiro | RJ | Brasil.
Tel.: + 55 21 3624.1449
www.geobrugg.com



Parceria:



The Best Solution!

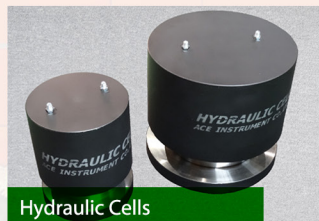
Tecnilab Portugal, S.A. will provide you with answers to your Geotechnical engineering needs.

Tecnilab Portugal, S.A. is a professional Geotechnical engineering company and has a lot of experience as a professional group that mainly engages in measurement engineering in dam, subway(Metro), harbor, power plant, soft ground and structure construction.

WE ARE THE DISTRIBUTOR OF PORTUGAL OF ACE INSTRUMENT CO., LTD. IN KOREA.

ACE INSTRUMENT CO., LTD. is a company that obtains worldwide reputation for supplying high precision, high reliability products in all Geotechnical instruments, data logger and in-situ test equipments. Independently developed automatic monitoring system can be used anywhere in the world, including buildings, bridges, ground and any constructions.

Data Acquisition System & Web Monitoring Program



Sales company



Tecnilab Portugal, S.A.

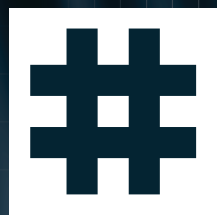
A: Rua Gregorio Lopes, Lote 1512B 1449-041 Lisboa Portugal
T: +351 217 220 870 F: +351 217 264 550
www.tecnilab.pt

Manufacturer



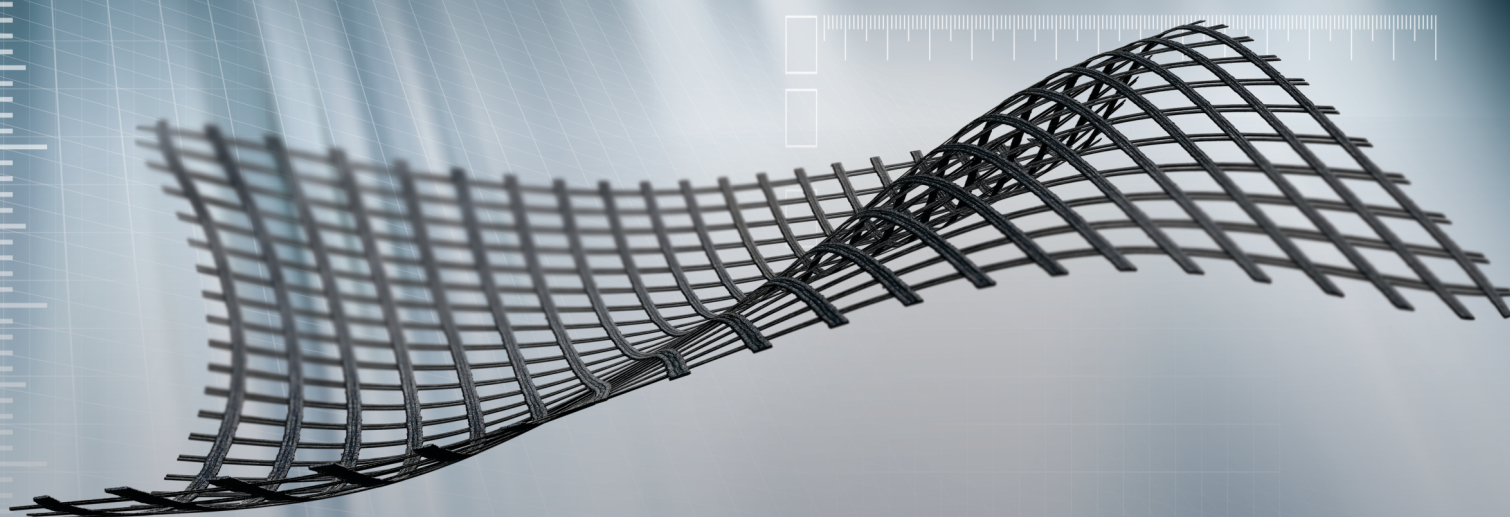
ACE INSTRUMENT CO., LTD.

The first value in Geotechnical & Structural Instrumentation
A: 9, Dangjung-ro 27 beon-gil, Gunpo-si, Gyeonggi-do, Korea
T: +82 31 459 8753-7 F: +82 31 459 8758 E: acens@naver.com
www.aceinstrument.com



HUESKER

Ideen. Ingenieure. Innovationen.



LEADER IN GEOSYNTHETICS

Experience HUESKER's geosynthetic building materials, systems and services now.



www.HUESKER.com

Find HUESKER in Social Media:



ENGINEERING AND ENVIRONMENTAL CONSULTANTS



COBA



GEOLOGY AND GEOTECHNICS

Hydrogeology • Engineering Geology • Rock Mechanics • Soil Mechanics • Foundations and Retaining Structures • Underground Works • Embankments and Slope Stability
Environmental Geotechnics • Geotechnical Mapping



- Water Resources Planning and Management
- Hydraulic Undertakings
- Electrical Power Generation and Transmission
- Water Supply Systems and Pluvial and Wastewater Systems
- Agriculture and Rural Development
- Road, Railway and Airway Infrastructures
- Environment
- Geotechnical Structures
- Cartography and Cadastre
- Safety Control and Work Rehabilitation
- Project Management and Construction Supervision



PORTUGAL

CENTER AND SOUTH REGION
Av. 5 de Outubro, 323
1649-011 LISBOA
Tel.: (351) 210125000, (351) 217925000
Fax: (351) 217970348
E-mail: coba@coba.pt
www.coba.pt

Av. Marquês de Tomar, 9, 6º.
1050-152 LISBOA
Tel.: (351) 217925000
Fax: (351) 213537492

NORTH REGION

Rua Mouzinho de Albuquerque, 744, 1º.
4450-203 MATOSINHOS
Tel.: (351) 229380421
Fax: (351) 229373648
E-mail: engico@engico.pt

ANGOLA

Praceta Farinha Leitão, edifício nº 27, 27-A - 2º Dto
Bairro do Maculusso, LUANDA
Tel./Fax: (244) 222338 513
Cell: (244) 923317541
E-mail: coba-angola@netcabo.co.ao

MOZAMBIQUE

Pestana Rovuma Hotel. Centro de Escritórios.
Rua da Sé nº114. Piso 3, MAPUTO
Tel./Fax: (258) 21 328 813
Cell: (258) 82 409 9605
E-mail: coba.mz@tdm.co.mz

ALGERIA

09, Rue des Frères Hocine
El Biar - 16606, ARGEL
Tel.: (213) 21 922802
Fax: (213) 21 922802
E-mail: coba.alger@gmail.com

BRAZIL

Rio de Janeiro
COBA Ltd. - Rua Bela 1128
São Cristóvão
20930-380 Rio de Janeiro RJ
Tel.: (55 21) 351 50 101
Fax: (55 21) 258 01 026

Fortaleza

Av. Senador Virgílio Távora 1701, Sala 403
Aldeota - Fortaleza CEP 60170 - 251
Tel.: (55 85) 3261 17 38
Fax: (55 85) 3261 50 83
E-mail: coba@esc-te.com.br

UNITED ARAB EMIRATES

Corniche Road - Corniche Tower - 5th Floor - 5B
P.O. Box 38360 ABU DHABI
Tel.: (971) 2 627 0088
Fax: (971) 2 627 0087

MACCAFERRI

Learn more about GAWAC® 3.0 software

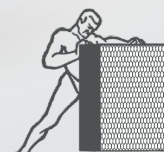
Developed to support engineers, designers and students in a fast and reliable way to perform the analyzes of gabion retaining wall.

The great advantage of **GAWAC® 3.0** is the inclusion of the stability analysis in serviceability conditions, through the GSC (Gabion Serviceability Coefficient). This type of analysis allows the user to evaluate the cross sections of the gabion walls in the most suitable conditions through the best performance and optimization of the gabion materials. The software allows the user to choose the type of gabion with the coating and mesh technologically appropriate to the work environment, in addition to allowing the use of international standards, various calculation analyzes with a detailed printable report.



NEW SOFTWARE FEATURES

- **New user-friendly** interface;
- Consider the **influence of the mesh**;
- **Service Limit State (SLS) and Ultimate Limit State (ULS)** are considered in the stability analysis;
- Consider the **long-term performance of the gabion** based on the type of mesh and coating;
- **Serviceability conditions** performed by layer;
- Optimized design with the use of **Strong Face Gabion**.



GABION
STRONG
FACE



Visit our website to **learn more**
about Strong Face Gabion and
download **GAWAC® 3.0**.



/maccaferri



/maccaferriamatrix



@Maccaferri_BR



/MaccaferriWorld



/maccaferriworld

Guide for Authors

Soils and Rocks is an international scientific journal published by the Brazilian Association for Soil Mechanics and Geotechnical Engineering (ABMS) and by the Portuguese Geotechnical Society (SPG). The aim of the journal is to publish original papers on all branches of Geotechnical Engineering. Each manuscript is subjected to a single-blind peer-review process. The journal's policy of screening for plagiarism includes the use of a plagiarism checker on all submitted manuscripts.

Soils and Rocks embraces the international Open Science program and is striving to meet all the recommendations. However, at this moment, the journal is not yet accepting preprints and open data, and has not adopted open peer reviews.

Soils and Rocks provides a manuscript template available at the journal's website.

1. Category of papers

Submissions are classified into one of the following categories:

Article – an extensive and conclusive dissertation about a geotechnical topic, presenting original findings.

Technical Note – presents a study of smaller scope or results of ongoing studies, comprising partial results and/or particular aspects of the investigation.

Case Study – report innovative ways to solve problems associated with design and construction of geotechnical projects. It also presents studies of the performance of existing structures.

Review Article – a summary of the State-of-the-Art or State-of-the-Practice on a particular subject or issue and represents an overview of recent developments.

Discussion – specific discussions about published papers.

Authors are responsible for selecting the correct category when submitting their manuscript. However, the manuscript category may be altered based on the recommendation of the Editorial Board. Authors are also requested to state the category of paper in their Cover Letter.

When submitting a manuscript for review, the authors should indicate the category of the manuscript, and is also understood that they:

- a) assume full responsibility for the contents and accuracy of the information in the paper;
- b) assure that the paper has not been previously published, and is not being submitted to any other journal for publication.

2. Paper length

Full-length manuscripts (Article, Case Study) should be between 4,000 and 8,000 words. Review articles should have up to 10,000 words. Technical Notes have a word count limit of 3,500 words. Discussions have a word count limit of 1,000 words. These word count limits exclude the title page, notation list (e.g., symbols, abbreviations), captions of tables and figures, acknowledgments and references. Each single column and double column figure or table is considered as equivalent to 150 and 300 words, respectively.

3. Scientific style

The manuscripts should be written in UK or US English, in the third person and all spelling should be checked in accordance with

a major English Dictionary. The manuscript should be able to be readily understood by a Civil Engineer and avoid colloquialisms. Unless essential to the comprehension of the manuscript, direct reference to the names of persons, organizations, products or services is not allowed. Flattery or derogatory remarks about any person or organization should not be included.

The author(s) of Discussion Papers should refer to himself (herself/themselves) as the reader(s) and to the author(s) of the paper as the author(s).

The International System (SI) units must be used. The symbols are recommended to be in accordance with Lexicon in 14 Languages, ISSMFE (2013) and the ISRM List of Symbols. Use italics for single letters that denote mathematical constants, variables, and unknown quantities, either in tables or in the text.

4. Submission requirements and contents

A submission implies that the following conditions are met:

- the authors assume full responsibility for the contents and accuracy of the information presented in the paper;
- the manuscript contents have not been published previously, except as a lecture or academic thesis;
- the manuscript is not under consideration for publication elsewhere;
- the manuscript is approved by all authors;
- the manuscript is approved by the necessary authorities, when applicable, such as ethics committees and institutions that may hold intellectual property on contents presented in the manuscript;
- the authors have obtained authorization from the copyright holder for any reproduced material;
- the authors are aware that the manuscript will be subjected to plagiarism check.

The author(s) must upload two digital files of the manuscript to the Soils and Rocks submission system. The size limit for each submission file is 20 MB. The manuscript should be submitted in docx format (Word 2007 or higher) or doc format (for older Word versions). An additional PDF format file of the manuscript is also required upon submission. Currently, the journal is not accepting manuscripts prepared using LaTeX.

The following documents are required as minimum for submission:

- cover letter;
- manuscript with figures and tables embedded in the text (doc or docx format);

manuscript with figures and tables embedded in the text for revision (PDF format);

- permission for re-use of previously published material when applicable, unless the author/owner has made explicit that the image is freely available.

4.1 Cover letter

The cover letter should include: manuscript title, submission type, authorship information, statement of key findings and work novelty, and related previous publications if applicable.

4.2 Title page

The title page is the first page of the manuscript and must include:

- A concise and informative title of the paper. Avoid abbreviations, acronyms or formulae. Discussion Papers should contain the title of the paper under discussion. Only the first letter of the first word should be capitalized.
- Full name(s) of the author(s). The first name(s) should not be abbreviated. The authors are allowed to abbreviate middle name(s).
- The corresponding author should be identified by a pound sign # beside his/her and in a footnote.
- The affiliation(s) of the author(s), should follow the format: Institution, (Department), City, (State), Country.
- Affiliation address and e-mail must appear below each author's name.
- The 16-digit ORCID of the author(s) – mandatory
- Main text word count (excluding abstract and references) and the number of figures and tables

4.3 Permissions

Figures, tables or text passages previously published elsewhere may be reproduced under permission from the copyright owner(s) for both the print and online format. The authors are required to provide evidence that such permission has been granted at the moment of paper submission.

4.4 Declaration of interest

Authors are required to disclose conflicting interests that could inappropriately bias their work. For that end, a section entitled “Declaration of interest” should be included following any acknowledgments and prior to the “Authors’ contributions” section. In case of the absence of conflicting interests, the authors should still include a declaration of interest.

4.5 Authors’ contributions

Authors are required to include an author statement outlining their individual contributions to the paper according to the CASRAI CRediT roles (as per <https://casrai.org/credit>). The minimum requirements of contribution to the work for recognition of authorship are: a) Participate actively in the discussion of results; b) Review and approval of the final version of the manuscript. A section entitled “Authors’ contributions” should be included after the declaration of interest section, and should be formatted with author's name and CRediT role(s), according to the example:

Samuel Zheng: conceptualization, methodology, validation. **Olivia Prakash:** data curation, writing - original draft preparation. **Fatima Wang:** investigation, validation. **Kwame Bankole:** supervision. **Sun Qi:** writing - reviewing and editing.

Do not include credit items that do not follow the Taxonomy established by CASRAI CRediT roles.

The authors’ contributions section should be omitted in manuscripts that have a single author.

5. Plagiarism checking

Submitted papers are expected to contain at least 50 % new content and the remaining 50 % should not be verbatim to previously published work.

All manuscripts are screened for similarities. Currently, the Editorial Board uses the plagiarism checker Plagius (www.plagius.com) to compare submitted papers to already published works. Manuscripts will be rejected if more than 20 % of content matches previously published work, including self-plagiarism. The decision to reject will be under the Editors’ discretion if the percentage is between 10 % and 20 %.

IMPORTANT OBSERVATION: Mendeley software plug-in (suggested in this guide) for MS-Word can be used to include the references in the manuscript. This plug-in uses a field code that sometimes includes automatically both title and abstract of the reference. Unfortunately, the similarity software adopted by the Journal (Plagius) recognizes the title and abstract as an actual written text by the field code of the reference and consequently increases considerably the percentage of similarity. Please do make sure to remove the abstract (if existing) inside Mendeley section where the adopted reference is included. This issue has mistakenly caused biased results in the past. The Editorial Board of the journal is now aware of this tendentious feature.

6. Formatting instructions

The text must be presented in a single column, using ISO A4 page size, left, right, top, and bottom margins of 25 mm, Times New Roman 12 font, and line spacing of 1.5. All lines and pages should be numbered.

The text should avoid unnecessary italic and bold words and letters, as well as too many acronyms. Authors should avoid to capitalize words and whenever possible to use tables with distinct font size and style of the regular text.

Figures, tables and equations should be numbered in the sequence that they are mentioned in the text.

Abstract

Please provide an abstract between 150 and 250 words in length. Abbreviations or acronyms should be avoided. The abstract should state briefly the purpose of the work, the main results and major conclusions or key findings.

Keywords

A minimum of three and a maximum of six keywords must be included after the abstract. The keywords must represent the

content of the paper. Keywords offer an opportunity to include synonyms for terms that are frequently referred to in the literature using more than one term. Adequate keywords maximize the visibility of your published paper.

Examples:

Poor keywords – piles; dams; numerical modeling; laboratory testing

Better keywords – friction piles; concrete-faced rockfill dams; material point method; bender element test

List of symbols

A list of symbols and definitions used in the text must be included before the References section. Any mathematical constant, variable or unknown quantity should appear in italics.

6.1 Citations

References to other published sources must be made in the text by the last name(s) of the author(s), followed by the year of publication. Examples:

- Narrative citation: [...] while Silva & Pereira (1987) observed that resistance depended on soil density
- Parenthetical citation: It was observed that resistance depended on soil density (Silva & Pereira, 1987).

In the case of three or more authors, the reduced format must be used, e.g.: Silva et al. (1982) or (Silva et al., 1982). Do not italicize “et al.”

Two or more citations belonging to the same author(s) and published in the same year are to be distinguished with small letters, e.g.: (Silva, 1975a, b, c.).

Standards must be cited in the text by the initials of the entity and the year of publication, e.g.: ABNT (1996), ASTM (2003).

6.2 References

A customized style for the Mendeley software is available and may be downloaded from this link.

Full references must be listed alphabetically at the end of the text by the first author's last name. Several references belonging to the same author must be cited chronologically.

Some formatting examples are presented here:

Journal Article

Bishop, A.W., & Blight, G.E. (1963). Some aspects of effective stress in saturated and partly saturated soils. *Géotechnique*, 13(2), 177-197. <https://doi.org/10.1680/geot.1963.13.3.177>

Castellanza, R., & Nova, R. (2004). Oedometric tests on artificially weathered carbonatic soft rocks. *Journal of Geotechnical and Geoenvironmental Engineering*, 130(7), 728-739. [https://doi.org/10.1061/\(ASCE\)1090-0241\(2004\)130:7\(728\)](https://doi.org/10.1061/(ASCE)1090-0241(2004)130:7(728))

Fletcher, G. (1965). Standard penetration test: its uses and abuses. *Journal of the Soil Mechanics Foundation Division*, 91, 67-75.

Indraratna, B., Kumara, C., Zhu S-P., Sloan, S. (2015). Mathematical modeling and experimental verification of fluid flow through deformable rough rock joints. *International Journal of Geomechanics*, 15(4): 04014065-1-04014065-11. [https://doi.org/10.1061/\(ASCE\)GM.1943-5622.0000413](https://doi.org/10.1061/(ASCE)GM.1943-5622.0000413)

Garnier, J., Gaudin, C., Springman, S.M., Culligan, P.J., Goodings, D., König, D., ... & Thorel, L. (2007). Catalogue of scaling laws and similitude questions in geotechnical centrifuge modelling. *International Journal of Physical Modelling in Geotechnics*, 7(3), 01-23. <https://doi.org/10.1680/ijpmg.2007.070301>

Bicalho, K.V., Gramelich, J.C., & Santos, C.L.C. (2014). Comparação entre os valores de limite de liquidez obtidos pelo método de Casagrande e cone para solos argilosos brasileiros. *Comunicações Geológicas*, 101(3), 1097-1099 (in Portuguese).

Book

Lambe, T.W., & Whitman, R.V. (1979). *Soil Mechanics, SI version*. John Wiley & Sons.

Das, B.M. (2012). *Fundamentos de Engenharia Geotécnica*. Cengage Learning (in Portuguese).

Head, K.H. (2006). *Manual of Soil Laboratory Testing - Volume 1: Soil Classification and Compaction Tests*. Whittles Publishing.

Bhering, S.B., Santos, H.G., Manzatto, C.V., Bognola, I., Fasolo, P.J., Carvalho, A.P., ... & Curcio, G.R. (2007). *Mapa de solos do estado do Paraná*. Embrapa (in Portuguese).

Book Section

Yerro, A., & Rohe, A. (2019). Fundamentals of the Material Point Method. In *The Material Point Method for Geotechnical Engineering* (pp. 23-55). CRC Press. <https://doi.org/10.1201/9780429028090>

Sharma, H.D., Dukes, M.T., & Olsen, D.M. (1990). Field measurements of dynamic moduli and Poisson's ratios of refuse and underlying soils at a landfill site. In *Geotechnics of Waste Fills - Theory and Practice* (pp. 57-70). ASTM International. <https://doi.org/10.1520/STP1070-EB>

Cavalcante, A.L.B., Borges, L.P.F., & Camapum de Carvalho, J. (2015). Tomografias computadorizadas e análises numéricas aplicadas à caracterização da estrutura porosa de solos não saturados. In *Solos Não Saturados no Contexto Geotécnico* (pp. 531-553). ABMS (in Portuguese).

Proceedings

Jamiolkowski, M.; Ladd, C.C.; Germaine, J.T., & Lancellotta, R. (1985). New developments in field and laboratory testing of soils. *Proc. 11th International Conference on Soil Mechanics and Foundation Engineering*, San Francisco, August 1985. Vol. 1, Balkema, 57-153.

Massey, J.B., Irfan, T.Y. & Cipullo, A. (1989). The characterization of granitic saprolitic soils. *Proc. 12th International Conference on Soil Mechanics and Foundation Engineering*, Rio de Janeiro. Vol. 6, Publications Committee of XII ICSMF, 533-542.

Indraratna, B., Oliveira D.A.F., & Jayanathan, M. (2008b). Revised shear strength model for infilled rock joints considering overconsolidation effect. *Proc. 1st Southern Hemisphere International Rock Mechanics Symposium*, Perth. ACG, 16-19.

Barreto, T.M., Repsold, L.L., & Casagrande, M.D.T. (2018). Melhoria de solos arenosos com polímeros. *Proc. 19º Congresso Brasileiro de Mecânica dos Solos e Engenharia Geotécnica*, Salvador. Vol. 2, ABMS, CBMR, ISRM & SPG, 1-11 (in Portuguese).

Thesis

Lee, K.L. (1965). *Triaxial compressive strength of saturated sands under seismic loading conditions* [Unpublished doctoral dissertation]. University of California at Berkeley.

Chow, F.C. (1997). *Investigations into the behaviour of displacement pile for offshore foundations* [Doctoral thesis, Imperial College London]. Imperial College London's repository. <https://spiral.imperial.ac.uk/handle/10044/1/7894>

Araki, M.S. (1997). *Aspectos relativos às propriedades dos solos porosos colapsíveis do Distrito Federal* [Unpublished master's dissertation]. University of Brasília (in Portuguese).

Sotomayor, J.M.G. (2018). *Evaluation of drained and non-drained mechanical behavior of iron and gold mine tailings reinforced with polypropylene fibers* [Doctoral thesis, Pontifical Catholic University of Rio de Janeiro]. Pontifical Catholic University of Rio de Janeiro's repository (in Portuguese). <https://doi.org/10.17771/PUCRio.acad.36102>*

* official title in English should be used when available in the document.

Report

ASTM D7928-17. (2017). Standard Test Method for Particle-Size Distribution (Gradation) of Fine-Grained Soils Using the Sedimentation (Hydrometer) Analysis. *ASTM International*, West Conshohocken, PA. <https://doi.org/10.1520/D7928-17>

ABNT NBR 10005. (2004). Procedure for obtention leaching extract of solid wastes. *ABNT - Associação Brasileira de Normas Técnicas*, Rio de Janeiro, RJ (in Portuguese).

DNIT. (2010). Pavimentação - Base de solo-cimento - Especificação de serviço DNIT 143. *DNIT -Departamento Nacional de Infraestrutura de Transportes*, Rio de Janeiro, RJ (in Portuguese).

USACE (1970). Engineering and Design: Stability of Earth and Rock-Fill Dams, Engineering Manual 1110-2-1902. Corps of Engineers, Washington, D.C.

Web Page

Soils and Rocks. (2020). *Guide for Authors*. Soils and Rocks. Retrieved in September 16, 2020, from <http://www.soilsandrocks.com/>

6.3 Artworks and illustrations

Each figure should be submitted as a high-resolution image, according to the following mandatory requirements:

- Figures must be created as a TIFF file format using LZW compression with minimum resolution of 500 dpi.
- Size the figures according to their final intended size. Single-column figures should have a width of up to 82 mm. Double-column figures should have a maximum width of 170 mm.
- Use Times New Roman for figure lettering. Use lettering sized 8-10 pt. for the final figure size.
- Lines should have 0.5 pt. minimum width in drawings.
- Titles or captions should not be included inside the figure itself.

Figures must be embedded in the text near the position where they are first cited. Cite figures in the manuscript in consecutive numerical order. Denote figure parts by lowercase letters (a, b, c, etc.). Please include a reference citation at the end of the figure caption for previously published material. Authorization from the copyright holder must be provided upon submission for any reproduced material.

Figure captions must be placed below the figure and start with the term "Figure" followed by the figure number and a period. Example:

Figure 1. Shear strength envelope.

Do not abbreviate "Figure" when making cross-references to figures.

All figures are published in color for the electronic version of the journal; however, the print version uses grayscale. Please format figures so that they are adequate even when printed in grayscale.

Accessibility: Please make sure that all figures have descriptive captions (text-to-speech software or a text-to-Braille hardware could be used by blind users). Prefer using patterns (e.g., different symbols for dispersion plot) rather than (or in addition to) colors for conveying information (then the visual elements can be distinguished by colorblind users). Any figure lettering should have a contrast ratio of at least 4.5:1

Improving the color accessibility for the printed version and for colorblind readers: Authors are encouraged to use color figures because they will be published in their original form in the online version. However, authors must consider the need to make their color figures accessible for reviewers and readers that are colorblind. As a general rule of thumb, authors should avoid using red and green simultaneously. Red should be replaced by magenta, vermillion, or orange. Green should be replaced by an off-green color, such as blue-green. Authors should prioritize the use of black, gray, and varying tones of blue and yellow.

These rules of thumb serve as general orientations, but authors must consider that there are multiple types of color blindness, affecting the perception of different colors. Ideally, authors should make use of the following resources: 1) for more information on how to prepare color figures, visit <https://jfly.uni-koeln.de/>; 2) a freeware software available at <http://www.vischeck.com/> is offered by Vischeck, to show how your figures would be perceived by the colorblind.

6.4 Tables

Tables should be presented as a MS Word table with data inserted consistently in separate cells. Place tables in the text near the position where they are first cited. Tables should be numbered consecutively using Arabic numerals and have a caption consisting of the table number and a brief title. Tables should always be cited in the text. Any previously published material should be identified by giving the original source as a reference at the end of the table caption. Additional comments can be placed as footnotes, indicated by superscript lower-case letters.

When applicable, the units should come right below the corresponding column heading. Horizontal lines should be used at the top and bottom of the table and to separate the headings row. Vertical lines should not be used.

Table captions must be placed above the table and start with the term “Table” followed by the table number and a period. Example:

Table 1. Soil properties.

Do not abbreviate “Table” when making cross-references to tables. Sample:

Table 1. Soil properties

Parameter	Symbol	Value
Specific gravity of the sand particles	G_s	2.64
Maximum dry density (Mg/m ³)	$\rho_{d(max)}$	1.554
Minimum dry density (Mg/m ³)	$\rho_{d(min)}$	1.186
Average grain-size (mm)	d_{50}	0.17
Coefficient of uniformity	C_u	1.97

6.5 Mathematical equations

Equations must be submitted as editable text, created using MathType or the built-in equation editor in MS Word. All variables must be presented in italics.

Equations must appear isolated in a single line of the text. Numbers identifying equations must be flushed with the right margin. International System (SI) units must be used. The definitions of the symbols used in the equations must appear in the List of Symbols.

Do not abbreviate “Equation” when making cross-references to an equation.